The Use of Non-ionic Surfactant Vesicles to Prevent Radiocontrast Media-Associated Damage

A thesis presented by

Rachel Donaghey

In fulfilment of the requirements for the degree of
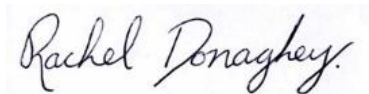Doctor of Philosophy

November 2018

Strathclyde's Institute of Pharmacy and Biomedical Science

Declaration of Authenticity

This thesis is the result of the author's original research. It has been composed by the author and has not been previously submitted for examination which has led to the award of a degree.

The copyright of this thesis belongs to the author under the terms of the United Kingdom Copyright Acts as qualified by University of Strathclyde Regulation 3.50. Due acknowledgement must always be made of the use of any material contained in, or derived from, this thesis.

Signed:

Date: 30/ 11/ 2018

Acknowledgements

List of Abbreviations

A

Acetonitrile (ACN)

Acetylcholine (ACh)

Acute kidney injury (AKI)

Analysis-of-variants (ANOVA)

Antidiuretic hormone (ADH)

Area under the curve (AUC)

Atomic Force Microscopy (AFM)

B

Bis-alanylalanyl-phenylalanyl-rhodamine 110 (bis-AAF-R110)

Bovine serum albumin (BSA)

C

Cardiovascular disease (CVD)

Cholesterol (chol.)

Chronic kidney disease (CKD)

Coefficient variant (CV %)

Computed tomography (CT)

Contrast media-induced nephropathy (CIN)

Contrast media (CM)

Critical packing parameter (CPP)

D

Danish Myo Technology (DMT)

Deionised (DI)

Dicetyl phosphate (DCP)

Differential scanning calorimetry (DSC)

1, 2-dipalmitoyl-sn-glycero-3-phosphocholine (DPPC)

Disintegrations per minute (dpm)

1, 2-Distearoyl-sn-glycero-3-phosphoethanolamine (DSPE)

1, 2-distearoyl-sn-glycero-3-phosphoethanolamine-N-[amino (polyethylene glycol)-2000] (DSPE-MPEG$_{2000}$)

Dynamic light scattering (DLS)

E

Eagle's minimum essential medium (EMEM)

Encapsulation Efficiency (EE)

Endothelial cells (ECs)

Endothelial nitric oxide synthase (eNOS)

Endoplasmic reticulum (ER)

Estimated glomerular filtration rate (eGFR)

European Society of Urogenital Radiology (ESUR)

F

Fetal calf serum (FCS)

Food and Drug Administration (FDA)

G

G-protein-coupled receptor (GPCR)

Glycyl-phenyl-alanyl-aminofluorocoumarin (GF-AFC)

Guanosine monophosphate (GMP)

Guanosine triphosphate (GTP)

H

Human embryonic kidney (HEK)

High Performance Liquid Chromatography (HPLC)

Human umbilical vein endothelial cell (HUVEC)

I

International Conference on Harmonisation of Technical Requirements for Registration of

Pharmaceuticals for Human Use (ICH)

Intravenous (IV)

Inositol triphosphate (IP$_3$)

Iohexol (IOX)

Isopropyl alcohol (IPA)

L

Left ventricular end-diastolic pressure (LVEDP)

Limit of detection (LoD)

Limit of quantification (LoQ)

M

Madin-Darby Canine Kidney (MDCK)

Magnetic resonance imaging (MRI)

Melting temperature (T$_m$)

Molecular weight (MW)

Molecular weight cut-off (MWCO)

Mononuclear phagocytic system (MPS)

Monopalmityl glycerol (MPG)

Multilamellar vesicles (MLVs)

Muscarinic receptors (MRs)

Myosin light chain (MLC)

N

N-acetylcysteine (NAC)

Nanoparticle (NP)

Nitric oxide (NO)

Non-ionic surfactant vesicle (NIV)

P

Paclitaxel (PTX)

Phase analysis light scattering (PALS)

Phenylephrine (PE)

Phosphate buffer saline (PBS)

Phosphatidylinositol 4, 5 – bisphosphate (PIP_2)

Phospholipase C (PLC)

Polydispersity index (PDI)

Polyethersulfone (PES)

Polyethylene glycol (PEG)

Prostaglandin E (PGE)

Protein kinase G (PKG)

R

Radiocontrast media (RCM)

Reactive oxygen species (ROS)

Relative fluorescence units (rfu)

Relative humidity (RH)

Relative standard deviation (RSD)

Renin-angiotensin-aldosterone system (RAAS)

Residual sum of squares (RSS)

Revolutions per minute (rpm)

Retention time (RT)

S

Scanning electron microscopy (SEM)

Serum creatinine (sCr)

Signal-to-noise (S/N)

Small unilamellar vesicles (SUVs)

Sodium stibogluconate (SSG)

Sodium nitroprusside (SNP)

Soluble guanylyl cyclase (sGC)

Standard deviation (SD)

T

Tangential flow filtration (TFF)

Thin film method (TFM)

Transmission electron microscopy (TEM)

Trichloroacetic acid (TCA)

Tritiated thymidine (^{3}H-dT)

U

Ultrasound (US)

Ultraviolet-high-performance liquid chromatography (UV-HPLC)

United States Pharmacopeia (USP)

V

Vascular smooth muscle (VSM)

Z

Zeta potential (ζP)

List of Figures

List of Tables

Abstract

Radiocontrast media administered during routine bio-imaging procedures represents a cause of hospital-associated, acute kidney injury or contrast-induced nephropathy. The exact mechanism of disease is not well characterised, although, a number of existing theories exist. The absence of adequate preventative or treatment measures poses a risk to poorly defined, susceptible patients. The initial goal is to formulate and characterise a novel iohexol-non-ionic surfactant vesicle (IOX-NIV) delivery system in line with FDA recommendations. This work adds to current knowledge of IOX-associated cytotoxicity and its influence on vessel function.

IOX-NIVs were prepared using a 3: 3: 1 mol. ratio of surfactant VIII/ cholesterol/ dicetyl phosphate using high shear homogenisation. Dynamic light scattering was used to determine physical characteristics including size, polydispersity index (PDI) and particle distribution. Phase analysis light scattering was used to measure surface charge. NIVs were purified using ultracentrifugation prior to the quantification of IOX encapsulation efficiency and release using high performance liquid chromatography. Toxicity of IOX, empty-NIV and IOX-NIV was tested on renal and vascular cells using assays including the Resazurin metabolic indicator assay, thymidine-incorporation, CellTox Green™ assay and ApoToxGlo™ assay.

IOX-NIVs were reproducibly produced (n = 3) with an average size of 204 ± 24 nm, low PDI of 0.13 ± 0.04, surface charge of -26 ± 1 mV and EE of $22 \pm 3\%$. Vesicle processing through ultracentrifugation or sterile filtration did not significantly alter physical properties. IOX-NIVs maintained physicochemical stability throughout 37 weeks storage at 4 and 25 °C. A time- and temperature-dependent change in IOX-NIV colour was observed prior to an increase in size (1671 ± 1498 nm) and PDI (0.7 ± 0.31), followed by a loss in negativity (-15 ± 3 mV) and EE (4 ± 3 %), specifically at temperatures of 37 and 50 °C ($p < 0.001$). Hydrated IOX-NIVs displayed a typical 'burst' release profile under physiological conditions *in vitro*, whereby 73 ± 2 % of IOX was released after 48 h. IOX exposure led to decreased renal and vascular metabolism where cells underwent rounding and a loss in adherence, features of which express similarities to cells undergoing apoptosis or as a result of exposure to hyperosmolar agents. In addition, IOX inhibited receptor-independent vasoconstriction, while IOX-NIV treated groups expressed a response similar to the control.

Characterisation of IOX-NIVs showed the synthesis of a stable system with physical features desirable for administration as an intravenous contrast agent. IOX-NIVs expressed relatively low toxicity *in vitro*. Overall, IOX-NIV show great potential as a clinically compatible product, however, future *in vivo* safety and efficacy studies are required.

Contents

Chapter 1

Introduction

1. Chapter 1 – Introduction

1.1. Contrast Media and its applications

A contrast medium (CM), or contrast agent, is a substance administered to patients prior to the performance of clinical biomedical imaging procedures. A major advantage of bio-imaging is the ability to visualise internal structures within the body in a non-invasive manner (Mastouri *et al.*, 2010). Techniques such as computed tomography (CT), magnetic resonance imaging (MRI), and ultrasound (US) are routinely carried out for the clinical diagnosis and prognosis of disease. As a result of their different mechanisms of action (i.e. x-ray imaging during CT scanning, nuclear magnetic resonance enhancement during MRI imaging or through the use of high-frequency sound waves during US imaging) each procedure requires a different reagent for the enhancement of image contrast and visualisation. This means that CM are often defined based on the procedure in which they are used for – radiocontrast media (RCM) are administered for the enhancement of CT imaging (Widmark, 2007), paramagnetic agents, such as gadolinium, for MRI (Tiderius *et al.*, 2003) and microbubble agents for ultrasound imaging (Stride and Saffari, 2003). In comparison to the other two techniques, CT imaging is enhanced through the use of RCM which either consist of iodinated small molecules or barium sulphate molecules. These are selected based on the desired route of administration. Iodinated RCM is primarily used during intravenous (IV) administration, particularly, in the process of angiography. Since their initial development, the safety of RCM has greatly improved, however, their use still poses a risk to certain groups of individuals who may benefit from additional protective measures.

1.1.1. CT Imaging and iodinated RCM

The Nobel prize in Medicine was jointly awarded to Cormack and Hounsfield in 1979 for their work in the development of CT imaging (Nobelprize.org). Initially, Cormack developed algorithms which described the absorption of x-rays by the human body and it was then postulated that differences in tissue absorbance could be used to differentiate between different materials in the body (Cormack, 1979). Hounsfield was the first to apply these mathematical calculations to a working CT system which resulted in the work being published in 1973. It was shown how *tomo*-graphic images could be obtained in the form of a '*slice*', and that a number of these slices could be pieced together to give a 3D image of internal structures within the body, which absorb x-rays at different intensities, within a whole patient in a non-invasive manner. In the clinical setting, a beam of x-rays is directed towards the patient then a detector measures the strength of those rays which pass through the body. The ability to detect x-rays is therefore dependent on the density of the material in which the beam has been passed

through. Hounsfield successfully managed to differentiate between brain, bone and tumour tissues by using this method and from this day the use of x-ray CT scanning has revolutionised how diseases of soft tissues are diagnosed, monitored and treated (Hounsfield, 1973). The administration of iodinated RCM to the patient enables enhanced imaging by creating a denser area which blocks x-rays from being detected, the greater the molecular weight of the molecule, the denser it is and the greater the contrast produced. However, RCM were being used to enhance radiographic images prior to the development of the CT scanner. In fact, shortly after the discovery of X-rays by Röntgen (1895), the desire to improve image quality quickly followed (Novelline, 1997). One month later, details of the first contrast-enhanced angiogram was reported, whereby a mixture of bismuth, lead and barium salts were injected into the vascular system of an amputated hand (Figure 1.1; Haschek and Lindenthal, 1896). IV administration of this concoction of heavy metals demonstrated the great medical potential of contrast-enhanced X-rays, however, this mixture of heavy metals would not be safe for human use and further development of radiocontrast agents was required.
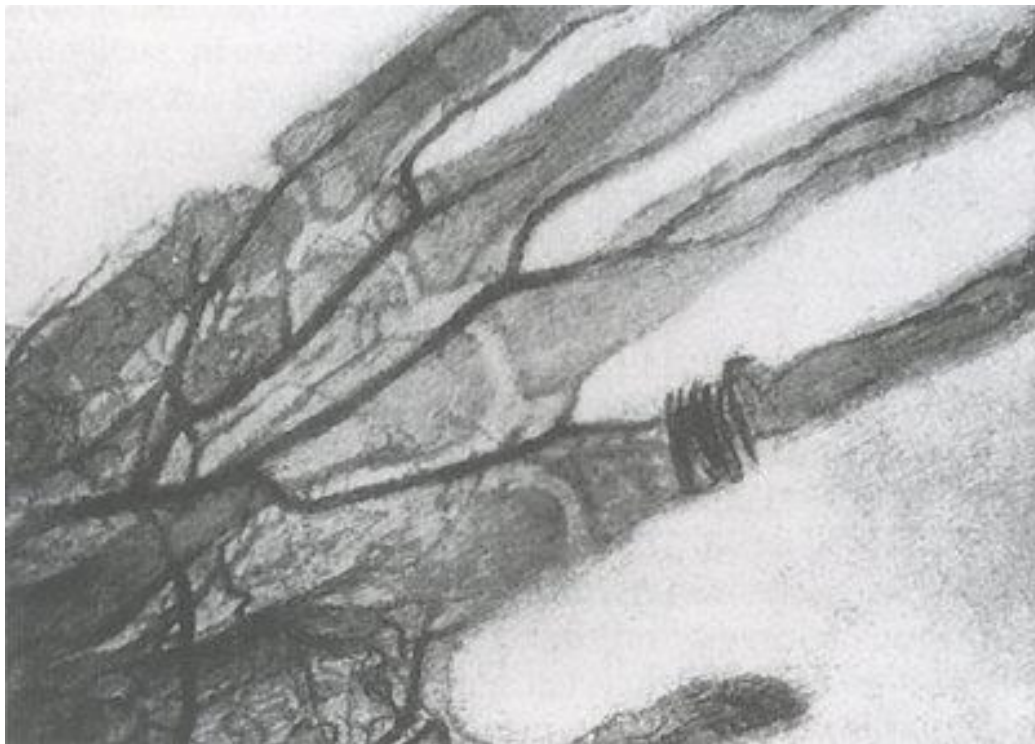
Figure 1.1: First angiographic image of an amputated hand with contrast-enhanced vascular system. *Darker regions contain the contrast-enhancing agent which expresses a higher atomic density in comparison to the surrounding tissues which allows for visualisation of the vasculature. Image reprinted from Haschek and Lindenthal (1896).*
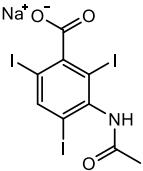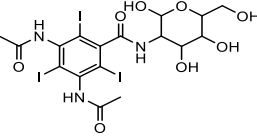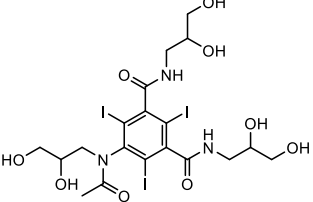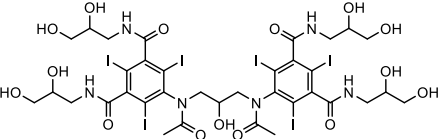
Table 1.1). Rather than RCM-development focusing on the improvement of image quality and resolution, the key driving force behind the development of new products was related to reducing the risk of adverse reactions whereby the transformation from ionic to non-ionic RCM was the first step in improving safety (Katayama *et al.*, 1990). Initial synthesis of iodinated-RCM led to production of the first generation of agents including the ionic, high osmolar CM, sodium acetrizoate. Sodium acetrizoate has a molecular structure consisting of a benzene aromatic ring with three covalently attached iodine atoms, in place of the original hydrogen atoms. This chemical was given the trade name Urokon® and it was believed to be one of the least toxic RCM available (Wallingford, 1953). Reports of severe and unpredictable neuro- and nephron-toxicity were later reported which lead to the removal of Urokon from the market (Killen *et al.,* 1962). Shortly after the manufacturing of Urokon® the synthesis of similar RCM took place, such as sodium diatrizoate (Urografin®) and meglumine iothalamate (Conray®) (Geenen *et al.,* 2013). Although it was shown that meglumine iothalamate offered a lower risk for the development of neurotoxicity, these complications were still prevalent in patients undergoing angiographic procedures (Chase and Kricheff, 1965).

It was not until 15 years later that the next generation of low-osmolar, non-ionic RCM were synthesised and marketed; allowing for the prevention of serious adverse effects which had been associated with first generation RCM. This was made possible due to the development of a chemical process that reduced toxic ionic strength and osmolality, leading to the production of metrizamide (Amipaque®) (Almén, 1969). Several other non-ionic RCM were later released with greater levels of solubility, making up the third generation of RCM, including iohexol (IOX; Omnipaque®), iopromide (Ultravist®), iomeprol (Iomeron®), ioversol (Optiray®) and iobitridol (Xenetix®). Dimeric compounds make up the final fourth class of RCM: iotrolan (Isovist®) is a chemical which was found to be iso-osmolar with blood (Sovak *et al.,* 1982). Although a reduction in the primary issues of toxicity were observed upon adapting the structure of RCM, the marketing of iotrolan was short lived due to the high incidence of delayed hypersensitive-type reactions and now, due to safety constraints, there is only one non-ionic dimer, iodixanol (Visipaque®), that is currently marketed as a RCM (Bolstad *et al.*, 1991; Kanzaki and Sakagami, 1991; Speck *et al.*, 1998). Initially, a decrease in RCM osmolality-induced toxicity was achieved by replacing ionising carboxyl groups with

hydrophilic structures leading to a reduction in potentially toxic Coulomb interactions which may occur between charged ions and biomolecules (Dawson, 1991). Removal of carboxyl groups also led to improved solubility and ionic strength. The inclusion of –OH groups improved neurological safety, while an even distribution of these hydroxyl groups enhanced this further (Katzberg, 1997). Regardless of minor alterations in chemical structure, IV administration of iodinated RCM leads to the dye rapidly spreading throughout the vasculature and filtration through highly vascularised organs including the kidneys, liver, and brain, while occupation within dense tissues including bone or fat occurs to a lesser extent (Pasternaka and Williamson, 2012). The estimated half-life of most RCM is in the range of 90-120 mins whereby it is excreted within the urine in an unmetabolised form (Katzberg, 1997).

Table 1.1: Examples of the alteration of iodinated-RCM throughout their development and the resultant changes in chemical and physical properties which were preformed to reduce side-effects.

	Radiocontrast media properties			
	1st generation	**2nd generation**	**3rd generation**	**4th generation**
Chemical name	Sodium acetrizoate	Metrizamide	Iohexol	Iodixanol
Commercial name	Urokon	Amipaque	Omnipaque300 (647 mg mL^{-1})	Visipaque 270 (550 mg mL^{-1})
Chemical structure				
Iodine concentration (mg iodine mL^{-1})	nr	300	300	270
Osmolality (mOsm kg^{-1} H$_2$O)	High-osmolar / nr	Low-osmolar / 484	Low-osmolar / 640	Iso-osmolar / 290
Ionic strength	Ionic	Non-ionic	Non-ionic	Non-ionic
MW (g mol^{-1})	578.84	789.1	821.24	1550.18

nr = not recorded

1.1.2 Estimated RCM usage

RCM can be administered to patients in a variety of different ways and in different doses depending on the organ of interest, demonstrating the versatility of RCM as an image-enhancing agent (Pasternaka and Williamson, 2012). An estimated 75 million RCM-enhanced procedures were reported to occur per year worldwide in 2002 (Christiansen, 2005). More recently, Persson (2005) reported on information gathered from the European Renal Association and the European Dialysis and Transplantation Association Meeting in Lisbon (2004) where it was estimated that in that year there would be over 80 million CT-imaging procedures requiring the administration of RCM. Its prevalence was also estimated to have increased by 800 % over the two decades prior to 2004 (Katzberg and Haller, 2006). These reports stress the popularity and importance of x-ray imaging techniques within the clinical environment, the incidences of which are being observed to increase over time (Kalra *et al.,* 2004).

1.2 RCM and adverse reactions

If RCM usage continues to increase at its current rate, an increase in the number of adverse reactions could be anticipated to follow. Although the risk to a healthy individual remains low (1-2 %; Lewington *et al.*, 2013), the incidence of RCM-associated disease, particularly acute kidney injury (AKI) and contrast-induced nephropathy (CIN), is estimated to occur in up to 50 % of the 'at-risk' population undergoing coronary angiography or percutaneous coronary intervention (Mehran and Nikolsky, 2006). The performance of retrospective analysis studies to define the incidences of these conditions are often contradictory meaning that the actual quantification of renal complications has been difficult to conclude (Andreucci *et al.* , 2017).

1.2.1 RCM-associated AKI and CIN

Contrast media-induced nephropathy (CIN) is a condition where there is a reduction in renal function as a result of the administration of RCM and is a third leading cause of hospital-associated kidney failure (Nash *et al.*, 2002; Hou *et al.*, 1983). A study performed by the European Society of Urogenital Radiology (ESUR; 1999) defined this condition by the detection of > 25 % absolute increase in serum creatinine (sCr) (44µM) during the 3 day period after initial administration of CM, in the absence of an alternative cause. This definition remains to be the most widely accepted and has proven to be the most reliable when compared to the use of calculating the relative increase in sCr or reductions in patients estimated glomerular filtration rate (eGFR) as outlined in an update of the ESUR guidelines on CIN (Stacul *et al.,* 2011).

Even with the wide range of research surrounding CIN, its existence still remains a controversial one. A recent retrospective meta-analysis on the development of CIN based on 53,439 patients who were either administered an IV injection of contrast media followed by a CT scan, or, had previously underwent a CT scan without the use RCM revealed no significant correlation between CIN and the use of CM (Mcdonald *et al.*, 2013). Although this study was a large, single-institute study which used propensity score adjustment for differences in reported risk factors, and patients were assessed using current definitions of CIN - differences in sCr from baseline measurements - it failed to take in to consideration any preventative and treatment measures which may have taken place within at-risk groups who were administered with RCM. Therefore, the results presented in this article may have been biased towards the groups who did not receive RCM, who in turn, would have been less likely to be receive preventative measures.

The risk factors that increase patient susceptibility have been under much deliberation throughout research involving CIN. However, a general consensus has been made on the fact that reduced renal and cardiac function, as well as haemodynamic instability, predispose patients to the development of CIN. Abnormal renal and cardiac function have been linked to a number of pre-existing co-morbidities (Table 1.2).

Table 1.2: Risk Factors Associated with the Development of CIN.

Risk factor	Associated disease state	Reference
Reduced renal function	Diabetes mellitus	Parfrey *et al.* (1989)
	Age	Stacul *et al.* (2011)
	Multiple myeloma	McCarthy and Becker (1992); Preda *et al.* (2011)
Reduced cardiac function	Congestive heart failure	Gruberg *et al.* (2000)
	Myocardial infarction	Stacul *et al.* (2011)
Haemodynamic instability	Anaemia	Stacul *et al.* (2011)
	Dehydration	Stacul *et al.* (2011)

In contrast to this, Kim *et al.*, (2012)conducted a study to determine any long-term effects of IV administration of 80-120 mL of the non-ionic, low osmolar, iodinated RCM, Iopromide, on 176 patients with pre-existing chronic kidney disease (CKD) who were undergoing CT imaging. Pre-existing CKD was defined in patients with kidney disease between stages 3-5, which is characterised based on the eGFR (Table 1.3). By performing retrospective analysis of patient's medical records, particularly the eGFR which was recorded on a monthly basis, no significant correlation between pre-existing renal damage and the use of this RCM was observed in the patient cohort analysed. This was also true when taking into consideration

additional risk factors such as age, sex, and the presence of diabetes. However, eGFR monitoring varied between patients in terms of duration from as little as 1 month up until a total of 8 months and analysis of any acute injury during the initial month was also not taken into consideration, which is the most critical time point in relation to the onset of CIN. It may be assumed that a number of these patients could have suffered from CIN but renal failure was prevented using current treatment measures including hydration resulting in the restoration of eGFR towards baseline measurements. This study also did not analyse the records of patients without CKD, therefore adequate control measures were not in place to determine the significance between damage in at-risk and healthy patients. Although this study does suggest that Iopromide is suitable for use within patients considered susceptible to CIN, the main issues arise in the percentage of patients where current treatment is not sufficient resulting in morbidity and mortality.

Table 1.3: UK characterisation of chronic kidney disease based on the eGFR. *Table adapted from:* NICE, 2014: https://www.nice.org.uk/guidance/cg182 [last accessed 2019 May 06] *; eGFR – estimated glomerular filtration rate).*

Grading	Description	eGFR (mL/min/1.73m^2)
Stage 1	Normal and high	≥ 90
Stage 2	Mild reduction	60-89
Stage 3A	Mild-moderate reduction	45-59
Stage 3B	Moderate-severe reduction	30-44
Stage 4	Severe reduction	15-29
Stage 5	Kidney failure	< 15

The ESUR came to an agreement that the development of CIN in the general population, who express normal renal function was < 5 %. It was also agreed that the literature supports the theory that the incidence of potentially fatal CIN increases to 25 % when considering susceptible patient groups (Morcos *et al.*, 1999). With incidences of predisposing co-morbidities including diabetes, obesity, cardiovascular and kidney disease on the rise, alongside a shift in demographics towards an aging population (Klonoff, 2009; Tonelli and Riella, 2014), it is likely that the number of patients requiring imaging procedures due to reduced health and existence of co-morbidities will also increase. It may also be predicted that increased patient exposure to RCM in combination with increased incidences of associated risk factors it will ultimately contribute to increasing incidences of CIN where current preventative measures are insufficient.

Development of AKI within NHS hospitals is reported to occur in 13-18 % of all patients admitted to hospital, part of which is attributed to patients receiving iodinated RCM this comes at an estimated cost of £434-620 million/ year (NICE, 2013).

An analytical model was developed to determine the 1 year financial cost of an in-patient developing CIN by(Subramanian *et al.*, 2007). Estimations were based on results obtained from a number of studies. Factors such as general hospital costs and also the cost of treatment were taken into consideration to estimate a cost of $11,812 USD/ patient over the course of 1 year after undertaking the imaging procedure. Additional costs that arise from this potentially preventable condition include patient morbidity, the requirement for prolonged dialysis, increased time spent in hospitals and intensive care units and also mortality. The existence of adequate preventative measures would reduce the large financial burden imposed on the healthcare system and improve patient health.

1.2.2   Theories behind renal and vascular RCM-associated toxicity and pathology

A number of theories exist to explain the toxicity of RCM, particularly in relation to the chemical properties of RCM dyes. Almén published some of the initial work looking at the effects of RCM ionic strength and its toxic influence on the cardiovascular system. It was his experience as a radiologist and patient suffering after the administration of RCM that led him down the path of developing safer and less toxic RCM which ultimately resulted in him being announced as 'the father of non-ionic iodine contrast media' (Nyman *et al.*, 2016). His research found that, when different RCM were administered at concentrations which eliminate the influence of differences in iodine concentration, ionic RCM exerted a significantly more toxic effect on the endothelial layer of rat aorta compared to non-ionic RCM, including IOX (Nyman and Almén, 1980). In addition to this, a randomised double-blind trial carried out on 1196 patients with and without diabetes and/ or renal insufficiency had shown a reduction in nephrotoxicity as a result of utilising the non-ionic RCM, IOX, in comparison to ionic meglumine/ sodium diatrizoate (Rudnick *et al.*, 1995). A reduction in ionic strength has been associated with reduced hydrophobic and Coulomb interactions occurring between the benzene ring-iodine groups of RCM and biomolecules, and hence a reduction in chemotoxicity (Dawson, 1991). Despite the improved safety of RCM over time, the development of adverse reactions after the administration of non-ionic RCM is still an issue.

In addition to reducing ionic strength, advances have also had a focus on reducing osmolality which is a secondary feature believed to contribute to the manifestation of adverse reactions. Despite the generation of iso-osmolar RCM from the initial high-osmolar agents, commonly used low-osmolar RCM, such as IOX, still express an osmolality 2x greater than blood. IV administration of materials which are hyperosmolar to blood have detrimental effects on blood cells as well as the endothelial and smooth muscle components of the blood vessel. Typical consequences of administration of hyperosmolar RCM include reduced oxygen delivery to

tissues, and in extreme cases anoxia, as well as increased blood vessel permeability, both of which can lead to complications in organ function (Grainger, 1980). A greater level of susceptibility to hyperosmolar-mediated damage occurs in organs which are highly vascularised with capillaries, such as the kidneys. Additional generalised effects which arise as a result of the administration of a hyperosmolar RCM include osmotic hypervolemia, vasodilation and systemic hypotension (Grainger, 1980).

RCM-associated toxicity has also been linked to iodine concentration. Despite this, the toxicity of iodine as a result of high intake in humans is rare, but has been known to arise as the result of increased consumption of vitamins, or from the environment in instances of nuclear disasters (Baker, 2004). The toxicity of iodine is more likely to be an issue for new-borns who have yet to develop a mature thyroid gland rather than patients who are most likely to receive iodine in the form of RCM. In addition, iodine is a micronutrient found in a number of food sources such as seafood, dairy and salt and its existence within humans is essential to enable healthy functioning of the thyroid. Iodine levels in pregnant woman is a critical feature required to promote healthy foetal development (Prado and Dewey, 2014). An estimation of the potential safety limit of RCM was previously defined as an LD50 of 8000 mg iodine kg^{-1}, however, the typical dose administered in the clinical setting, when considering the performance of a urogram for example, is 300 mg iodine kg^{-1} meaning that in theory the actual administered dose is much less than the level required to induce iodine-induced toxicity (Dawson and Clauss, 1998). As safer non-ionic low-osmolar RCM now exist, it means that the LD50 of more commonly used RCM would be greater and the patient would be able to withstand greater doses. Key adverse reactions relating to the iodine content of RCM has also been linked to hypersensitivity reactions, however, this is a controversial area which is discussed later in this chapter (Section 1.2.3).

RCM-associated increases in urine viscosity was observed when testing the urine output from pigs injected with iodixanol, one of the only iso-osmolar RCM (Jost *et al.*, 2010). The initially viscous RCM becomes diluted by the blood upon IV administration where it is then rapidly cleared from the body via the kidneys without the occurrence of any metabolic alterations. As the RCM-containing blood becomes filtered through the kidneys, the urine viscosity subsequently increases leading to a drop in urine flow rate and reduced clearance of RCM. This in turn is likely to prolong renal exposure to RCM leading to pressure-related damage of tubular cells in addition to the renal medulla (Lenhard *et al.*, 2012). Vascular constriction of the vasa recta of the kidneys has also been reported to occur *ex vivo* and has been attributed to the high viscosity of RCM (Sendeski *et al.*, 2010). Viscosity-associated renal injury may be

linked to a shift in red blood cell structure from their typical concave disc shape to an irregular, rigid echinocyte (Mrowietz *et al.*, 2012). Alteration of the typical blood cell morphology will reduce the bloods capacity to deliver oxygen leading to ischaemic damage, particularly within the kidneys. Decreased blood flow and ischaemic damage within the medullary portion of the kidneys has also been linked to the high viscosity of RCM in a dog model (Lancelot *et al.*, 2002). The prevalence of increased urine viscosity could be inter-linked to renal impairment due to alterations in blood flow and hypoxia within highly sensitive portions of the kidneys. The relationship between high RCM viscosity, development of viscous urine output and potential for hypoxia-mediated renal damage as a result of altered medullary blood flow was also observed in subsequent studies (Seeliger *et al.*, 2007).

Overall, the toxicity of RCM on the vasculature and renal filtration system appears to be the result of a multi-factorial insult relating to the RCM chemical structure, whereby interactions between the RCM and biomolecules comprise cardiovascular and renal tissues leading to injury, as well as features such as RCM ionic strength, osmolality and viscosity which can all interfere with haemodynamics and down-stream renal filtration. Regardless of the inability to identify a single cause of RCM-associated vascular and renal damage, it is often reported that the pathological outcomes include renal and cardiovascular cell death through apoptosis *in vitro* (Romano *et al.*, 2008; Rowe *et al.*, 2016; Zhang, *et al.*, 2000). An increase in reactive oxygen species (ROS) production has been associated with renal tubular cell death via apoptosis, even in the instance of exposure to low-osmolar RCM which are believed to be less toxic (Yang *et al.*, 2014; Gong *et al.*, 2010). Studies which focused on the effects of RCM *in vivo* detected signs of apoptosis in both cardiac and renal tissues. A change in cellular morphology to indicate apoptosis (or programmed cell death), detection of DNA fragmentation, and immunohistochemical identification of apoptotic biomarkers Bcl-2, Bax and p53 were all reported in the kidneys of rats exposed to RCM (Zhang *et al.*, 1999). The combined insults derived from RCM administration is likely to have contributed to difficulties in defining disease states, in addition to problems in developing effective preventative measures. A multifactorial approach to preventing RCM interactions within the body may represent a more appropriate treatment mechanism to protect 'at-risk' patients from RCM-associated damage.

1.2.3   Alternative side-effects relating to RCM-exposure

Other than potential RCM-associated renal and cardiovascular complications, reported adverse reactions include allergic-type reactions which can take the form of immediate anaphylaxis (< 1 h) or delayed (> 1 h) cutaneous type-reactions (Meth and Maibach, 2006).

Patients experiencing hypersensitive reactions to RCM are commonly reported to develop urticaria (Bumbăcea *et al.*, 2013). Studies have shown that administration of antihistamines or corticosteroids prior to repeat exposure to RCM did not prevent immediate hypersensitivity from developing. Prior administration of anti-allergic treatments was found to significantly increase the likelihood of developing urticaria (Kolbe *et al.*, 2014). Additional studies have shown that the most successful method for the prevention of hypersensitivity is through the use of an alternative RCM in comparison to that used during the primary performance of RCM-enhanced imaging rather than the use of pharmacological intervention (Abe *et al.*, 2016).

The development of RCM-associated allergic-type reactions has previously been linked to seafood and iodine allergies (Witten *et al.*, 1973). Taking precautions in patients with seafood and/ or iodine allergies who are undergoing bio-imaging procedures is often recommended, however, this link is controversial and more recently has been disproved (Baig *et al.*, 2014). Skin tests of patients who previously expressed an immune response to RCM revealed a role for T-cell-mediated immunity as well as cross-reactivity between different RCM *(Kanny et al.*, 2005). Cross-reactivity after exposure to inorganic iodine has not been observed. Both of these studies show a link between RCM structure and immunogenicity, as well as a lack of iodine immunogenicity (Akiyama *et al.*, 1998). In addition to this, IgE-mediated immune responses to RCM have been reported through the use of skin tests and identification of basophil activation (Trcka *et al.*, 2008). Conclusions on the exact cause of RCM-hypersensitivity has been difficult to define due to variations between patients in addition to the fact that preventative pharmacological measures have shown to be of little benefit. A greater understanding of patient response to RCM is essential in order to develop preventative strategies.

1.3 Current prophylactic measures for the prevention of RCM-associated toxicity

1.3.1   Patient hydration for the prevention of RCM-AKI and CIN

When patient assessment leads to the identification of a requirement for RCM administration and bio-imaging, without the identification of major risk factors or a way to improve safety through the use of alternative methods, a number of prophylactic steps can be implemented to reduce the risk to patients. The ESURs first consensus report highlighted hydration as a key prophylactic measure for the prevention of renal complications after RCM exposure, in addition to the selection of low- or iso-osmolar RCM, rather than high-osmolar RCM (Morcos *et al.*, 1999). This report also highlighted the consideration of patient withdrawal from the use of any nephrotoxic drugs at least 24 h prior to RCM administration. A more recent review of

the 1999 report remains in agreement with these prophylactic measures meaning that patient hydration is the primary method used both before and after RCM administration to restore renal function, as well as preventing CIN and potential renal failure (Stacul *et al.*, 2011).

The exact beneficial mechanisms behind this prophylactic measure remain to be confirmed, the uncertainty surrounding RCM-AKI and its prevention is likely to be related to the multifactorial nature in which both injury and protection occur. A number of theories of describing RCM-damage and its prevention can be explained as a result of improving patient hydration. One of the key factors associated with RCM-CIN, as mentioned previously, is a loss in haemodynamic stability leading to hypoxia and cell death within the kidneys. The susceptibility of the kidneys is related to the non-metabolised excretion of RCM through this organ. The tubular and medullary regions of the kidneys are often reported to be the most significantly affected and are highly vascularised due to the fact that salt, water and nutrient secretion and reabsorption occurs in the distal and proximal tubules which make up the renal cortex, as well as the Loop of Henle and collecting ducts of the nephron which make up the medulla (Figure 1.2). The requirement for diffusion of salts and water across the nephron and blood barriers highlights the fragile nature of these structures which may represent a key link to damage sensitivity associated with hypoxia.
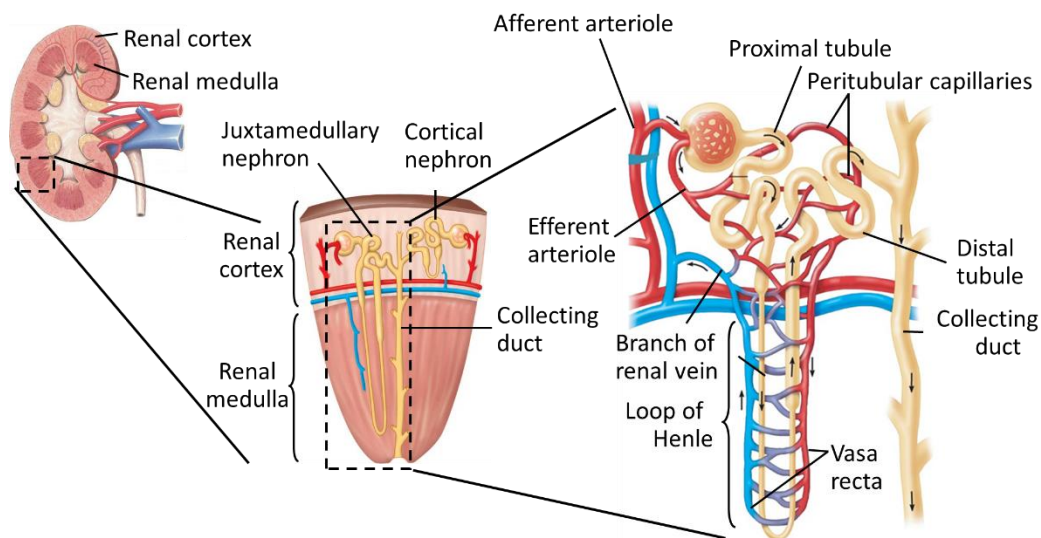
Figure 1.2: Diagrams showing the gross, macro- and micro-structures of the kidneys. *The kidney is composed of different structural units which have essential functions in the reabsorption of nutrients and excretion of waste. At the macro-scale, the existence of two key parts, which are reported to be most susceptible to RCM-AKI, are the renal cortex which surrounds 'pyramid-like' structures termed the medulla. Closer analysis of these structures show that both the medulla and the cortex support different portions of the nephron which is highly vascularised, to promote the passage of nutrients and water. The medullary tissue*

contains the proximal and distal tubules of the nephron while the cortex contains the Loop of Henle and collecting ducts. Images adapted from Pearson Education, Inc. Copyright 2008.

One theory behind the protective nature of IV saline administration relates to its influence on neurohormonal signalling which would help overcome RCM-induced medullary hypoxia. The increase in blood volume after the administration of fluids may lead to suppression of antidiuretic hormone (ADH) and increase the synthesis of vasodilatory prostaglandins leading to improved blood flow and oxygen delivery resulting in attenuation of RCM-induced renal damage (Chou *et al.*, 1990). Prostaglandin E (PGE)-2 has been shown to prevent hypoxia-induced medullary damage by inhibiting oxygen consumption. Li *et al.*, (2014) compared patient response up to 48 h post-exposure to a non-ionic, low osmolar RCM and showed that CIN development was more likely to occur in the control patient group when compared to the patient group pre-treated with PGE prior to the administration of RCM, however, the benefit associated with PGE treatment was not paired with a decrease in blood pressure. A second theory is that RCM exposure directly leads to chemical cytotoxicity. Reduced damage as a result of hydration, or blood 'volume expansion', may therefore be related to enhanced safety as a result of the dilution factor generated within the blood leading to reduced chemical, viscosity or osmolality-based toxicity (Weisbord and Palevsky, 2008).

The rate and volume of fluid replacement is likely to effect the safety and efficacy of hydration as prophylactic protection against RCM-AKI or CIN. The ESUR committee recommended IV administration of saline at a rate of $1\text{-}1.5$ mL^{-1} kg^{-1} h^{-1} for at least 6 h before and after the administration of RCM. A more rapid process, suited for outpatients, involves administration of sodium bicarbonate 3 mL^{-1} kg^{-1} h^{-1} for 1 h prior to RCM exposure and for 6 h after (Stacul *et al.*, 2011). In order to avoid under-hydration or over-hydration, which could induce secondary complications such as acute pulmonary oedema, the administration of fluid should be considered on an individual basis. The left ventricular end-diastolic pressure (LVEDP) is commonly used for monitoring the risk of heart failure development. The application of this method during protection against RCM-AKI in potentially 'at-risk' individuals saw a significant reduction in complications when patients were administered saline following LVEDP-guided method (6.7 %) in comparison to the control group who were administered with saline using standardised clinical conditions (16.3 %). However, it is also important to consider that termination of saline administration occurred in 3 patients per treatment group as a result of signs of pulmonary complications (Brar *et al.*, 2014). Although a benefit of more controlled fluid administration was observed, this prophylactic measure is not sufficient enough to completely eliminate the risk of further complications.

1.3.2   Pharmacological intervention for the prevention of RCM-AKI and CIN

Pharmacological intervention is commonly believed and reported to offer protection to 'at-risk' individuals. *N*-acetylcysteine (NAC) is an antioxidant which promotes glutathione synthesis (Whillier *et al.*, 2009), ROS scavenging (Ates *et al.*, 2008) and vasodilation (Han *et al.*, 2009). A key link which describes CIN predisposition within susceptible patient groups is vascular dysfunction, such as the presence of underlying vasoconstriction within the diabetic patient (Caiazza *et al.*, 2014). The vasodilatory effect of NAC may therefore be beneficial in the prevention of RCM-AKI and CIN by relaxing blood vessels, preventing renal ischaemia and preserving normal eGFR (Safirstein *et al.*, 2000). In addition to this, there is evidence to suggest that RCM-AKI pathology is linked to the generation of ROS and cell death via apoptosis, as described previously (Section 1.1.2). It may be proposed that increased glutathione synthesis and ROS scavenging through the administration of NAC has the potential to prevent damage. *In vitro* experiments performed with a focus on pre-treatment with NAC or NAC amide reported a reduction in ROS and reduced expression of apoptotic proteins associated with RCM-cell death (Gong *et al.*, 2010; Yang *et al.*, 2014).

In the clinical setting NAC dosage to 'at-risk' patients before and after RCM administration, along with typical clinical IV saline interventions, lead to the detection of a significant reduction in RCM-associated increase in sCr in comparison to control groups (Tepel *et al.*, 2000). Similar results were obtained in a later study by Briguori *et al.* (2002), however, the benefit of NAC was found to be dependent on the dosage of RCM and its protective effect was found to diminish after patient exposure to high volumes (> 140 mL) and a similar degree of renal deterioration occurred in both NAC and control groups. Other randomised controlled trials have shown contrasting results, where a link between NAC treatment and avoidance of renal damage, predominantly determined through the measurement of sCr, was not observed (Kwok *et al.*, 2013). A meta-analysis of 16 clinical trials performed by Kshirsagar *et al.* (2004) tested the efficacy of NAC in the prevention of CIN to show that a clear consensus could not be reached due to inter-study variability. This meant that the ESUR were unable to support this pharmacological intervention as an effective prophylactic measure against RCM-AKI and CIN (Stacul *et al.*, 2011). Therefore, there remains to be a requirement for the development of more reliable preventative measures to protect vulnerable patients.

1.4 Potential application for lipid-based delivery systems for the prevention of RCM-associated toxicity

Lipid or polymeric-based delivery systems have been a key focus in research looking to prevent unwanted side-effects of drugs, particularly in relation to non-targeted and widespread

toxicity as a result of chemotherapy during cancer treatment. Currently there is approximately 14 clinically approved liposome-based products, one of which is Caelyx®/ Doxil®, which was developed to deliver the chemotherapeutic doxorubicin. The administration of free doxorubicin in the treatment of cancer can have severe toxicity risks for patients, such as life-threatening cardiotoxicity (Von Hoff *et al.*, 1979), while entrapping the drug within polyethylene gylcol (PEG) coated liposomes has been shown to reduce cardiotoxicity through alteration of the drugs typical pharmacokinetic profile (Ansari *et al.*, 2017) and reduced exposure of free-doxorubicin to cardiocytes which can be attributed to liposome stability and minimal drug leakage (Gabizon and Martin, 1997). Despite the observation of secondary side-effects, as a result of the subcutaneous accumulation of PEGylated liposomes containing doxorubicin (Jacobi *et al.*, 2005), phase III clinical trials have found that the benefits of Caelyx administration include improved survival rates and reduced adverse reactions such as cardiotoxicity, alopecia, nausea, vomiting and neutropenia (O'Brien *et al.*, 2004). In addition to this, hypersensitive reactions to platinum are a common severe reaction observed in patients who require additional carboplatin treatment due to cancer reoccurrence, while co-treatment with Caelyx has been observed to circumvent unwanted hypersensitivity (Alberts *et al.*, 2008). The scope of the research described in this thesis is based on this evidence which highlights a reduction in patient renal and cardiovascular complications, as well as reduced immune sensitivity, when administering liposomal-based chemotherapy in comparison to free-drug administration. This theory may therefore be translatable to reducing side effects upon administration of RCM in a lipid-based delivery system.

The primary goals behind the development of a safe and effective RCM should be focused on obtaining high efficacy where the RCM should have a strong propensity to attenuate X-rays, leading to a high contrast in relation to surrounding tissues. The second most important point is that entrapped RCM has reduced adverse reactions in comparison to free RCM. This is particularly important in patients undergoing investigative medical procedures for certain conditions which should not be exacerbated or further complicated upon entering the hospital environment. Different variations of lipid delivery systems exist which contain similarities and differences.

1.4.1 Liposomes

Lipids constitute a group of molecules including fatty acyls, sterol lipids and phospholipids which have a variety functions such as providing support and structure to cell membranes. By taking advantage of the natural properties of these lipids, it is possible to create self-assembling vesicles which have the potential to encapsulate and deliver a number of agents useful in

human medicine, such as drugs and RCM for bio-imaging purposes. The discovery that the hydration of amphipathic lipids using an aqueous solution results in the formation of multilamellar vesicles (MLVs) was first described by Bangham and Horne (1964). Initial research focused on the application of these phospholipid-based vesicles, termed liposomes, as models to study the interaction and diffusion of molecules across similarly structured biological plasma membranes that make up the outer structure of all cells (Sessa and Weissmann, 1968). The idea that lipid vesicles could be used as carriers of drugs as a novel way to treat disease was first proposed by Gregoriadis and Ryman (1971). It was shown that the entrapment of enzymes and drugs within liposomes offered a number of advantages for the treatment of lysosomal storage diseases. Soon after, the application of liposomes as drug delivery systems in a range of important diseases, such as cancer and fungal infections, were described (Gregoriadis, 1973). Current investigation for the application of lipid particles in the clinical environment involve gene delivery (Vitor *et al.*, 2013), drug and vaccine delivery (Gregoriadis and Perrie, 2010), multimodal bio-imaging (Zheng *et al.*, 2015) and improvement of drug bioavailability (Gawrys *et al.*, 2014).

Liposomes are comprised of amphiphilic lipid molecules, such as phospholipids, which form a bilayer structure where the hydrophilic phosphate groups become positioned towards the outer aqueous environment and the hydrophobic fatty acid chains remain hidden within the bilayer interior which in turn creates an aqueous core. The molecular weight of the drug has been shown to influence encapsulation efficiency, specifically in the instance of poorly soluble drugs (Ali *et al.*, 2010). Poorly soluble, lipophilic drugs have a distinct method of entrapment dependent on the drugs solubilisation within the lipid bilayer in contrast to the entrapment of hydrophilic drugs within the aqueous core (Figure 1.3). Solubility was found to have a greater influencing factor on encapsulation efficiency (EE) when compared to other parameters, including MW. In comparison, the predominant limiting factors for the entrapment of water soluble drugs is related to the spatial volume available within the vesicle, the hydrophilicity of the drug, as well as the lipid concentration used within the formulation (Torchilin and Weissig, 1990). This means that the EE of water soluble drugs is commonly limited to ~30 % of the total amount of lipid (Akbarzadeh *et al*., 2013). Similar to the structure and function of cholesterol within mammalian cell membranes, the addition of cholesterol to lipid-based formulations can provide structure and support (Krause and Regen, 2014).
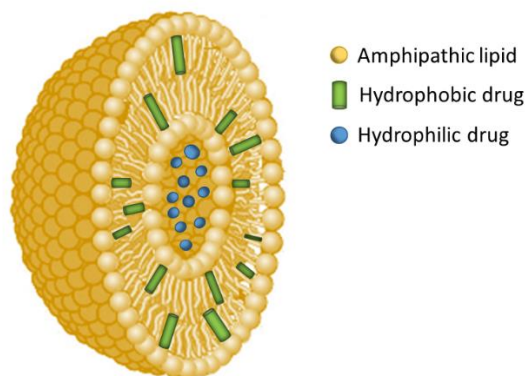
Figure 1.3: Structure and drug distribution within liposomes. *Common arrangement of amphipathic phospholipids (yellow) into a bilayer structure after self-assembly in aqueous solution. Hydrophobic (green) drugs become distributed throughout the lipid bilayer while hydrophilic (blue) drugs are solubilised in the aqueous phase meaning they become entrapped within the aqueous core of the vesicle. Image adapted from: Reema Zeineldin Research Liposome;* http://www.reemazeineldin.com/Liposome.html *last accessed: 27th November 2018.*

A number of studies have reported the use of liposomes as delivery vectors for RCM which have been prepared using a variety of different materials and methods in order to optimise their properties (Table 1.4). The most common liposomal formulation used throughout the literature is based on DPPC/ chol/ DSPE-MPEG$_{2000}$ (55: 40: 5), while the most common method of synthesis is the Thin Film Method (TFM) followed by extrusion which enables controlled and homogeneous particle sizes of around 100 nm. Although the TFM allows for the production of a homogenous particle suspension, it is very time consuming and involves many steps which are not compatible with industrial-scale manufacturing. Therefore, the identification of a method which may be more practical during large-scale manufacturing is essential for the development of a product suitable for clinical use. A variety of different RCM in both typical and concentrated forms has led to reporting of a range of EE, the majority of which is within the reported range of ~30 % for hydrophilic drugs (Akbarzadeh *et al*., 2013).

Table 1.4: Formulation, methodologies and characteristics of liposomes prepared to encapsulate RCM.

Liposome Components	Contrast Media/ Iodine Conc.	Method	Size (d.nm)	EE	Reference
DOPC/ chol/ DPPG/ triolein (36: 53: 12: 6)	Iohexol (350 mg I mL^{-1})	Double emulsion method	4000	30 %	Wei *et al.* (2005)
DPPC/ chol/ DSPE-MPEG$_{2000}$ (55: 40: 5)	Iohexol (300 mg I mL^{-1})	TFM and extrusion	70-85	Iodine/ lipid weight ratio 1: 1.8	Zheng *et al.* (2007)
	Concentrated Iodixanol (118.6 mg I mL^{-1})	TFM and extrusion	113 ± 1	83-105 mg I mL^{-1} (17-22 %)	Mukundan *et al.*, (2006)
	Iopamidol (65 ± 5 mg I mL^{-1})	TFM and extrusion	113	65 mg I mL^{-1}	Samei *et al.*, (2009)
	Iohexol (350 mg I mL^{-1})	TFM and extrusion	93 ± 0.1	88 mg I mL^{-1} (25 %)	Burke *et al.* (2007)
	Concentrated iodixanol (650mg mg I mL^{-1})	TFM and extrusion	102 ± 11	165 mg I mL^{-1} (100 %)	Karathanasis *et al.* (2009a)
	Concentrated iodixanol (650 mg I mL^{-1})	TFM and extrusion	96 ± 8	155 mg I mL^{-1} (100 %)	Karathanasis *et al.* (2009b)
	Concentrated iodixanol (550 mg I mL^{-1})	TFM and extrusion	102 ± 12	110 mg I mL^{-1}	Karathanasis *et al.* (2008)
DPPC/ chol/ DSPE-PEG$_{2000}$-COOH (3: 1: 0.3)	100mM MES-IOX (2:1 or 8:1 phospholipid/ IOX)	TFM and extrusion	149 ± 0.7	30-38 mg I mL^{-1} (18-19 %)	Danila *et al.* (2009)

1.4.2   Niosomes

Since the development of liposomes, a number of subfamilies of lipid-based vesicles have been described which offer advantages under certain conditions. Niosomes are defined as non-ionic surfactant vesicles (NISVs or NIVs) and were developed as a way to improve the stability of vesicles by replacing the main structural phospholipids of liposomes with a non-ionic synthetic material less susceptible to degradation (Baillie *et al.*, 1985; Handjani-Vila *et al.*, 1979). Phospholipid degradation readily occurs through hydrolysis of ester linkages which constitute the bond between the glycerol backbone and alkene groups (Grit *et al.*, 1993a). The use of non-ionic surfactant in place of phospholipids reduces the chance of peroxidation which is known to occur at sites of unsaturated alkene groups present in phospholipids (Figure 1.4; Konings, 1984).
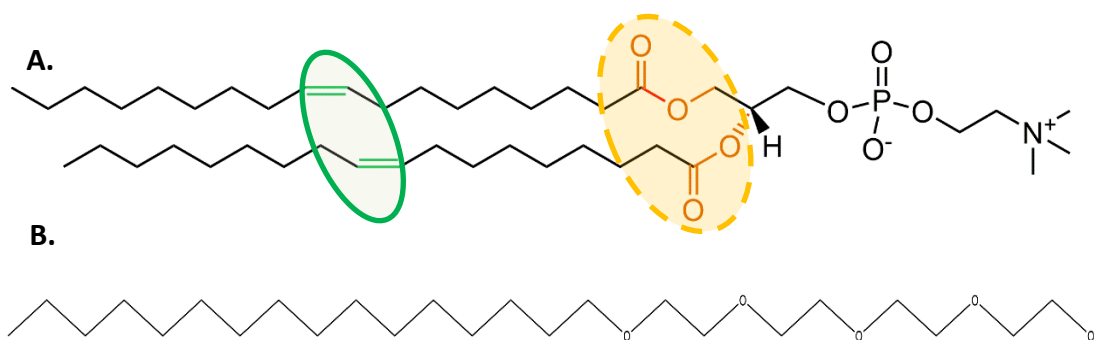
Figure 1.4: Comparison of points of degradation susceptibility of typical key chemical structural components used in the synthesis of both liposomes and niosomes. *(A) Unsaturated phospholipid, DOPC, compared to (B) the chemical structure of the non-ionic surfactant used throughout this study, tetra ethylene glycol monohexadecyl ether. In image A. the green enclosed circle highlights the presence of unsaturated alkene groups while the orange broken circle highlights the presence of ester linkages. Chemical structures were generated on ChemDraw Professional 15.0.*
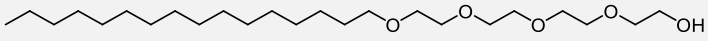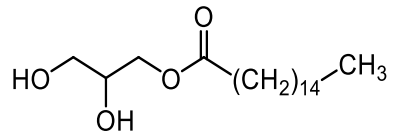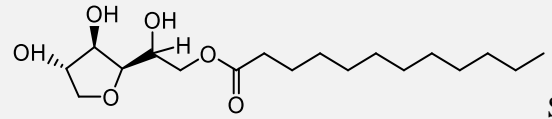
Bilosomes are an example of an additional sub-category of vesicle, termed so due to the incorporation of bile salts within the lipid bilayer. The addition of bile salts into vesicle formulations has been shown to infer a selective advantage upon administration via the oral route and enhanced stability within the acidic environment of the gastrointestinal tract (Conacher *et al.*, 2001). Another key structural difference between phospholipids used in the synthesis of liposomes and synthetic surfactants is the number of alkyl chains. Phospholipids have two alkyl chains while most surfactants used in the synthesis of NIVs tend to only have one (Figure 1.4; Uchegbu *et al.*, 1995; Mullen *et al.*, 2000; Obeid *et al.*, 2016). Despite

differences relating to structure and stability, liposomes and NIVs have been found to be similarly effective as a delivery system for sodium stibogluconate (SSG) as an anti-leishmanial treatment (Baillie *et al.*, 1986). After IV administration, both liposomal and niosomal formulations expressed similar preferential liver uptake, rather than remaining in the bloodstream as observed with free drug. As a result delivery of SSG within a lipid delivery system promoted liver-targeting for the treatment of leishmaniasis. In later studies, the *in vivo* administration of NIVs, in combination with SSG resulted in acute SSG dose-dependent toxicity in some treatment groups, as observed by a loss in body and spleen weights. Symptoms of toxicity were not linked to the NIV formulation, which was the same as that described within this thesis, or uptake within the liver (Carter *et al.*, 2003).

Similar to other vesicle- and nanoparticle-based drug delivery systems, NIV properties, such as particle size and surface chemistry largely dictate how they will behave *in vivo* (Senior, 1987). These factors influence everything from drug encapsulation, particle stability to bio-distribution, and occurrence of molecular interactions between particles and an *in vivo* system. The properties exhibited by the final product are largely controlled by the formulation and method of synthesis. An in depth review on the effects of NIV formulation and production method on characterisation, stability, toxicity and efficacy as a drug delivery system can be found elsewhere (Abdelkader *et al.*, 2014), the roles and application of common non-ionic surfactants used in the synthesis of NIVs are variable (Table 1.5).

Table 1.5: Examples of the key characteristics of lipids commonly used for the synthesis of non-ionic surfactant vesicles.

Lipid	Structure	Application	Ref
Surfactant VIII		A saturated surfactant which has strong chemical stability in comparison to unsaturated lipids. This is due to the reduced opportunity for oxidation and hydrolysis. Surfactant VIII has been successfully used as a delivery system for SSG, an anti-leishmanial drug.	Alsaadi *et al.*, (2013); Mullen *et al.*, (2000)
MPG		Has been used as the main structural component of NIVs within the context of vaccine delivery.	Obeid *et al.*, (2017)
Span (20-85)		Commonly used as a stabiliser for emulsions and suspensions and can be selected as a surfactant of choice for the synthesis of NIVs. The numerical value of Span refers to differences in the length of the carbon chain.	Taymouri and Varshosaz, (2016); Uchegbu *et al.*, (1995)
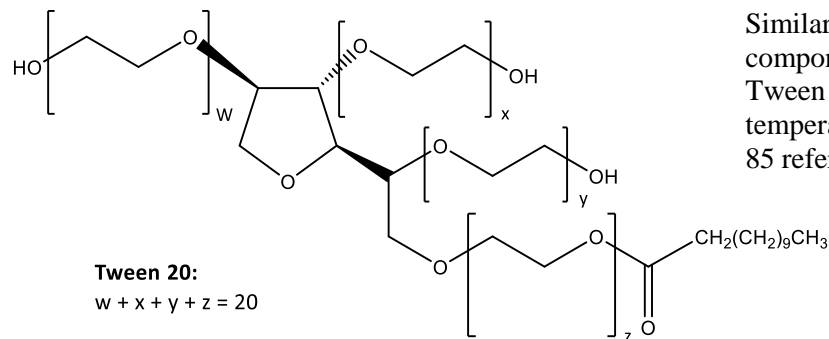
Tween (20-85)	 **Tween 20:** w + x + y + z = 20	Similar to the use of Span as a co-structural component during the synthesis of NIVs. Alone Tween exists as a liquid state at room temperature. The characterisation of Tween 20-85 refers to the number of carbon chain repeats.	Shehata, *et al.* (2016)
Cholesterol		Cholesterol is a key stabilising molecule that is found in all cell membranes. As well as offering stability in lipid bilayers, cholesterol reduces membrane fluidity due to an increased packing density of lipids and surfactants. In addition, the incorporation of cholesterol commonly leads to an increase in transition temperature in comparison to the transition temperature of the raw materials.	Nematollahi *et al.,* (2017)
DCP		Commonly added in NIV formulations to add a negative surface charge to alter specific biological interactions or promote electrochemical stability.	Alsaadi *et al.,* (2013); Mullen *et al.,* (2000)
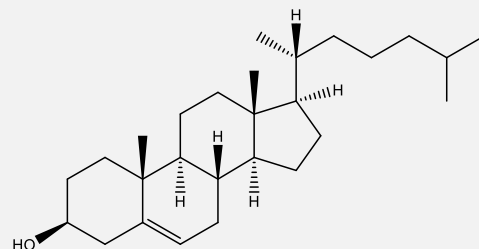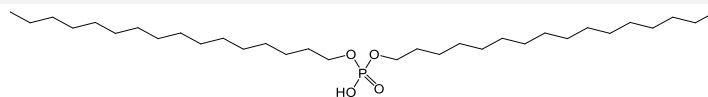
1.4.3 Potential benefits of RCM-encapsulation within NIVs

As discussed previously, successful RCM-enhanced imaging is based on the principle that the greater the electron density of a given material (i.e. iodine), the higher the x-ray attenuation and the greater resolution of the final image (Section 1.1.1). Although the entrapment of iodine-based RCM will not necessarily increase the iodine concentration, it could provide an advantage in its ability to localise the electron dense RCM within the NIV core which may reduce the effects of rapid haemodilution when administered as a free drug subsequently promoting image resolution. Usually when RCM is administered during angiographic procedures for example, the concentration of iodine becomes rapidly diluted within the blood, leading to reduced detail or timing in which RCM-enhanced imaging can be successfully achieved. By sequestering the RCM within NIVs it could be possible to retain the density of the RCM within the NIV core, as observed with IOX-liposome systems (Mukundan *et al.*, 2006). This may have the potential to allow for the detection of smaller pathological conditions such as those observed in arteriosclerosis or micro-aneurysms which may have easily been missed (Almén, 1995). One theory is that RCM-NIV entrapment could potentially lead to the development of a more efficient diagnostic procedure with a greater sensitivity to smaller pathologies as a direct result of RCM-encapsulation (Ding et al., 2018).

One application of RCM-enhanced bio-imaging is for the diagnosis and prognosis of cancer. The enhanced-permeability and retention (EPR) effect is a phenomenon which has been used to describe the advantage of entrapping anticancer therapeutics within nano-sized vesicles to promote tumour regression (Matsumura and Maeda, 1986). This passive, tumour-specific advantage occurs due to the natural way in which tumours grow in comparison to normal healthy tissue. Due to their rapid proliferative state, the tumour blood supply becomes leaky as the vessels are unable to form properly leading to reduced nanoparticle clearance at the tumour site (Maede, 2012). Upon IV administration of a chemotherapeutic liposomal-based delivery system, particles permeate through the vessel and become trapped resulting in higher concentrations of chemotherapeutics residing within the tumour. This promotes tumour cell death leading to a significant improvement in the treatment of cancer (Gabizon *et al.*, 1994). The theory that small nano-sized drug carriers become trapped in tumour sites may also offer an advantage of improved bio-imaging of tumours which may be applied at a diagnostic and prognostic level. The success of the EPR effect is ultimately influenced by the size of nanoparticles and the tumour type. Some particles as small as 5 nm are reported to be effective, while an upper size limit of ~200 nm is commonly used to promote effective residence within a tumour site (Peer et al., 2007).

The entrapment of RCM inside NIVs could reduce chemical toxicity by sequestering previously identified toxic chemical groups behind a non-toxic lipid bilayer. Entrapment could also prevent the toxic effects associated with RCM ionic strength and osmolality, similar to the prevention of chemical toxicity, interactions associated with high osmolar and ionic RCM could be avoided upon entrapment within NIVs. As mentioned, entrapment of doxorubicin within liposomes has successfully protected against unwanted side-effects such as direct chemical toxicity and immune responses (Section 1.4.1), therefore, the same theory may be applied to RCM entrapment within NIVs. In addition to this, it is likely that IOX-NIVs will express a vastly different pharmacokinetic profile in comparison to free-IOX which is typically rapidly filtered by the kidneys upon administration. NIVs prepared with a size ~200 nm are likely to avoid the narrow capillaries of the renal system, instead they are more commonly transported to other areas of the body such as the liver (Uchegbu, 1998). Transportation of lipid vesicles of this size to the liver is facilitated by particle recognition and uptake by macrophages as a result of particle opsonisation, where they then may be preferential taken up by phagocytic Kupffer cells present in the sinusoids of the liver (Koppele and Thurman, 1990; Sosale *et al.*, 2015). This theory of altering the pharmacokinetic profile of IOX could provide a key mechanism to prevent AKI and further development to CIN.

1.5 Experimental hypothesis, aim and objectives

Adverse reactions to RCM and the reasons behind them are widely debated in the literature, while current preventative measures are inadequate in protecting vulnerable patient groups, whether the adverse reaction is renal, vascular or immune orientated. Lipid-based delivery systems have already proven to reduce adverse reactions associated with chemotherapeutics. Their advantages lie in their role in decreasing vascular and wide-spread organ exposure, altering the drugs typical pharmacokinetic profile, as well as reducing immunogenicity. Previous studies have successfully prepared liposomal-RCM formulations which have shown good efficacy, however, their ability to prevent toxic interactions and reduce the risk of AKI or CIN has not been directly analysed. In addition, NIVs are known to have advantages in comparison to phospholipid-based liposomal formulations such as a reduction in cost and improved stability due to reduced susceptibility to oxidation. As far as a literature search (PubMed, Science Direct and Google Scholar) was able to determine, the work described in this thesis is the first to characterise a RCM-NIV. The formulation and method of choice have provided advantages in the delivery of anti-leishmanial drugs, antibiotics and chemotherapeutic agents. This works hypothesises that NIVs have the ability to entrap the RCM, IOX, alter the toxicity profile, and subsequently reduce the risk of adverse reactions in patients who are susceptible to RCM-associated damage. To test this theory, the objectives of this thesis are to:

1) Prepare a novel IOX-NIV formulation of desirable characteristics using methods established by the Mullen group (Alsaadi *et al.*, 2015; Alsaadi, 2011; Mullen *et al.*, 2000).

2) Determine the physical properties of an IOX-NIV system as well as its stability under specified storage conditions as advised by the FDA during the development of a novel lipid delivery system.

3) Validate an efficacious and robust analytical method for the determination of IOX entrapment within an IOX-NIV system post-synthesis and under specified storage conditions and times.

4) Characterise the toxicity profile of IOX and IOX-NIV in key cell types including those derived from the kidneys and those of vascular origin.

5) Analyse the effect of free IOX and IOX-NIV on the vasculature using an *ex vivo* model.

Chapter 2

Formulation and physical characterisation
of IOX-NIV

2 Chapter 2 – Formulation and physical characterisation of IOX-NIV

2.1 Introduction

The Food and Drug Administration (FDA; 2015) released a set of guidelines which include recommendations on the criteria to be met in order to assist those in the development of liposomes with an end goal of getting a suitable medicinal product to market. Some of the key physical parameters which should be defined include particle size (expressed as a mean size as well as the size distribution), surface characterisation and charge analysis (typically described as the zeta potential; ζP), as well as morphology and lamellarity (FDA, 2015). Often additional processing steps are required post-synthesis - this may be related to improving the purity or sterilisation of the final product. It is therefore also important that physical characteristics determined post-synthesis are not altered by any additional processing. The long-term stability of the system should be monitored as this has implications on the potential shelf-life and could be used to necessitate additional secondary processing considerations, such as the use of lyophilisation to preserve lipid vesicle integrity (Franzé *et al.*, 2018).

2.1.1 NIV formulation

There are a range of different surfactants which can be used in the synthesis of NIVs: polyoxyethylene ethers (Mullen *et al.*, 2000), alkyl polyglycerols (Handjani-Vila *et al.*, 1979), Span 60 (Uchegbu *et al.*, 1995) and monopalmitin glycerol (MPG; Obeid *et al.*, 2016). Many of these non-ionic surfactants offer advantages over phospholipid components, not only in relation to chemical stability and low cellular toxicity, but also because they are commercially available at high purity and at low cost (Brewer and Alexander, 1992). The effect of the use of polyoxyethylene ether non-ionic surfactants with increasing alkyl chain lengths has been well characterised in the context of developing SSG-NIVs for the treatment of Visceral leishmaniasis, a potentially fatal parasitic disease which affects organs including the liver, spleen and bone marrow (Mullen *et al.*, 2000). The benefits of SSG-NIV residence within the liver in the treatment of this condition were mentioned previously (Section 1.4.2). As well as the chemical structure of surfactant having an effect on NIV physical size, the hydrating drug concentration and volume, surfactant concentration and overall lipid composition, homogenisation parameters and temperature were all shown to influence average particle size. Although Mullen *et al.* (2000) focuses on the impact of altering process parameters on NIV size, it is likely that they would also affect other parameters such as drug loading.

The mol. % of cholesterol used in the synthesis of SSG-NIV has been shown to significantly influence physical size measurements of drug loaded NIVs (Mullen *et al.*, 2000). An increase in average size was observed when decreasing the proportion of cholesterol from 3: 3: 1 to 3:

2: 1 (Surfactant VIII/ cholesterol/ dicetyl phosphate; DCP) which correlated to a subsequent decrease in vesicle stability. The inclusion of cholesterol within the lipid bilayers has been prevalent right from the beginning of liposomal research. As with the role of cholesterol in offering stability to cell plasma membranes, cholesterol can be used to improve the stability of lipid bilayers used as drug delivery systems. It has long been known that cholesterol can infer stabilisation through condensation of 'fluid-like' phospholipids. When maintained at a temperature above the transition temperature, phospholipids change from having a well-defined solid-gel structure, to one where the hydrocarbon chains are in a disordered configuration and are more fluid-like. This dramatically increases membrane permeability which may impact potentially important feature of NIVs such as drug entrapment and retention. When a sufficient amount of cholesterol is incorporated within a phospholipid bilayer the hydrocarbon chains become more ordered and compact together exhibiting less mobility and a more stable structure. There are a number of different theories which have been developed to describe the specific interactions behind this process (Krause and Regen, 2014).The cholesterol composition within cellular plasma membranes has been found to vary depending on species and cell type, however it is known to exist at levels between 30 and 40 % of the total amount of lipid in the cells of vertebrates (van Meer, 1989). It is not then surprising that the stability of lipid vesicles may also be maximised through the incorporation of similar proportions of cholesterol. Kirby *et al.* (1980) had shown that the incorporation of 29-50 % cholesterol lead to increased stability *in vitro* and *in vivo* compared to those without. A formulation incorporating 50 % cholesterol was observed to have the greatest benefit. In addition to cholesterol, the incorporation of a negative charge led to faster clearance after IV injection in comparison to both neutral and positively charged vesicles.

2.1.2 Synthesis of NIVs

Methods of NIV synthesis are shared with those utilised for the synthesis of liposomes and can be selected based on the final desired characteristics of the delivery system to be produced. The classic thin film method (TFM) describes the formation of a lipid film on a surface upon evaporation of an organic solvent used to dissolve the lipid mixture. Subsequent hydration using aqueous solution and agitation of the film results in the spontaneous formation of heterogeneous multi-lamellar vesicles (Baillie *et al.*, 1985). Baillie's experiments make a comparison between the TFM and the ether injection method for the synthesis of NIVs. The ether (or alcohol) injection method is based on the injection of amphipathic lipids into an aqueous solution which results in the spontaneous formation of small unilamellar vesicles. The ether method requires heating the mixture to a temperature above the boiling point of the ether leading to its evaporation and vesicle formation. It was shown that the ether injection method

is capable of increasing the encapsulation efficiency of a hydrophilic dye within the core of NIVs in comparison to the TFM.

More novel methods of synthesis include the use of microfluidics whereby lipids dissolved in solvent are rapidly mixed with an aqueous solution leading to reproducible batch production of vesicles. Vesicle physical properties can be easily manipulated upon altering parameters such as the flow rate of each component (Walsh *et al.*, 2004). The development of bench-top microfluidic systems could enable the generation of a product which may be personalised towards the treatment of specific diseases tailored to the requirement of specific patients. Due to the flexibility of the process, vesicles can be easily manipulated to incorporate different drugs or generate different sizes through the control of mixing parameters in a way where they may be administered in a point-of-care setting (van Swaay and deMello, 2013).

One-limiting factor in the wide-spread availability of vesicle delivery systems within the clinical setting is the requirement for a continuous or large scale manufacturing process. Current research is working on developing the process of microfluidics into a system which can be up-scaled and offer a continuous manufacturing system which has the capability to purify, concentrate and characterise vesicles in a one step process (Vladisavljević *et al.*, 2013; Carugo *et al.*, 2016). Homogenisation has been previously identified as a reproducible method for manufacturing up-scaled NIV systems (Alsaadi, 2011). Homogenisation offers the benefit of being a simple process that generates homogeneous vesicle dispersions which do not require additional down-sizing stages. This is in contrast to additional down-sizing after the synthesis of MLVs using the traditional TFM. The requirement for subsequent down-sizing, using extrusion or sonication after synthesis using the TFM offers an advantage of improving homogeneity, however, this can come at the cost of other essential parameters such as stability and encapsulation efficiency (Solanki *et al.*, 2013; Gryparis *et al.*, 2007). In comparison, homogenisation can lead to the immediate synthesis of uniform vesicles, the properties of which can be altered and optimised by changing the homogenisation time and speed meaning that additional down-sizing techniques are not required (Mullen *et al.*, 2000). It would be fair to suggest that the resultant vesicle polydispersity achieved through the use of homogenisation may be broader than that observed through the use of microfluidic systems. Despite this, evidence suggests that a PDI, much less than the acceptable level of 0.3 can be obtained, highlighting the generation of a homogenous size distribution which is important for the IV administration of lipid delivery systems. Homogenisation also offers an advantage of shorter processing times which do not require additional steps, i.e. for the removal of organic solvents,

as required during current Microfluidic manufacturing, the requirement of which has the potential to compromise physicochemical stability of vesicles or the active excipients.

2.1.3 Characterisation of NIV size distribution

Determination of NIV size is an important feature due to the fact that vesicle size is a controlling factor of drug encapsulation within the system (Torchilin and Weissig, 1990). In addition, the size must be well defined due to factors of clinical importance. The ideal size required for an IV drug delivery is often reported to be between 100 and 200 nm (Petros and DeSimone, 2010). Particles > 200 nm are more prone to uptake by the mononuclear phagocytic system (MPS), whereby protein interaction with large particles and subsequent innate immune responses facilitate the clearance of potentially harmful molecules from the circulation (Harashima *et al.,* 1994). Size has also been found to hinder protective properties exhibited by liposomal vesicles as a result of the addition of PEG to the surface. As particle size supersedes ~200 nm, the 'stealth' properties exhibited by PEG coated vesicles can be lost (Awasthi *et al.*, 2003). Although MPS clearance could be recognised as a negative consequence for the delivery of drugs within the body, it has actually been exploited for the development of anti-leishmanial treatment (Carter *et al.*, 1999). This method of passive immune cell 'targeting' is so successful because it is the host's macrophages which harbour the leishmanial parasite. Therefore the uptake of anti-leishmanial drugs can be enhanced upon encapsulation within large vesicles in comparison to the administration of free drug on its own. Size is also an important factor in the development of nano- and micro-particle-based vaccines for example, relating to their ability to induce an immune response (Gutierro *et al.,* 2002). Small particles, < 5.5 nm in diameter, have a half-life of mere minutes as they become rapidly filtered through the kidneys (Choi *et al.*, 2007).

There is much debate regarding size-mediated responses to drug delivery systems and how it may alter bio-distribution *in vivo*. The great variation between results reported in the literature can be attributed to varying formulations as well as the numerous influencing parameters which affect the way in which particles behave. A comparison of the physical characteristics of some commercially available liposomal formulations highlights the variation depending on the medical application and route of administration (Table 2.1). Liposomal formulations suitable for IV administration often report a size < 250 nm, in comparison, larger μm sized vesicles are usually administered directly to the CNS or subcutaneously, depending on the application. Based on this, this research aims to prepare IOX-NIVs with an average size between 100 and 200 nm in the development of a stable, long-circulating, bio-imaging system which can offer protection to the kidneys upon encapsulation of potentially nephrotoxic RCM.

Table 2.1: Outline of clinically available liposome formulations, characteristics and advantages.

Liposome	API	Treatment	Administration	Size	Formulation	Advantages
DaunoXome®	Daunorubicin	Kaposi's sarcoma	IV	45 nm	DSPC/ chol. (2: 1)	Avoidance of the MPS leading to prolonged circulation (Forssen and Ross, 1994)
Onivyde™	Irinotecan	Metastatic adenocarcinoma of the pancreas	IV	~110 nm	DSPC/ chol/ MPEG-2000-DSPE (3:2:0.015)	Prolonged circulation, higher drug loading and retention (Hong *et al.,* 2016)
Inflexal® V	Influenza surface protein	Influenza virus	IM/ SC	~150 nm	lecithin/ cephalin/ (DOPC/DOPE) (70: 20: 10)	Enhanced immunogenicity to viral antigens in comparison to alternative vaccines (Glück *et al.*, 1994)
Myocet®	Doxorubicin	Breast cancer	IV	150-250 nm	eggPC/ chol (55: 45)	Minimise drug exposure to normal tissues and reduced toxicity (Kanter *et al.*, 1993)
Depocyt®	Ara-C	neoplastic meningitis	Ventricular/ lumbar	3–30 µm	DOPC/ DPPG/ chol./ triolein	Improved drug delivery and exposure time within the meninges and CSF (S. Kim et al., 1993)
Exparel®	bupivacaine	local anaesthetic	SC	24–31 µm	DEPC/ DPPG/ cholesterol/ tricaprylin	Enhanced deposition and sustained release (Davidson *et al.,* 2010)

API – active pharmaceutical ingredient; IV – intravenous; IM – intramuscular; SC – subcutaneous; DSPC - 1,2-distearoyl-sn-glycero-3-phosphocholine; Chol – cholesterol; MPEG-2000-DSPE– methoxy-(polyethylene glycol)-2000-distearoylphosphatidyl ethanolamine.

These physicochemical properties are known to control factors such as particle clearance (Harashima *et al.*, 1994), toxicity (Lai, 2015), biodistribution (Oussoren *et al.*, 1997) and pharmacokinetics (Romberg *et al.*, 2007). Dynamic light scattering (DLS) is a technique often used to determine the size of particles within a suspension and is dependent on the theory of Brownian motion. Brownian motion describes the random movement of particles within a suspension as a result of particle interactions with water molecules of the suspending media. Using DLS, larger particles move more slowly which means the light reflected by them occurs over a longer time scale when compared to particles of smaller dimensions (Figure 2.1). The light reflected from moving particles is converted to obtain a hydrodynamic diameter (m), *d(H),* using the Stokes-Einstein equation (.

Equation 2.1). Within this equation it is assumed that particles follow the same kinetic law applied to gas molecules at a specific temperature, in such a way that an increase in temperature will increase the kinetic energy of particles within a suspension. This factor is represented by the Boltzmann's constant (kg x m^2 x s^{-2} x K^{-1}), *k*, while *T* represents the absolute temperature (K). The viscosity (kg x m^{-1} x s^{-1}) of the suspending medium, *η*, also influences the measured particle size - as viscosity increases particles will diffuse through the suspension at a slower rate – hence affecting size measurements. It is also assumed that the movement of the particles is the same as that of a spherical particle which forms the basis of translational diffusion coefficient (m^2 x s^{-1}), *D*.
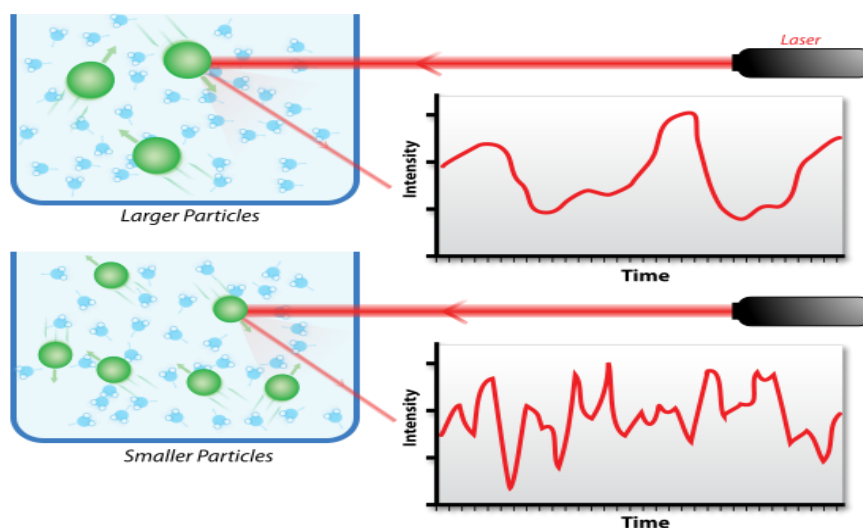
Figure 2.1: Particle size analysis using DLS. *Light scattering is influenced by the size of the particles and how they are able to diffuse through their suspending media. Image obtained from "DLS" by Mike Jones - Own work. Licensed under CC BY-SA 3.0 via Wikimedia*

Equation 2.1: Stokes-Einstein equation used to determine particle size using DLS.

$$d(H) = \frac{kT}{3\pi\eta D}$$

A number of different particle sizes are obtained upon use of the Malvern ZetaSizer which depends on the method in which they were calculated. Particle size distribution within a suspension can be based on the measurement of light intensity, number of particles, or calculated particle volume. Each of the measurements have their own advantages and disadvantages. However, the most accurate measurement is obtained from the Z-average hydrodynamic diameter and is the recommended value for quality control analysis within the pharmaceutical industry as outlined in ISO 22412. The Z-average calculation is dependent on intensity-based measurements, and therefore cannot be directly compared to results obtained using alternative size measurements including those based on volume or number as determined by DLS, in addition to results obtained from alternative size-analysis techniques.

The polydispersity index (PDI) is another important value obtained upon analysis using the Zetasizer which refers to the width of the distribution of particle sizes within a sample. The PDI ranges from 0-1, where a PDI < 0.05 is usually only observed upon analysis of standard monodispersed latex particles. A range between 0.05 and 0.08 would indicate a sample very close to having the qualities of a completely monodispersed sample, however, most commonly, measurements are between the range of 0.08 to 0.7, which is where the application of this analysis is most reliable. A PDI $\geq$ 0.7 implies that the variation in detected signalling is too great for DLS analysis and that alternative methods of size analysis may be more suited (Malvern, n.d.).

2.1.4 Characterisation of particle surface charge

Measuring the zeta potential (ζP) of vesicles within a suspension provides key details on the surface charge which may be altered in order to gain desired pharmacokinetic characteristics. Control of the surface charge is important as it can be utilised to promote stability as well as being a controlling factor as to how vesicles interact with specific cells (Miller *et al.*, 1998). The relationship between charge and stability is described by the Derjaguin, Landau, Verwey and Overbeek (DLVO) theory. This outlines the fact that stability within a suspension is dependent on the attractive and repulsive interactions between the particles and molecules in

the surrounding environment. If particles are designed to repulse each other the suspension will remain stable, however, if the strength of attracting Van der Waal forces overcome this, particles will begin to aggregate and the suspension will eventually separate into different phases (Carrion *et al.,* 1994). It is generally accepted that either a positive or negative charge of ~ 30 mV ensures the development of a stable suspension (Malvern, n.d.). DCP incorporation within a formulation is commonly used to induce a negative surface charge while the addition of cationic stearylamines can be used to induce a positive charge (Junyaprasert *et al.*, 2008). Positively charged vesicles offer specific advantages in relation to the synthesis of vesicles capable of delivering genetic material across the cell membrane for gene therapy. Negatively charged nucleic acids are attracted to the positively charged vesicle surfaces promoting entrapment as well as subsequent cellular endocytosis upon interaction with cell membranes (Felgner *et al.,* 1987; Monnard *et al.*, 1997).

The ζP can be determined through the use of phase analysis light scattering (PALS) which measures the velocity of particles within a suspension after the introduction of an electric field. The ζP reflects the charge present at the verge of the hydrodynamic diameter of the vesicle, rather than the direct surface charge of the particle itself. The hydrodynamic diameter is composed of ions which are strongly bound to the surface of the particle to the extent where the particles and ions both move as one, creating an electrical double layer around the surface of the particle. It is the conductivity between these ion boundaries and external ions within the suspending media which is referred to as the ζP (Figure 2.2).
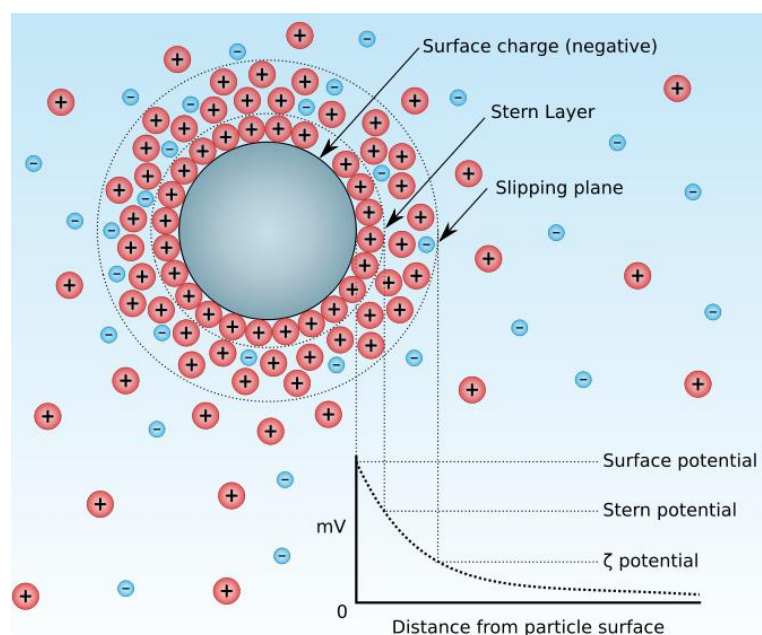
Figure 2.2: Interaction between ions within a solution and negatively charged particles expressing an electrical double layer. *The ζP refers to the conductivity between the double layer and external environment. Original work by Larr. Licensed under CC BY-SA 3.0 via Wikimedia Commons (Image taken from: https://en.wikipedia.org/wiki/Zeta_potential; Date last accessed: 29th September 2018).*

Physical characterisation of vesicle size and charge is important for the initial definition of NIV parameters. In addition to this, the measurement of size and charge over time is closely related to the chemical stability of the vesicles, whereby alterations in chemical stability, i.e. the degradation of a specific lipid component, has the potential to alter physical characteristics due to their dependence on the underlying chemistry (Danila *et al.*, 2009; Taymouri and Varshosaz, 2016). PALS analysis is based on a number of different assumptions relating to the properties of particles within a suspension. The effect of storage time and temperature on the quantification of drug components will be described in future experiments in order to gain more detail regarding this intertwining relationship between physical and chemical vesicle properties (Chapter 3 - Validation of HPLC detection of IOX and quantification of encapsulation efficiency and release).

2.1.5 Confirmation of particle size and morphology

As mentioned previously, DLS makes many assumptions on sample parameters, which, if these are not met, can easily interfere with final measurements. In addition, the fusion or presence of large particles in a suspension of predominantly smaller particles can significantly impact final measurements. Although filtration of solutions used throughout vesicle formation is advisable to maximise the removal of contaminants including dust or excess lipid particles,

it is not possible to completely eliminate this risk. Additional qualitative measurements can be used to provide supporting data to that obtained from DLS analysis.

Microscopic imaging can enable visualisation of nanoscale structures non-visible to the human eye. Scanning electron microscopy (SEM), transmission electron microscopy (TEM), cryo-TEM and atomic force microscopy (AFM) are all common methods for visualisation of nanostructures which cannot be observed using light or confocal microscopy. Cryo-TEM is advantageous due to the absence of stages, such as fixation and staining, which may disrupt vesicle structures. Instead, rapid cooling and maintenance of sample temperatures to that of liquid nitrogen, enables direct, unaltered imaging of nanostructures at a high resolution. There are some limitations in relation to the sizes of structures which may be visualised. Those >500 nm lead to over-scattering electrons and poor resolution while structures <5 nm, such as the lipid bilayer thickness of a vesicle, may not be visible using this technique (Almgren *et al.,* 2000). AFM creates an image of surfaces and is most easily performed under dry conditions. A 3D µm-sized surface map is obtained due to the detection of a laser signal as it is reflected from a cantilever arm with a µm sized tip (Figure 2.3). The cantilever taps the surface creating an image based on deviations in height which change depending on where the cantilever tip makes contact with the surface and subsequently where the light signal is detected (Figure 2.4). These deviations may be reported based on the height of the surface, as mentioned, while more complex measurements can provide information based on sample stiffness and elasticity, for example.
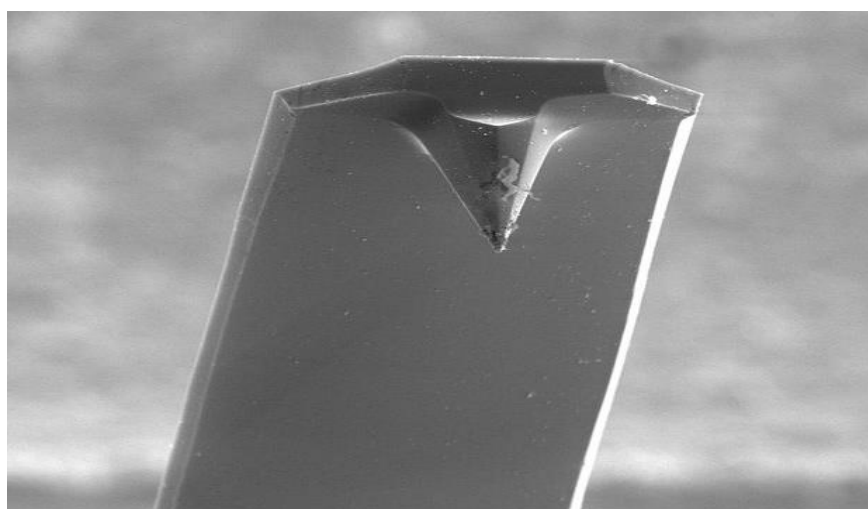
Figure 2.3: SEM image of an AFM cantilever (x1000). Original image from Materialscientist. *Licensed under CC BY-SA 3.0 via Wikimedia Commons (Image taken from: https://en.wikipedia.org/wiki/Atomic_force_microscopy; Date last accessed: 29th September 2018).*
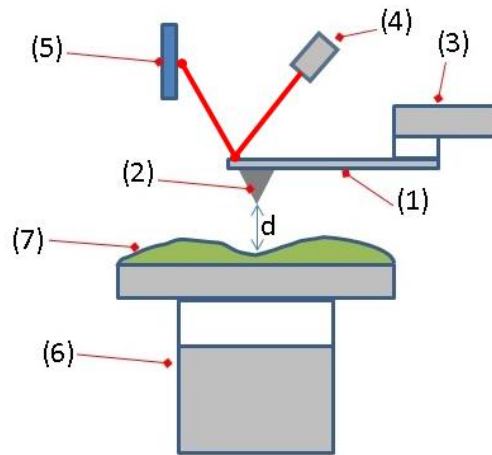
Figure 2.4: Typical set-up of an AFM. *The cantilever arm (1) has a µm-sized tip (2) attached and is connected to a support system (3) through a piezoelectric charge which allows the cantilever to oscillate during imaging. A laser diode (4) is aligned with the tip of the cantilever and the light is reflected into the path of a detector (5). As the distance, d, between the cantilever and sample stage (6) change due to artefacts present in the sample (7), the positioning of the light reflected from the cantilever is detected and transformed to produce an image. Image adapted from Tom Toyosaki. Licensed under CC 4.0 via Wikimedia Commons (Image adapted from: https://en.wikipedia.org/wiki/Atomic_force_microscopy; Date last accessed: 29ᵗʰ September 2018)*

AFM also has the power be used to determine the elastic modulus, stiffness and morphology. Having the ability to do so within live cells has contributed to knowledge of complex cellular processes and their relationship with pathological disease states. For example, the stiffness of red blood cells, as determined by the calculation of Young's modulus (i.e. the linear elasticity of a material defined by the relationship between stress and strain in a uniaxial deformation), has been observed to play a role in the pathology of a number of blood-related diseases including haemolytic anaemia (Dulińska *et al.*, 2006). The altered modulus of tumour cells has been identified as a potential biomarker for use in cancer diagnostics, prognostics and treatment, as potential connections between the metastatic profile of tumour cells have been described (Swaminathan *et al.*, 2011). The applications and potential of AFM imaging are vast and powerful. In the context of the work described for the characterisation of NIV, AFM will enable the confirmation of physical dimensions and visualisation of morphological features in conjunction with DLS.

2.2   **Chapter aims and objectives**

The aim of this chapter is to prepare an IOX-NIV is suitable for further pre-clinical and clinical testing. It is important that the system satisfies criteria in agreement with current literature and that outlined by regulatory bodies such as the FDA. This chapter has a focus on formulating an IOX-NIV system with the desired physical properties to enable IV administration leading to prolonged circulation and avoidance of IOX toxicity. In order to meet these requirements the objectives of this chapter are to:

- Prepare both empty- and IOX-NIVs using a pre-tested formulation and method of synthesis.
- Compare and contrast the physical and electrochemical properties expressed by empty- and IOX-NIVs.
- Determine any influence of processing procedures, such as ultracentrifugation and sterile filtration, on the physical properties of IOX-NIVs.
- Determine the effect of typical storage and extreme temperatures on physical and electrochemical properties of IOX-NIVs over 37 weeks.

After completion of these aims it will be decided whether this system expresses physical characteristics which promote suitability as a delivery system for RCM. Validation of processing parameters, in terms of expressing an ability to retain desired physical properties post-processing, will create an argument as to whether these techniques will be beneficial for further analysis of chemical properties, such as the accurate quantification of encapsulation efficiency. In combination with the work described here, future chemical analysis will be used to define NIV characteristics, shelf-life and recommended storage conditions, as well as using *in vitro* experiments to predict efficacy and release *in vivo*. Each of these factors must be defined in order to meet the standards required for the transition of a product from research and development to the clinical setting.

2.3 Materials and methods

2.3.1 NIV synthesis using the homogeniser

NIVs were prepared using the homogenisation method, details of which have been described elsewhere (Mullen and Carter, 1997; Alsaadi *et al.*, 2015). The non-ionic surfactant tetra-ethylene glycol mono n-hexadecyl ether (Nikkol Chemicals Co. Ltd.), the membrane stabiliser, cholesterol (Croda Chemicals Ltd.) and negatively charged DCP (Fine Chemical Products Ltd) were combined at a molar ratio of 3: 3: 1, respectively. Lipids were melted at 130 °C for 5 min before reducing the temperature to 70 °C and hydrating with preheated Omnipaque300, containing 647 mg ml^{-1} IOX, (70°C; GE Healthcare, UK) to achieve a lipid concentration of 150 mM. As a control, empty-NIVs were also prepared using the same method but exchanging IOX with filtered-PBS (pH 7.4) or H_2O as the hydrating agent. After the addition of hydrating media, the preparation was homogenised at 8000 rpm for 15 min using a Silverson L4R SU rotor and five-eighth inch tubular work head.

IOX-NIVs were prepared in 3 separate batches and aliquoted into low volume glass vials, sealed, and stored in darkness at an appropriate temperature for future stability analysis. Temperatures of 4 and 25 °C were selected as potential storage conditions typical for storage in a fridge and RT, respectively, higher temperatures of 37 and 50 °C were used to compare the potential effects of IOX-NIV storage at high to extreme temperatures. IOX-NIV and empty-NIV were subjected to additional processing steps such as ultracentrifugation prior to analysis of loading efficiency, as well as sterile filtration using 0.22 µm Millipore PES (polyethersulfone) syringe filters prior to the performance of *in vitro* and *ex vivo* experiments. IOX-NIVs were centrifuged using a T40 Beckman ultracentrifuge rotor and each tube was balanced according to weight prior to centrifugation at 36 k rpm for 1 h at 4 °C, removal of supernatant and resuspension of the pellet in to a volume of PBS equivalent to a final volume of 10 ml IOX-NIV. The effects of these processing steps on NIV physical characteristics were also determined.

2.3.2 DLS analysis of particle size distribution

Size measurements were taken immediately post-synthesis and at specified time points over a period of 37 weeks in order to determine the effect of long term storage and temperature on IOX-NIV physical characteristics. IOX-NIVs were aliquoted into 100 µl volumes and stored in constant temperature rooms at 4, 25, 37 and 50 °C. At different time points over the 37 weeks samples were removed from the controlled temperature room and suspended in 12 ml filtered PBS (pH 7.4) to obtain a final lipid concentration of 1.25 mM. Size measurements were performed using DLS in a Zetasizer Nano ZS® (Malvern) at an attenuation of either 6

or 7. Analysis was performed by adding a 500 µl volume of diluted IOX-NIV to a disposable polystyrene micro-cuvette. Triplicate measurements were recorded at 25 °C with a minimum of 11 measurement runs/ reading. The average particle size of 3 combined batches was reported as the Z-average (d.nm) based on the measured intensity of scattered light. The PDI was recorded as a measurement of sample homogeneity.

2.3.3 PALS analysis of particle surface charge using PALS

The surface charge of NIV was reported as the ζP as determined through PALS. The same equipment and sample conditions described for particle size (Section 2.3.2) were used for the measurement of ζP upon transferring the sample to a disposable folded capillary zeta cuvette. Triplicate measurements were recorded at 25 °C until a minimum particle count was reached. The minimum particle count will be influenced by the sample concentration, but defined by the ZetaSizer software. The detection of the electrophoretic mobility of individual particles within a suspension was converted to ζP by assuming Smoluchowski's model.

2.3.4 Atomic force microscopy analysis of particle size and morphology

AFM was utilised in conjunction with DLS to enable visualisation of IOX-NIV morphology. Before and after the dilution of IOX-NIVs, 5 µl of sample was added to a freshly cleaved mica surface and allowed to air-dry. Sample analysis was performed within the first hour after addition to the mica surface in order to minimise alteration of vesicle structure as a result of prolonged exposure to a dry environment. Images were obtained using the ScanAsyst method and represented by the change in peak force error. The scale bar of these images reflect the extent of cantilever deflection as it taps across the surface (i.e. as the cantilever scans a particle in comparison to an empty space, deflection will increase to a greater extent). Particle size distributions and SD were obtained from 3 separate images of IOX-NIV using the Particle Analysis function available on NanoScope Analysis software.

2.3.5 Statistical analysis

Statistical analysis such as average measurements ± SD were obtained using Microsoft Excel 2013, while more complicated statistical analysis including analysis-of-variants (ANOVA) with Tukey tests comparisons was performed using Minitab statistical software v 17. Statistical significance was assumed where $p < 0.05$.

2.4 Results

2.4.1 Comparison of the appearance and physical properties of empty- and IOX-NIV

Empty- and IOX-NIV were prepared using the formulation and method described previously (section 2.3.1). When comparing empty- and IOX-NIV, there was no significant difference in average particle size which was 192 ± 3 nm and 204 ± 24 nm, respectively, as determined using DLS (Figure 2.5A). In comparison, empty-NIVs expressed a significantly lower PDI when compared to IOX-NIV which was found to be 0.07 ± 0.01 and 0.12 ± 0.04, respectively ($p < 0.05$; **Error! Reference source not found.**B). In terms of surface charge, empty-NIVs were significantly more negative at -30 ± 1 mV, compared to an average surface charge of -25 ± 2 mV for IOX-NIVs ($p < 0.001$; Figure 2.6).
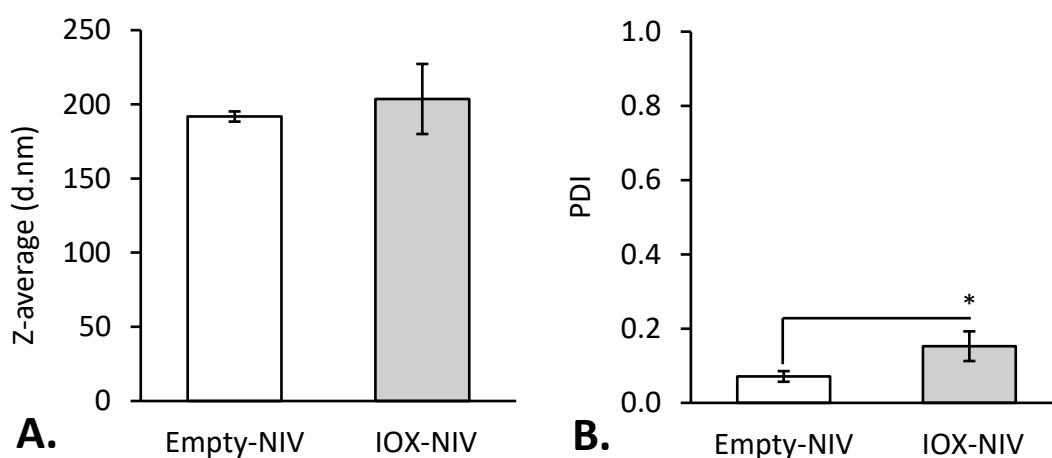
Figure 2.5: Comparison of average (A) size and (B) PDI of empty- and IOX-NIVs *(n = 3 ± SD; * p < 0.05).*
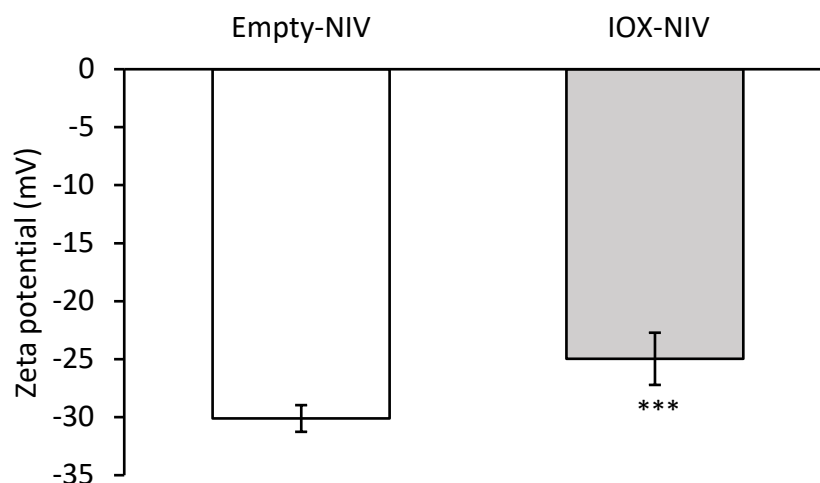
Figure 2.6: Comparison of empty- and IOX-NIV average surface charge *(n = 3; ± SD; *** p < 0.001).*

Empty-NIV prepared to encapsulate PBS had a typical opaque appearance, which can be expected during the synthesis of a suspension of vesicles. In comparison NIVs prepared by hydrating lipids in IOX expressed a relatively clear and viscous appearance (Figure 2.7). Interestingly, it was observed that when IOX-NIV was diluted in an aqueous solution, whether this was H_2O or PBS (pH 7.4), a change in colour from transparent to a similarly milky suspension occurred (Figure 2.8). In comparison, dilution of empty-NIV, prepared using H_2O or PBS resulted in a comparably diluted change in colour.
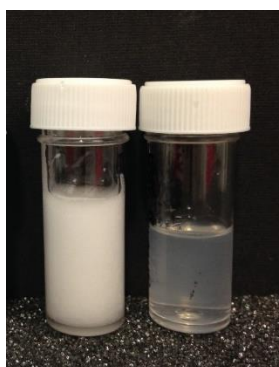
Figure 2.7: Comparison of the physical appearance of 150 mM empty-NIV (left) and IOX-NIV (right).
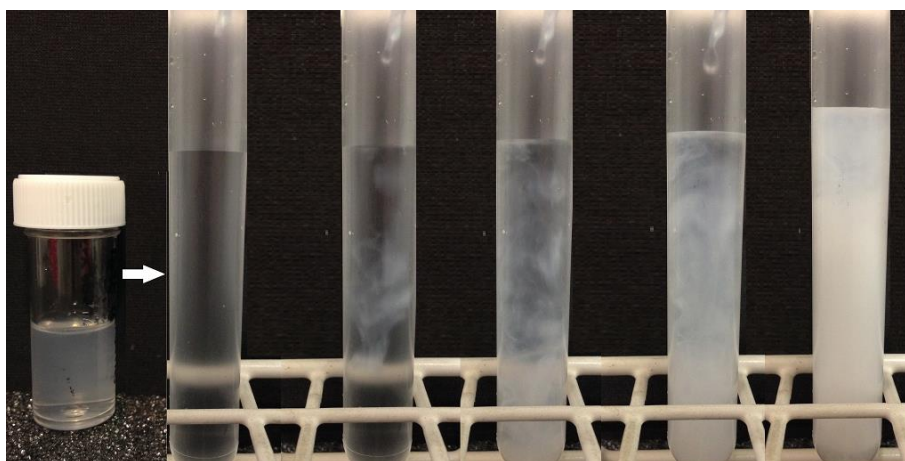
Figure 2.8: The change in IOX-NIV appearance after diluting in PBS (pH 7.4).

AFM was used to gain qualitative data relating to the presence of vesicles and their morphology in the IOX-NIV solution before and after dilution. AFM failed to detect the presence of any fully formed vesicles in the solution obtained immediately post-synthesis (Figure 2.9). In comparison, analysis of diluted IOX-NIV detected the presence of round, monodispersed vesicles with an average diameter of 288 ± 12 nm and an average NIV distribution between 187 and 534 nm as determined through AFM (Figure 2.10). 3D imaging of the IOX-NIV solution obtained immediately post-synthesis showed the presence of spikes associated with a high level of background noise (Figure 2.11). In contrast, vesicle-like structures were observed after IOX-NIV dilution, AFM imaging was also able to identify the spherical morphology expressed by these NIVs (Figure 2.12).
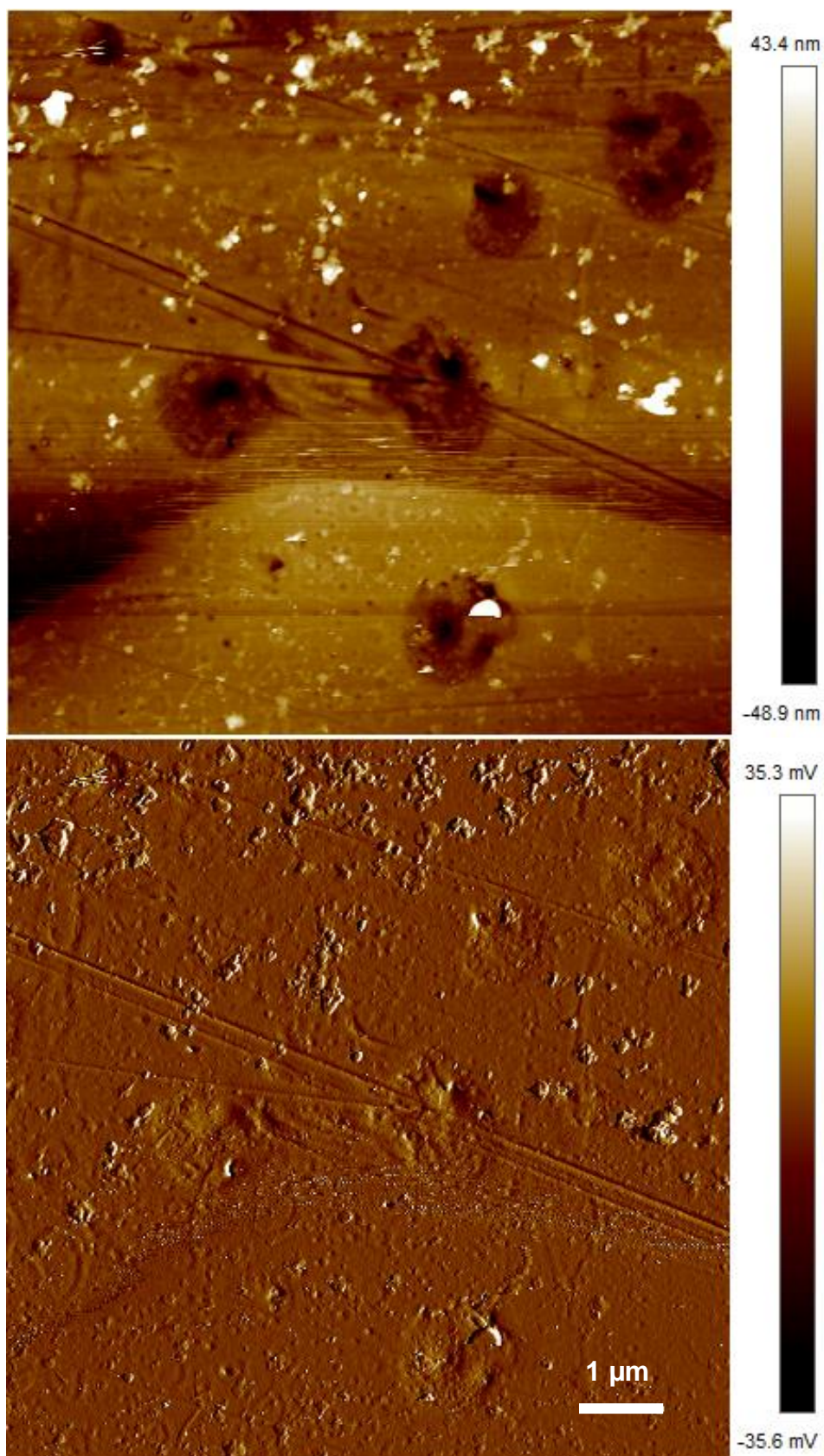
Figure 2.9: Representative height (top) and peak force error (bottom) images obtained from AFM analysis of IOX-NIV immediately post-homogenisation.
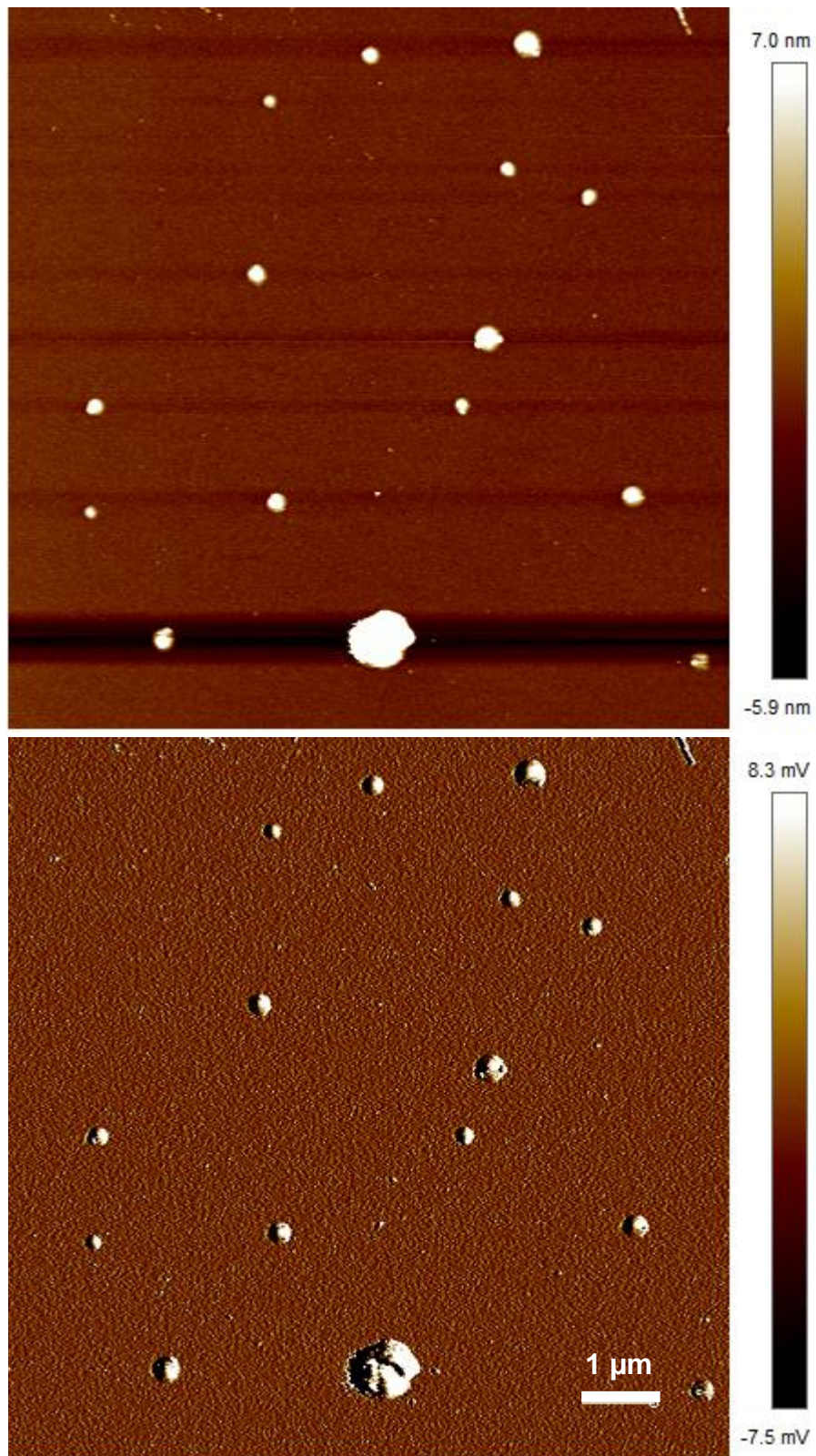
Figure 2.10: Representative height (top) and peak force error (bottom) images obtained from AFM analysis of IOX-NIV post-dilution.
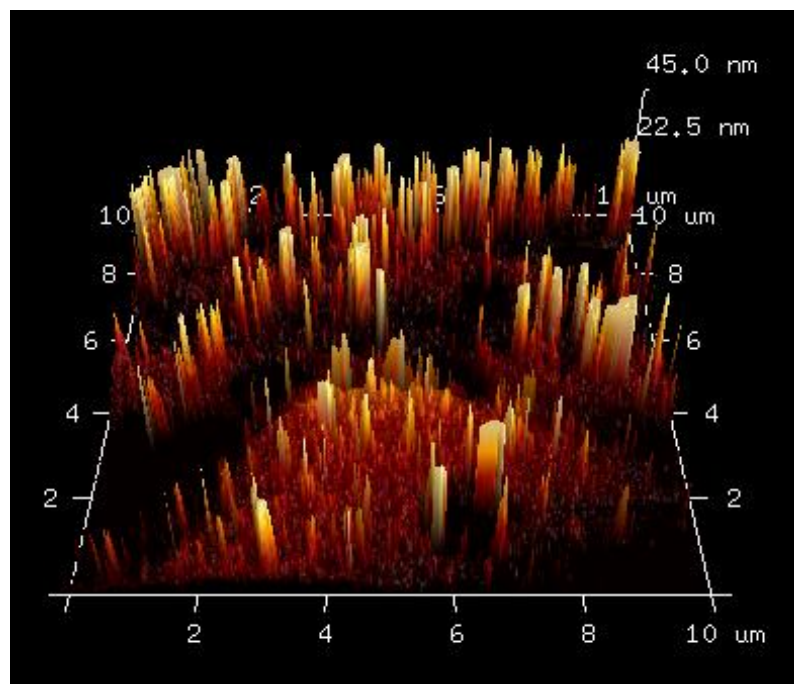
Figure 2.11: 3D representation of IOX-NIV solution immediately post-homogenisation using AFM.
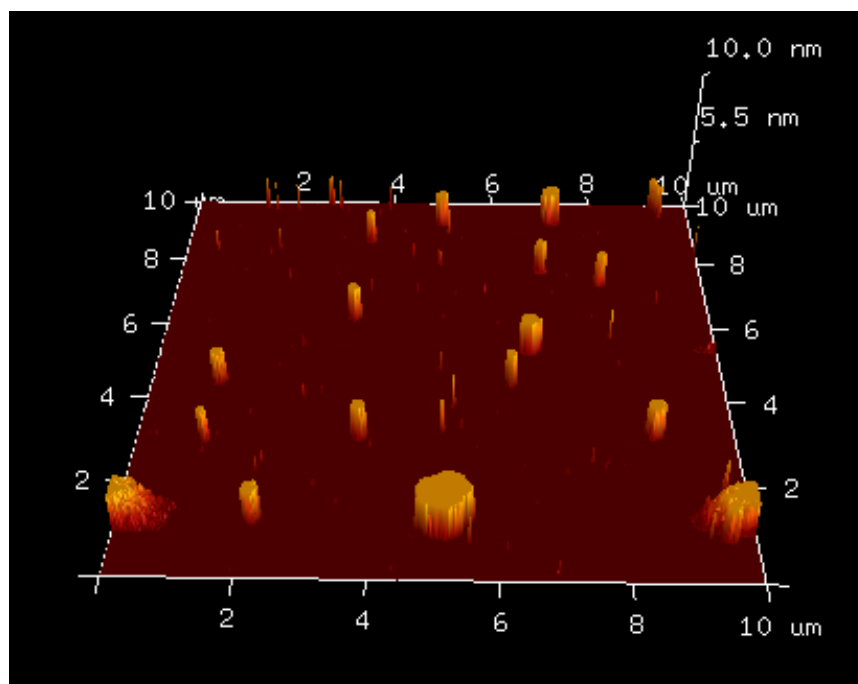
Figure 2.12: 3D representation of IOX-NIV vesicles after dilution in aqueous solution and imaging using AFM.

2.4.2 Homogenisation leads to the production of a negatively charged, monodispersed population of IOX-NIVs

Analysis of 3 separately prepared IOX-NIV suspensions which were diluted in a 10-fold volume of aqueous media lead to the detection of a monomodal, homologous particle suspension with average size distribution between 79 and 531nm (Figure 2.13). Diluted IOX-NIV expressed an average size of 204 ± 24 nm and low average PDI of 0.12 ± 0.04 and ζP of -25 ± 2 mV (Table 2.2).
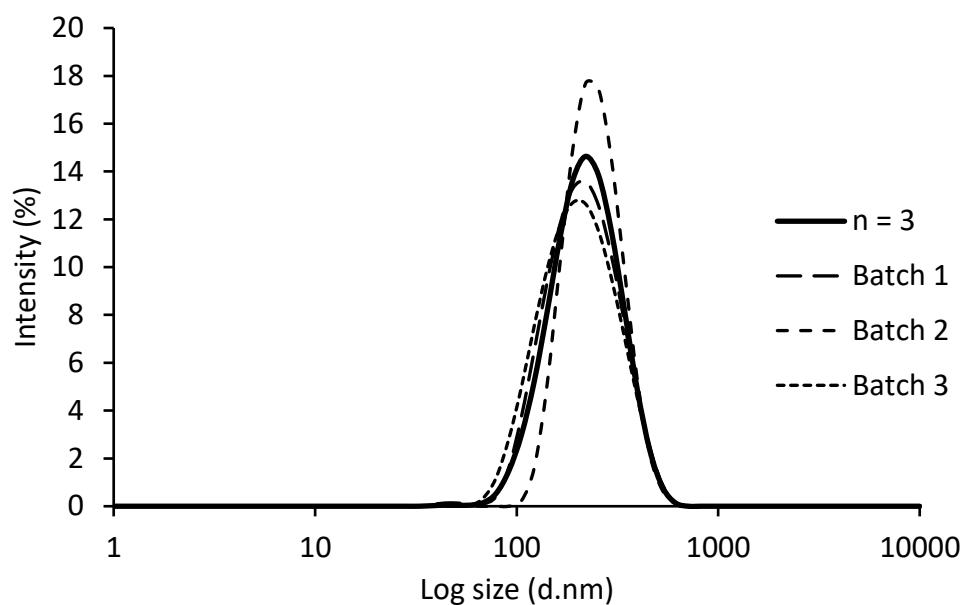
Figure 2.13: Individual and average intensity-based size distributions of 3 separately prepared batches of diluted IOX-NIV (1.5 mM total lipid) suspensions (n = 3).

Table 2.2: Average and individual size and surface charge measurements after the additional hydration of 3 individually prepared batches of IOX-NIV.

	Z-ave (d.nm)	Peak mean intensity (d.nm)				PDI	ζP (mV)
		1	**2**	**3**	**4**		
Batch 1	193	228	17	-	-	0.14	-24
Batch 2	231	255	-	-	-	0.08	-27
Batch 3	187	220	-	-	-	0.15	-25
Average	**204**	**234**	6	-	-	**0.12**	**-25**
SD	**24**	**18**	10	-	-	**0.04**	**2**

Differences between average particle size and overall particle size distribution obtained from DLS and AFM can be expected due to differences in the methods of analysis. The average size of diluted IOX-NIV obtained using DLS was lower, while the size distribution was broader, suggesting greater polydispersity, when compared to the data obtained from AFM (Table 2.3).

Table 2.3: Comparison of IOX-NIV size data obtained from DLS and AFM analysis.

Method of Analysis	*Mean size (d.nm) ± SD*	*Size distribution (d.nm)*
DLS	204 ± 24	79 – 531
AFM	288 ± 12	187– 534

2.4.3 Effect of sample processing on IOX-NIV physical and electrostatic stability

Prior to further characterisation of NIV, or for use during *in vitro* or *ex vivo* experiments, additional processing steps are required. Ultracentrifugation was used to separate IOX-NIVs from their external media containing unentrapped IOX, enabling the quantification of EE %. Sterile filtration was essential prior to the treatment of cells *in vitro*, as well as prior to *in vivo* administration. Therefore, it is vital to assess whether these processes impact NIV physical characteristics compared to the characteristics determined originally. Filtration of empty-NIVs did not lead to a significant reduction in average size, which was 192 ± 3 d.nm post-synthesis and 185 ± 40 d.nm (Figure 2.14A). The effect of ultracentrifugation on empty-NIV was not presented due to the inability to separate empty-NIV using this method. It was noted that even after ultracentrifugation empty-NIVs remained as a cloudy suspension, it could have been that empty-NIVs were not dense enough to form a pellet under the described conditions. A significant alteration in average particle size was observed after filtration of IOX-NIVs whereby size was reduced from 204 ± 24 d.nm to 157 ± 2 d.nm ($p < 0.001$), however,

ultracentrifugation did not have a negative impact on size (Figure 2.14B). In addition to the decrease in IOX-NIV size after filtration, the PDI of both empty- and IOX-NIV was significantly reduced in comparison to the PDI measured post-synthesis ($p < 0.001$; Figure 2.15 A and B). Similarly, ultracentrifugation did not alter IOX-NIV PDI.
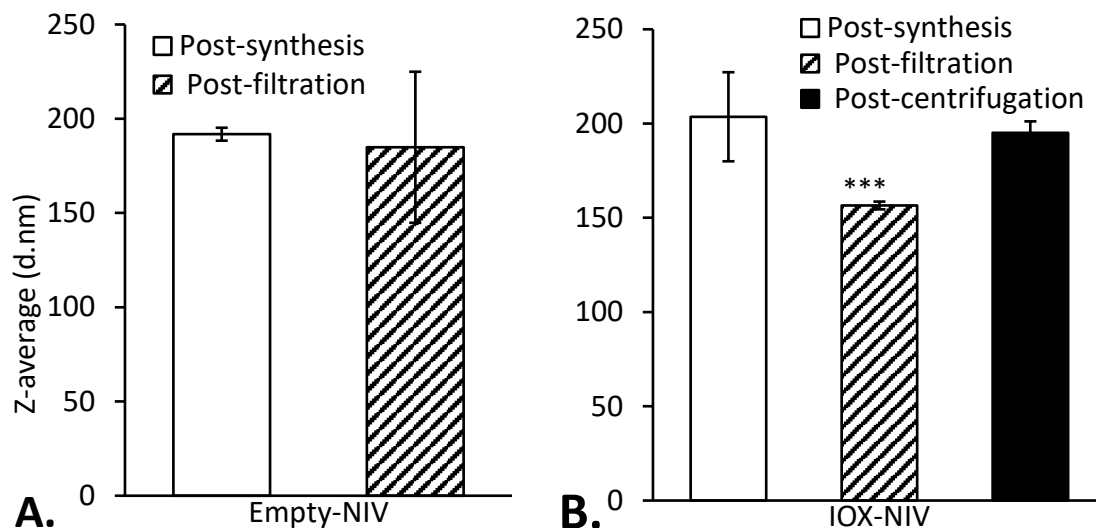
Figure 2.14: Effect of processing on (A) empty- and (B) IOX-NIV average size. Measurements were taken at final lipid concentrations of 1.5 mM *(*** $p < 0.001$ in comparison to NIVs post-synthesis; n = 3; ± SD).*
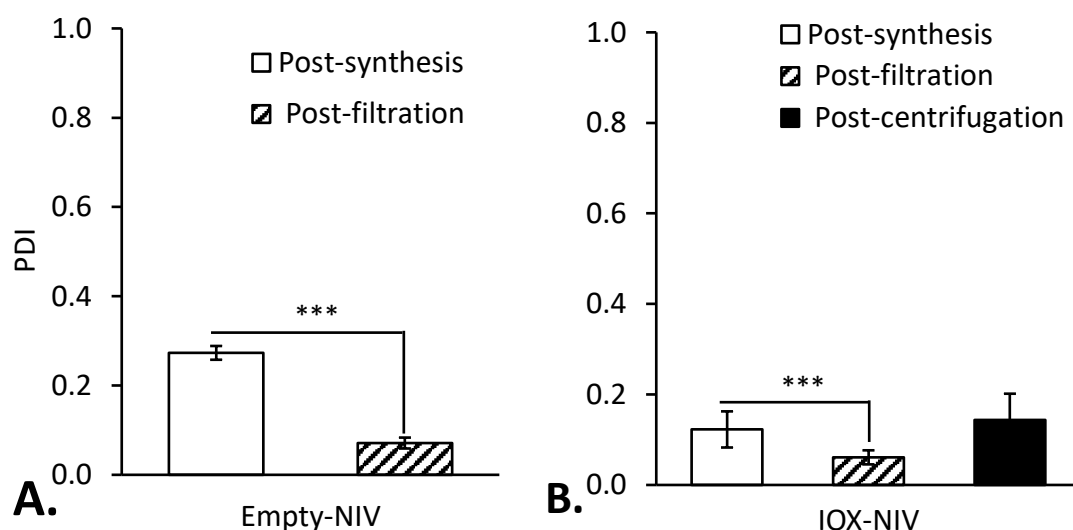
Figure 2.15: Effect of processing empty- (A) and IOX-NIV (B) (1.5 mM) on PDI *(*** $p < 0.001$ in comparison to NIVs post-synthesis; n = 3; ± SD).*

Analysis of empty-NIVs before and after filtration showed no deviation in surface charge which was -30 ± 1 mV and -30 ± 1 mV, respectively (Figure 2.16A). There was a slight

increase in the measured electronegativity, from -25 ± 2 mV post-synthesis to -28 ± 3 mV, after filtration and ultracentrifugation (Figure 2.16B), however, these differences were not significant.
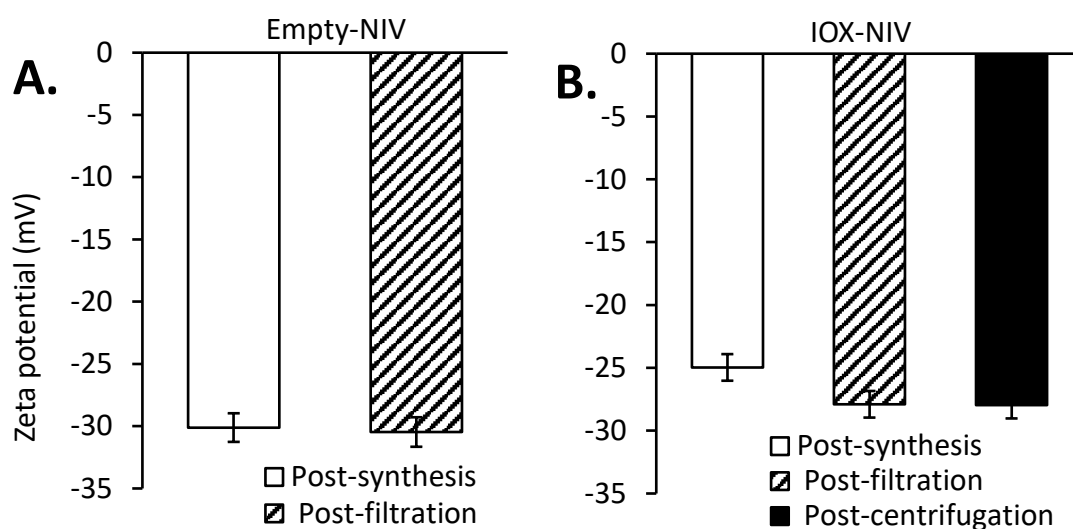
Figure 2.16: Effect of processing on (A) empty- and (B) IOX-NIV surface charge *(n = 3; ± SD).*

2.3.4   Effect of time and temperature of IOX-NIV appearance

Volumes of 100 µl IOX-NIV were aliquoted in small vials and stored in darkness within constant temperature rooms as described previously (Section 2.3.2). The impact of storage time and temperature on IOX-NIV appearance became visibly apparent at higher temperatures of 37 and 50 °C (Figure 2.17). After as little as 8 weeks, samples stored at 37 and 50 °C expressed a noticeable change in colour, from a clear solution to a yellow colour, which was darker in samples were stored at 50 °C. In comparison, samples stored at either 4 or 25 °C remained unchanged in appearance even after 28 weeks.
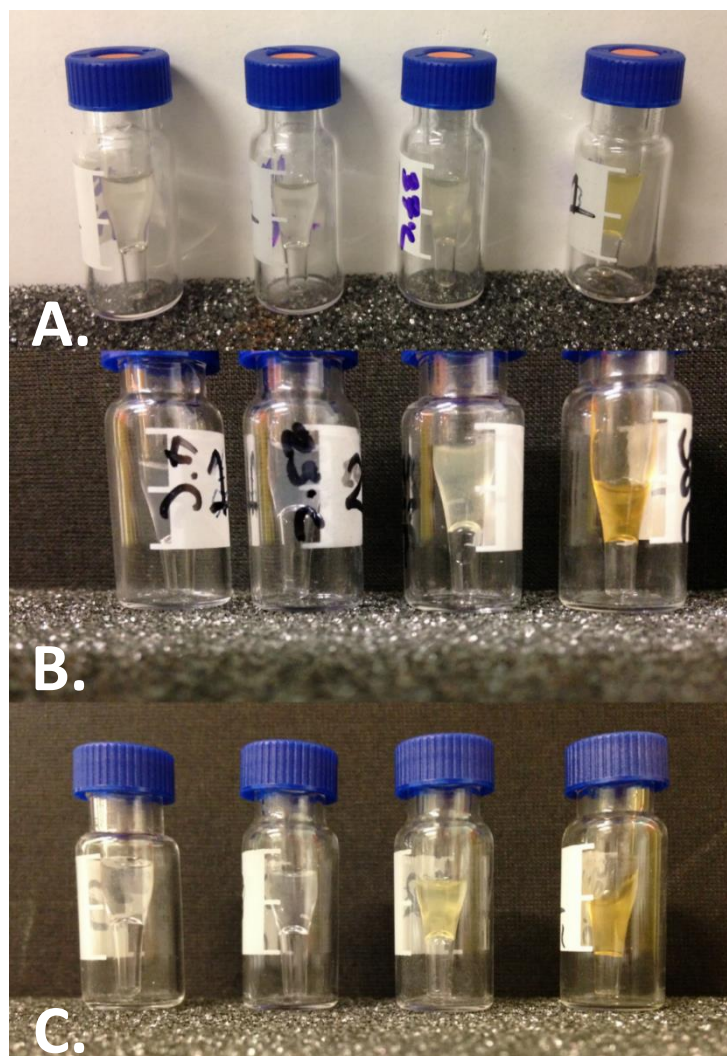
Figure 2.17: Effect of storage temperature and time on IOX-NIV appearance. *L- R: 4, 25, 37 and 50 °C and time (A) 8 weeks, (B) 16 weeks and (C) 28 weeks.*

2.3.5   Effect of time and temperature on IOX-NIV size and PDI

Measurement of average particle size and PDI of 3 individually prepared batches of IOX-NIV was performed after storage at a range of temperatures for different time points in order to determine the physical stability of IOX-NIV. After a total of 37 weeks at 4 °C, there was no significant change in average particle size compared to newly prepared IOX-NIV. An increase in PDI from 0.13 ± 0.04 to 0.20 ± 0.06 after 24 weeks was the only time point observed to show a significant change ($p < 0.001$). Despite this, measurements obtained at 28 and 37 weeks were not found to be significantly different when compared to IOX-NIV at $t = 0$ (Figure 2.18). Similar results were obtained after long-term storage at 25 °C where none of the time points showed any significant change in size and PDI when compared to the data obtained immediately post-synthesis (Figure 2.19). At day 0 average IOX-NIV size was 204 ± 24 nm

while the PDI was 0.1 ± 0.04, after a storage period of 37 weeks at 25 °C the size was 187 ± 10 nm and the PDI was 0.2 ± 0.04.
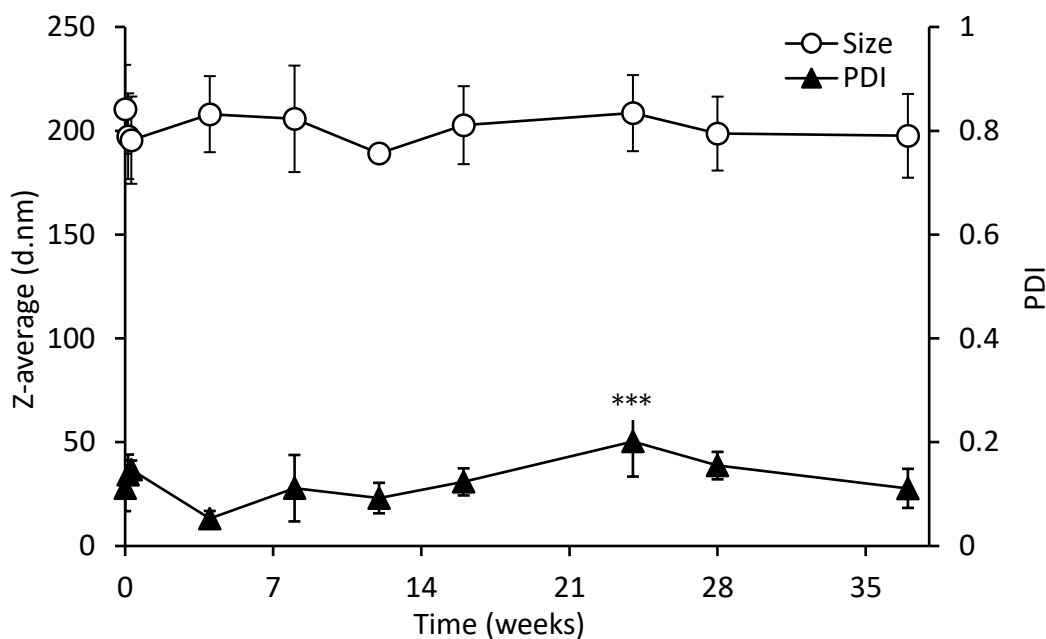
Figure 2.18 Effect of 37 week storage of IOX-NIV at 4 °C on average size and PDI *(*** p < 0.001 when comparing the PDI to that measured where t=0; n = 3; ±SD).*
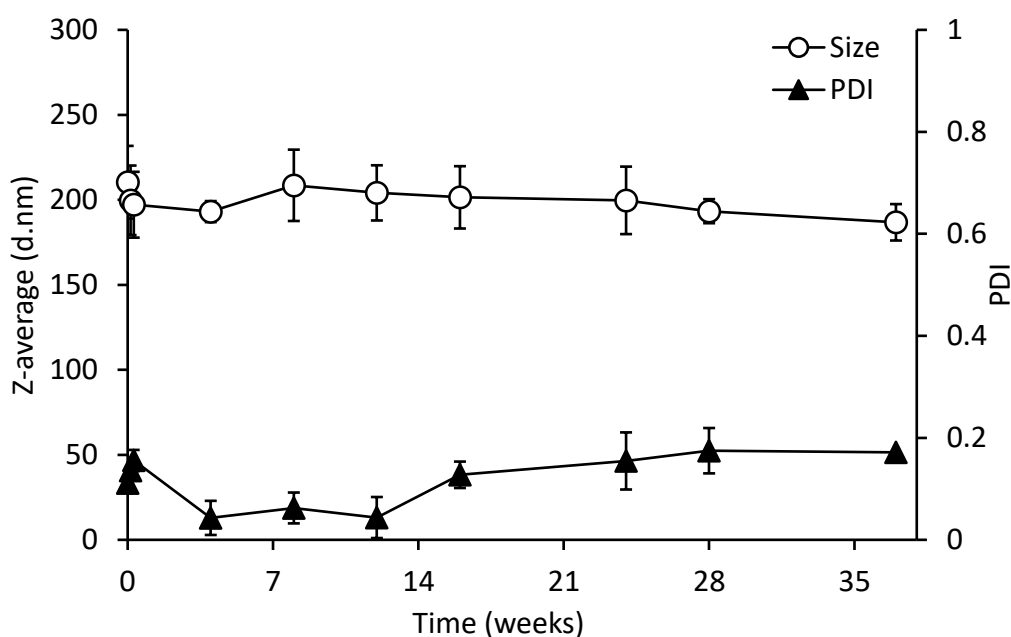
Figure 2.19: Effect of 37 week storage of IOX-NIV at 25 °C on average size and PDI *(n = 3; ±SD).*

After 37 weeks storage at 37 °C, IOX-NIV expressed similar physical stability to those stored at lower temperatures (Figure 2.20). Again there was no significant difference in size at any

of the time points measured. However, a drift towards a larger average size of 236 ± 44 nm was observed at week 37. In terms of PDI, there was no significant change for the initial 12 weeks at 37 °C, however, by weeks 24-37 the PDI had significantly increased ($p < 0.001$; Figure 2.20). At 24, 28 and 37 weeks respectively, the PDI of IOX-NIV was 0.2 ± 0.04, 0.2 ± 0.07 and 0.3 ± 0.09, respectively.
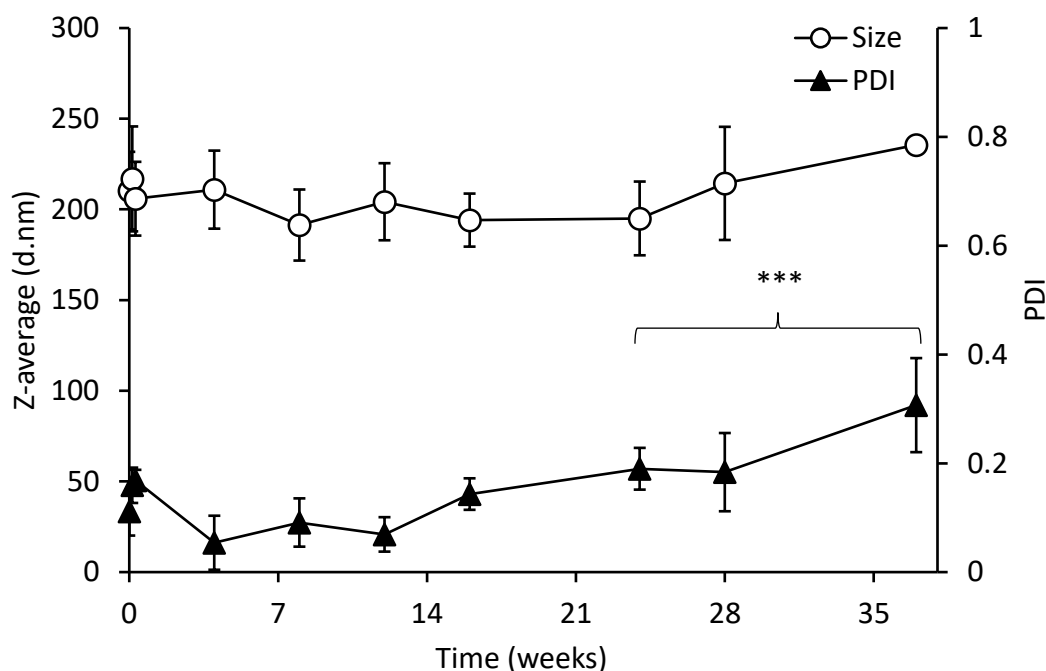
Figure 2.20: Effect of 37 week storage of IOX-NIV at 37 °C on average size and PDI *(*** p < 0.001 when comparing the PDI to that measured where t=0; n = 3; ± SD).*

The negative impact of storage on IOX-NIV physical characteristics was accelerated at temperatures above 37 °C (Figure 2.21). During the first 8 weeks of storage, the Z-average and PDI remained stable with no significant changes. At $t = 0$ IOX-NIV expressed a Z-average of 204 ± 24 nm and PDI of 0.13 ± 0.04, after 8 weeks at 50 °C the size and PDI showed no change at 209 ± 21 nm and 0.06 ± 0.03, respectively. Beyond 8 weeks, an increase in size and PDI, as well as SD, was observed and results became less reliable. The large variability between size measurements of the 3 individually prepared batches when stored at 50 °C for longer than 8 weeks meant that the size increases were not found to be statistically significant. One of the only significant increases was found to be the final measurement obtained at 37 weeks which was recorded as 1671 ± 1498 nm; PDI 0.7 ± 0.31 ($p < 0.0001$). In addition, the increase in PDI to 0.4 ± 0.30 at 24 weeks was statistically significant when compared to the initial PDI (0.1 ± 0.04) ($p < 0.001$).
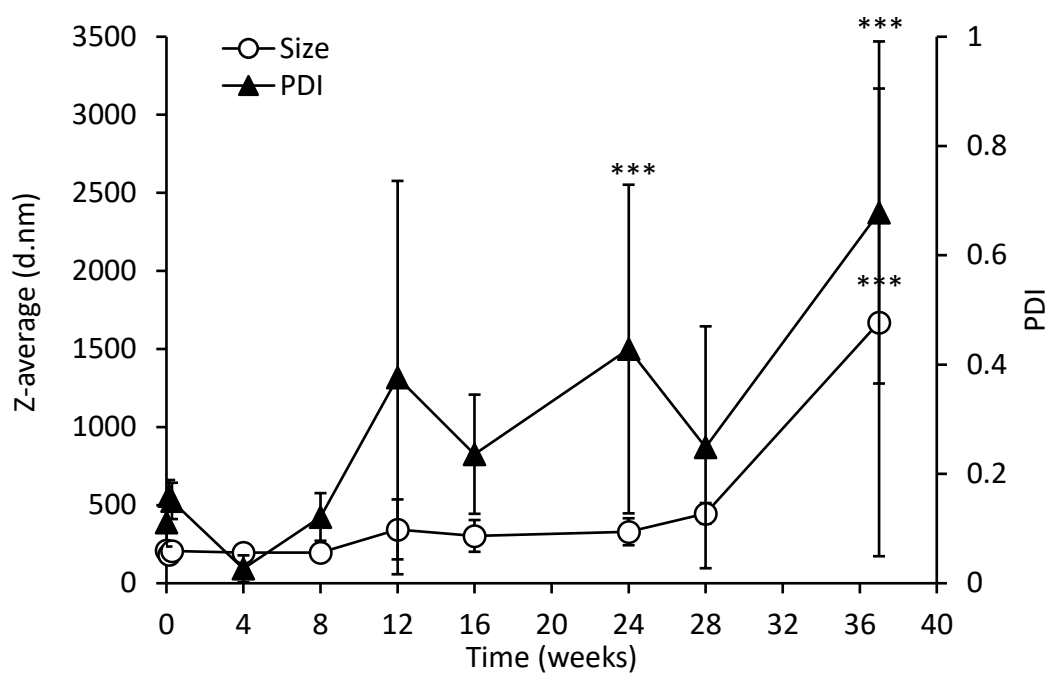
Figure 2.21: Effect of 37 week storage of IOX-NIV at 50 °C on average size and PDI *(*** p < 0.001 when comparing the size and PDI to that measured where t=0; n = 3; ±SD).*

2.3.6   Effect of storage time and temperature on IOX-NIV surface charge

During long-term stability experiments, the effect of storage time and temperature on average IOX-NIV surface charge of 3 individually prepared batches was analysed in addition to earlier size measurements. A similar pattern of results, detailed upon size analysis (Section 2.3.5), was also observed upon the measurement of vesicle charge. Storage of IOX-NIV at 4 °C resulted in no significant differences in surface charge at any time point throughout the 37 week incubation period when compared to the surface charge of IOX-NIV at day 0 (Figure 2.22).
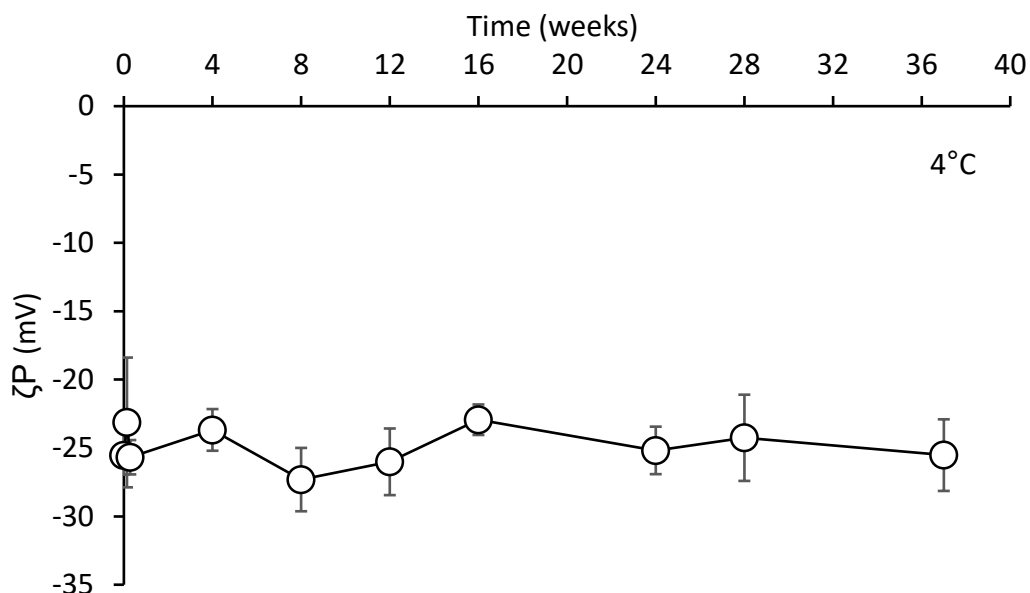
Figure 2.22: Effect of 37 week storage of IOX-NIV at t 4 °C on surface charge *(n = 3; ± SD).*

After storage of IOX-NIV at temperatures of 25 and 37 °C there were some significant changes in surface charge at specific time points when compared to the surface charge measured post-synthesis ($p < 0.0001$), however, no significance was observed when comparing initial measurements with the final measurement taken after 37 weeks storage (Figure 2.23, Figure 2.24). For example, at t = 0 the average IOX-NIV surface charge was -26 ± 1 mV, after storage at 25 °C for 8 weeks, a significantly more negative charge was recorded at -29 ± 2 mV. Despite this none of the following surface charge measurements were significantly altered and a final reading of -26 ± 2.23 mV was recorded after 37 weeks. Similarly there was no significant change when comparing the final measurement taken after 37 weeks of storage at 37 °C (-24 ± 1.55 mV) when compared to the initial charge. However, significant changes were detected at 16 and 24 weeks, where the surface negativity had dropped to -22 ± 1.71 mV and -23 ± 1.02 mV, respectively (Figure 2.24; $p < 0.001$).
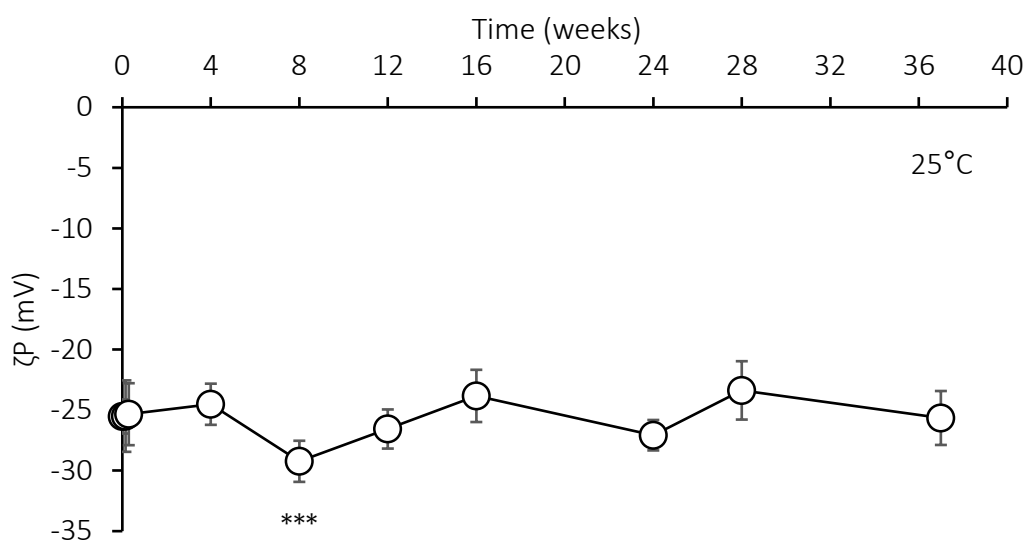
Figure 2.23: Effect of 37 week storage of IOX-NIV at 25 °C on surface charge *(*** p < 0.001 when comparing the zeta potential to that measured where t=0; n = 3; ± SD).*
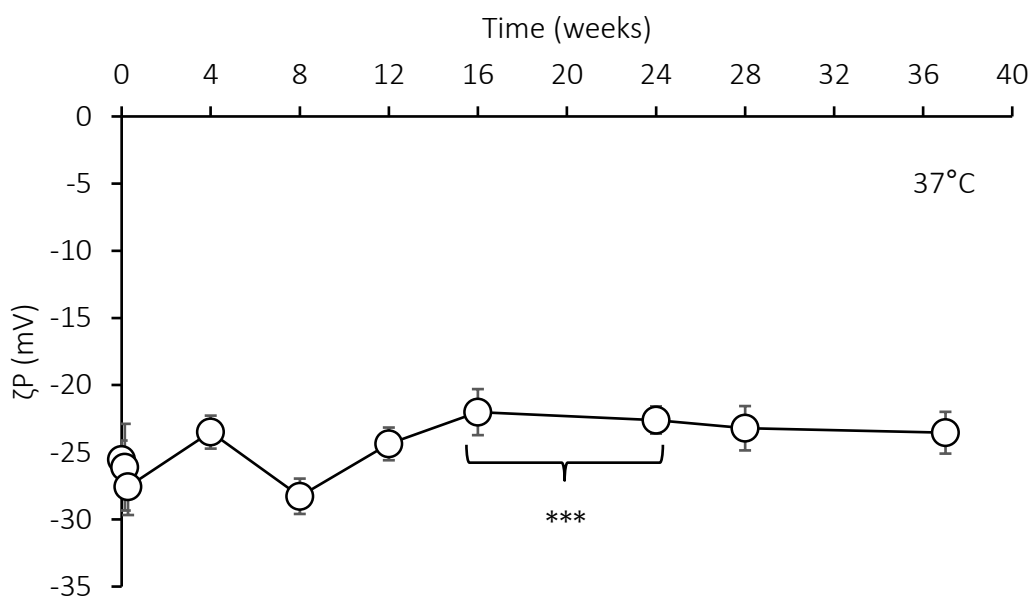
Figure 2.24: Effect of 37 week storage of IOX-NIV at 37 °C on surface charge *(*** p < 0.0001 when comparing the zeta potential to that measured where t=0; n = 3; ± SD).*

When IOX-NIV were stored at an extreme temperature of 50 °C the surface charge remained stable for the initial 12 weeks of storage. After 16 weeks, the charge negativity had significantly reduced from -26 ± 1mV to -22 ± 2 mV when compared to the surface charge measured post-synthesis (p < 0.001; Figure 2.25). In comparison to the initial charge expressed by newly prepared particles, every time point after 16 weeks was significantly reduced (p < 0.0001; Figure 2.25). After a total of 37 weeks storage at 50 °C the electronegativity of IOX-NIV had dropped from -26 ± 1 mV to -15 ± 3 mV.
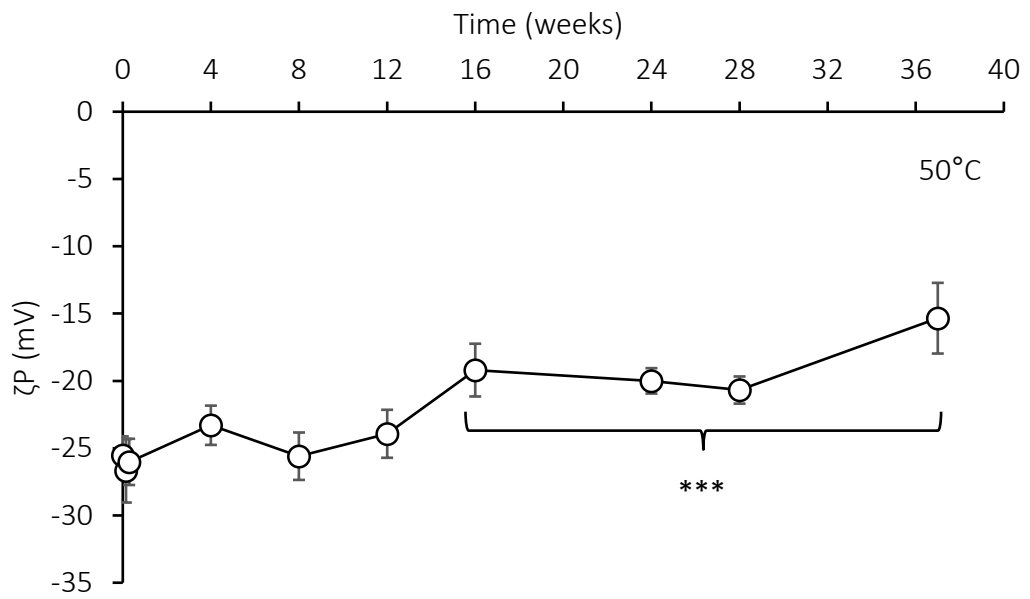
Figure 2.25: Effect of 37 week storage of IOX-NIV at 50 °C on surface charge *(n = 3; ± SD; *** p < 0.001 when comparing the zeta potential to that measured where t=0).*

2.5 Discussion

2.5.1 Differences in the appearance of IOX- and empty-NIVs before and after hydration

Cloudy suspensions of lipid vesicles are often anticipated to be the final product obtained post-synthesis. However, the IOX-NIV solution obtained in these experiments was an off-clear viscous solution, with little resemblance to the opaque suspension obtained for empty-NIV whereby molten lipids were hydrated using an aqueous solution. The appearance of vesicle suspensions are largely dictated by the size and stability of particles and their ability to reflect light, as well as the lipid concentration and entrapped agent. Despite the poor statistical power of AFM for the analysis of average particle sizes within a suspension, AFM was able to provide further evidence to support the theory that IOX-NIVs form spontaneously as a result of hydration using an aqueous solution. The evidence suggests that it was not until IOX-NIV were diluted with an aqueous solution that a cloudy suspension of IOX-NIV particles were formed. The development of a turbid suspension can sometimes be indicative of large vesicle sizes or suspension instability and aggregation of vesicles (Sobral *et al.*, 2008), however, the measured size, PDI and surface charge were indicative of a stable suspension with a small average size of ~ 200 nm. AFM successfully imaged vesicles present in diluted IOX-NIV which were found to have a spherical morphology while there were no other signs of suspension instability that have been described to proceed turbidity; such as flocculation, coagulation and sedimentation, prior to the final stage of phase separation (Sobral *et al.*, 2008).

One theory that describes the formation of vesicles after hydration is the synthesis of a pro-vesicle system. Here, the self-assembly of amphipathic non-ionic surfactant molecules into IOX-NIV was initiated as a result of the addition of an aqueous phase. Pro-liposomes were the first system reported to have this behaviour and were prepared in the form of a free-flowing powder consisting of sorbitol coated with amphipathic lipids which could be hydrated to produce vesicles when required (Payne *et al.*, 1986b). Sometime after, a similar system for the synthesis of pro-NIVs was also reported (Hu and Rhodes, 1999). A key difference in the way in which IOX-NIVs form in comparison to descriptions of pro-vesicle systems is their physical state. As mentioned previously, pro-vesicles are typically in the form of a dry, granular powder, whereby hydration causes vesicles to bud-off from sugar (i.e. sorbitol) support components resulting in the generation of smaller, more homogeneous size distributions, when compared to those prepared by the hydration of a lipid film (Payne *et al.*, 1986a; Payne *et al.*, 1986b). However, in this instance, the IOX-NIV formulation obtained post-synthesis was in the form of a solution, rather than a granular powder. Similar to the conditions described in this research, Vora *et al.* (1998) described the synthesis of a pro-NIV

formulation as a 'liquid crystalline-compact niosome hybrid' which spontaneously formed NIVs after hydration. This formulation could be described as a gel equivalent of the thin film layer prepared during the TFM of vesicle synthesis. Tightly packed lipids which take on the form of a film or gel can be diluted with an aqueous phase, resulting in the budding and release of vesicular structures. After hydration of the film prepared using TFM, vesicles tend to be very heterogeneous, in comparison, Vora *et al.* (1998) had recorded a very low PDI using gel hydration, between 0.14 and 0.18, which could be further reduced using agitation or ultrasonication. The PDI obtained for IOX-NIV after dilution was as low as some the values observed by Vora *et al.* (1998) after ultrasonication, at 0.11. This highlights the surprising level of homogeneity obtained after IOX-NIV hydration using such a crude, uncontrolled method, particularly without the need for additional down-sizing processes.

Concentrated IOX-NIV was found to be in a liquid-like state, rather than a gel, but expressed a viscous consistency with a clear colour, similar to the film and gel methods. (Israelachvili (2011)described the theory that amphipathic molecules, including surfactants, can be in the form of lyotropic crystals with the potential to spontaneously rearrange and form a variety of structures, including micelles, bilayer vesicles, or more complex structures depending on a critical packing parameter (CPP) (Israelachvili, 2011). This CPP is dependent on the characteristics and ratio of lipid, drug, and aqueous components (Uchegbu and Vyas, 1998). The incorporation of cholesterol within a formulation has been shown to significantly influence the CPP and transformation of surfactant from a gel-state to self-assembling, drug-loaded vesicles (Yoshioka *et al.*, 1994). In this instance, when comparing empty-NIVs prepared using the same total lipid concentrations and ratio as IOX-NIV, the only difference being that the lipids were homogenised with PBS rather than IOX, vesicles were formed immediately during homogenisation and a cloudy suspension was obtained. Therefore, the key component which influences the CPP of IOX-NIV using the method and formulation outlined in this chapter appears to be linked to IOX as the encapsulated agent and specifically, the IOX interaction with NIV lipids. Alternative NIVs prepared within the Mullen group which utilised the same method and formulation, but with different encapsulated agents, did not report the development of a pro-NIV system. However, Alsaadi (2011) had faced complications in relation to the development and characterisation of a highly viscous suspension of empty-NIV, prepared to encapsulate 0.9 % (*w/v*) NaCl, which may be indicative of a more ordered arrangement of lipid molecules. This evidence suggests that the chemical properties of IOX, and its interaction with surfactant, was the main determining factor relating to the formation of vesicles post-dilution. IOX itself is non-ionic with a neutral pH and is particularly hydrophilic, expressing a logP value of -3, however, there are a number of chemical

differences in comparison to PBS. Even though IOX is considered to be of low osmolality, it still expresses an osmolality ~2x greater than PBS, also the viscosity of IOX (Omnipaque300) at 37 °C is 10.4 Cps, while PBS expresses a viscosity of 1.0 Cps. It is likely that a combination of these factors contribute to the physical state of IOX-surfactant mixtures (Uchegbu and Vyas, 1998). The specific IOX/ lipid ratio required for spontaneous IOX-NIV self-assembly was not a parameter further investigated within this study. Difficulties were observed when trying to utilise AFM to detect IOX-NIV formation post-hydration, relating to the requirement to analyse a dry sample, while light microscopy utilised to visualise large vesicle budding in previous studies (Vora *et al.*, 1998). Light microscopy does not express a high enough resolution to detect IOX-NIVs at ~200 nm. Many advantages associated with the synthesis of a pro-NIV formulations have been described in comparison to conventional methods. These include improved stability without loss of entrapment efficiency after long periods of storage (Vora *et al.*, 1998).

Measurement of the average particle size and size distribution of formed IOX-NIVs was reported using two alternative techniques – DLS and AFM. Differences observed when comparing these two techniques could be expected due to fundamental differences between the underlying principles of these techniques. DLS measures the hydrodynamic diameter of vesicles within a suspension by detecting fluctuations in light reflected off particles which cross its path. On the other hand, samples prepared for AFM are aliquoted on to a flat surface and allowed to air-dry prior to imaging. The process of drying a lipid vesicle on a flat surface could easily influence the perceived diameter. This explains the differences observed when comparing data obtained from DLS and AFM.

A significant difference in the electronegative surface charge of empty- and IOX-NIV was detected, whereby, empty-NIVs were slightly more negative in comparison to IOX-NIV, however, a ζP of +/ -30 mV is suggestive of an electrochemically stable particle suspension (Malvern, n.d.). The difference in surface charges should be considered when interpreting data which examines the biological interactions of the systems and when comparing the toxicity of empty- and IOX-NIVs, however, the biggest influence on the toxicity of lipid nanoparticles is reported to be those which express a positive charge (Soenen *et al.* , 2009).

2.5.2   Homogenisation and dilution of IOX-NIV leads to the formation of homogeneous vesicles with desirable size and charge characteristics

DLS analysis of IOX-NIV after dilution in aqueous solution led to the detection of one, uniform size distribution peak. These measurements support the application of IOX-NIV as a clinically relevant drug delivery system due to size homogeneity and narrow size distribution.

The results presented in this chapter represent the analysis of 3 separately prepared batches of IOX-NIV, the similarity of which highlight the reproducibility and robustness of both the formulation and method of production. The average size of 3 batches of IOX-NIV was ~200 nm. Entrapment of IOX within vesicles of this characteristic size may offer a selective advantage in avoiding damage within the renal system. Free IOX has a half-life of 2 h as it is rapidly filtered through the kidneys (R. Katzberg, 1997). After 24 h, IOX has been completely eliminated from the body as an unmetabolised product within the urine (Olsson *et al.,* 1983). Encapsulation of IOX within NIVs of this size could offer a passive mechanism for bypassing the usual filtration of contrast media through the kidneys, which may be a contributing to CIN related damage. Uchegbu (1998) compared the biodistribution of PMA and Span60 NIVs, although the surface charge of the vesicles was not reported, negatively charged DCP was incorporated within the NIV formulations which would infer a negative charge. Span60 NIVs were observed to have a size of 177 nm, close to the average size of IOX-NIV described in this study. Here it was shown that after IV injection in mice, most of the drug encapsulated in Span60 NIVs was detected in the liver, at ~18 and 12.5 %, after 5 and 24 h, respectively. In comparison, the amount residing in either the plasma, spleen or heart was ≤ 1.5 % at both of these times. This data was in agreement with previous data looking at the administration of NIVs encapsulating different drugs, where NIVs had a tendency to become deposited in the liver and there is often no report of accumulation within the kidneys (Baillie *et al.*, 1986; Azmins *et al.*, 1985). Shehata *et al.* (2016) had shown that the incorporation of a PEG layer on NIV circulation could be used to prevent typical uptake within the liver. While the incorporation of a negative charge through the inclusion of DCP has been found to dramatically increase liver uptake in comparison to neutral and positively charged liposomes (Liu and Liu, 1996). It may therefore be assumed that the strong negative charge expressed on the surface of IOX-NIVs formulated with negatively charge DCP will lead to a similar biodistribution pathway and that much of the particles will end up within the liver.

Accumulation of lipid vesicles within the liver, and also the spleen, is related to the uptake of opsonised vesicles > 100 nm by specialised macrophages of the MPS. Vesicles smaller than 100 nm avoid interaction with circulating proteins and subsequent recognition by immune cells which tends to result in increased circulation within blood (Bozzuto and Molinari, 2015). In comparison, larger vesicles (> 1 µm) have the potential to cause serious adverse effects upon IV administration as they are likely to become trapped in capillary beds where the smallest blood vessels have diameters ranging from 5-10 µm. An incident resulting in the death of man following IV administration of a clinically available amphotericin B-lipid complex system, Abelcet, was previously reported (Tolentino *et al.*, 2004). The cause of death was

linked to the development of a fatal fat embolism as a result of lipid-complex deposition within the capillaries. In comparison to the IOX-NIV developed in this study, Abelcet is a lipid-amphotericin B complex with a large size reported to be between 1.6 and 11.1 μm (Adler-Moore and Proffitt, 2008). A vesicular drug delivery system of ~200 nm could be used to avoid negative consequences linked to the administration of large lipid materials. Overall, analysis of currently available data supports the development of an IOX-NIV system at a size of ~200 nm. A PDI of 0.11 ± 0.04 is on the lower end of the scale indicating the presence of a monodispersed sample (Malvern, n.d.). A highly monodispersed product provides obvious advantages in the development of a system for clinical use. The administration of IOX-NIV, rather than free IOX, could offer a number of potential benefits, including: protection of the body from IOX chemical insult, increased IOX blood circulation time leading to greater potential for bio-imaging, and finally IOX avoidance of the renal system and redirection to the liver may provide preventative measures against CIN development.

As expected, the incorporation of DCP in NIV formulations resulted in the synthesis of vesicles with a negative charge. The dilution of either empty- or IOX-NIVs in PBS resulted in the measurement of particles with a ζP of -30 ± 2 mV and -25 mV ± 2 mV, respectively. Similar to the results described here, previous research into the use of the same NIV formulation and method of synthesis had shown a slightly more negative potential in empty-NIV compared with drug-entrapped vesicles at -25 to -35 mV, for SSG and PBS-entrapped vesicles (Mullen *et al.*, 2000). In comparison, Alsaadi (2011) reported a much more negative ζP expressed by empty-NIV at > -60 mV post-synthesis, when compared to NIV encapsulating cisplatin, the electronegativity increased further leading to a surface charge > -70 mV. The differences in measured charge can be attributed to the material to be entrapped within the NIVs rather than the formulation or methodology (Mullen *et al.*, 2000). Obeid *et al.* (2016) had shown a great increase in negativity when comparing NIVs prepared with distilled water to the use of other solvents, including PBS or 'normal' (0.9 % (*w/v*) NaCl) saline. In this instance, the electronegativity had increased from ~ -30mV when prepared with PBS to > -75 mV when prepared with distilled H_2O. This data therefore highlights how the ionic strength of the material used to prepare vesicles has a significant impact on the measured surface charge as described by the classic DLVO theory (Derjaguin and Landau, 1993).

Regardless of difference in surface charge, it is commonly accepted that vesicles with a ζP of +/ -30 mV are stable within a suspension. The inclusion of a charge of -25 mV on the surface of IOX-NIV was shown to promote electrostatic repulsion between similarly charged vesicles preventing them from colliding and forming aggregates (Malvern, n.d.). Aggregation of NIVs

would be detrimental to their ability to retain encapsulated IOX and would decrease their suitability as a successful nanomedicine (Taylor and Elhissi, 2016).

2.5.3 Processing IOX-NIV did not impact physical IOX-NIV characteristics

Ultracentrifugation was used to later enable the chemical characterisation of IOX encapsulation within NIVs and for the purification of vesicles. It was shown that the majority of IOX-NIV were successfully separated from the suspending media upon ultracentrifugation at 36 k rpm as detected upon the formation of a vesicle pellet, clear suspension and similarities in size measurements before and after ultracentrifugation. In comparison, ultracentrifugation of empty-NIV did not allow for this separation and a cloudy suspension was still present even after centrifugation. The reason for this difference could be attributed to the increased mass of NIVs when IOX was entrapped. The additional mass of IOX within NIV would allow the centrifugal force to separate IOX-NIV from their external environment. The maintenance of size, PDI and charge characteristics after ultracentrifugation suggests that any shear force was not great enough to negatively impact the structural integrity of IOX-NIVs.

Prior to further *in vitro* toxicological analysis of IOX-NIV, it is important that the product is sterile, this is also an important consideration prior to IV administration of IOX-NIV within a clinical setting. Filter sterilisation offers many advantages when compared to other methods of sterilisation. The extreme conditions of an autoclave are not appropriate due to the temperature-labile nature of lipid vesicles. UV and γ-irradiation are both known to accelerate peroxidation and subsequent degradation of lipids leading to release of vesicular contents (Mandal and Chatterjee, 1980; Erdogan *et al.*, 2006). IOX-NIV showed no significant differences in average size measurements despite potential concerns relating to the shear forces vesicles are subjected to when passing through the syringe filtration system under pressure. This highlights the physical stability of IOX-NIV as well as the suitability of this method for *in vitro* and future clinical testing. A significant reduction in IOX-NIV PDI was observed post-filtration which may be expected due to the removal of particles greater than the filters pore size of 0.22 µm (Goldbach *et al.*, 1995). Despite this, the reduction in PDI, as a result of the removal of larger IOX-NIVs, was not significant enough to affect average particle size.

2.5.4 Long term physical stability of IOX-NIVs under different storage temperatures

The long-term stability of pro-IOX-NIVs was analysed by monitoring the effect of temperatures of 4, 25, 37 and 50 °C on physical characteristics for a total of 37 weeks. A visible change in appearance was observed in the form of discolouration, from what was initially a clear solution, to one which was yellow/ brown in colour. The change in IOX-NIV appearance was time-dependent and occurred more rapidly, and to a greater extent, at higher

temperatures. No obvious discolouration was observed throughout the 37 week storage time at temperatures of 4 and 25 °C, which was in conjunction with an ability to retain typical physical characteristics up until the 37 week time point. Upon storage at 37 °C, the first signs of instability were associated with an increase in average particle size while a loss in surface charge was only observed after longer incubation times at 50 °C. Surfactant VIII, the main structural component of IOX-NIV, has a melting temperature (T_m) of 37-38 °C. Therefore, a loss of stability at temperatures ≥ 37 °C may have been anticipated as bilayers approach the T_m of the main structural component, increased membrane fluidity occurs. However, the incorporation of cholesterol within lipid membranes has long been known to alter the phase transition temperature of the main structural component and will hence influence the stability of IOX-NIV at different temperatures (Ladbrooke *et al.*, 1968). Characterisation of IOX-NIV phase transition temperatures can be defined through the use of differential scanning calorimetry (DSC) which would have provided additional information regarding the stability and fluidity of NIV membranes in relation to temperature, however, this was not performed within the scope of this study. Despite this, there is a relationship between increasing environmental temperatures and increased expression of membrane defects which promote fusion of neighbouring vesicles (Cevc and Richardsen, 1999). As lipid molecules fuse it is likely that entrapped hydrophilic drug will be lost due to the disruption and reformation of membranes (Taylor and Elhissi, 2016). The increase in PDI at 37 °C still resulted in the detection of a suitably homogeneous size distribution as the PDI remained ≤ 0.3. Strong discolouration of IOX-NIV was observed as early as 8 weeks after storage at 50 °C, prior to any significant changes in average particle size, PDI or surface charge. The greatest alteration in IOX-NIV size was found after 12 weeks storage at 50 °C, however, the significance of these changes in comparison to initial measurements were masked by large standard deviations, which in itself, may be attributed to an increase in heterogeneity. Interestingly, the increase in size and PDI observed coincided with a decrease in surface charge at 50 °C. A loss in surface charge may have been related to an increase in membrane fluidity or lipid degradation, which in turn decreases the electrostatic repulsion and stability of IOX-NIV leading to aggregation and the measurement of increased particle size.

Similar changes in colour with increasing temperature was reported in previous research carried out in the Mullen group, however, these earlier experiments concluded that the change in sample colour may have been more likely attributed to the precipitation of cisplatin over time rather than lipid oxidation (Alsaadi, 2011). The presence of lipids in combination with IOX alone are unlikely to have had an effect on the appearance and physical properties of IOX-NIVs. It is known that the iodine molecules of low-osmolar ionic RCM, such as IOX, do

not dissociate leading to the presence of free iodine molecules, therefore some form of degradation would need to occur before iodine atoms were free to interact and degrade the unsaturated bonds of lipids (Thomsen and Morcos, 2000), such as those present in cholesterol or DCP. The manufacturer's instructions state that IOX in the form of Omnipaque is colourless to pale-yellow in appearance. In terms of IOX stocks stored throughout the course of these experiments, no significant alteration in the typical colourless appearance of IOX was observed, however the inclusion of control group of IOX only and empty-NIVs at the defined temperatures and time periods would have provided additional information relating to the change in appearance of undiluted IOX-NIVs as observed in these experiments.

In addition, the final stages of IOX manufacturing, in the form of a RCM solution such as Omnipaque, involves autoclaving as a sterilisation step, as described in the manufacturer's leaflet. Due to the fact this sterilisation procedure typically involves maintaining the product at high temperatures of at least ~121 °C for between 15 and 20 mins, it may be assumed that a change in IOX structure alone is unlikely to be responsible for the alteration in IOX-NIV appearance at temperatures of 37 and 50 °C. As described in the manufacturer's instructions Omnipaque should be stored at a temperature range between 20 and 25 °C and is reported to have a shelf-life of up to 3 years when stored in polypropylene bottles. An acceptable storage time of up to 1 month is described when maintained at warmer temperatures of 36-38 °C. It should be noted that the visual change in colour of undiluted IOX-NIV did not become apparent until after 1 month storage at 37 °C. If IOX had become broken down during long-term storage (> 1 month) at 37 and 50 °C, this may have resulted in the presence of free iodine within the IOX-NIV sample which in turn could promote the risk of lipid breakdown through the interaction of iodine with the unsaturated lipid bonds. Due to the strong interaction between iodine and unsaturated lipid bonds, the presence of unsaturated bonds can be quantified using a known amount of iodine which may be converted to an 'iodine value' reflecting the degree of lipid unsaturation and this technique is used throughout food science (Firkins and Eastridge, 1994).

A second theory to explain the temperature- and time-dependent change in NIV colour, may be related to chemical alteration of lipid components which are susceptible to oxidation due to exposure to atmospheric oxygen, in a process termed the Maillard reaction, whereby sample 'browning' occurs over time (Hidalgo and Zamora, 2005). Despite the fact that non-ionic surfactants have reduced susceptibility to oxidation, particularly in comparison to the main phospholipid components of liposomes, autoxidation over long storage times has been reported to occur in ethoxylated surfactants, similar to surfactant VIII, which was utilised as

the main structural component of NIVs prepared in this study (Bodin *et al.*, 2003). Other molecules included in the formulation, such as cholesterol are also susceptible to oxidation (Valenzuela *et al.*, 2003). The speed at which chemical reactions, including oxidation, occur can be increased upon increasing temperature which would explain the considerably more noticeable effect of storage time on IOX-NIV appearance at temperatures > 25 °C (Matumoto-Pintro *et al.*, 2017). IOX-NIV stability may have been further enhanced by storing vesicles in inert gas, such as nitrogen, resulting in the removal of oxygen and reduced occurrence of oxidation. This method has been described to enhance the shelf-life of lipid vesicles incorporating haemoglobin, as well as commonly being used to prolong shelf-life throughout the food industry (Marasca *et al.*, 2016; Sakai, *et al.*, 2000).

2.5.5   Additional physical characterisation

The definition of additional parameters, including lamellarity, is recommended by the FDA during the development of a vesicular product for clinical use (Food and Drug Administration, 2015). Although this characteristic was not defined within the scope of this study, it may be performed using techniques such as freeze-fracture electron microscopy (FFEM) (Pereira-lachataignerais *et al.*, 2006). FFEM was utilised in previous research by the Mullen group to determine the lamellarity of this NIV formulation in the encapsulation of cisplatin. In this study Alsaadi (2011) obtained inconclusive results which had been altered by the presence of artifacts associated with the techniques itself. Overall it was suggested that NIVs prepared using the method commonly used within the Mullen group, and as described here, lead to the development of a NIV system containing a mixture of unilamellar and multilamellar vesicles.

2.6   Conclusion

Immediately post-synthesis IOX-NIV appeared to be in a pro-NIV lyotropic-state under the influence of the chemical properties of IOX. Long-term storage of IOX-NIV in a pro-vesicle form could have the potential to offer a protection in comparison to storage of formed IOX-NIV. After further hydration with an aqueous solution, homogeneous vesicles of ~200 nm were detected using DLS and their round morphology was visualised using AFM. The synthesis of vesicles of this size could offer advantages including enhanced IOX circulation time upon IV administration, protection of the patient from IOX-associated damage, and passive avoidance of usual IOX filtration through the kidneys, potentially preventing the risk of CIN in susceptible patients. A narrow IOX-NIV size distribution and low PDI enhances its potential success as a clinically available product which satisfies criteria outlined by regulatory bodies such as the FDA. A negative surface charge of -25 mV demonstrates the development of an electro-stable system with reduced opportunity for aggregation and alteration of physical and chemical parameters. For the consideration of a robust and stable product, suitable for use in the clinical environment, it is important that physical characteristics are defined after each processing step. Additional processing, such as ultracentrifugation for purification and chemical characterisation and filter sterilisation required for *in vitro* characterisation, were not found to negatively influence the structural integrity of IOX-NIV. This supports the suitability and requirement for further experimental analysis of the system to promote its development towards a clinical stage.

Long-term physical characterisation of IOX-NIV over 37 weeks showed that a protective environment could be maintained at storage temperatures of 4 and 25 °C. As temperatures increased to 37 °C after a period of 9 weeks, average IOX-NIV size was observed to increase, while the surface charge remained relatively stable. In comparison, the increase in size and PDI during storage at 50 °C coincided with a decrease in surface charge which is suggestive of IOX-NIV aggregation and a loss of electrostatic stability between formed vesicles. A change in physical appearance, in terms of colour, was also observed at temperatures of 37 and 50 °C. Further experimentation is required before the exact cause of this change may be concluded, however, a review of the literature implies that a change in colour may be attributed to alterations in IOX structure leading to further iodine interactions with unsaturated lipid bonds, or as a result of lipid oxidation and potential degradation of IOX-NIV lipid components. The impact of these physical changes on the ability of NIV to entrap IOX will be described in future chapters.

In order to further satisfy criteria recommended by the FDA for the development of a clinically translatable medicinal nanomedicine, future research should include additional characterisation such as the definition of bilayer lamellarity.

Chapter 3

Validation of an HPLC method for
IOX quantification and determination
of IOX-NIV encapsulation efficiency
and release

3. Chapter 3 – Validation of an HPLC method for IOX quantification and determination of IOX-NIV encapsulation efficiency and release

3.1 Introduction

Throughout the design and formulation of lipid-based delivery systems, the characterisation of particles based on physical characteristics including size distribution and particle charge is a fundamental aspect of analysis. In addition, the amount of drug entrapped within NIVs is another important parameter that should be characterised as this will determine the efficacy of an IOX-NIV delivery system. The FDA (2018) released a report outlining key recommendations to assist with applications relating to novel liposomal drug development - which includes advice on the characterisation of the drug component. Drug entrapment is a highly recommended characteristic to be analysed and can be done so in a number of complimentary ways including representing the final drug concentration as: mg mL^{-1}, drug-to-lipid ratio, and encapsulation efficiency. The EE % refers to the amount of drug successfully entrapped within a vesicular drug delivery system post-synthesis as a percentage of the amount of drug used in the preparation of vesicles (Xu *et al.*, 2012b).

NIV formation occurs as a result of the self-assembly of lipid components that become attracted to each other, creating a vesicle structure. IOX-NIVs were found to take on a spherical structure upon visualisation using AFM during physical characterisation experiments (Chapter 2 – Formulation and Physical Characterisation of IOX-NIV). A spherical structure is often reported to be the main structural shape of vesicles due to the requirement for the lowest amount of energy during formation, although other complex and asymmetrical geometries have been reported (Svetina and Zeks, 2002). In the instance of passive encapsulation of water soluble drugs, such as IOX, whereby the drug becomes entrapped as a result of vesicle formation around the IOX aqueous phase, the encapsulation efficiency (EE %) can be limited by the method of production, lipid-drug interactions and lipid concentrations, as well as the volume available within each vesicle (Xu *et al.*, 2012a). After separation of the outer media containing un-encapsulated IOX the amount which remains entrapped within NIVs may then be quantified. The capacity of IOX-NIV to retain IOX will provide an estimation of how the system may perform as an image enhancing agent. More quantifiable data could be obtained upon measuring the x-ray attenuation strength both *in vitro* and after IV administration *in vivo*.

The FDA (2018) also advise on running experiments to determine a lipid delivery systems ability to maintain drug encapsulation, both over time and under specified storage conditions. The detection of a minimal loss in NIV EE throughout the defined storage conditions would

highlight the preparation of a chemically stable delivery system, in addition to defining appropriate storage conditions and potential storage limitations. The inclusion of drug delivery performance under stress conditions, such as high temperatures, will provide information relevant to the storage of IOX-NIV in certain climates or in incidences of accidental heating. In addition to the identification of appropriate IOX-NIV storage conditions and definition of shelf-life, the stability of IOX-NIVs within the body is also an important consideration (FDA, 2018). The estimation of how IOX is released from NIVs and in to the blood stream should be analysed in order to define the amount of IOX that patients may be exposed to and whether IOX-NIV may be used to alter the renal- and vascular-toxicity profile of IOX.

3.1.1 Separation of NIVs from unentrapped IOX

The separation of lipid-vesicles from their suspending medium is an essential stage prior to the quantification of the EE % of IOX within NIVs. The appropriateness of selecting a specific separation technique is dependent on the properties of the particles. Large, micrometre-sized vesicles may be easily separated through filtration or regular centrifugation while smaller vesicles within the nanometre range can be more problematic, although a number of different methods exist. Vesicles may be separated using centrifugation and ultracentrifugation methods by applying a centrifugal force leading to the sedimentation of particles which express a greater density than the suspending medium. After sedimentation, the concentration of IOX within NIVs can be determined indirectly by quantifying the amount of free drug present in the supernatant or directly, by first removing the supernatant and destroying the lipid pellet to release entrapped drug (Wallace *et al.*, 2013). Key concerns regarding the use of ultracentrifugation relates to the possibility that the centrifugal force induces leakage of drug out of the vesicles or leads to the collapse of vesicle structures, leading to a false representation of the maximum encapsulation potential (Heeremans *et al.*, 1995). Earlier physical characterisation experiments which focused on the analysis of the size of IOX-NIVs post-centrifugation revealed no significant alteration of average IOX-NIV size and PDI after ultracentrifugation which highlights the stability of the system regardless of the applied centrifugal force (Chapter 2 - Formulation and Physical Characterisation of IOX-NIV).

Alternative methods of separation and purification of vesicles include dialysis whereby vesicles are aliquoted into a dialysis bag containing pores with an appropriate molecular weight cut-off (MWCO), which is then submerged in dialysis buffer. This selected MWCO should only allow the passage of unentrapped drug out of the dialysis membrane and in to the dialysis buffer, while larger formed vesicles are retained within the dialysis bag (Saarinen-Savolainen *et al.*, 1997). Disadvantages in the accuracy of purification though the use of

dialysis has been outlined previously, particularly related to the choice of a relevant methodology. Through the use of DLS analysis, a comparison to alternative techniques highlighted ultracentifugation as the most viable method (Wallace *et al.*, 2013). In addition, dialysis is most commonly reported as a key technique for the analysis of vesicular release profiles and offers advantages in determining how drug may be released from particles under physiologically relevant conditions (Avgoustakis *et al.*, 2002; Saarinen-Savolainen *et al.*, 1997). In the experiments described in this chapter, free IOX was first removed from self-assembled NIVs through centrifugation and then the release of entrapped IOX from NIVs was performed using dialysis.

Older traditional methods of separation include the use of size-exclusion chromatography which can involve the use of a column, commonly prepared using Sephadex beads of micron size ranges. The separation of materials is dependent on gravity whereby smaller particles such as unentrapped drug will pass through the column at a slower rate in comparison to larger particles, or those with a higher MW, which will take longer to pass through the column. Size-dependent fractions are obtained from the column and can be analysed for the quantification of free-drug prior to obtaining fractions containing separated drug-containing vesicles. This has a complex set up and optimisation procedure. Furthermore, uncertainties over the interaction of lipids within this system, plus the inability to apply this method to an industrial setting, is a cause for concern (Ruysschaert *et al.*, 2005). Tangential flow filtration (TFF) represents a more modern technology which has a similar principle to dialysis whereby vesicles are run through a column containing pores with a specified MWCO, which is selected so that unentrapped drug pass out the column within the perfusate, while larger vesicles are retained. The continuous flow of the systems helps to overcome specific disadvantages such as blocking of pores and the requirement for media changes which are required through the performance of dialysis (O'Sullivan *et al.*, 2012). TFF has been reported to have great potential within an industrial setting and may even be used in conjunction with specific microfluidic methods used for the synthesis of nano-vesicles to create a rapid continuous manufacturing and purification system (Dimov *et al.*, 2017).

Despite the advantages reported through the use of TFF, initial experiments provided evidence to suggest the retention of vesicle stability and successful separation of NIVs from their external media using ultracentrifugation within the scope of this thesis (Chapter 2 – Formulation and Physical Characterisation of IOX-NIV). In addition to its ease of use, this work highlighted the suitability of ultracentrifugation as a purification and separation

technique for IOX-NIVs. Further experiments focused on the use of ultracentrifugation for the determination of EE % post-synthesis and throughout defined stability experiments.

3.1.2   Quantification of drug encapsulation

Ultraviolet-high-performance liquid chromatography (UV-HPLC) is a technique commonly used in analytical chemistry to separate, identify and quantify components within a mixture. Due to various polar and hydrophobic interactions between the functional groups of molecules dissolved within a mobile phase, a characteristic elution time through a stationary phase offers a sensitive method for the separation and identification of materials. The use of a UV detector allows for drug quantification upon the measurement of light attenuation at a specific wavelength. Drug quantification can be achieved upon comparison with known standards in accordance with the Beer-Lambert Law, whereby an increase in light absorbance has a linear relationship with an increase in drug concentration (Ingle and Crouch, 1988). HPLC is a highly sensitive technique which has many applications within pharmaceutical analysis including separation of chemical components, quality control, the occurrence of drug degradation and the presence of impurities (Siddiqui *et al.*, 2017; USP, n.d.). A number of variations of HPLC exist with the two most commonly used being normal-phase (NP) and reverse-phase (RP)-HPLC which are based on opposing interactions.

During NP-HPLC the stationary phase column is comprised of polar, hydrophilic silica particles and the mobile phase which flows through the stationary phase is hydrophilic and non-polar. In this instance, the analyte to be separated and quantified may be polar resulting in strong interactions between the analyte and the similarly polar stationary phase. Overall, the stronger the polarity, the longer it takes for the analyte to pass through the column. In comparison, non-polar molecules will rapidly elute through the column without interacting with the stationary phase. In the instance of RP-HPLC, the opposite set-up is used whereby the silica particles are modified to be non-polar, this commonly occurs by binding carbon molecules, such as C18, to the surface of the silica particles. Similarly, the mobile phase of choice should be polar. In this instance, non-polar molecules are attracted to the stationary phase so that they can be separated from polar molecules which pass through quickly. Non-polar molecules show the strongest interactions to the non-polar stationary phase and will take the longest time to travel through the column, in comparison, polar molecules are weakly retained by the non-polar column and pass at a faster rate (Figure 3.1).
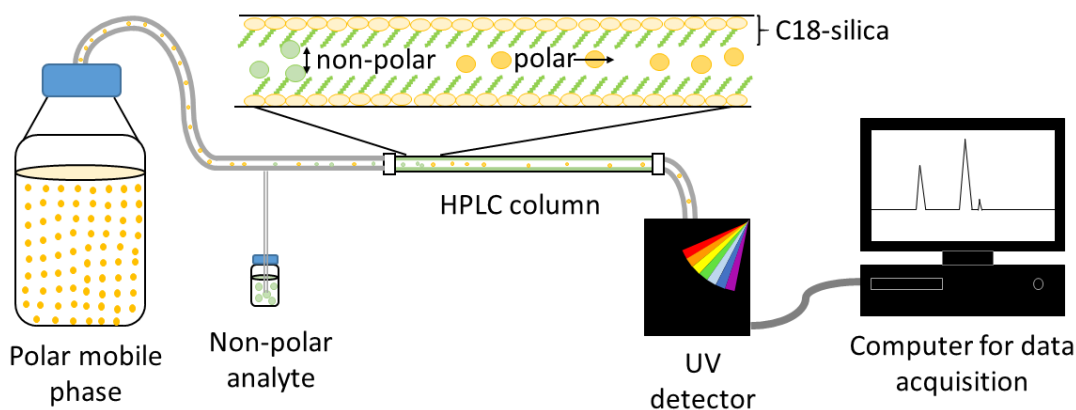
Figure 3.1: A schematic representation of RP-HPLC separation of materials based on polarity and detection and quantification using UV-analysis. *A polar mobile phase flows through a non-polar stationary phase, whereby non-polar analytes interact with the stationary phase leading to slower transition through the HPLC column. When the drug of interest is eluted through the column, its presence is detected as a result of a change in absorbance at a wavelength specific for that molecule. The change in absorbance over time is then picked up by a computer in the form of an HPLC spectra which may then be utilised to determine unknown drug concentrations.*

Despite the naming systems used for HPLC, RP-HPLC is most commonly used due to its ease of use and adaptability as well as enabling the separation and quantification of a wide range of molecules. In comparison, NP-HPLC is advantageous in instances where the material to be detected is insoluble or degrades in water, if the molecule is highly hydrophobic (Vaisman *et al.*, 2005), or to promote the separation of molecular isomers (Perrin *et al.*, 2002).

3.1.3   Defining parameters for the development of a successful HPLC method

Upon development of a suitable HPLC method for the quantification of IOX within test samples, it is important to achieve high levels of accuracy, specificity, precision and sensitivity as outlined in the International Conference on Harmonisation of Technical Requirements for Registration of Pharmaceuticals for Human Use (ICH) Harmonised Tripartite Guidelines (2005). These guidelines are often referenced in information published by both the FDA (2015) and the United States Pharmacopeia (USP), which describe the validation of analytical techniques upon highlighting the parameters which must be met to ensure a reliable and robust method of work. These parameters include the measurement of range and linearity, accuracy, precision, specificity and limits of detection and quantification.

The range of the analytical method refers to all samples tested between the upper and lower concentrations while the linearity describes the relationship between these increasing concentrations and the peak area detected using HPLC. It is important that the range of standard samples tested express an acceptable level of linearity, accuracy and precision in order to be used to determine unknown concentrations of lipids or IOX within liposomal

samples. In order to obtain reliable results, unknown test sample concentrations should fall somewhere within the range of concentrations prepared for standard analysis. Method accuracy is defined as the degree of closeness between test sample concentrations and the true concentration where the measured concentration is taken as a percentage of the expected concentration to determine the similarity when compared between these values. Analytical precision is tested in order to determine the degree of closeness between repeat measurements of a single sample at a specified concentration under identical experimental conditions, also known as intra-day precision. In comparison, inter-day precision accounts for differences observed between random variations which may arise through analysis of samples on different instruments or on different days. The relative standard deviation (RSD) value, also known as the coefficient of variance, is calculated to compare the degree of uncertainty between different measurements as a method of defining precision and repeatability. Acceptable ranges are identified where RSD $\leq$ 2 %. The limit of detection (LoD) refers to the lowest concentration of the test sample which can be detected, while the limit of quantification (LoQ) refers to the lowest concentration which can be accurately and reproducibly quantified. Usually analysis of these limits is determined as a ratio when comparing the baseline signal/ noise ratio; however, in instances where baseline noise is not present, an alternative method can be used. In this instance, the LoQ was measured as the lowest concentration measured within a defined acceptance range of $\pm$ 10 % and the LoD estimated as the lowest concentration which produced a visible representative peak. Both of these parameters will be tested using the method developed for the quantification of IOX within a solution of 90: 10 % (*v/v*) IPA and PBS (pH 7.4). The validation criteria for each parameter must be met in order to confirm HPLC method quality and robustness for the quantification of IOX within unknown test samples.

3.1.3.1 *Range and linearity*

In accordance with the European Medicines Agency (EMEA)'s ICH guidelines (2006) Q2 (R1) on the validation of analytical procedures such as HPLC, a minimum of 5 drug concentrations should be prepared for standard sample analysis. The target concentration of IOX was considered to be 125 µg mL^{-1} and standard samples are to be prepared within a range between 0 and 200 % of this target concentration, as described by Shabir (2004). The line of regression should be plotted in order to show the linearity of increasing drug concentration on the area under the curve measured using HPLC. In addition to this, the description of correlation coefficient (R^2) and y-intercept should be reported. The acceptance criteria for of linearity has been reported to be where the $R^2 \geq 0.998$ (Shabir, 2004).

3.1.3.2 Accuracy

The accuracy is a third parameter which should be determined in order to support the use of HPLC as a process for the quantification of IOX. The ICH guidelines prepared by the EMEA (2006) define this as 'the closeness of agreement between the value which is accepted either as a conventional true value or an accepted reference value and the value found' at a specified drug concentration. Accuracy is measured as the percentage of sample recovered in comparison to a defined standard response (Equation 3.1). A minimum of 9x measurements of individual sample preparations are recommended over 3 concentrations. Acceptability of these measurements has been recognised as a percentage recovery of 100 ± 5 % over the range of 50 – 150 % of the target concentration.

Equation 3.1: Calculation used for the determination of IOX recovery.

$$Recovery\ (\%) = \frac{mean\ measured\ conc.}{true\ conc.} \times 100$$

3.1.3.3 Precision

In comparison to accuracy measurements, the precision of an analytical procedure is 'the closeness of agreement (degree of scatter) between a series of measurements obtained from multiple sampling of the same homogeneous sample' (EMEA, 2006). In this instance, a minimum of 6 measurements at the target concentration should be taken which is defined as the measurement of intra-day precision, the same repeated measurements performed on different days, or in a different lab using different analytical equipment is defined as inter-day precision. Both of these criteria can be defined as being acceptable if the RSD is < 1 % for intra-day precision and < 2 % for inter-day precision measurements (Shabir, 2004). Precision analysis may also be measured in a number of different ways, but is generally used to analyse the repeatability of an analytical method under specified conditions.

3.1.3.4 Specificity

The specificity of the described HPLC method for the detection of IOX was tested in order to determine if the presence of other components in tests samples, such as surfactant and cholesterol, exerted any interference with results. Due to the choice of a direct method for the quantification of IOX encapsulation, whereby NIVs are destroyed in the presence of solvent, it is important to show that the presence of these molecules do not alter the interpretation of results. In comparison to indirect methods of measuring encapsulation efficiency, which involves measuring the amount of free drug not encapsulated by NIVs and subtracting this from the initial amount added during synthesis, direct methods offer an advantage of being more accurate due to a reduction in the opportunity for experimental error. Specificity can be

determined upon visualisation of a spectra without any interfering peaks at the time point whereby IOX is eluted (Shabir, 2004).

3.1.3.5 *Limit of quantification and limit of detection*

The limit of quantitation can be used to describe the lowest level of IOX which can be quantified with an appropriate level of precision and accuracy, in comparison, the LoD is defined as the lowest amount of IOX which can be detected, without being accurately quantified (EMEA, 2006). These values are usually determined as a ratio of peak height, or signal, in comparison to the baseline noise (S/N), whereby an S/N ratio of 10 is used to define the LoQ. The LoD is the lowest amount of IOX that can be detected above the baseline noise and is typically described as being three times the noise level, whereby the S/ N ratio is equal to 3. In order to determine the S/N ratio, the baseline must exhibit some degree of background noise. Using the method outlined in these experiments, little to no baseline noise was observed, even at low concentrations of IOX which were not accurately quantifiable but still produced a peak representative of IOX. Instead this study based the LoQ on the lowest dose which could be accurately measured and expressed a mean sample recovery within the acceptable range of $\pm$ 10 %. The LoD was estimated upon visualisation of IOX peaks at low concentrations.

3.2 Chapter aims and objectives

The aim of this chapter is to first validate a robust and accurate HPLC method for the quantification of IOX based on methods previously described in the literature, enabling the determination of drug encapsulation within NIVs post-synthesis and during stability analysis. Finally, the described HPLC method will be used to determine the release profile of IOX-NIVs under physiologically relevant conditions. The objectives to be met in this chapter are to:

- Successfully validate an HPLC method suitable for IOX quantification while meeting FDA and USP-recommended criteria upon defining the following parameters:
  - The quantifiable IOX concentration range, linearity of the range of concentrations tested, accuracy between different IOX preparations, precision of repeat measurements, the specificity of the method towards IOX quantification, in addition to the LoD and LoQ values.
- Quantify IOX entrapment within IOX-NIV post-synthesis after separation using ultracentrifugation.
- Determine the effect of typical storage and extreme temperatures on IOX entrapment after hydration with PBS over a 37 week period.
- Quantify the release of IOX from IOX-NIV under physiologically relevant conditions.

Upon completion of these objectives it will be possible to accurately quantify IOX-entrapment within NIVs in order to define NIV characteristics, shelf-life and recommended storage conditions, as well as using *in vitro* experiments to predict efficacy and release *in vivo*. Each of these factors must be defined in order to meet the standards required for the transition of a product from research and development to the clinical setting.

3.3   Materials and methods

3.3.1   HPLC quantification of IOX

HPLC-grade acetonitrile (ACN) and isopropyl alcohol (IPA) were purchased from VWR Chemicals and Fisher Chemicals, respectively, while water was purified using a Millipore Milli-Q system. IOX was obtained in the form of Omnipaque300 (GE Healthcare, Norway).

HPLC analysis was performed using the DIONEX system with GINA 50 autosampler, P580 pump and UVD1705 UV detector. IOX was isocratically eluted through a C18 Kromasil® column (250 x 4 mm; particle size: 5 µm; Hichrom Ltd) and detected at a wavelength of 245 nm. The method used was similar to that described by Cavalier *et al.* (2008), whereby the mobile phase was prepared as a mixture of 95: 5 % H$_2$O/ ACN) and the pH adjusted to 3.0 using 85 % (*v/v*) orthophosphoric acid. Prior to use, the mobile phase was filtered and degassed by passing it through a cellulose nitrate membrane (Whatman; 5 µm pore size) under vacuum. In comparison to the method described by Cavalier *et al.*, (2008) the flow rate of the mobile phase was lowered from 1.0 mL min^{-1} to 0.7 mL min^{-1} which typically resulted in a pressure between ~270 bar when maintained at room temperature. Data was obtained using Chromeleon software (v 6.80 SP2) and peak integration was determined manually by following baseline-to-baseline integration which was maintained consistent for both standard and test sample analysis. The peak area of unknown concentrations of IOX was compared to a standard concentration graph previously prepared where the peak area (mAU*min) of IOX was plotted against known concentrations.

3.3.2   Preparation of unknown samples and IOX standards

Standard samples used to validate the HPLC method for IOX quantification were prepared by first creating a stock solution whereby Omnipaque 300 (647 mg mL^{-1}) was diluted in a 9: 1 solution of IPA/ PBS to obtain an IOX stock concentration of 647 µg mL^{-1}. The use of 9: 1 IPA/ PBS was selected as a diluent in order to mimic test sample preparation. The stock solution, was diluted to achieve a maximum standard concentration of 300 µg mL^{-1} which was serially diluted 1 in 2 so that triplicate concentrations ranging from 18.75 to 300 µg mL^{-1} were obtained. Standard samples were prepared every 1 month, based on the analysis of inter-day precision, prior to the analysis of IOX encapsulation and release from NIVs during long- and short-term stability experiments.

After ultracentrifugation of test samples, the supernatant was discarded and the lipid pellet dissolved in 9 mL filtered IPA which was sonicated for 10 mins in order to ensure complete disruption of NIVs and release of entrapped IOX. A 1 mL volume of PBS was added to the solvent-lipid mix in order to solubilise IOX and a sample was diluted 1 in 10 in a 9: 1 solution

of IPA/ PBS in order to obtain IOX at a concentration within the target range prior to HPLC analysis. The encapsulation efficiency of IOX-NIVs post-synthesis and after specified storage conditions was determined by taking the amount of IOX quantified after pellet destruction as a percentage of the initial amount of IOX used during IOX-NIV synthesis (Equation 3.2). The determination of short-term release of IOX from NIVs was performed by measuring the amount of IOX released through a dialysis membrane.

Equation 3.2: Calculation for the direct determination of IOX encapsulation.

$$Encapsulation\ (\%)\ =\ \frac{encapsulated\ conc.}{initial\ iohexol\ conc.}\times 100$$

3.3.3 Acceptance criteria for HPLC method validation for the detection of IOX

The acceptance criteria was dependent on the parameter being tested as described earlier (Section 3.1.3). For all measurements the RSD % was also reported. In general, an RSD < 2 % validates the performance of an appropriate method of IOX quantification. The only exception to this rule is observed upon the measurement of intra-day precision, whereby repeat measurements of the same concentration of IOX is expected to have an RSD < 1 %. The RSD is defined as the standard deviation (σ) of measurements as a percentage of the mean (μ) (Equation 3.3).

Equation 3.3: Calculation for determining the RSD between standard measurements.

$$RSD\ (\%)\ =\ \frac{\sigma}{\mu}\times 100$$

3.3.4 Separation of IOX from IOX-NIVs using ultracentrifugation

IOX encapsulation within NIVs was determined by first separating external media containing free IOX from IOX-NIVs. Previous research performed by the Mullen group (Alsaadi, 2011), in combination with earlier size characterisation highlights the appropriateness of this method (Section 2.5.3). Immediately after the synthesis of 3x individual batches of IOX-NIV, 100 µl of pro-IOX-NIV was hydrated to a volume of 12 mL PBS within ultracentrifugation tubes and a cloudy suspension was observed to form. The same hydration process was performed for pro-IOX-NIV samples which were stored at various temperatures (4, 25, 37 and 50 °C) for different time points up to 37 weeks, The tubes were placed into a T40 Beckman ultracentrifuge rotor and each tube was balanced according to weight. Samples were centrifuged using a Beckman ultracentrifuge at 36 k rpm for 1 h at 4 °C.

3.3.5 Performance of short-term IOX-NIV release studies

Cellulose dialysis membrane (14 kDa MWCO; Sigma) was prepared by boiling in dH_2O 1 h followed by several rinsing stages using fresh dH_2O. A 1 mL volume of IOX-NIV, obtained after ultracentrifugation and resuspension in 10 mL PBS, was added to a small length of dialysis membrane. The tubing was submerged in 5 mL pre-warmed PBS (pH 7.4, 37 °C) which was subjected to constant agitation by the presence of a magnetic stirrer and maintained at 37 °C for a total of 72 h. At specified time points a 500 µl aliquot of dialysate was removed for testing and replaced with 500 µl fresh PBS. Samples removed from the dialysate were diluted in a 10x volume of IPA (4.5 ml) to obtain a similar sample composition to that obtained upon destruction of NIVs during EE % studies. The amount of IOX released from IOX-NIVs over time was represented as a percentage of the entrapped concentration of IOX which was determined in EE % studies (Equation 3.4).

Equation 3.4: Calculation for the quantification of IOX short-term release from IOX-NIVs.

$$IOX\ release\ (\%)\ =\ \frac{released\ IOX}{encapsulated\ IOX}\ \times 100$$

3.3.6 Statistical analysis

Microsoft Excel was used to determine averages, SD, and RSD % values for all data. Minitab was used to perform ANOVA tests with Tukey comparisons when analysing the effect of time on the EE % of IOX-NIVs. Statistical significance was assumed where $p < 0.05$.

3.4 Results

3.4.1 HPLC method validation for the quantification of IOX

3.4.1.1 Range and Linearity

IOX was identified as a single narrow peak at a RT of 4.6 min (Figure 3.2). The measured HPLC response, in the form of the area under the curve (AUC) was plotted against 7 increasing IOX concentrations, between the range of 0 and 250 µg mL^{-1}, correlating to concentrations between 25 to 200 % of the target concentration. An $R^2 = 0.998$ highlights the strong linear relationship between IOX concentration and peak area within the range tested (Figure 3.3). The y-intercept was found to be 2.287, which, as a percentage of the target concentration response of 59.28 mAU*min, correlates to 4 %. The residual sum of squares (RSS) of the line of regression was found to be 31. RSD % values calculated for each triplicate sample preparation was < 2 %, highlighting the suitability of this HPLC method for the quantification of IOX at concentrations between 25 and 200 % of the target concentration of 125 µg mL^{-1} (Table 3.3.1: **Assessment of linearity and range of IOX calibration standards**.
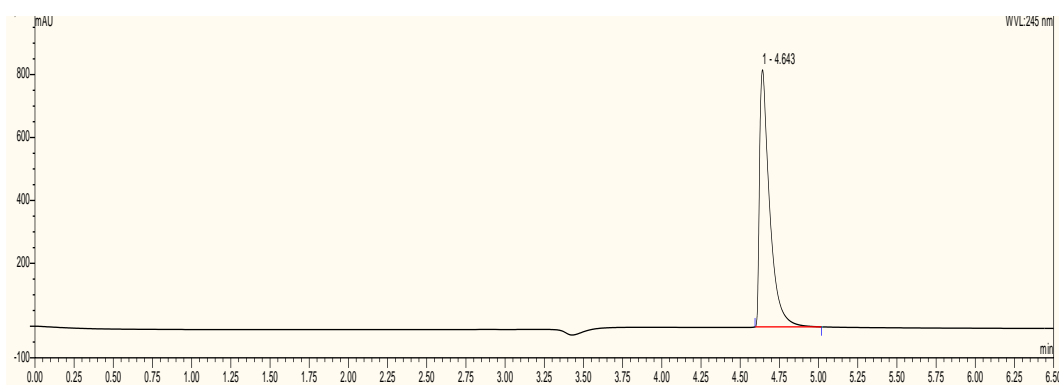
Figure 3.2: HPLC chromatograph of IOX at a target concentration of 125 µg mL^{-1}. *The sample dilution was prepared in a solution of 90 % IPA.*
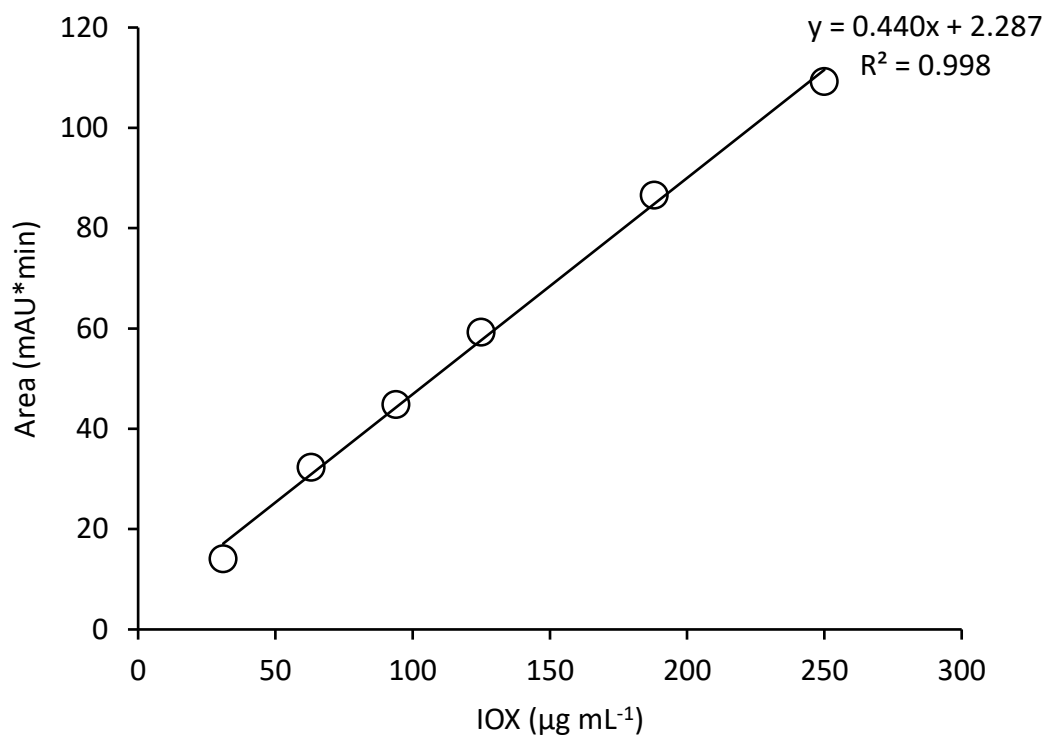
Figure 3.3: Linearity of HPLC calibration curve for the quantification of IOX *(n = 3; ± SD – values are too small to be visualised).*

Table 3.3.1: Assessment of linearity and range of IOX calibration standards.

IOX (% of target)	IOX (µg mL⁻¹)	Peak area (mAU*min) (± SD, n = 3)	RSD (%)
25	31	14.05 ± 0.06	0.43
50	63	32.38 ± 0.08	0.24
75	94	44.84 ± 0.04	0.08
100	125	59.28 ± 0.14	0.24
150	188	86.59 ± 0.33	0.38
200	250	109.25 ± 0.31	0.29

R^2 = 0.998; slope of regression = 0.440; y-intercept = 2.287; RSS = 31

3.4.1.2 Accuracy

The method accuracy was reported to be 96 ± 3 % across the range of the 4 IOX concentrations tested (63 - 188 µg mL⁻¹) (

Table 3.3.2). The recovery (%) for 63, 94, 125 and 188 µg mL⁻¹ was 98, 100, 101 and 95 %, respectively. All RSDs were < 2 % for all concentrations.

Table 3.3.2: **Assessment of accuracy of IOX calibration standards.**

IOX (% of target)	IOX (µg mL⁻¹)	Recovery (%)	RSD (%)
50	63	98	0.24
75	94	100	0.25
100	125	101	0.14
150	188	95	0.18
	Average	96	
	± SD	3	

3.4.1.3 Intra-day precision

Intra-day precision was determined by comparing the results obtained from 6 repeat measurements of a single standard IOX sample, prepared at a target concentration of 125 µg mL⁻¹. Each repeat measurement, performed on the same day, expressed similar RTs (4.63 ± 0.01 min), peak heights (779.73 ± 1.67 mAU) and peak areas (60.25 ± 0.10 mAU*min). The low standard deviations were reflected by low RSD values for each measurement reported (Table 3.3.3). The RSD values for RT, peak height and peak area was 0.15, 0.21 and 0.16, respectively.

Table 3.3.3: Demonstration of repeatability of IOX quantification at a target concentration of 125 µg mL⁻¹.

Measurement	RT (min)	Peak height (mAU)	Peak area (mAU*min)
1	4.62	779.19	60.09
2	4.63	779.04	60.25
3	4.63	779.79	60.33
4	4.62	781.11	60.32
5	4.63	782.01	60.34
6	4.64	777.26	60.19
Average	4.63	779.73	60.25
± SD	0.01	1.67	0.10
RSD (%)	0.15	0.21	0.16

3.4.1.4 Inter-day precision

In comparison to the analysis of intra-day precision, inter-day precision was determined by comparing repeat IOX standard sample measurements over the course of different days. The inter-day precision and stability of IOX standards in 9: 1 IPA/ PBS was monitored over a total of 28 days. When comparing t = 0 and 28 days there was little difference between the lines of regression for increasing IOX concentration vs the area under the curve and the R^2 value

remained unchanged at 0.996 for across both time points (Figure 3.4). The precision of quantification of 94 µg mL^{-1} IOX (75 % of the target concentration) over the 28 days storage at RT was plotted to show that the values remained relatively consistent and close to the desired value of 100 % (Figure 3.5; Table 3.3.4). The RSD values of both the RT and recovery % were both ≤ 2 % over the course of the 28 day analysis period.
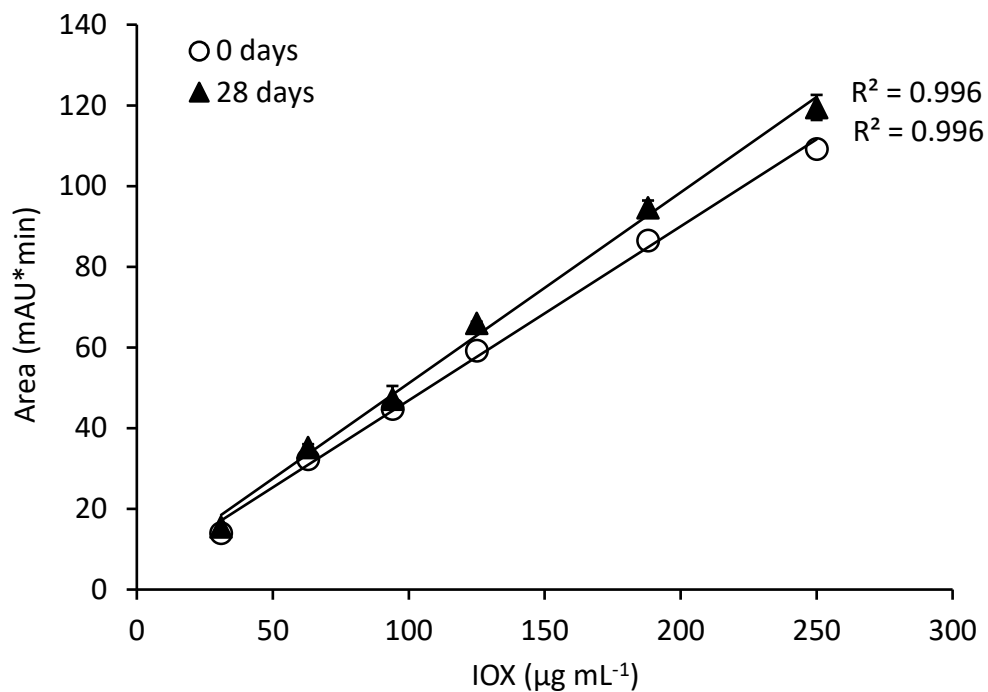
Figure 3.4: Linear relationship between increasing IOX concentrations and stability after 28 days. *Standard dilutions were prepared in 90 % IPA (n = 3; ± SD).*
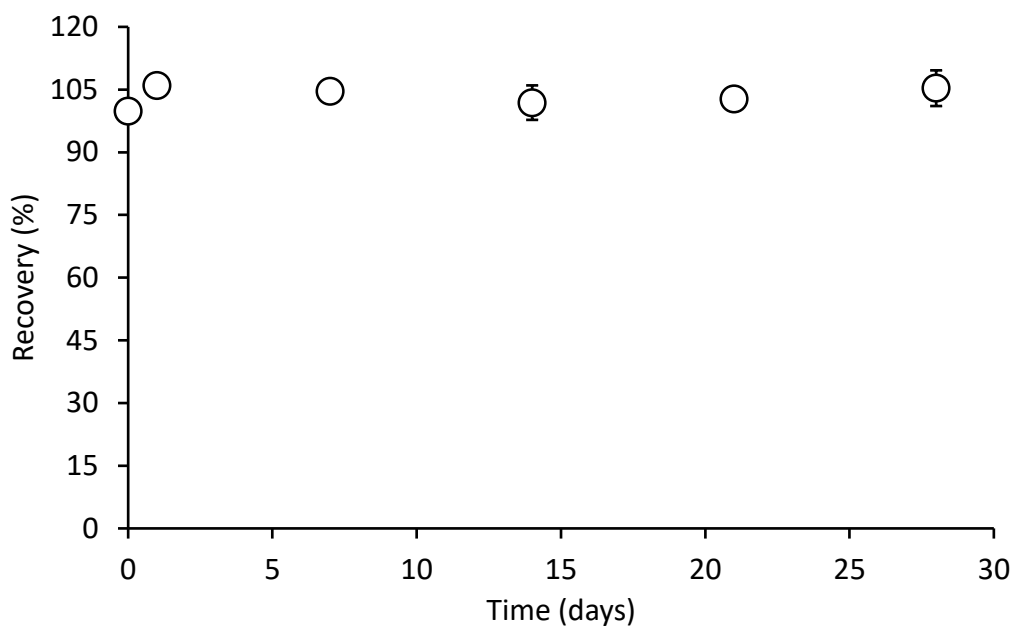
Figure 3.5: Effect of standard sample storage time on IOX quantification and intraday precision at a concentration of 94 μg mL^{-1} IOX over a total period of 28 days at RT *(n = 3; ± SD).*

Table 3.3.4: **Assessment of intraday precision of IOX.** *Statistical comparisons were performed on the average RT and % recovery of repeat measurements of a single preparation of 94 μg mL^{-1} IOX over a total period of 28 days at RT.*

Time (days)	*IOX (μg mL^{-1})*	*RT (min)*	*Recovery (%)*
0	94	4.63	100
1	94	4.63	106
7	94	4.63	105
14	94	4.65	102
21	94	4.71	102
28	94	4.71	106
Average		4.66	104
± SD		0.04	2
RSD		0.87	2

3.4.1.5 Specificity

In order to identify any potential interference in the ability to quantify IOX in unknown test samples, where NIVs were dissolved in 9x excess IPA, standards were prepared at the target concentration and spiked with 10 % (*v/v*) empty-NIVs. Analysis of this sample lead to the generation of a spectra with no additional or interfering peaks which may have been related to the presence of NIV components. In addition, the presence of the lipid components of NIV had no effect on characteristic IOX retention time (4.6 min) or peak shape (Figure 3.6).
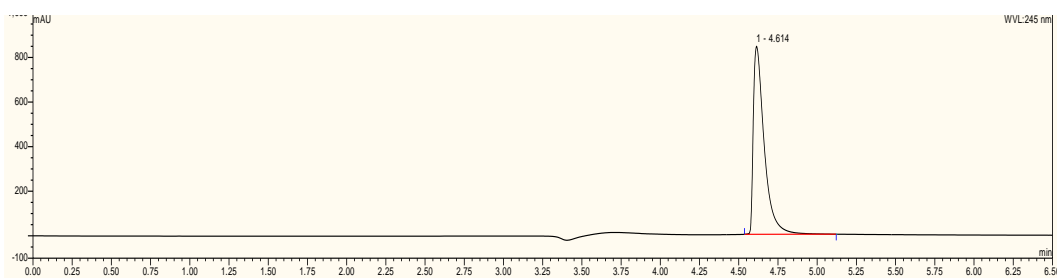
Figure 3.6: HPLC chromatogram showing method specificity for IOX quantification in the presence of 10 % (*v/v*) NIV.

3.4.1.6 Limit of quantitation and detection

In this set of experiments, the LoQ was determined based on the lowest concentration of IOX measured which expresses an average sample recovery within the acceptable error range of $\pm$ 10 %. Out of the all the concentrations tested, 25 µg mL^{-1} was the most appropriate concentration tested to describe the LoQ. Analysis of 25 µg mL^{-1} IOX lead to an average recovery of 93 %. As the concentration decreased to 19 µg mL^{-1}, the relative error became greater than the 10 % range deemed to be acceptable (Figure 3.7). Visualisation of the IOX chromatogram at 25 µg mL^{-1} showed a clear, quantifiable peak at the expected RT (Figure 3.8). The LoD of IOX was defined as 13 µg mL^{-1}.
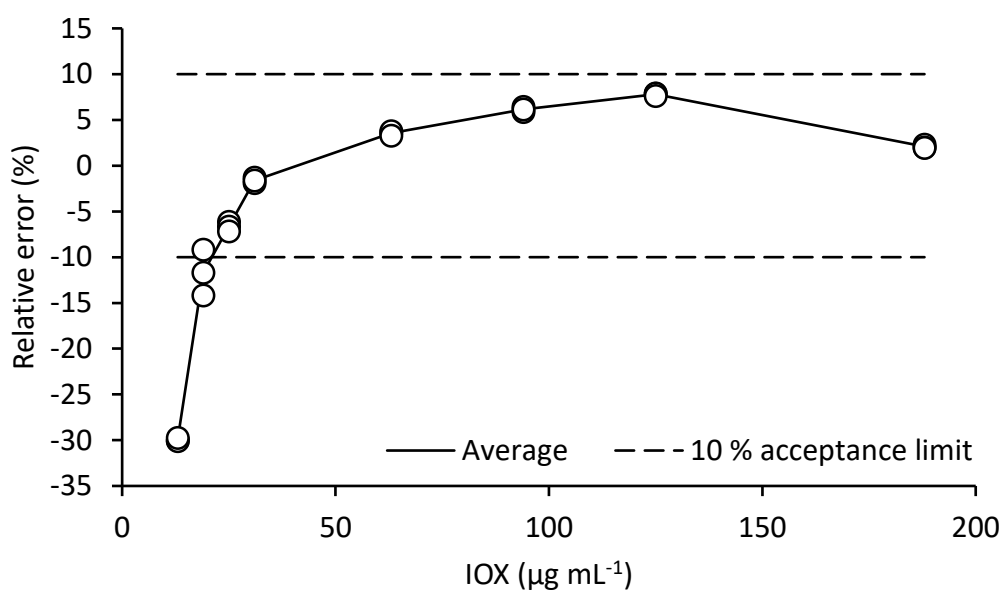
Figure 3.7: Range of relative error in HPLC analysis of increasing concentrations of IOX for identification of the estimated LoQ for IOX quantification. *Three repeat measurements are represented by open circles while the average response was plotted as a solid line. The acceptable 10 % error range for defining the LoQ was represented by 2 dashed lines.*
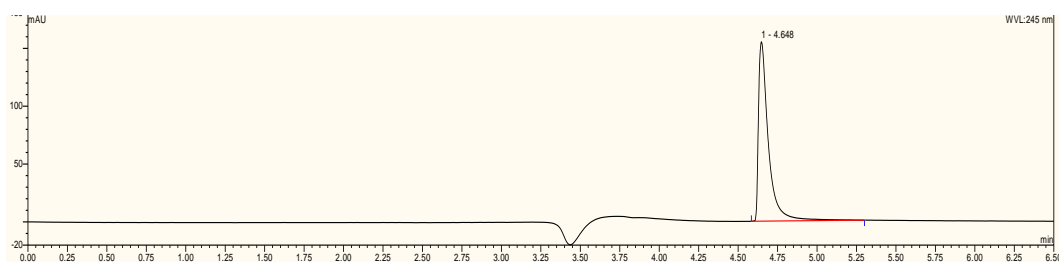
Figure 3.8: **HPLC chromatogram of IOX at the estimated LoQ defined as 25 µg mL^{-1} IOX.**

3.4.2 Encapsulation efficiency of IOX-NIVs before and after long-term storage

IOX entrapment was directly quantified, using the aforementioned HPLC method, after the synthesis of three separately prepared batches of IOX-NIV. Similar IOX entrapment efficiencies were quantified regardless of batch (Table 3.3.5). The average encapsulation efficiency was determined to be 22 ± 3 %. The EE % of IOX-NIVs, after storage in the pro-NIV form, was monitored over 37 weeks at temperatures of 4, 25, 37 and 50 °C in order to determine the effect of long-term storage conditions on the chemical stability of IOX-NIVs. A time- and temperature-dependent effect on the ability of NIVs to encapsulate IOX was observed (Figure 3.9). Throughout the 37 week storage period at 4 and 25 °C there was no significant decrease in IOX EE %. When t = 0, IOX-NIVs expressed an EE % of 22 ± 3 %, over the course of the 37 week storage period at 4 °C EE % ranged from 18 ± 4 % after 2 days and 26 ± 7 % after 28 weeks, with a final EE of 25 ± 2 %. The differences in EE % immediately post-synthesis were not significantly different when compared to these time points. A similar pattern was observed at 25 °C whereby EE ranged from 16 ± 7 % after 2 days storage, and 22 ± 4 % after 27 weeks. Again these differences were not found to be significant in comparison to the EE post-synthesis.

Table 3.3.5: Summary of encapsulation efficiency and physical characteristics of 3 batches of IOX-NIV.

Batch	Encapsulation efficiency (%)	Size (Z-average; d.nm)	PDI	Zeta potential (mV)
1	19	193	0.14	-24
2	24	231	0.08	-23
3	22	187	0.15	-28
Average	22	204	0.13	-26
± SD	3	24	0.04	1

Storage of pro-IOX-NIVs at increased temperatures of 37 and 50 °C led to an overall decrease in hydrated IOX-NIV EE %, which was further reduced as time increased (Figure 3.9). The first significant reduction in EE was observed after 16 weeks storage at 37 °C where IOX-NIV

EE % was 9 ± 1 % (p < 0.005). A gradual decline in EE was observed as time increased and the lowest measurement was 5 ± 2 % after 37 weeks (p < 0.005). A similar loss in EE was observed when pro-IOX-NIVs were stored at 50 °C - EE dropped from 22 ± 3 % (t = 0) to 15 ± 1 % after 4 weeks storage, although this decrease was not found to be significant. As storage time increased to 12 weeks at 50 °C, the EE of IOX-NIV significantly decreased to 9 ± 4 % which continually decreased until an EE % of 4 ± 3 % was reached after the total 37 week storage period (p < 0.0001).
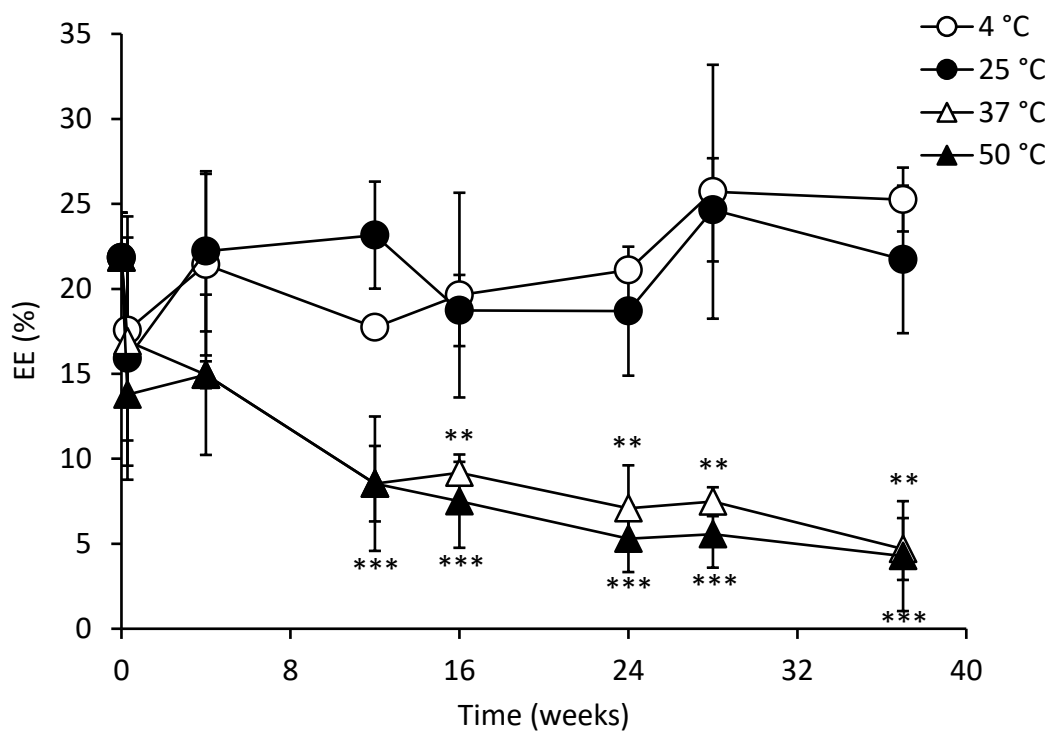
Figure 3.9: Effect of storage time and temperature on IOX-NIV encapsulation efficiency *(** p < 0.005; *** p < 0.0001; n = 3; ± SD).*

3.4.3   Release of IOX from NIVs under physiological conditions *in vitro*

IOX-NIV EE % following ultracentrifugation and resuspension in PBS was carried out as described previously (Section 3.3.5). Measurement of IOX release from hydrated NIVs into PBS at 37 °C generated a typical release curve whereby the majority of IOX (67 ± 6 %) was released within 24 h (Figure 3.10). After 48 h, 73 ± 2 % of IOX initially encapsulated within NIVs leaked out without any further significant changes with increased incubation time.
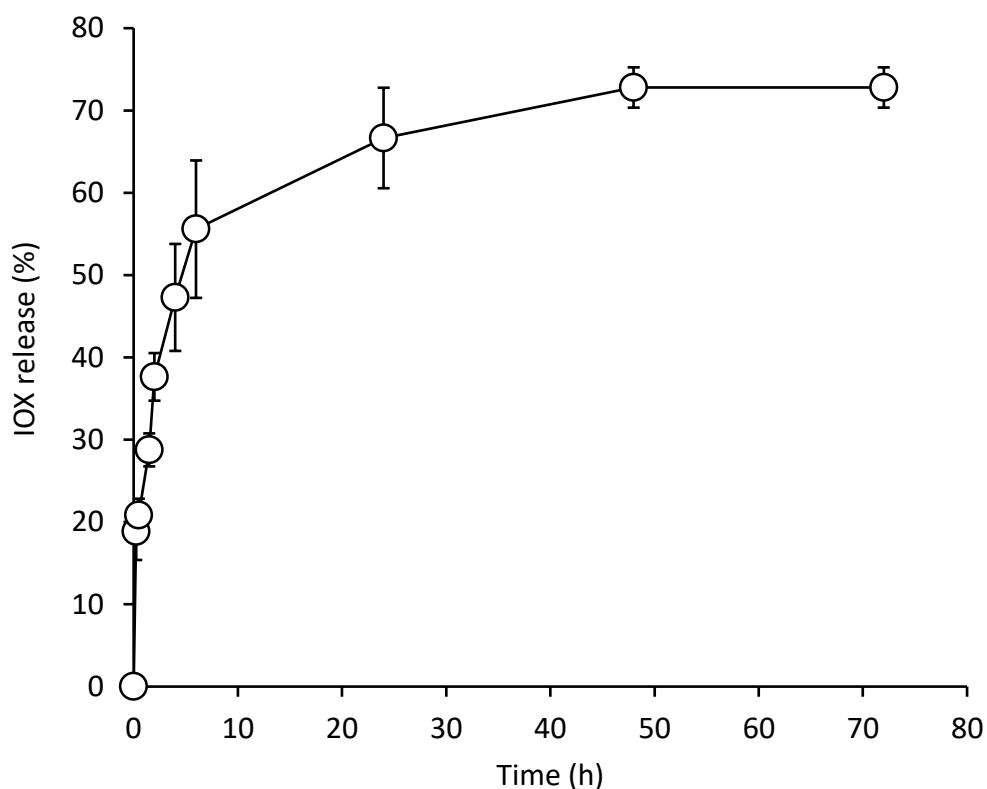
Figure 3.10: Short-term release of IOX from NIVs across dialysis membrane and into PBS under physiologically relevant conditions *(37 °C; n = 3; ± SD).*

3.5 Discussion

3.5.1 Validation of an HPLC method for the quantification of IOX

An adapted version of the HPLC method described by Cavalier *et al.* (2008) was validated for IOX samples prepared in a 9: 1 (*v/v*) solution of IPA/ PBS whereby a singular peak representative of IOX could be obtained. The visualisation of two IOX peaks during chromatographic detection of IOX is not uncommon due to the chemical nature of IOX. Although a number of potential points of IOX isomerisation were initially described, only the N-acetyl endo-/exo-isomers were identifiable using HPLC (Foster and Sovak, 1988). Here it was shown that conversion between these forms occurs rapidly at physiological temperature in H_2O, and it was concluded that the two isomers visualised using this HPLC method could be assumed to represent a single molecule of IOX. Successful validation of an HPLC method for the quantification of IOX, represented as two isomeric peaks, has been reported using a number of different methods (Cavalier *et al.*, 2008; Chaloemsuwiwattanakan *et al.*, 2016; De Baere *et al.*, 2012; Farthing *et al.*, 2005; Schwertner and Weld, 2015).

Previous research which has focused on the clear separation of IOX isomeric forms using HPLC described a preference for the use of increasing proportions of MeOH during gradient separation, in comparison to ACN, as the main solvent of choice (De Baere *et al.*, 2012). Therefore, it may be assumed that the use of ACN as the mobile phase solvent, instead of MeOH, could improve single peak resolution as observed here. IOX is also a highly polar molecule that readily dissolves in H_2O. The interaction of IOX as a single unit or in its isomeric form, with a non-polar C18 stationary phase would be poor. This will explain the low retention time (4.6 min) and inability to visualise the different isomers.

Schwertner and Weld (2015) described improved peak resolution through the use of a C18 column in comparison to a C8. Their method also saw the visualisation of both isomeric forms of IOX. However, it was noted that sensitivity could be increased if the two isomers could be combined upon analysis. The visualisation of 1 singular peak in these experiments suggests improved sensitivity of the HPLC method for the quantification of IOX. Despite this, Schwertner and Weld (2015) described a more sensitive assay with an LoQ of 10 µg mL^{-1} in comparison to the LoQ described here (25 µg mL^{-1}).

3.5.1.1 Range and linearity

Over an IOX concentration range, spanning 25-200 % of the target concentration of 125 µg mL^{-1}, a high level of linearity with an R^2 of 0.998 confirms the acceptability of this range as defined by Shabir (2004). Low RSD values (< 2 %) obtained from the analysis of triplicate dilutions of IOX were also in line with defined acceptability criteria. The

appropriateness of the described HPLC method for quantifying IOX was deemed satisfactory in terms of range and linearity. The maximum range of linearity was not tested in this set of experiments; however, other research has described good linearity over a wide range of concentrations between 10 and 1500 µg mL^{-1} (Schwertner and Weld, 2015).

3.5.1.2 Accuracy

In order to determine method accuracy, the percentage of recovered IOX was calculated from a second batch of test samples spiked with known IOX concentrations. As outlined by the EMEA's ICH (2006), triplicate samples over a minimum of 3 different concentrations were tested for accuracy – in this instance, 4 concentrations ranging from 63 - 188 µg mL^{-1} IOX were reported. The concentrations selected include those within the range of 50-150 % of the target, which is recommended for the validation of a quantitative assay (Shabir, 2004). The % recovery of IOX at each level remained within the acceptable range of ± 5 %, while all RSD values calculated upon analysis of triplicate samples were within the acceptable limit of < 2 % (Shabir, 2004). This data supports the potential for the described HPLC method for the accurate quantification of IOX. In comparison, alternative methods which tested accuracy at greater concentrations (50-1500 µg mL^{-1}) reported accuracies between 89 and 108 % of the expected values (Schwertner and Weld, 2015).

3.5.1.3 Intra-day precision

Intra-day precision was measured by performing 6 repeat measurements of a single preparation of IOX at the target concentration of 125 µg mL^{-1}. The precision of the method was deemed acceptable for IOX quantification due to the low RSD values (< 1 %) which were reported for IOX RT, peak height and peak area.

3.5.1.4 Inter-day precision

Shabir (2004) defined the inter-day precision acceptability as an RSD value ≤ 2 % after repeat measurements of a preparation of a defined analyte concentration. Upon analysis of IOX at 94 µg mL^{-1} over a total of 28 days, the accuracy when comparing each measurement taken on different days was found to express an RSD of 2 which is within the acceptance criteria. The RSD value calculated between RTs was also ≤ 2. This highlights the stability of IOX after dilution within a solution of 9: 1 IPA/ PBS, even after a storage time of 28 days at RT. In addition this provides evidence to support the accuracy of the HPLC method. Based on this data standard samples were prepared fresh every 1 month during the analysis of IOX-NIV long-term stability.

3.5.1.5 Specificity

The specificity of the HPLC method for IOX in the presence of dissolved lipid components that would be present in samples obtained after the destruction of NIVs was tested. Analysis of the spectra showed an absence of any interfering peaks and the measurement of an unaltered RT which supports method specificity for IOX even in the presence of materials likely to be found in test samples. The lack of chromophores on lipid components such as surfactant 8, cholesterol and DCP explain the reason for the absence of peaks or interference using UV detection which was observed upon the analysis of a sample which mimics test sample conditions.

3.5.1.6 Limit of quantification and detection

The LoQ obtained in this experiment correlates well with previous experiments which describe the validation of an HPLC method for the detection of IOX within patient serum samples. Shihabi and Constantinescu (1993) defined the LoQ for IOX as 25 µg mL^{-1} upon development of an HPLC method for the direct quantification of IOX within serum. Despite this, alternative HPLC methods, such as that reported by Schwertner and Weld (2015), were found to be more sensitive and reported an LoQ as low as 10 µg mL^{-1} and an LoD of 6 µg mL^{-1}. However, the LoD and LoQ of the protocol adopted in these studies was sufficient for the chemical characterisation of IOX entrapment and release as conducted within this thesis.

3.5.2 Encapsulation efficiency of IOX within NIVs

Direct quantification of IOX encapsulation within NIVs was performed by first destroying the lipid pellet in IPA, followed by the addition of 1 % (*v/ v*) PBS to ensure solubilisation of the IOX component. HPLC quantification and calculation of EE as a % of the initial concentration used during IOX-NIV synthesis detected a typical EE % of 22 %. An EE of 22 % for IOX-NIVs which, after hydration and resuspension (1 in 10 dilution) would leave a final IOX concentration of 14.23 mg mL^{-1} IOX (6.6 mg I mL^{-1})/ 31.74 mg mL^{-1} lipid, equivalent to a 1: 2 weight ratio of drug/ lipid components. Previous research describing IOX encapsulation within liposomes report similar IOX encapsulation efficiencies to that described here (Zheng *et al.*, 2006). A common liposome formulation used in a number of studies utilises DPPC/ cholesterol/ DSPE-PEG2000 at molar ratio of 55: 40: 5. In the work described by Zheng, liposomes were prepared by first dissolving lipids in EtOH prior to hydration and down-sizing using high pressure extrusion. This lead to the formation of IOX-liposomes with an EE of 19.6 ± 2.8 % when loaded alongside an MRI imaging agent (Zheng *et al.*, 2006). Other research which focused on the same formulation and method of production, but this time loaded IOX alongside a fluorescently conjugated version of DSPE reported a much lower encapsulation

efficiency of 5.9 ± 0.5 % (Huang *et al.*, 2012). The low EE presented by Huang *et al.* (2012) may be reflective of disadvantages related to the DSPE-fluorescent conjugation or it may be related to the use of extrusion as a down-sizing method. Extrusion has been reported to reduce EE as well as leading to a loss in overall lipid content (Jousma *et al.*, 1987; Patil and Jadhav, 2015). This is related to the destruction and reformation of vesicles which occurs as a result of the extrusion process leading to release of originally entrapped IOX from the aqueous core. The small size of these IOX-liposomes (82 ± 2 nm) may also have a disadvantage in achieving higher levels of drug entrapment due to the fact that a much smaller internal volume is available for IOX to reside (Huang *et al.*, 2012). An additional key difference observed when comparing these two publications may relate to the lipid concentration in which IOX-liposomes were prepared - Zheng *et al.* (2006) prepared IOX-liposomes at a lipid concentration of 200 mM while Huang *et al.*, (2012) prepared their formulation at a much lower lipid concentrations of 100 mM. In comparison, IOX-NIVs were prepared at a final lipid concentration of 150 mM which is likely to improve EE % due to the greater amount of lipid components which may form vesicular bodies leading to increased IOX entrapment. Previous research has shown potential for improving EE % upon increasing lipid concentration (Maherani *et al.*, 2012).

Despite differences in EE %, both researchers reported IOX-enhanced visualisation of organs after IV administration of IOX-liposomes *in vivo*, highlighting the efficacy of this product, even at a range of encapsulation efficiencies. Using the same formulation and similar methodology as Zheng *et al.* (2006) and Huang *et al.*, (2012), Burke *et al.* (2007) reported enhanced x-ray attenuation using IOX-liposomes in comparison to free-IOX. IOX-liposomes were monodispersed with an average diameter of 93 nm expressing a greater IOX encapsulation efficiency of ~25 % of the initial iodine content. Additional experiments have shown that liposomes with an iodine entrapment of 34.8 mg I mL^{-1} delivered intravenously to rabbits at 475 mg I kg^{-1} body weight successfully provided contrast enhancement (Kao *et al.*, 2003). The iodine-equivalent concentration of IOX within NIVs prepared in this study was 52 % greater than that reported in previous studies. It may be assumed at this stage, a non-toxic IOX-NIV system may present a safe and effective option for contrast-enhanced bio-imaging. Further experiments should be performed to determine the attenuation power of this vesicle system.

Danila *et al.*, (2009) tested the effect of lipid/ IOX ratio on the ability of liposomes to encapsulate IOX after synthesis using the TFM, followed by down-sizing using extrusion. A molar ratio of 2: 1 or 8: 1 phospholipid/ IOX had shown that there was not a great difference

between the ratio of IOX to lipid in relation to encapsulation efficiency (~ 20 %); however, the 8: 1 lipid/ IOX molar ratio enabled the highest concentration of IOX to be encapsulated at 38 mg I mL^{-1} compared to 30 mg I mL^{-1} at a ratio of 2: 1. In agreement with this previous research, it has been shown that EE % can be enhanced upon increasing the overall lipid concentration used during synthesis which is likely related to the fact that more lipid vesicles will be formed with the capability of encapsulating drug (Maherani *et al.*, 2012).

The lipid/ drug ratio is a key factor in the ability of IOX-NIV to form, as a CPP effect was observed in initial formulation experiments (Chapter 2 – Formulation and Physical Characterisation of IOX-NIV). The exact determination of this concentration was untested. However, it was concluded that immediately post-synthesis IOX-NIVs were in a pro-NIV form until further hydration with PBS. In contrast, empty-NIV were observed to form immediately upon hydration of the melted lipids, the CPP required for IOX-NIV self-assembly was most likely to be linked to the ratio of IOX-to-lipid. This feature of IOX-NIV may have been a determining factor for EE, despite this, IOX-NIV expressed a comparable EE % when compared with liposomal formulations throughout the literature.

As mentioned previously, the use of passive methods of drug entrapment, such as when a soluble drug becomes entrapped due to formation of vesicles within a drug-containing aqueous phase, hydrophilic drug entrapment is often low (< 30 %) due to limitations in the volume available within the aqueous core. This in turn highlights the potential correlation between the drug-to-lipid ratio used within the formulation and the number of vesicles formed (Akbarzadeh *et al.*, 2013). IOX entrapment within liposomes has been reported to reach 30 % upon formulation of vesicles expressing a size within the micrometre range (Wei *et al.*, 2005). Disadvantages in the administration of large vesicles have been associated with increased interactions with serum proteins, opsonisation and rapid removal from the blood (Harashima *et al.*, 1994; Liu *et al.*, 1995).

Huang *et al.* (2010) prepared IOX-liposomes that were negatively charged and expressed an average diameter of ~80 nm. These were found to have a half-life of 29 h, which is significantly greater than the half-life of free IOX. IOX-liposomes expressed a tendency to accumulate in the spleen and liver, with a portion of iodine also being detected within the kidneys. This would suggest that the bio-distribution of IOX lipid-based nanomedicines is different to that of free-IOX. It is known that IOX does not get metabolised in the body and instead is rapidly filtered through the kidneys and excreted in urine, while the kidney is the key organ affected by negative side-effects as a result of exposure to RCM. It is likely that the administration of IOX-NIV will change the biodistribution profile in comparison to free IOX,

whereby IOX-NIVs are more likely to be deposited within the liver and spleen. Pharmacokinetic experiments previously performed by the Mullen group in relation to cisplatin-NIVs, of the same formulation and delivered intravenously, had shown that the main tissues in which NIVs were deposited were the lungs, spleen, kidneys and liver, in addition to enhanced circulation and detection within the serum (Manal Alsaadi, 2011). A significant increase in the detection of cisplatin within the kidneys, in comparison to free-cisplatin, was also reported, however, in combination with other researchers, the use of lipid delivery systems has been shown to reduce the nephrotoxic properties of various drugs due to encapsulation-based inhibition of drug transport across renal tissues (Manal Alsaadi, 2011; Júnior et al., 2007). Transportation of IOX to the liver and spleen when administered within lipid vesicles may help to contribute to renal protection in patients susceptible to RCM-AKI.

IOX expresses a MW of 821 g mol^{-1} (or ~821 Da) while the glomerular filtration system of the kidneys is reported to have an estimated MWCO of 30-50 kDa (Ruggiero et al., 2010), while electron tomography identified the diaphragm slits of the nephron to be 30-40 nm wide (Wartiovaara *et al.*, 2004). The small size of free-IOX explains the ease and speed in which it is filtered from the blood by the kidneys. In comparison 30-40 nm pore sizes are vastly less than the measured diameter of IOX-NIVs which expressed a diameter closer to 200 nm, highlighting the physiological incompatibility of IOX-NIVs with the renal system. In comparison to the 15 nm physiological upper limit of certain capillaries of the renal vasculature, the capillaries of the liver have been reported to express diameters of 100-200 nm (Sarin, 2010) while splenic capillaries express a terminal diameter of 5 μm (Chen, 1978). The physiological spatial environment of the liver and spleen appears to be more favourable for the biodistribution of IOX-NIVs, particularly in comparison to the kidneys. Despite some evidence showing greater cisplatin concentrations within the kidneys as a result of its administration within liposomes and NIVs, the nephrotoxicity of cisplatin was believed to be reduced when administered in the liposome formulation due to drug sequestering and reduced drug adsorption into the renal tissues (Manal Alsaadi, 2011; Júnior et al., 2007). Similar to IOX, the majority of cisplatin is excreted through the kidneys (Siddik *et al.*, 1988), therefore it could be expected that NIVs have the potential to similarly reduce IOX nephrotoxicity based on the principles described within the literature for cisplatin.

3.5.3 Effect of storage temperature on the stability of pro-IOX-NIVs

Initial IOX-NIV stability studies were carried out to monitor the effect of time and temperature on the physical appearance of pro-IOX-NIVs as well as the size, PDI and surface charge of self-assembled IOX-NIVs after hydration (Chapter 2 – Formulation and Physical

Characterisation of IOX-NIV). In this chapter it was shown that pro-IOX-NIVs were able to maintain their typical physical appearance as a clear solution at temperatures of 4 and 25 °C for up to 37 weeks. This was paired with the observation that after storage, hydration with PBS led to the same self-assembly of IOX-NIVs expressing the same characteristic size, PDI and charge compared to that described immediately post-synthesis. Chemical analysis of IOX entrapment after long-term storage had shown a similar protective effect at 4 and 25 °C. Across the 37 week storage period, the EE % of pro-IOX-NIVs at 4 and 25 °C was observed to deviate between values ranging from 16 to 25 %. Despite the range in EE %, none of the differences were found to be significant. This may be suggestive of batch-to-batch variation and/ or variability associated with processing parameters including NIV hydration, ultracentrifugation and resuspension, rather than chemical stability of NIVs. Overall, both physical and chemical characterisation experiments highlight the suitability of long-term storage (37 weeks) of IOX-NIVs in a pro-NIV form at 4 and 25 °C. A number of publications which describe the release of IOX from liposomes upon storage at physiological conditions have been reported and will be compared to the results obtained for determining the release profile of IOX-NIV at 37 °C (Section 3.5.4). The reduced EE capability of IOX-NIV after storage at higher temperatures coincides with changes in size, PDI and charge of hydrated IOX-NIV, as well as changes in the visual appearance of the pro-IOX-NIV solution (Chapter 2 – Formulation and Physical Characterisation of IOX-NIV). Despite the evidence supporting a change in physical and chemical properties of hydrated IOX-NIV over the course of 37 weeks at temperatures of 37 and 50 °C, previous work by the Mullen group, which utilised this NIV formulation to entrap cisplatin, saw consistent cisplatin retention over a total of 469 days (i.e. 67 weeks) at temperatures of 4, 25 and 40 °C, however, cisplatin precipitation was a feature commonly observed in stored samples and there was some degree of deviation in measurements throughout the course of the experiments (Alsaadi, 2011). The reduced ability to retain entrapped drug when comparing storage of IOX-NIV and cisplatin-NIV at temperatures around 37 °C, i.e. 37 and 40 °C, respectively, may be linked to the drug itself or perhaps the interaction between the drug and lipid. Due to the fact that commercially available IOX is autoclaved for sterilisation during the manufacturing process, it seems unlikely that prolonged incubation at this temperature would significantly degrade IOX. RCM such as IOX are known to be sensitive to UV-degradation (Giannakis *et al.*, 2017), however, storage vessels were maintained in darkness at their described temperatures, and the time and temperature-dependent reduction in IOX entrapment did not appear to be associated with UV-light exposure.

Signs of lipid oxidation were identified previously after a change in physical appearance of pro-IOX-NIV, from a clear to a more yellow colour, was observed as storage time increased at higher temperatures (37 °C and 50 °C). In addition to this, the ability of hydrated IOX-NIVs to form monodispersed, charged vesicles of a typical size of ~ 200 nm were altered at similar time points to when the EE of IOX-NIVs was observed to decrease. A change in pro-IOX-NIV physical appearance was apparent after 16 weeks storage at 37 °C. It was also at this time point where the first significant reduction in EE % was observed. Alteration in pro-IOX-NIV appearance and EE % after storage at 37 °C was followed by alterations in the size and PDI of hydrated IOX-NIV after 24 weeks storage. At higher temperatures an earlier alteration in physical appearance was observed. After 8 weeks storage at 50 °C, pro-IOX-NIV expressed a strong dark-yellow colour. The earliest detection of a decrease in EE % at 50 °C was observed as early as 4 weeks, but a statistically significant difference was not observed until the 12 week time point, which coincides with the length of time taken for changes in IOX-NIV size and PDI. Alterations in surface charge after storage and hydration were not as significant as other chemical and physical properties although a significant decrease in IOX-NIV negativity was observed after 16 weeks at 50 °C.

A link between the timing of changes in appearance of pro-IOX-NIV, IOX-NIV formation and retention of initial physical and chemical characteristics were observed. A greater reduction in EE % at high temperatures and over time can be explained due to the fact that lipid degradation as a result of lipid oxidation and hydrolysis occurs over time and at a faster rate at high temperatures (Matumoto-Pintro *et al.*, 2017). Although non-ionic surfactants are less susceptible to oxidation due to the absence of unsaturated bonds, autoxidation of ethoxylated surfactant, similar to surfactant VIII, has been reported after long storage times (Bodin *et al.*, 2003). Autoxidation of unsaturated fatty acids typically arises through the generation of lipid radicals (Loftsson, 2014). The cholesterol component of IOX-NIV is also reported to be susceptible to oxidation (Valenzuela *et al.*, 2003). IOX contains a number of hydroxyl groups in its chemical structure and the presence of such are known to catalyse the hydrolysis of non-ionic surfactants (Toh and Chiu, 2013). Therefore, hydrolysis reactions may have also contributed to lipid degradation and reduced EE. Despite this, storage of surfactants below their critical concentration for the formation of vesicles has been reported to offer a level of protection (Stjerndahl and Holmberg, 2003). Similarly to the process of oxidation, the rate in which hydrolysis occurs is accelerated as temperature and time increases (Grit *et al.*, 1993b) which explains why the most significant reductions in EE was observed at a storage temperature greater than 25 °C but not at 4 or 25 °C.

3.5.4 Release of IOX from NIVs under physiological conditions

IOX-NIV expressed a release profile typical of niosomal and liposomal drug-delivery systems - whereby the majority of water-soluble drugs rapidly escape from the aqueous core. Analysis of the IOX release profile using similar dialysis methods to that described here show a 'burst' release of IOX within the initial 24 h and then reaching a plateau after 48 h at 37 °C (Huang *et al.*, 2012; Zheng *et al.*, 2006). The maximum release after the duration of analysis was ~15 %, after 96 h incubation in 45 mg mL^{-1} bovine serum albumin (BSA), and 9.1 ± 2.5 % after 15 days, as described by Huang *et al.*, (2012) and Zheng *et al.* (2006), respectively. In contrast, the total IOX release from IOX-NIVs under physiological conditions was much greater. A total of 73 % of the initially encapsulated IOX had leaked out by the end of the 72 h incubation period. This difference may be partly explained by the greatly reduced EE % (5.9 ± 0.5 %) described by Huang *et al.* (2012), whereby the initial amount of IOX available for release is much lower than the amount successfully entrapped within IOX-NIVs, rather than being related to disadvantages in IOX-NIV stability or capability for drug retention. In contrast, a similar EE of ~20 % was achieved upon the synthesis of IOX-liposomes as prepared by Zheng *et al.* (2006). In addition they had also shown minimal release of IOX under physiologically relevant conditions. This suggests the presence of alternative factors relating to the formulation may explain the reduced capability of NIVs to retain IOX under physiological conditions in comparison to liposomal formulations reported in the literature.

The phase transition temperatures of IOX-NIV was not a parameter that was tested in the scope of this thesis, nevertheless, it may have been these factors which influenced the rapid and high release of IOX under physiological conditions. A T_m of 37-38 °C for surfactant VIII, as the main structural component of IOX-NIV, is likely to lead to the rapid release of IOX when at physiological temperature. When a lipid system approaches its T_m, the lipids become more disorganised and fluid-like, meaning that IOX could easily escape due to increased membrane permeability. The lipid composition of vesicular systems has been shown to control the T_m and phase transition behaviours which subsequently influences the bilayer fluidity and hence the ability to retain encapsulated materials (Nasseri, 2005; Park *et al.*, 2014; Stott *et al.*, 2008). The incorporation of cholesterol and other lipids within the IOX-NIV formulation would increase lipid packing and reduce membrane fluidity leading to altered phase transition behaviours, such as increased T_m (Sułkowskia *et al.*, 2005), which may be characterised in future work using DSC analysis.

Any IOX which remains trapped within NIVs after administration is likely to be transported to other areas within the body, such as the spleen and liver, prior to its eventual release and

excretion through the kidneys. This could provide a mechanism for avoiding large volume (5-30 ml) acute exposure to IOX which could be of benefit to prevent direct IOX nephrotoxicity within the renal system. It is also important to consider the potential damage of re-directing IOX to organs such as the liver and spleen. A previous study which tested the effects of IOX on liver function after the performance of an angiogram did not detect an increase in liver enzymes, even in patients with pre-existing impaired liver function, however, a slight increase in creatine kinase was measured after exposure to IOX, which may in fact be indicative of renal or muscular damage (Billström *et al.*, 1987). Due to the fact that the specific time and location where IOX-NIV is likely to reside within the body has yet to be tested, caution should be taking when interpreting the potential safety benefits of entrapping IOX within NIVs, while further *in vitro* and *in vivo* work is essential. Despite this, the overall delayed renal exposure time upon administration of IOX-NIV and its ability to sequester IOX from surrounding tissues may assist in minimising the immediate risk to susceptible patients with underlying kidney and vascular problems.

3.6   Conclusion

Standard samples analysed across the concentration range of 18.5-250 µg mL^{-1} IOX showed acceptable linearity with RSD values < 2 %, in accordance with acceptance criteria and guidelines set by the ICH and FDA. An ability of the HPLC method to accurately quantify IOX within this range was shown, alongside minimal changes during the analysis of intra-day measurements (RSD < 1 %) which were analysed on the same day, and inter-day precision (RSD < 2 %) which was monitored over the course of one month. Even in the presence of NIV lipid components, IOX was successfully quantified at its characteristic retention time without any interference. This proves the specificity of this method for the identification of IOX in test samples which would include NIV lipids dissolved in solvent. Despite the description of more sensitive methods of IOX quantification in the literature, the method outlined here was found to be accurate and robust to an extent which allows for the characterisation of IOX encapsulation which is essential for both NIV characterisation and future product development. The determination of IOX EE % within NIVs is important for IOX-NIV efficacy as this will influence radiocontrast opacity and image quality *in vivo*.

An EE of 22 % is in agreement with IOX-liposomal formulations which have been reported in the literature. In addition to the work described here, it has been shown that a range of EE %, including those much less that 20 %, have shown success in enhancing CT imaging *in vivo* which suggests that IOX-NIVs will express similar potential for bio-imaging. Future work should include the measurement of IOX-NIV x-ray attenuation in comparison to free-IOX. *In vivo* work should be performed to allow for the analysis of safety and efficacy. In addition, the analysis of the toxicity profile *in vitro* is a key stage in the development of a product suitable for market and is discussed in future experiments (Chapter 4 - In vitro Toxicity of IOX, IOX-NIV and Empty-NIV).

Storage of IOX-NIVs in the pro-form, at 4 and 25 °C for up to 37 weeks, allows for the same successful IOX formation and encapsulation. The FDA recommends performing stability experiments for up to 2 years, therefore, IOX-NIV stability should be monitored for an addition 1 year and 15 weeks in order to satisfy this criteria, however, initial stability experiments showed acceptable stability at 4 and 25 °C for the initial 37 weeks and it may be anticipated that storage at lower temperatures of 4 °C may protect against degradation. IOX-NIV physical and chemical characteristics were also monitored at an increased temperature of 37 °C and an extreme temperature of 50 °C. Under both of these conditions an increase in time was associated with a decreased ability of hydrated NIV to successfully encapsulate IOX, as well as altered physical characteristics which were observed in Chapter 2

– Formulation and Physical Characterisation of IOX-NIV. The decrease in EE % coincided with a change in physical appearance of pro-IOX-NIVs which became more yellow as time increased and at a faster rate at higher temperatures. A combination of these factors suggest that lipids were degrading through oxidation and potentially hydrolysis. In order to ensure stability the delivery system should be stored in the pro-IOX-NIV form at a temperature no greater than 25 °C.

The release of IOX from hydrated IOX-NIVs under physiological conditions which mimic the body showed a burst release profile. A typical feature of lipid-based delivery systems which entrap hydrophilic agents is that there is fast release of drug within the first 24 h. Specific consideration of IOX-liposomes previously reported in the literature show that IOX-NIVs had a much greater plateau in IOX release in (73 %) after monitoring for 72 h. Other IOX-liposomes characterised in the literature expressed as little as = 10 % release. The rapid release of IOX from NIVs at 37 °C may be linked to the T_m of surfactant VIII as the main structural component of NIVs. Even at the lower transition temperature lipid molecules present within a bilayer become more fluid-like and the membrane more porous. Despite this, the presence of other lipids will alter the exact phase transitions of IOX-NIV, therefore, future experiments could include DSC analysis to determine these values. The delayed release of IOX over several hours or days may be of benefit to the kidneys, and the redistribution of IOX within a NIV formulation towards alternative organs such as the liver and spleen may contribute to reduced nephrotoxicity. Despite the fact that there is no current evidence to suggest that IOX is toxic to the spleen and liver, care should be taken to thoroughly test safety and toxicity of an IOX-NIV delivery system.

Chapter 4

In vitro Toxicity of IOX, IOX-NIV and Empty-NIV

4.   Chapter 4 - *In vitro* Toxicity of IOX, IOX-NIV and Empty-NIV

4.1   Introduction

In vitro cell culture experiments offer the opportunity to gain information regarding the safety and efficacy of novel pharmacological agents on specific tissue derivatives without the immediate and unnecessary use of whole animal models. The direct correlation between *in vitro* and *in vivo* systems, as well as their translation to safety and efficacy in humans, should be approached with caution as differences in interspecies biochemistry can massively influence cellular responses to drugs. One example of this is observed when comparing interspecies variation in hepatoxicity of paracetamol where mouse, rat and human hepatocytes show a range of sensitivities (Jemnitz *et al.*, 2008). Despite this, *in vitro* systems offer many advantages as a rapid and high-throughput drug screening technique, the performance of which is currently a key stage in pre-clinical pharmaceutical drug development (van Norman, 2016). The identification of relevant cell and isolated organ models, to assist with designing future *in vivo* studies, is in support of the 3 R principles – replacement, reduction and refinement (Törnqvist *et al.*, 2014). Whereby, initial identification and quantification of tissues sensitivity to the unknown effects of IOX and IOX-NIV *in vitro* will work to: (1) replace the initial use of animals to identify previously unknown toxicities; (2) reduce the number of animals used in *in vivo* studies through better experimental design and (3) refine experimental conditions by first identifying toxic *in vitro* drug concentrations, leading to improved animal welfare and a reduction in potential suffering.

There are a number of ways in which cells are obtained for *in vitro* use. Cell immortalisation using a virus, or tumour-derived cells, are advantageous due to their ability to replicate rapidly while expressing an 'infinite' lifespan. The typical lifespan of transformed and tumour- derived cells is long, at around 50-100 cell divisions, or passages. Despite this, it is important to be aware of how immortalisation may impact normal cell metabolism and hence how the cells respond to substances. In contrast, immortalised cell lines can include cells cultured upon primary isolation from tissue. Primary cell lines offer an advantage due to their ability to maintain biochemical processes more closely related to their behaviour within their natural environment (Kaur and Dufour, 2012). However, the use of cells directly isolated from tissues comes with disadvantages which may include a reduced growth rate and limited lifespan – these cells are often only utilised for a small number of cell divisions, typically between 40 and 60, however, this is dependent on the cell of origin being used (Geraghty *et al.*, 2014). Monitoring cells based on doubling time and typical morphology is the most common method for ensuring a cell response closely related to their natural behaviour. Purification and identification of a pure population of the target cell is an additional quality

assurance step which is required due to the fact that tissues in which cells are isolated from typically include a range of cell types that work together to form the tissue structure.

4.1.1   *In vitro* models of kidney and vascular function and RCM-associated toxicity

It is generally accepted that the introduction of low-osmolar, non-ionic RCM such as IOX, has contributed to a significant reduction in RCM-associated complications. Despite IOX being considered to be a low-osmolar RCM, commercially available Omnipaque300, used throughout the experiments described in this thesis, expresses an osmolality of 672 mOsm kg^{-1}. In comparison, blood plasma levels typically range from 275-299 mOsm kg^{-1}, meaning that the osmolality of IOX is ~2.3x greater than blood. RCM osmolarity is often reported as a factor which influences both endothelial and VSMCs (Zhang *et al.*, 2000; Takatsuki *et al.*, 2004) and is believed to be an issue for certain patient groups, such as those with underlying cardiovascular disease (Barrett *et al.,* 1992). Despite this, the link between RCM osmolality and its direct effect on toxicity is debated in the literature. Zhang *et al.* (1999) highlighted the fact that rather than RCM toxicity and osmolarity being directly linked, there was evidence to suggest that both mechanisms of toxicity could lead to the initiation of apoptosis, but this is mediated through different pathways (Zhang *et al.*, 1999). Another theory linked to RCM toxicity is a role for the level of iodine present. This was tested in a range of kidney cells, of dog and mammalian origin, to show that cell viability, after normalising RCM iodine concentration against a preparation of sodium iodide, that no association between cell death and iodine concentration (Romano *et al.*, 2008). In this study iodine concentrations of 100 and 200 mg ml^{-1} were completely non-toxic which was in contrast to the significant reduction in viability detected after treatment with RCM at equal iodine concentrations. In addition, this study observed a link between reduced HEK-293 viability and the presence of DNA laddering, and caspase-3/ -9. Regardless of the cause of cytotoxicity, this study provides evidence to suggest that the mechanism of death is associated with apoptosis, or programmed cell death, and specific activation through the intrinsic pathway. A range of information exists to support the reasoning behind RCM-associated toxicity, the occurrence of which is likely to be multifactorial, however, a common theme of RCM-associated cytotoxicity is the detection of apoptotic markers. The application of apoptotic inhibitors *in vitro* have also been shown to inhibit RCM-associated toxicity in nucleus polposus cells (Matheny and Moehlenbruck, 2010).

For *in vitro* studies the use of human embryonic kidney (HEK-293) cells, which are undifferentiated human renal cells, may be useful in the analysis of the effects of NIV, IOX and IOX-NIV due to the ease in which they can be handled and also because they are

human-derived. The use of these cells may provide relevant data with the aim of making IOX-NIVs suitable for bio-imaging in human medicine. Quintavalle *et al.* (2011) performed a study in order to analyse the route of cell death taken by renal cells after exposure to RCM. *In vitro* analysis focused solely on the use of Madin-Darby Canine Kidney (MDCK) cells which - along with HEK-293 cells - have been used in other studies to examine the cytotoxic effects of RCM (Romano *et al.,* 2008). MDCK cells offer advantages for the analysis of the effect of RCM and prevention of associated toxicity due to the fact that the distal epithelial tubular cells of the kidneys are more prone to insult from RCM and also for the ease in which they can be handled (Quintavalle *et al.*, 2011). Other cells that have been used in the analysis of RCM cytotoxicity *in vitro* include the porcine proximal renal tubular (LLC-PK1) cell line which show similarities to the distal tubule renal cells in humans (Romano *et al.*, 2008). For the purpose of this thesis HEK-293s were selected as the cell of choice for further investigation of IOX-related toxicity and its prevention after its entrapment within NIVs. Renal and vascular cell types are of particular interest due to the fact that upon IV administration the vasculature is the first site of contact for RCM, in addition to the sensitivity of these organs to the toxicity of RCM and their potential role in the development of AKI and CIN (Sadat *et al*., 2015). The lipid components used to formulate NIVs are generally perceived to be non-toxic, therefore, it may be assumed that the formulation of these lipids in to a nano-vesicular structure is similarly non-toxic.

4.1.2   *In vitro* analysis of cell metabolism and replication

Resazurin is a dye commonly used as an *in vitro* indicator for cytotoxicity in addition to being used as a measurement of cellular proliferation, metabolism, viability and drug sensitivity in prokaryotes (Sarker *et al.*, 2007), eukaryotes (Ducker *et al.*, 2016) and protostomes (Duarte *et al.*, 2009). Alternative commercially available forms of Resazurin include Alamar Blue™ (Trek Diagnostic Systems) and UptiBlue™ (Interchim). Resazurin has the ability to cross cellular membranes as a blue dye where it is then reduced to Resorufin by NADH present in metabolically active cells (Figure 4.1). This change in chemical structure results in a colour change (blue to pink) and a change in fluorescence and absorbance which may then be detected spectroscopically (Candeias *et al.*, 1998). The Resazurin assay offers the advantage of being a one-step process and has been shown to be more sensitive than alternative techniques such as the MTT assay, which similarly reflects the presence of mitochondrial NAD(P)H reductase enzymes that are key to mitochondrial metabolism (Hamid *et al.*, 2004), and the radioactive monitoring of cell division through DNA incorporation of tritiated thymidine (^{3}H-dT) (Ahmed *et al.*, 1994). The acceptance of the measurement of cellular metabolism to determine cell viability is common due to the direct correlation between metabolism and viable cell number

(Gonzalez and Tarloff, 2001; Hamid *et al.,* 2004; Rampersad, 2012). In comparison to the ^{3}H-dT-incoproration assay, Resazurin analysis offers advantages such as avoidance of laborious techniques, acting as a high-throughput technique without the use of harmful reagents (Ahmed *et al.*, 1994), as well as enabling the maintenance of sterility due to the ability to perform the single-step reagent addition within a biological safety cabinet.
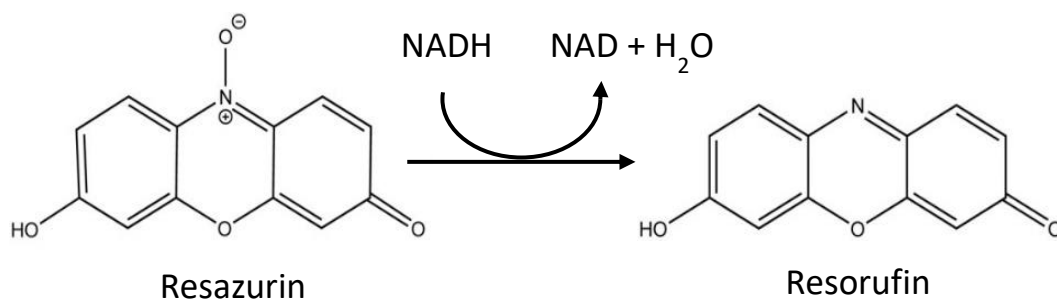
Figure 4.1: Metabolic reduction of Resazurin to Resorufin. *Exposure of viable cells to Resazurin leads to its irreversible reduction by NADH to produce Resorufin and by-products NAD and H_2O. Image prepared using ChemDraw Professional v15.*

4.1.3 Cell viability analysis

The CellTox™ Green cytotoxicity assay is a commercially available kit which can be used to analyse the effect of cytotoxic compounds. The principle of the assay is based on the ability of an intercalating dye to bind to nucleic acids present in cells with compromised membranes, while viable cells will remain unstained. Upon interaction of the dye with DNA the fluorescent signal becomes significantly enhanced and the signal produced is proportional to the number of dead cells. The CellTox™ Green assay may provide an advantage over indirect methods of toxicity screening, such as Resazurin, the signal of which may be influenced by a number of factors. In conjunction with initial analysis of the influence of IOX on cellular metabolism and proliferation, CellTox™ Green can be used a complimentary test for the direct determination of cytotoxicity.
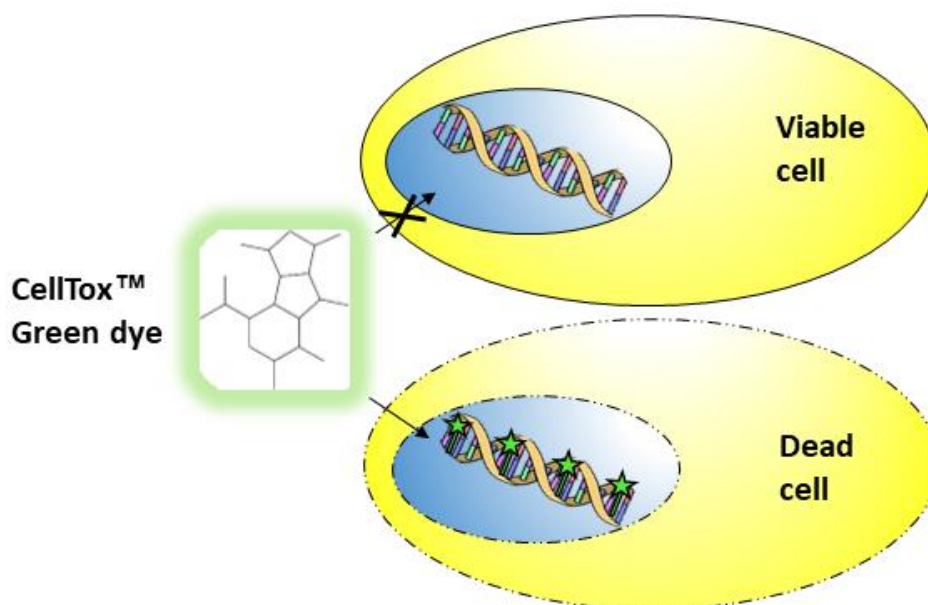
Figure 4.2: Principle behind *in vitro* toxicity analysis using CellTox™ Green. *The CellTox™ Green assay has the ability to kinetically determine test sample toxicity upon exposure to an intercalating dye which binds to DNA leading to enhanced fluorescence at wavelengths of 485_{ex} and 535_{em} nm. The dye is unable to cross the cell membrane of viable cells, however, increased cellular and nuclear membrane permeability in dying cells enables interaction of the dye with DNA and subsequent detection of a fluorescent signal. Images reproduced from the manufacturer's protocol and prepared using Microsoft PowerPoint 2013 and ChemDraw Professional v15.*

The ApoTox-Glo™ assay is another commercially available kit which incorporates 3 separate methods for the measurement of cell viability, toxicity, and the specific identification of controlled cell death through apoptosis within a single triplex experiment (Figure 4.3A). This technique is complementarily to the experiments described previously due to the different way in which viability and toxicity is measured. The principle of viable cell detection is based on the uptake of a membrane-permeable peptide which incorporates the fluorophore glycyl-phenyl-alanyl-aminofluorocoumarin (GF-AFC). A fluorescent signal, proportional to the number of viable cells, can be measured when GF-AFC becomes cleaved by intracellular proteases within the cytoplasm of membrane-intact viable cells. Dying cells express a loss of membrane-integrity and intracellular proteases leak out into the extracellular media, therefore no fluorescent signal is generated by dead cells. A second fluorescent peptide with a distinct excitation and emission spectra is included for the measurement of cytotoxicity. In comparison to GF-AFC, the peptide bis-alanylalanyl-phenylalanyl-rhodamine 110 (bis-AAF-R110) is not membrane permeable, instead this molecule becomes cleaved within the extracellular

110

environment in the presence of proteases released from dying cells which have lost membrane integrity and hence the signal can be used as a measurement of toxicity.

The final feature of this assay is the detection of a luminescent signal which may be measured after the cleavage and release of a luciferase-specific substrate (Figure 4.3B). Substrate cleavage is performed only in the presence of proteolytic enzymes, caspase-3 and -7, which makes this reaction specific towards cells undergoing apoptosis. These enzymes are important for the progression of the apoptotic cascade required for programmed cell death. RCM-induced cell death has previously been linked to the initiation of apoptosis (Rowe *et al.*, 2016), therefore the performance of this assay can be used to gain more information regarding IOX-associated toxicity and whether this may be avoided through the use of NIV delivery systems.
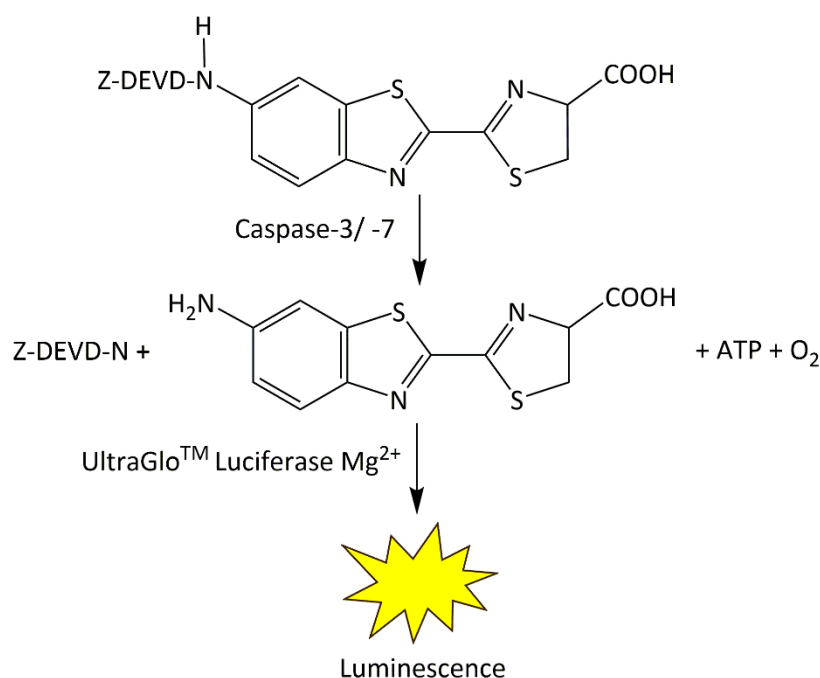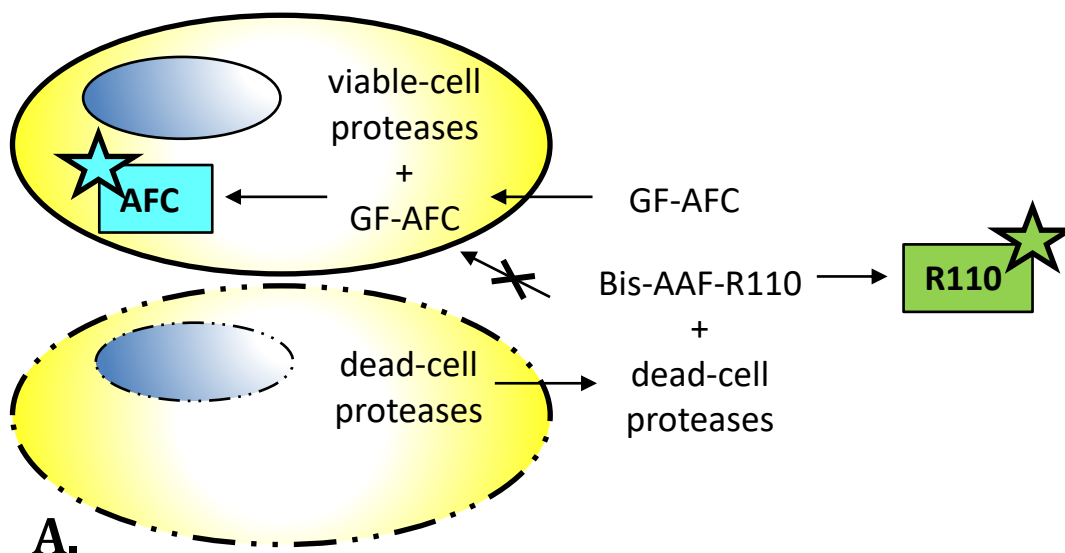
Figure 4.3: Principle behind viability and cytotoxicity analysis using ApoTox-Glo™. A)
The ApoTox-Glo™ assay enables the fluorescent detection of viable cells in vitro due to the incorporation of the dye GF-AFC which has the ability to cross viable cell membranes where it is cleaved by proteases present in the cytoplasm. Protease cleavage leads to the generation of AFC which expresses enhanced fluorescence which can be detected at wavelengths of 400_{ex} and 505_{em} nm. A second, membrane impermeable dye called bis-AAF-R110 is cleaved by proteases which are released from dead cells leading to the generation of R110 which produces a fluorescent signal which can be detected at wavelengths of 485_{ex} and 520_{em} nm. GF-AFC - glycyl-phenyl-alanyl-aminofluorocoumarin; bis-AAF-R110 - bis-alanylalanyl-phenylalanyl-rhodamine 110. **B)** *Apoptotic activity is detected upon cleavage of the DEVD molecule by caspase-3/ -7 resulting in a luciferase reaction producing a detectable luminescent signal. Images reproduced from the manufacturer's protocol and prepared using Microsoft PowerPoint 2013 and ChemDraw Professional v15.*

4.2   Chapter aims and objectives

In vitro pre-clinical testing will be performed in order to estimate safety *in vivo* and data will be compared to similar experiments which have been reported in the literature. Due to the novelty of IOX encapsulation in NIVs, this chapter will be the first to examine the effects of NIVs and IOX-NIVs on renal and vascular cell metabolism and viability. After the initial isolation, identification and routine culture of cells of renal and vascular origin, a range of *in vitro* tests will be compared and contrasted. There will be a focus on renal and vascular metabolism, viability and cell death. The overall aim of this chapter is to gain a better understanding of IOX interactions that may contribute to RCM-AKI or CIN, while also analysing the potential of IOX encapsulation within NIVs as a way to prevent damage. In doing so, the objectives of this chapter are to:

- Isolate and confirm the identity of VSMCs obtained through primary isolation techniques.
- Optimise *in vitro* experimental conditions for different cell types prior to the introduction of test materials.
- Utilise a range of complementary and alternative *in vitro* tests to determine the effect of IOX on renal and vascular cell viability and function.
- Compare the toxicity profile of empty- and IOX-NIVs on renal and vascular cell lines.

4.3   Materials and methods

4.3.1   Cell culture

A range of cell lines were cultured and used as *in vitro* models to determine the effect of free-IOX, empty-NIV and IOX entrapped within NIVs on cells derived from the kidneys and vasculature (

Table **4.1**). HEK-293 and human umbilical vein endothelial cell (HUVEC) cell lines were purchased from ATCC, in comparison, VSMCs were isolated using a variation of the early explant method as it offers a simple and effective method for the isolation of a pure culture of VSMCs as described elsewhere (MacAskill, 2014; Al-sulti, 2017). Male Sprague Dawley rats (12-20 weeks, 200-400 g) were housed and cared for following standards outlined by the Animals Procedure Act (1986). Rats had *ad lib* access to standard laboratory chow and water prior to being sacrificed using cervical neck dislocation. The rat's fur was decontaminated with 70 % (*v/v*) ethanol (Sigma) and transferred to a class II biological safety cabinet - sterile scissors and forceps were used to open the chest cavity. The thoracic aorta was dissected and placed in ice-cold VSMC media before immediate transportation to the tissue culture lab. Further dissection was carried out within a sterile class II biological safety cabinet to remove blood, adventitia and connective tissue before cutting the aorta into 3 mm segments. Two or three segments were aseptically transferred into T25 tissue culture flasks along with 5 ml VSMC media. Aorta rings were incubated undisturbed at 37 °C, 5% CO_2, 80 % relative humidity (RH) for at least 48 h prior to the performance of a media change. VSMCs were allowed to reach confluency before dissociation and transfer to T75 flasks for routine culture prior to use in experimental assays. To ensure maintenance of typical VSMC characteristics, cells were only utilised for experimental analysis between 1 and 5 passes. During experimental analysis 'n' represents the number of experiments performed using VSMCs isolated from different rats, while other 'n' values refer to the performance of 3 repeat measurements stemming from that particular cell line.

Table 4.1: Details of culture media preparations utilised for different cell types. *Both basal media and supplement composition for each cell type is described along with details of manufacturers*

Cell type	Culture media	Supplements
HEK-293 (ATCC)	Eagle's minimum essential medium (EMEM) (Sigma, UK)	1% (*v/v*) penicillin-streptomycin; 10% (*v/v*) FCS
HUVEC (Cellworks, UK)	Human large vessel endothelial cell basal media (Cellworks, UK)	0.1% (*v/v*) antibiotic supplement; 2% growth supplement (Cellworks)
VSMC (primary isolation)	50: 50 % (*v/v*) Ham's F-12 nutrient mixture/ Weymouth medium (ThermoFisher, UK)	1% (*v/v*) penicillin-streptomycin (Sigma); 10% (*v/v*) FCS (Biosera, UK)

4.3.2   Immunohistochemical confirmation of VSMC isolation

Upon isolation and growth of VSMCs, morphological analysis and immunohistochemical staining was performed to confirm the isolation of a population of VSMCs using methods similar to those described elsewhere (Xu *et al.*, 2009). VSMCs were seeded and allowed to proliferate on coverslips prior to fixing for 10 min in 4 % paraformaldehyde (VWR). VSMCs were permeabilised with 0.1 % (*v/v*) triton X-100 (Sigma) for 10 min to enable antibody interaction with targeted intracellular protein markers. Cells were blocked with 1 % (*w/v*) BSA (Fisher) in PBST (PBS plus 0.1 % (*v/v*) Tween 20 (Thermo Scientific) and 22.52 mg mL^{-1} glycine) for 1 h at RT and then incubated overnight at 4 °C with a primary Ab specific for VSMC protein markers (Table 4.2). Coverslips were washed for 3 x 5 min in ice-cold PBS prior to 1 h incubation in darkness with an appropriate fluorescein-labelled secondary Ab prepared in 0.1 % BSA as per the manufacturer's protocol (Table 4.2). While maintaining the coverslips in darkness, they were washed 3 x 5 min in ice-cold PBS. Hoechst 33342 (Molecular Probes) was used as a counterstain for the visualisation of nuclei. A 1 µg mL^{-1} solution was prepared in PBS and aliquoted onto cells for 1 min followed by rinsing with PBS. Coverslips were mounted on to slides using DPX Mountant Media (Sigma) and stored in darkness prior to visualisation using an Epifluorescent Upright microscope with Nikon Eclipse E600 camera. A FITC filter was used for visualisation of fluorescein-labelled proteins while a DAPI filter was selected for visualisation of Hoechst stained nuclei.

Isolation and routine culture revealed the typical VSMC spindle-like morphology with an expected size of 100-200 µm x 10-15 µm (Chamley-Campbell *et al.*, 1979; Appendix - Section 4.8.1; Figure 4.27). The successful identification of VSMC markers confirmed the isolation of a homologous populations of VSMCs (Appendix - Section 4.7.1; Figure 4.25 and Figure 4.26).

These experiments validated the use of the explant method for further analysis of the effect of IOX, empty-NIV and IOX-NIV on VSMCs.

Table 4.2: Preparation of antibodies for IHC identification of VSMCs

	Antibody	*Manufacturer*	*Concentration*
Primary	Myosin Heavy Chain mouse mAb	R&D Systems	$10\,\mu g\,mL^{-1}$ (1: 100)
	α-SM-actin mAb	Sigma	(1: 400)
Secondary	Fluorescein anti-mouse (horse) IgG	Vector Labs	$10\,\mu g\,mL^{-1}$ (1: 150)
	Fluorescein anti-rabbit (goat) IgG	Vector Labs	$10\,\mu g\,mL^{-1}$ (1: 150)

4.3.3 Resazurin assay

Upon reaching 70-80 % confluency cell culture media was aspirated and cells were enzymatically lifted from the flask upon the addition of 5 ml TryplE™ Express Enzyme (Gibco). . Cells were incubated in TryplE™ Express at 37 °C, 5 % CO_2 for 5 mins, with the exception of VSMCs where the incubation time was increased to 8 mins. It was noted that some VSMCs remained attached to the flask despite increasing the incubation time and agitation. Enzymatic action was inhibited upon addition of 1 % (*v/v*) FCS to the cell suspension which was then centrifuged at 2500 g for 4 mins. The supernatant was aspirated and cell pellet suspended in fresh culture media. Cell viability was determined using the trypan blue exclusion assay upon mixing a volume of cells in an equal volume of 0.4 % trypan blue (Gibco).Viable and non-viable cells were counted using a Neubauer Haemocytometer. After confirmation of ≥ 90 % cell viability, cells were seeded in 100 µL volumes within a 96-well plate at an appropriate density as determined by optimisation studies (Appendix – Section 4.7; Figure 4.27 and Figure 4.28; Figure 4.29 and Figure 4.30). Cells were then allowed to adhere overnight prior to treatment with 100 µL of IOX, empty-NIV, IOX-NIV or control sample at appropriate concentrations prior to incubation for a specified time.

Resazurin stock solution was prepared as a 0.01 % (*w/v*) stock by dissolving 5 mg Resazurin sodium salt (Sigma) in 50 mL DI water before filter sterilisation using 0.2 µm syringe filters (Whatman). Sterile Resazurin was stored at -20 °C and thawed prior to the performance of experiments. A volume of 20 µl was added to each well in order to obtain a final concentration of 1 % (*w/v*) Resazurin. Plates were incubated in darkness at 37 °C, 5 % CO_2, 80 % RH for a time determined in optimisation experiments (section 5.3.1 Optimisation). The fluorescence was measured using a SpectraMaxM5 fluorescent plate reader (Molecular Devices v0.008) at a wavelength of $560_{ex}/ 590_{em}$ nm. The percentage of metabolically active cells was determined

after normalising results against the fluorescence of blank wells containing the test sample without cells, and then taking each test results as a percentage of the untreated control wells (Equation 4.1). Microscopic images were taken to show any changes in morphological features.

Equation 4.1: Calculation of metabolic activity in cells treated in the Resazurin assay.
The fluorescent signal of unknown test samples and controls was subtracted from blank measurements without cells which was divided by the fluorescent signal obtained for control, untreated cells.

$$\% \ of \ Metabolically \ Active \ Cells$$
$$= \left(\frac{Test \ sample \ fluorescence - background \ fluorescence}{Fluorescence \ of \ untreated \ cells}\right) \times 100$$

Upon analysis of HEK-293, VSMC and HUVEC metabolic responses to increasing concentrations of IOX, automatic EC50 calculation using PRISM software was not possible. This was due to a number of factors including the absence of a plateau in cellular response at the upper and lower IOX concentration ranges (i.e. 2 data points whereby cell metabolism was 100 % and two data points whereby the cell metabolism was 0 %), in addition to the poor sigmoidal distribution of data across the concentration range tested, The relative EC50s were instead determined from the maximum and minimum metabolic responses exhibited by cells within the linear response range. The EC50 concentration for each cell type was defined by the median response and calculated using the equation of the line of regression. Other EC50s used to describe the cellular response to empty- and IOX-NIVs was successfully determined through the use of PRISM software.

4.3.4 Use of an Osmometer for the measurement of test solution and control sample osmolality

The Osmomat 030 (Gonotec) measures osmolality based on the solutions freezing point and determines how that deviates from the freezing point of dH_2O. The Osmomat 030 was calibrated as described by the manufacturer's protocol. Firstly, a 50 µl volume of dH_2O was used to calibrate the osmometer so that the osmolarity of dH_2O was determined to be 0.000. This was followed by the use of a 300 mOsmol kg^{-1} calibration standard. A stock solution of mannitol was prepared to achieve a final concentration of 11 % (*w/v*). The osmolality of IOX

and the 11 % mannitol solution were measured to confirm that the test samples expressed a similar osmolality, as anticipated. The preparation of a mannitol solution with a similar osmolality to IOX was performed to test the role of osmolality in the influence of IOX on HEK-293 metabolism, as determined through the Resazurin metabolic indicator assay.

4.3.5 CellTox™ Green cytotoxicity assay

The CellTox™ Green Cytotoxicity Assay (Promega) was performed as per the Manufacturer's instructions for the performance of the Express, No-step experiment whereby the CellTox™ Green reagent is added at the point of dosing to enable kinetic analysis regarding the effect of IOX treatment on HEK-293 cytotoxicity. HEK-293s were routinely cultured as mentioned previously (Section 4.3.1). Viable HEK-293s were dissociated using TryplE, stained using trypan blue and counted using a haemocytometer before seeding into a 96-well plate at a seeding density of 1×10^4 cells well^{-1}. HEK-293s were allowed to adhere over night at 37 °C, 5 % CO_2 and 80 % RH.

All kit components were thawed in a water bath at 37 °C and vortexed to ensure homogenisation. A 2x CellTox™ Green solution was prepared by diluting the stock solution 1: 500 in assay buffer while protecting from light sources. Serial dilutions of IOX was preformed prior to the addition of 50 % (*v/v*) IOX to HEK-293s. A lysis buffer control for the detection of cytotoxicity, which was included in the kit, was added to HEK-293s in 8 µl volumes. The 2x CellTox™ Green working stock was added to each well in 100 µl volumes and then the plate was incubated in darkness prior to measuring fluorescence at 485_{ex} and 535_{em} nm at various time points (1, 2, 4, 6 and 24 h). The analysis of toxicity at incubation times > 24 h could lead to inaccurate representation of toxicity due to the build-up of waste metabolites which occurs with increasing incubation time *in vitro*.

4.3.6 ApoTox-Glo™ triplex assay

In addition to the analysis of the effect of IOX and NIVs on vascular cell metabolism, further experiments were performed to uncover potential mechanisms behind the altered function of vascular cells after free-IOX, empty-NIV and IOX-NIV exposure using a commercially available toxicity assay. The ApoTox-Glo™ triplex assay (Promega) has the potential to measure live cells, dead cells and apoptotic activity. The assay was performed as described in the manufacturer's protocol. Firstly, VSMCs were seeded in a 96-well plate at 1×10^6 cells well^{-1} and left to adhere over night at 37 °C, 5 % CO_2 and 80 % RH. In comparison, larger HUVECs were seeded at 1×10^4 cells well^{-1}. Cells were treated for 4 h with free-IOX at concentrations higher and lower than the EC50 value determined after initial Resazurin

experiments, or empty-NIV and IOX-NIV at a concentration equivalent to the Resazurin-detected EC50 as well as lower concentrations (Section 4.4.3).

Cells were treated with test or control samples for 4 h prior to the addition of the viability/ cytotoxicity reagent. In the first set of experiments, which focused on VSMC response to IOX and NIVs, paclitaxel (PTX) was used as a control for cytotoxicity and apoptosis after 4 h incubation at a final concentration of 100 nM (Tan *et al.*, 2002). Therefore, a 200 nM PTX stock was prepared in DMSO prior to a further 1 in 1000 dilution in cell culture media. A 50 µl volume of the 200 nM stock was then added to each control well. Due to unexpected signalling from PTX, subsequent testing using HUVECs made use of the same dead cell control used in the Resazurin assay, whereby HUVECs incubated in 50 % (*v/v)* DMSO were included to act as a positive control for cytotoxicity.

The kit assay buffer, GF-AFC and bis-AAF-R110 substrates were thawed in a water bath at 37 °C and the contents of both substrates were combined in 2 ml of assay buffer which was vortexed for 20 sec. The caspase-Glo® 3/ 7 substrate was prepared by first thawing the substrate and caspase-Glo® 3/ 7 buffer at RT before combining them followed by mixing for 20 sec. A 5 µl volume of the viability/ toxicity reagent was added per well and the plate was placed on an orbital shaker at 1,300 rpm for 30 sec prior to incubation at 37 °C for 30 min. Viability fluorescence was measured at wavelengths of 400_{ex} and 505_{em} nm while toxicity was measured at 485_{ex} and 520_{em} nm. After the measurement of fluorescence, the caspase-Glo® 3/ 7 reagent was added to each well at a volume of 25 µland again the plate was placed on an orbital shaker at 1,300 rpm for 30 sec. Luminescence was recorded after a further 30 min incubation at RT. Results were obtained after subtraction of background signal which was measured from wells without cells but containing blank media with the appropriate test sample concentrations.

4.3.7 Statistical analysis

Microsoft Excel was used to determine average and SD values for all data. GraphPad PRISM was used to determine EC50 values in Resazurin-based experiments. Minitab was used to perform student-unpaired T-tests and ANOVA tests with Tukey comparisons when analysing the effect of time and concentration on cellular processes. Statistical significance was assumed where $p < 0.05$. The T-test was used to compare the average results from two groups (i.e. empty-IOX vs IOX-NIV EC50s for a particular cell type), while ANOVA analysis was used to compare the average data across more than two sample populations (i.e. the effect of increasing IOX concentration on cell metabolism).

4.4 Results

4.4.1 The role of IOX hyperosmolality on HEK-293 metabolism

Initial investigations into the effects of IOX *in vitro* focused on the theory that IOX-associated renal toxicity may be related to exposure to a hyperosmolar agent. Firstly, equi-osmolar concentrations of mannitol were prepared to mimic IOX osmolality (Table 4.3). The hyperosmolalilty of IOX was highlighted upon the measurement of an osmolality of 648 ± 13.05 mOsmol kg^{-1}. An 11 % (*w/v)* mannitol solution (110 mg mL^{-1}) was analysed using the Osmomat 030 to reveal an osmolality of 630 ± 1.00 mOsmol kg^{-1}. In comparison, dH$_2$O and PBS were analysed as controls and were found to express an osmolality of 1.33 ± 0.58 and 369 ± 1.53 mOsmol kg^{-1}, respectively. The influence of hyperosmolar IOX and mannitol on HEK-293 metabolism was compared to determine whether there is an association between osmolality and IOX-associated toxicity.

Table 4.3: Measurement of solution osmolality using an Osmometer prior to the treatment of HEK-293 *(n = 3; ± SD).*

Solution	Average Osmolality (mOsmol kg^{-1})
dH$_2$O	1.33 ± 0.58
PBS	369 ± 1.53
IOX (647 mg mL^{-1})	648 ± 13.05
Mannitol (110 mg mL^{-1})	630 ± 1.00

A concentration-dependent decrease in HEK-293 metabolism was observed upon exposure to IOX (Figure 4.4A). Each IOX concentration tested, between the range of 128 and 647 mg mL^{-1}, was observed to significantly reduce HEK-293 metabolism in comparison to untreated cells after 2 h exposure ($p < 0.001$). The most significant difference was observed at the IOX concentration with the highest level of osmolality which lead to a 40 % reduction in HEK-293 metabolism ($p < 0.001$). The IOX-associated reduction in HEK-293 metabolism did not appear to be solely related to exposure to a hyperosmotic environment as treatment with mannitol concentrations with similar osmolality had the opposite effect on HEK-293 metabolism (Figure 4.4B). Instead, exposure of HEK-293s to increasing mannitol concentrations lead to a significant rise in HEK-293 metabolism, specifically at higher concentrations ($p < 0.001$). HEK-293s treated with 22 and 110 mg mL^{-1} mannitol solution expressed increased metabolic activity at 118 ± 0.57 and 127 ± 3.78 % of the control, respectively ($p < 0.001$). A negative control of non-metabolic dead cells exposed to 50 % (*v/ v*) DMSO were found to express a level of metabolism equivalent to 1 ± 0.04 % in comparison to untreated, viable cells.
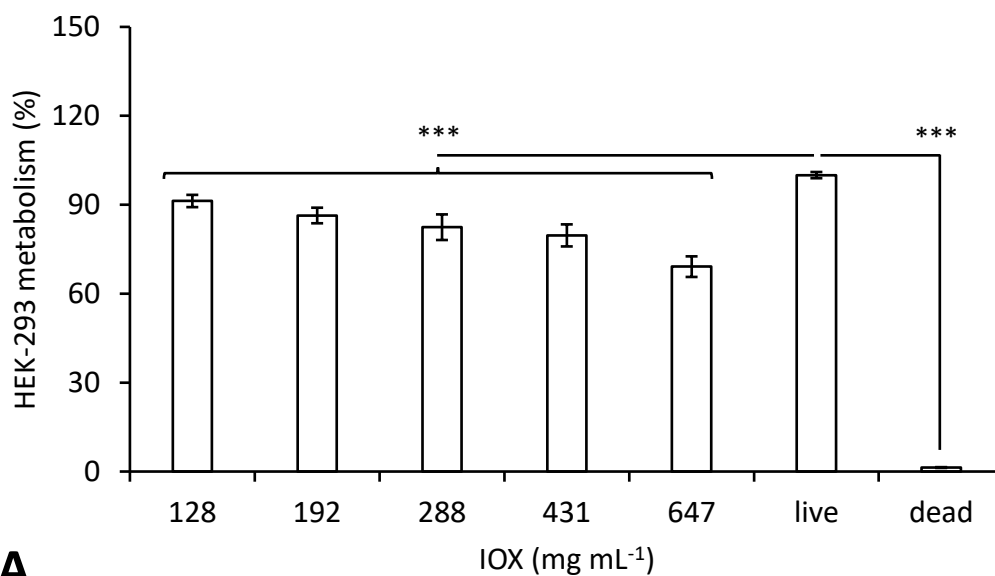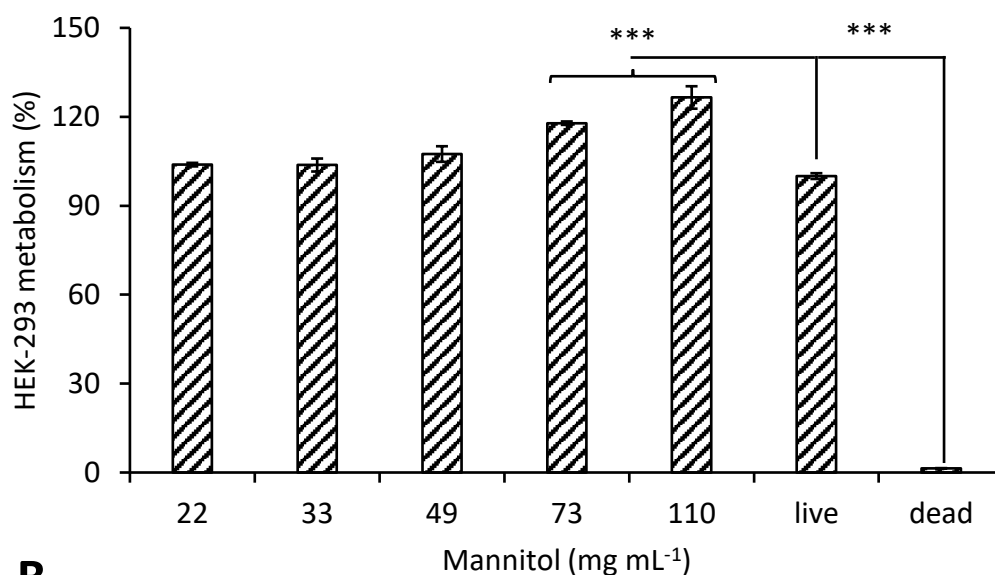
Figure 4.4: Determination of the role of osmolality on IOX-associated toxicity. A. *HEK-293s were incubated with a range of IOX concentrations or* **B.** *increasing mannitol concentrations, the 100 mg mL^{-1} mannitol stock was prepared to express a similar level of osmolality to IOX. Reagent exposure was performed for a 2 h incubation time and a negative control of dead cells was included by exposing HEK-293s to 50 % (v/v) DMSO (*** $p < 0.001$ in comparison to the live control; $n = 3$; ± SD).*

4.4.2 Kinetic analysis of IOX toxicity on HEK-293s using the CellTox™ Green assay

As per the manufacturer's protocol, the kinetic "no-step" analysis of the effects of IOX on HEK-293 toxicity was directly analysed using the CellTox™ Green assay whereby CellTox reagent is added at the point of treatment and the fluorescent signal generated was measured over time. Analysis of fluorescence at time points between 1 and 6 h showed similar results

(data not shown). The measured fluorescence at 2 h represented each of these time points whereby no significant increase in fluorescence was observed at any IOX concentration. In fact, the live control sample expressed a higher level of fluorescence at 3 ± 0.89 x 10^3 rfu when compared to HEK-293s exposed to 324 mg ml^{-1} IOX which expressed a fluorescent signal of 1 ± 0.19 x 10^3 rfu. The only significant difference in fluorescence was observed in the dead control group, where HEK-293s exposed to kit lysis buffer expressed fluorescence at 16 ± 2.70 x 10^3 rfu (p < 0.001; Figure 4.5).
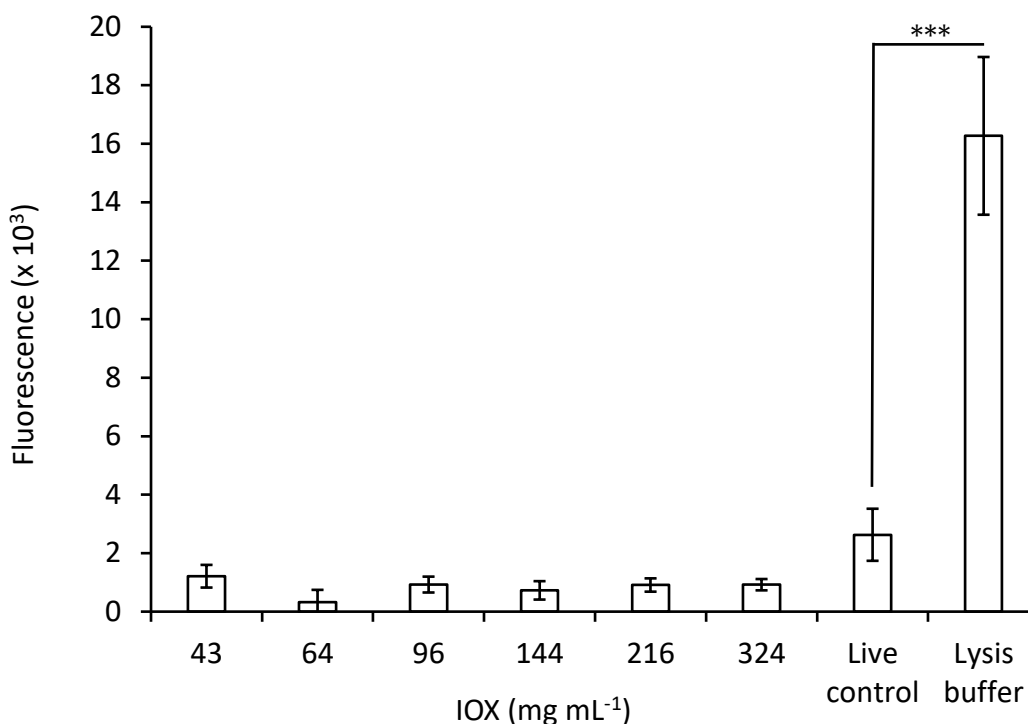
Figure 4.5: Direct analysis of IOX toxicity on HEK-293s after a 2 h exposure time. *CellTox™ Green reagent was added to cells at the point of seeding and HEK-293s were exposed to increasing IOX concentrations. The data presented was obtained upon measurement of fluorescence at wavelengths of 485_{ex} and 535_{em} nm at the 2 h time point (n = 3; ± SD; *** p < 0.001 in comparison to the live control).*

Despite the manufacturer's protocol describing the performance of kinetic analysis 24, 48 and 72 h after treatment with a cytotoxic agent, a significant decrease in lysed control signal strength was observed at the 24 h time point in comparison to fluorescent measurements made at earlier time points (p < 0.05; Figure 4.6). A peak in fluorescence was observed 2 h after the addition of lysis solution to HEK-293s where the fluorescence was measured to be 16 ± 2.70 x 10^3 rfu and there was no significant difference in signal over the initial 6 h where lysed HEK-293s expressed a fluorescent signal of 14 ± 2.80 x 10^3 rfu, however, after 24 h the signal was found to drop to 5 ± 0.77 x 10^3 rfu. A decrease in live control fluorescence was also observed over time. After 1 h incubation live cells expressed a fluorescent signal of 3 ± 0.92

x 10^3 rfu which reduced to 1 ± 0.57 x 10^3 rfu after 24 h, however, this decrease in fluorescence was not significant (p = 0.177; Figure 4.6).
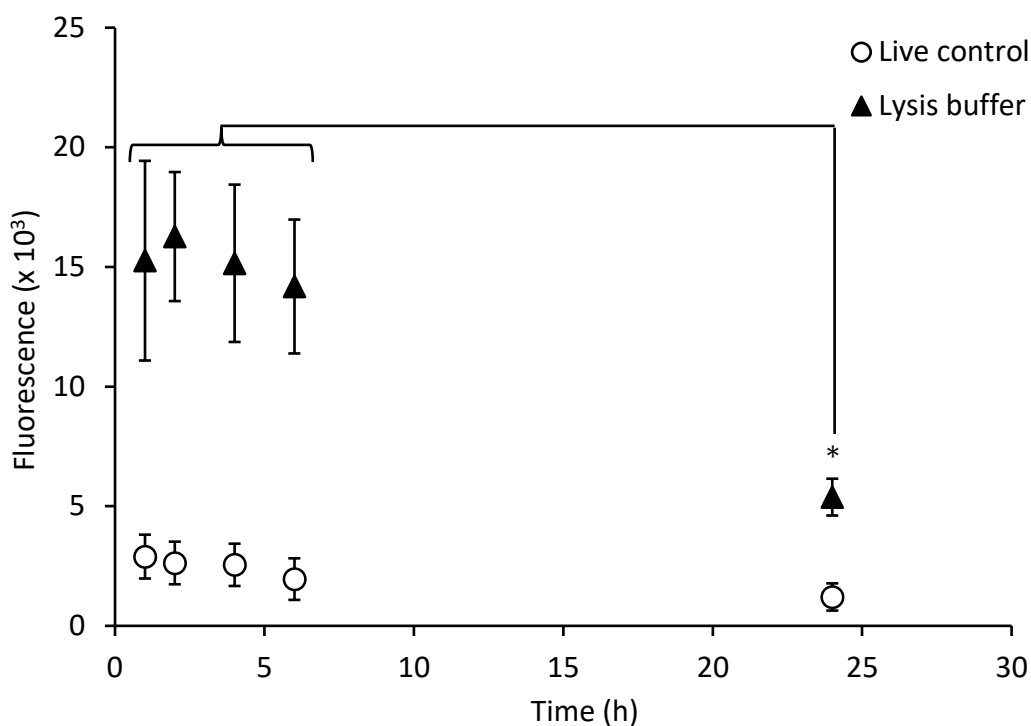
Figure 4.6: Effect of increasing time on control sample fluorescence during the performance of the kinetic "no-step" CellTox™ Green assay. *Two control sample groups were included – a positive control of dead HEK-293s, which had been treated with the kit lysis buffer at the start of the experiments, and a negative control of live HEK-293s which were untreated and maintained in cell culture media throughout the duration of the experiment (n = 3; $\pm$ SD; * p < 0.05 in comparison to all earlier time points).*

HEK-293 morphology and confluency was visualised using light microscopy 24 h after the initiation of the CellTox™ Green assay which showed altered HEK-293 adherence and morphology which was more significant as IOX concentration increased (Figure 4.7). Treatment of HEK-293 cells with IOX concentrations as low as 64 mg ml^{-1} appeared to reduce HEK-293 confluency, possibly linked to a reduction in adherence, this effect was further enhanced after treatment with an increased concentration of 96 mg ml^{-1}. As concentrations increased to 216 mg ml^{-1} IOX, the defined cell walls of neighbouring HEK-293s became blurred and cells formed a web-like pattern. After treatment with 324 mg ml^{-1} IOX no cells were found to remain adhered to the surface and there was little resemblance to viable untreated HEK-293s, instead large agglomerates were found to be floating in the media. There were no visible HEK-293s in the sample treated with lysis solution which was utilised as a positive control of cell death.
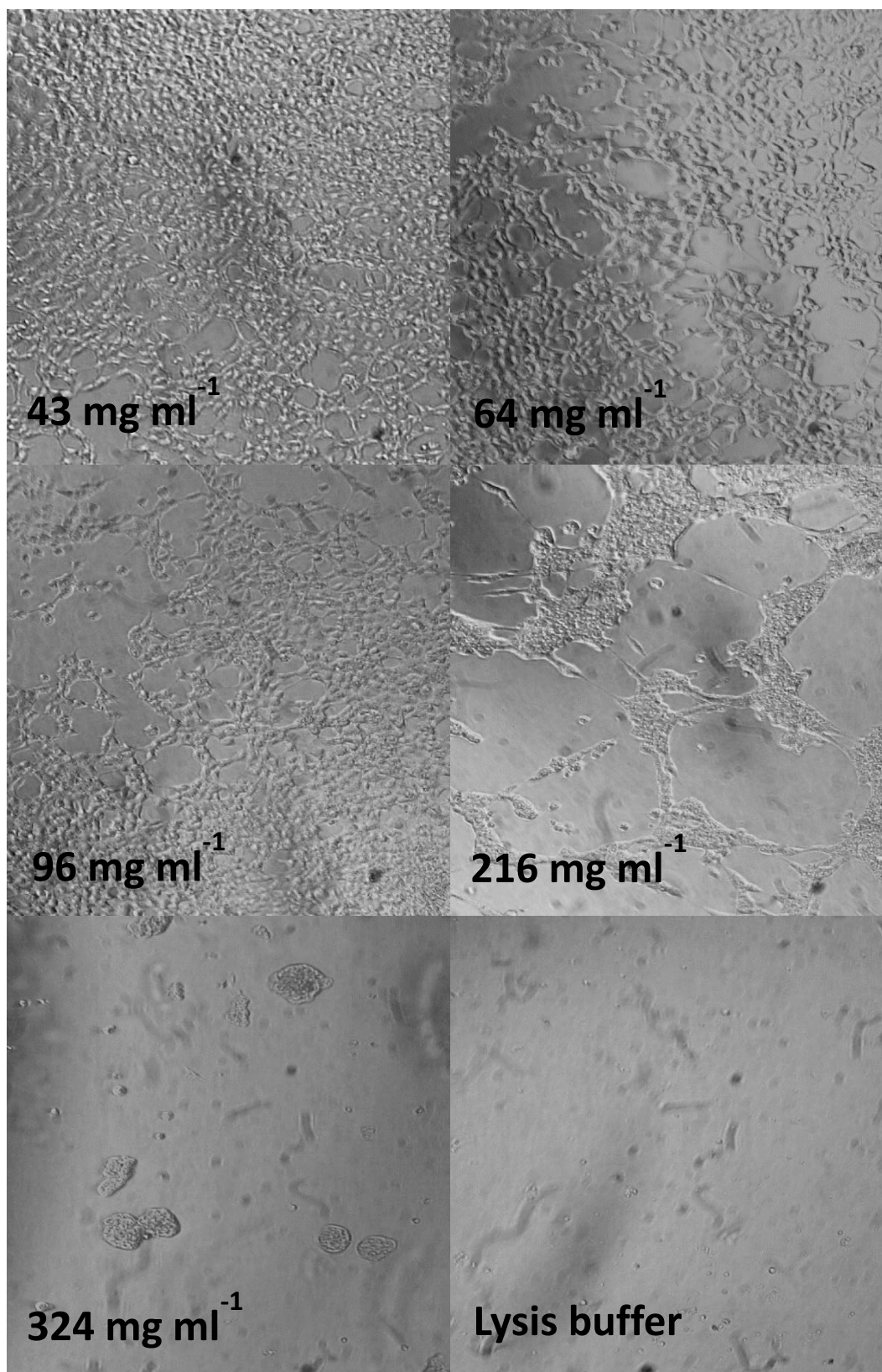
Figure 4.7: Effect of increasing IOX concentration on HEK-293 morphology 24 h after treatment and initiation of the CellTox™ Green assay. *HEK-293s were seeded with CellTox™ Green reagent and incubated with increasing concentrations of IOX. Images were taken after completion of kinetic time course analysis after a total of 24 h. 100x magnification.*

4.4.3 Effect of IOX exposure on HEK-293, VSMC and HUVEC metabolism and morphology

HEK-293s were exposed to increasing concentrations of IOX, from 32 to 324 mg mL^{-1}, whereby 324 mg mL^{-1} was the maximum concentration that could be tested as a result of reaching the maximum well capacity (200 μL) after the addition of an equal volume (50 % *v/v*) of Omnipaque300 (647 mg mL^{-1} IOX) to culture media. As IOX concentration increased, a decrease in HEK-293 metabolism was observed when each test sample was taken as a percentage of the untreated control HEK-293s (Figure 4.8). The line of best fit represents the concentration range where a linear decrease in HEK-293 metabolism was observed. The average level of metabolic activity which represented 50 % of the maximum and minimum HEK-293 metabolic responses within the line of regression was calculated to be 68 ± 3 %. This median response correlated to an average EC50 value of 152 ± 5 mg mL^{-1}.

Morphological changes observed after 24 h exposure of HEK-293s to 324 mg mL^{-1} IOX were recorded. Untreated, control HEK-293s expressed a similar morphology to that which has been described by the supplier – whereby adherent HEK-293s have a structure typical of epithelial cells (Figure 4.9A). Although a loss in typical HEK-293 morphology was observed at lower concentrations, the effect of higher concentrations > 162 mg mL^{-1} lead to the most striking morphological transformation. After 24 h exposure to 324 mg mL^{-1} IOX, HEK-293s lost their adherent properties and most of the cells were observed to take on a round morphology and were floating as groups in the culture media (Figure 4.9B).
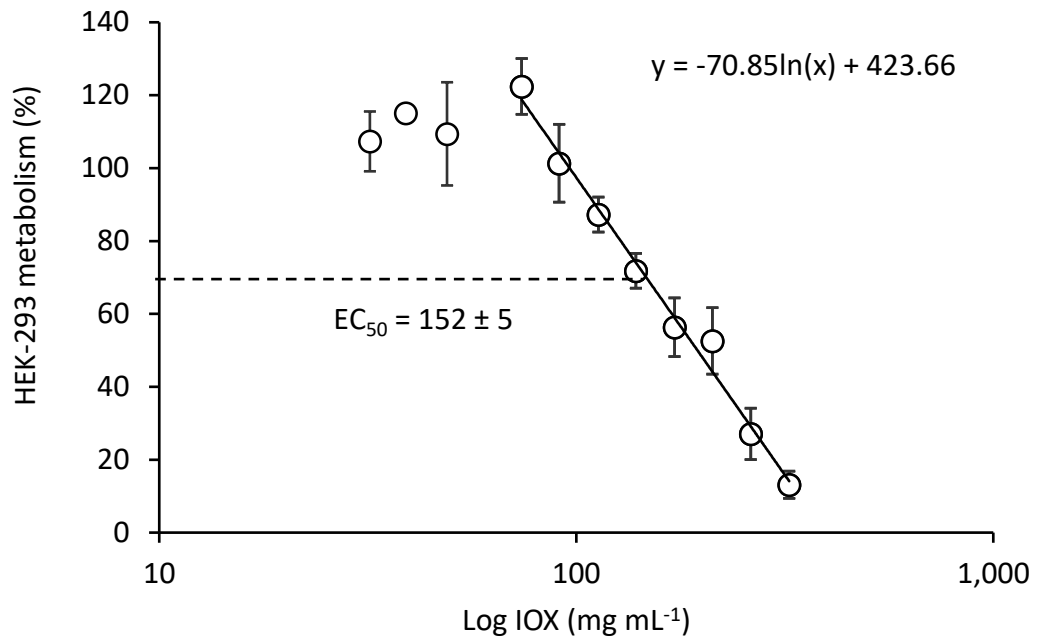
Figure 4.8: Effect of increasing IOX concentration on HEK-293 metabolism after 24 h exposure. *The fluorescent convergence of Resazurin to Resorufin was measured after exposure of HEK-293s to increasing IOX concentrations. The equation of the line used to determine the EC50 value (n = 3; ± SD).*
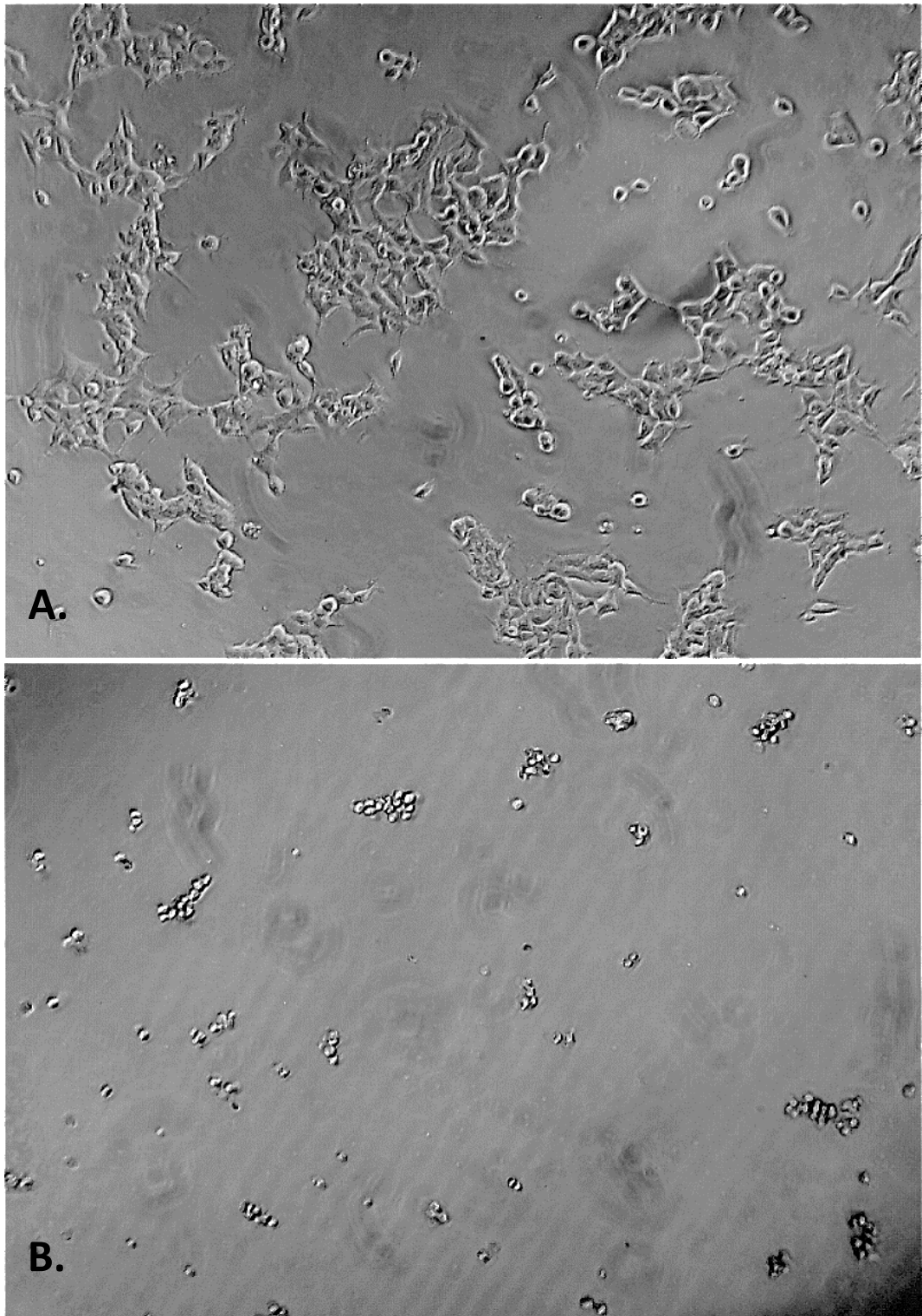
Figure 4.9: Comparison of the effect of HEK-293 exposure to IOX on typical cell morphology. A) *Untreated viable HEK-293s with typical epithelial morphology and* **B)** *HEK-293s exposed to 324 mg mL^{-1} IOX for 24 h.*

As well as analysing the effect of IOX on renal-derived HEK-293 cells, the effect of IOX on cells derived from the vasculature was also tested. A similar experimental design was used for each cell type. Firstly, the effect of IOX on VSMC metabolism was tested across the range of 2.53-324 mg mL^{-1} and the linearity between increasing IOX concentrations and decreasing metabolic activity was plotted to determine the median metabolic response was 48 ± 2 % which correlated to an average EC50 value of 124 ± 15 mg mL^{-1} (Figure 4.10). Even at lower concentrations of IOX, between 2.53 and 10.13 mg mL^{-1}, VSMC metabolism was reduced to 77 ± 1 and 84 ± 4 %, respectively, in comparison to control wells. It was observed that the flat nature of VSMCs can result in poor image contrast between cells and the surface in which they are grown on, however, confluent healthy VSMCs were shown to express their typical spindle-like morphology (Figure 4.11A). In contrast, VSMCs exposed to the maximum IOX concentration of 324 mg mL^{-1} for 2 h were observed to lose their typical morphology and confluency and become more rounded and detached from its surface (Figure 4.11B).
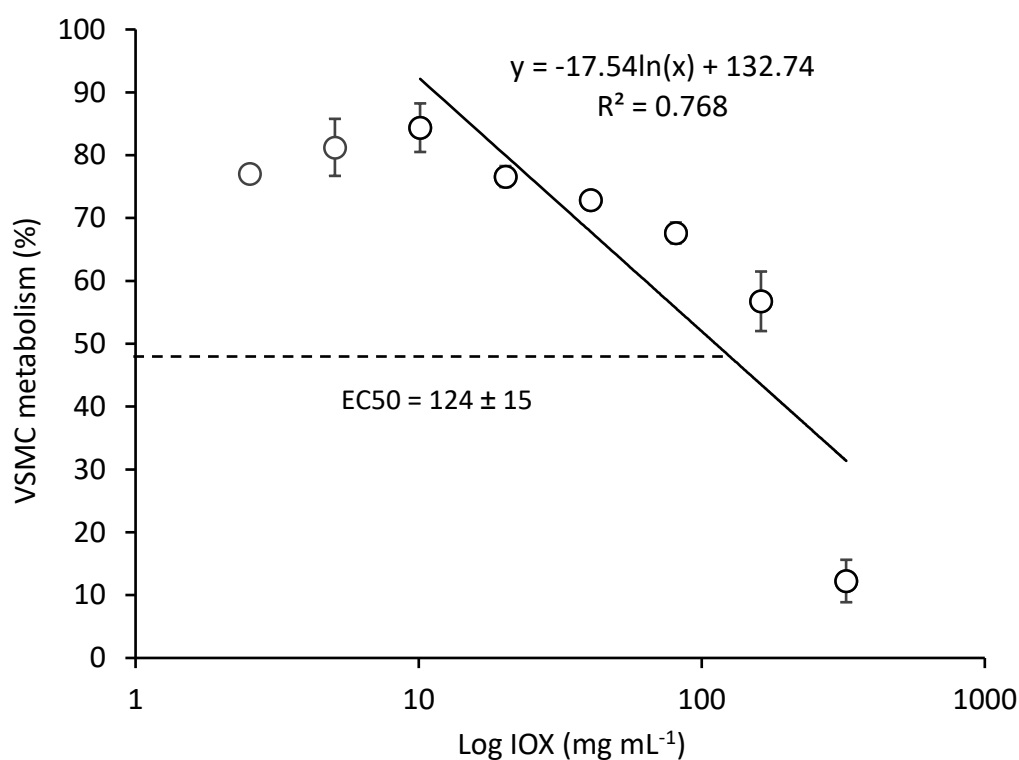
Figure 4.10: Effect of increasing IOX concentration on VSMC metabolism after 2 h exposure. *The change in fluorescence associated with the reduction of Resazurin to Resorufin during viable cell metabolism after exposure of VSMCs to increasing IOX concentrations. The equation of the line was used to determine the EC50 value (n = 3; ± SD).*
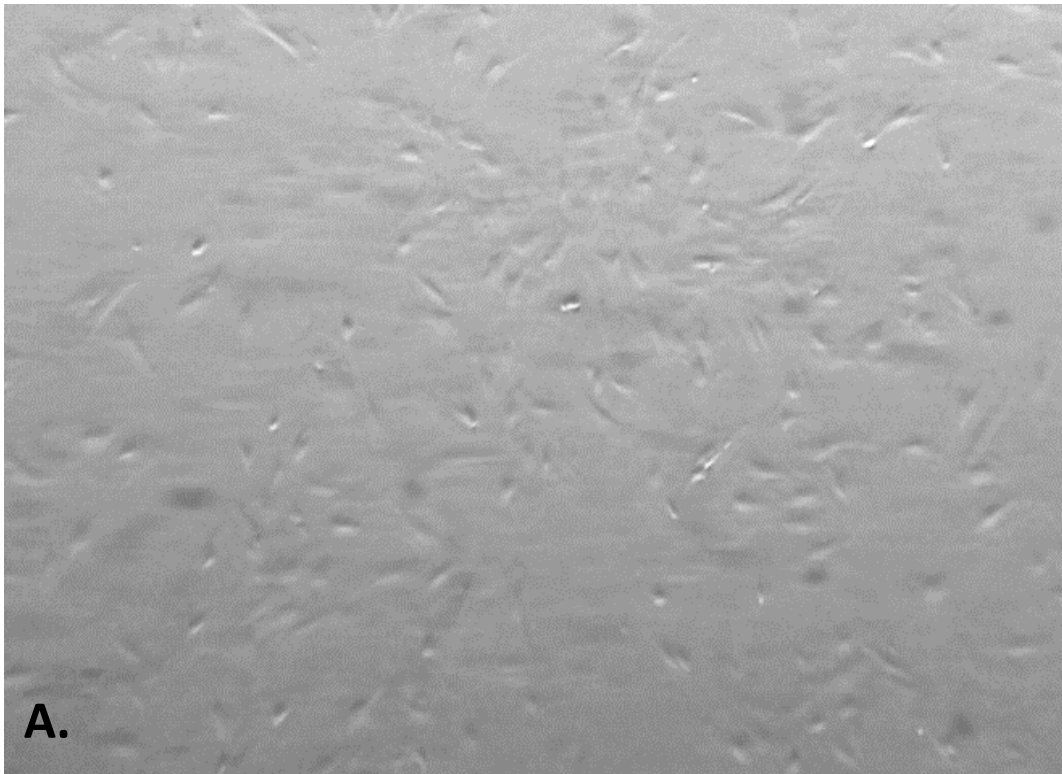
Figure 4.11: Comparison of the effect of VSMC exposure to IOX on typical cell morphology. A) *Untreated viable VSMCs with typical SMC morphology and* **B)** *VSMCs exposed to 324 mg mL^{-1} IOX for 2 h.*

The effect of IOX on HUVEC metabolism as determined through NADH reduction of resazurin was also tested. Similar to other cell types, the metabolic capacity of HUVECs after 2 h treatment led to a concentration-dependent decrease in metabolism, the median response in the range of linearity was 57 ± 3 % the equivalent concentration which reduced HUVEC metabolism to this level was estimated to be calculation of an EC50 value of 114 ± 12 mg mL^{-1} IOX (Figure 4.12). A similar effect on cell morphology, at the highest concentration of 324 mg mL^{-1}, was observed in comparison to the effects observed after HEK-293 and VSMC exposure to IOX. After 2 h treatment with IOX, HUVECs lost their typical endothelial morphology and became rounded and detached from their surface (Figure 4.13A and Figure 4.13B). A summary of IOX EC50s for each cell type was prepared and ANOVA analysis with Tukey comparisons were performed to show a significant difference between EC50 values for all cell types ($p < 0.001$; Table 4.4).
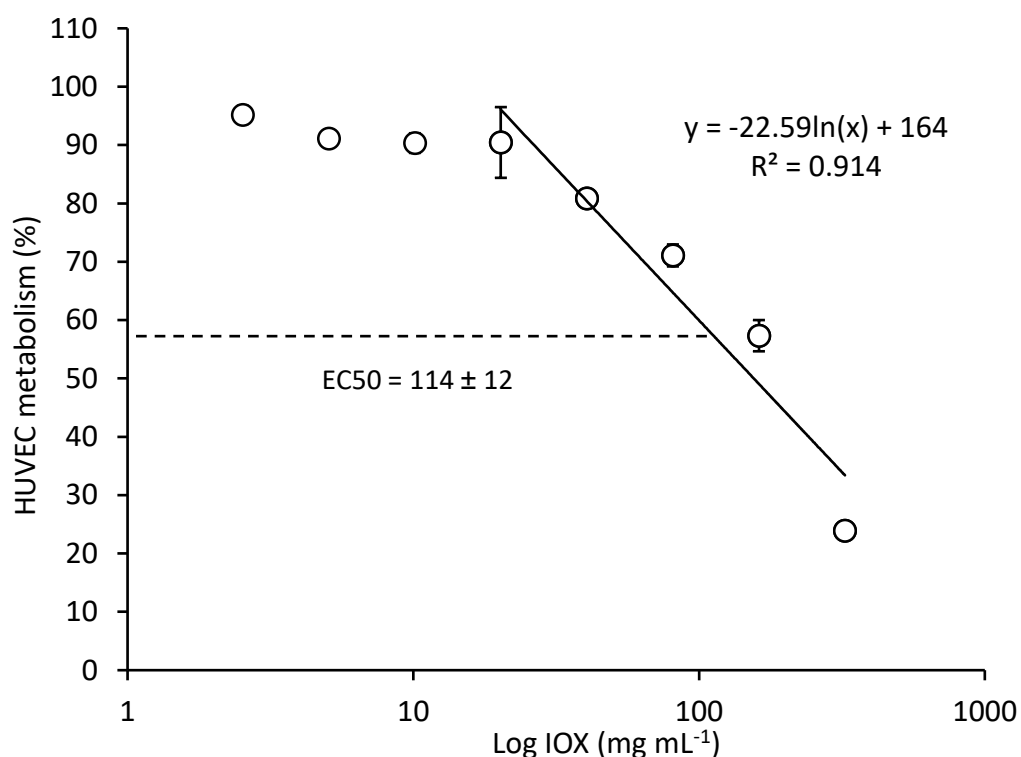
Figure 4.12: Effect of increasing IOX concentration on HUVEC metabolism after 2 h exposure. *The fluorescent reduction of Resazurin to Resorufin was measured after exposure of HUVECs to increasing IOX concentrations. The equation of the line was used to determine the EC50 value (n = 3; ± SD).*
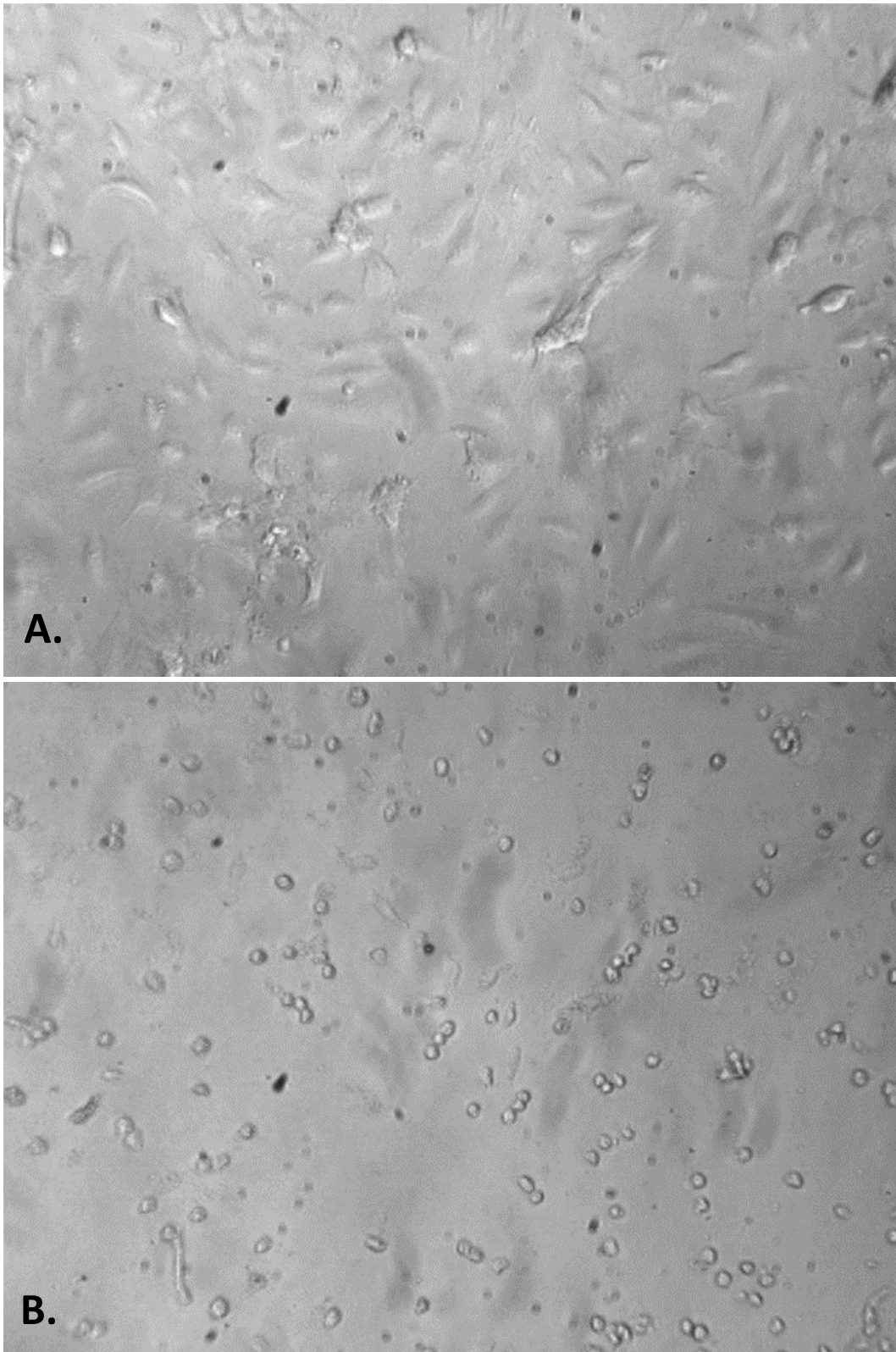
Figure 4.13: Comparison of the effect of HUVEC exposure to IOX on typical cell morphology. A) *Untreated viable HUVECs with typical endothelial morphology and* **B)** *HUVECs exposed to 324 mg mL^{-1} IOX for 24 h 100x.*

Table 4.4: Summary of experimental conditions and EC50 values for the analysis of the effects of IOX exposure on cell metabolism in vitro *(n = 3).*

Cell type	EC50 (mg mL^{-1})	± SD	p-value*	Treatment time
HEK-293	152	5	< 0.001	24 h
VSMC	124	15	< 0.001	2 h
HUVEC	114	12	< 0.001	2 h
	ANOVA with Tukey comparisons was performed for each EC50			

4.4.4 Comparison of the effect of empty- and IOX-NIV on vascular metabolism *in vitro*

The influence of both empty- and IOX-NIV on the metabolism of VSMC and HUVEC metabolism was analysed in a concentration-dependent manner using the Resazurin assay. Interestingly, it was found that VSMC metabolism was reduced to a greater extent by empty-NIVs in comparison to IOX-NIVs across a final lipid concentration range between 0.97 and 2.5 mM (Figure 4.14). Differences in the extent of NIV-associated metabolism reduction could also be visualised as a result of the change in colour directly related to the reduction of Resazurin to Resorufin (Figure 4.15). EC50 values based on NIV lipid concentration on VSMC metabolism was determined using PRISM where it was shown that a significantly lower concentration of empty-NIVs was required to reduce VSMC metabolic activity by 50 % in comparison to IOX-NIVs (p < 0.01; Table 4.5). The VSMC EC50 response to empty- and IOX-NIVs was 0.99 ± 0.001 mM and 1.36 ± 0.29 mM (1.29 mg mL^{-1} IOX equivalent), respectively.
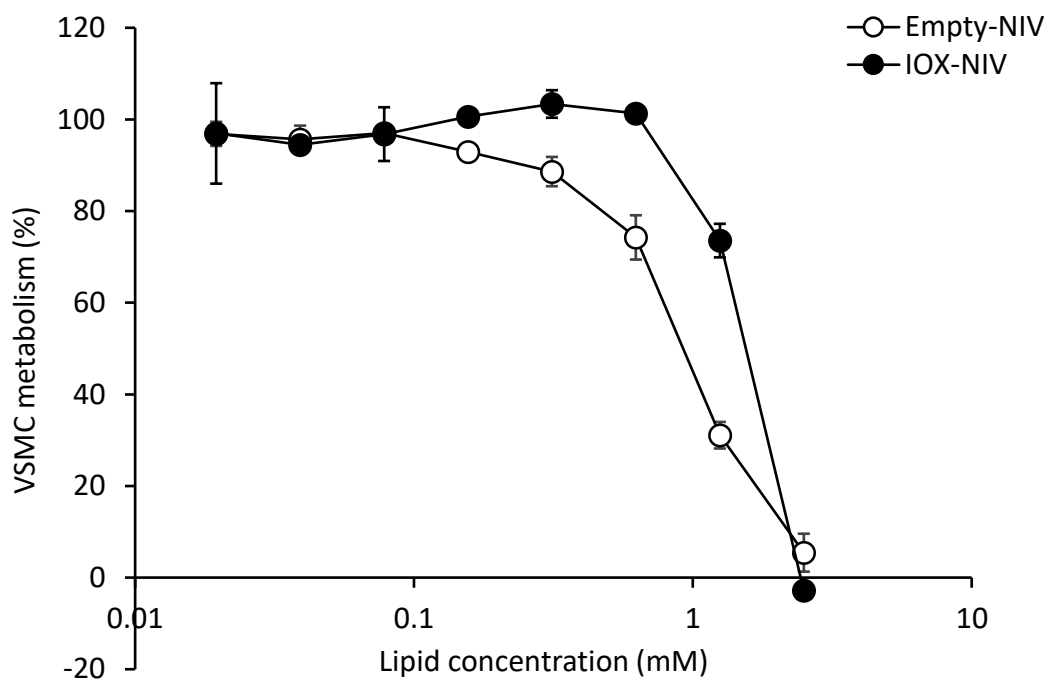
Figure 4.14: Relationship between increasing lipid concentration of empty- and IOX-NIV and VSMC metabolism. *VSMCs were treated with NIV for 2 h. Fluorescence was measured at wavelengths of 560_{ex} and 590_{em} nm. Equivalent encapsulated IOX concentration range within IOX-NIVs between 0.02 and 2.37 mg mL^{-1} (n = 3, whereby cells were isolated from 3x different rats, ± SD).*
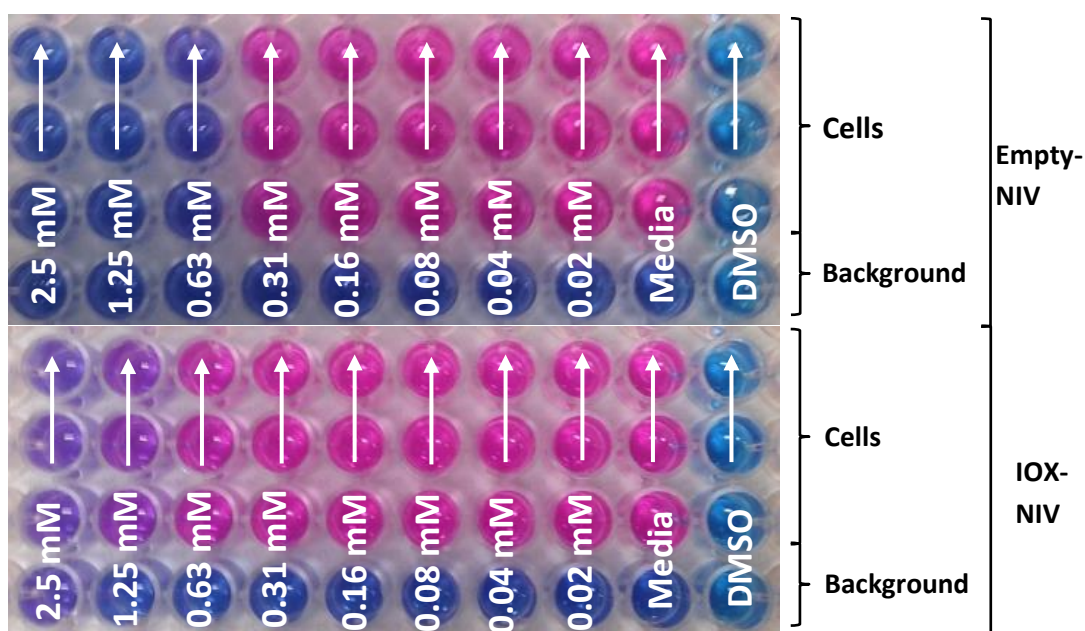
Figure 4.15: Colourimetic change in cell media observed after the metabolic reduction of Resazurin to Resorufin (blue-pink) by viable VSMCs in the presence of decreasing concentrations of NIVs. *Cells incubated in media was used as a positive control and cells destroyed using 50 % (v/v) DMSO was used as a negative control. Top – Empty-NIV, bottom – IOX-NIV.*

Table 4.5: EC50 values describing the effect of empty- and IOX-NIVs on VSMC metabolism. *VSMCs were treated with empty- and IOX-NIV for 2 h. Comparative p-values were determined using PRISM software (n = 3).*

Cell type	Treatment	EC50 (mM)	± SE	p-value*
VSMC	Empty-NIV	0.99	0.001	< 0.01
	IOX-NIV	1.36[†]	0.29	

* Statistical comparisons between empty vs IOX-NIV
[†]*Equivalent encapsulated IOX concentration of 1.29 mg mL^{-1}*

Similar to the greater reduction in metabolic activity observed after empty-NIV treatment of VSMCs in comparison to IOX-NIV, the reduction in HUVEC metabolism was also affected by lower concentrations of empty-NIVs (Figure 4.16). Again, visual analysis of the plate saw a change in cell media colour across the tested concentration range in agreement with the levels of fluorescence measured from the presence of Resorufin in cell media (Figure 4.17). Therefore, the EC50 value of empty-NIVs on HUVEC metabolism was also significantly lower, at 0.45 ± 0.001 mM, in comparison to IOX-NIVs which expressed an EC50 value of 1.28 ± 0.001 mM (Table 4.6).
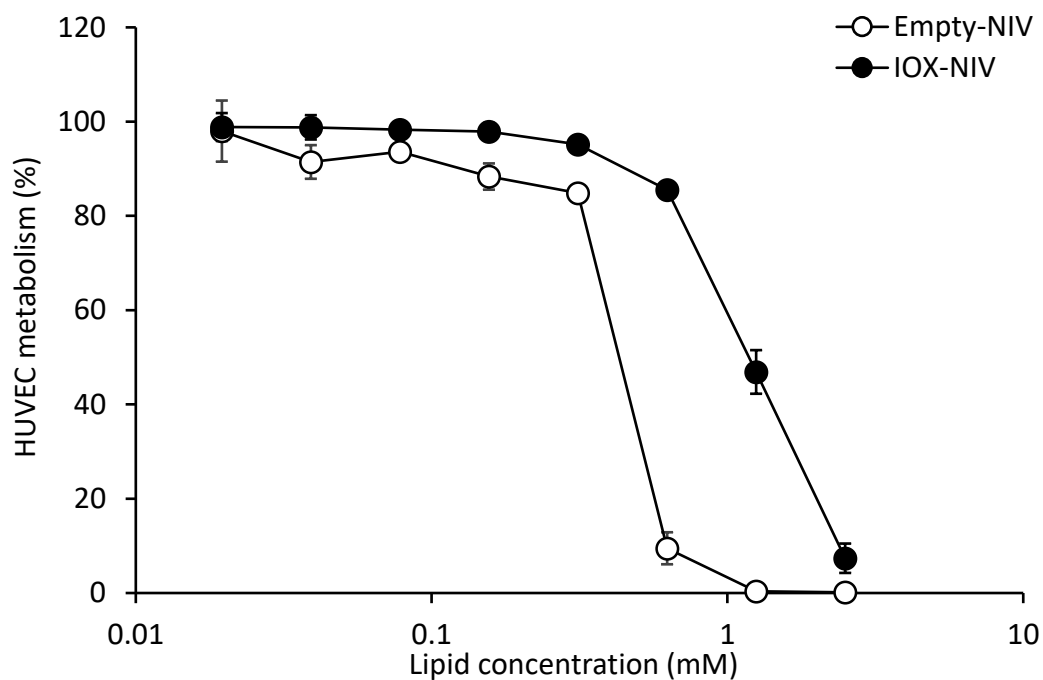
Figure 4.16: Relationship between increasing lipid concentration of empty- and IOX-NIV and HUVEC metabolism. *HUVECs were treated with NIV for 2 h. Fluorescence was measured at wavelengths of 560_{ex} and 590_{em} nm. Equivalent encapsulated IOX concentration range within IOX-NIVs between 0.02 and 2.37 mg mL^{-1}. (n = 3; $\pm$ SD).*
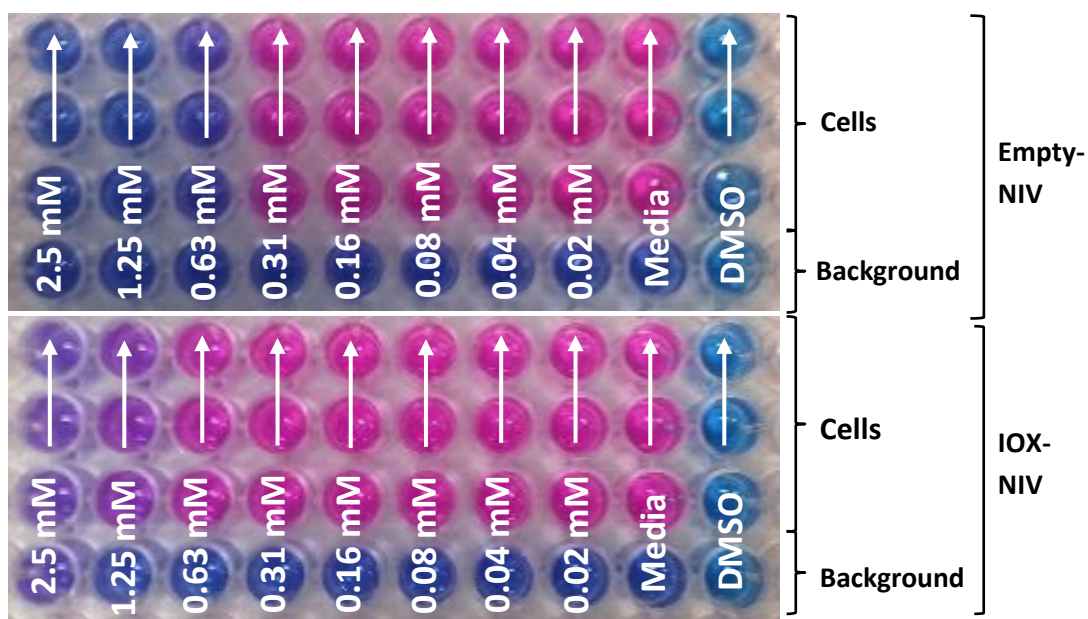
Figure 4.17: Colourimetic change in cell media observed after the metabolic reduction of Resazurin to Resorufin (blue-pink) by viable HUVECs in the presence of decreasing concentrations of NIVs. *Cells incubated in media was used as a positive control and cells destroyed using 50 % (v/v) DMSO was used as a negative control. Top – Empty-NIV, bottom – IOX-NIV.*

Table 4.6: EC50 values describing the effect of empty- and IOX-NIVs on HUVEC metabolism. *HUVECs were treated with empty- and IOX-NIV for 2 h. Comparative p-values were determined using PRISM software (n = 3).*

Cell type	Treatment	EC50 (mM)	± SE	p-value*
HUVEC	Empty-NIV	0.45	0.001	<0.001
	IOX-NIV	1.21[†]	0.001	

*Statistical comparisons between empty vs IOX-NIV
[†]*Equivalent encapsulated IOX concentration of 1.29 mg mL^{-1}*

Statistical analysis was also used to test the relationship between NIV concentration and cell metabolism based on the cell's origin, whether it was HUVECs or VSMCs. With a focus on the effects of empty-NIV treatment, VSMCs required a greater lipid concentration to induce similar reductions in metabolism in comparison to HUVECs. VSMCs expressed an EC50 of 0.99 ± 0.001 mM for empty-NIVs while HUVECs EC50 was significantly less at 0.45 ± 0.001 mM (p < 0.001; Table 4.7). In comparison to the responses observed when comparing the effect of IOX-NIV on HUVEC and VSMC metabolism, VSMCs were found to have a slightly greater EC50 at 1.36 ± 0.29 mM in comparison to HUVECs which expressed an EC50 of 1.28 ± 0.001 mM, however, the difference between cell types was non-significant.

Table 4.7: EC50 values describing the effect of empty- and IOX-NIVs on VSMC and HUVEC metabolism. *VSMCs and HUVECs were treated with increasing concentrations of either empty- or IOX-NIV for 2 h. Comparative p-values were determined using PRISM software (n = 3; ± SEM).*

Treatment	Cell type	EC50 (mM)	± SEM	p-value
Empty-NIV	VSMC	0.99	0.001	< 0.001
	HUVEC	0.45	0.001	
IOX-NIV	VSMC	1.36[1]	0.29	N/ a*
	HUVEC	1.28[2]	0.001	

* PRISM software accepts EC50 values as the same for VSMC and HUVECs
Equivalent encapsulated IOX concentrations of [1] 1.29 and [2] 1.21 mg mL^{-1}

4.4.5 Comparison of the effect of free-IOX, empty- and IOX-NIV on vascular cell viability *in vitro*

For the performance of the ApoToxGlo™ assay, cells were treated with free-IOX at concentrations higher and lower than the EC50 value determined after initial Resazurin experiments. Empty- and IOX-NIVs were tested at concentrations equivalent to the Resazurin-EC50, as well as a slightly lower concentration (Section 4.4.3). All treatment types were observed to induce a loss in VSMC viability in a concentration-dependent manner as

determined by the ApoToxGlo™ assay. Higher concentrations lead to a greater reduction in viable VSMC signalling. Despite reductions in overall viability after 4 h exposure in each treatment group, only VSMCs treated with 1.36 mM IOX-NIV or 80 and 170 mg mL^{-1} IOX expressed statistically significant reductions in fluorescence (Figure 4.18). VSMCs treated with 1.36 mM IOX-NIV expressed a fluorescence of 129 ± 27 rfus while control VSMCs expressed fluorescence of 324 ± 46 rfus ($p < 0.001$). HUVECs exposed to 80 and 170 mg mL^{-1} IOX were 74 ± 37 and 63 ± 0.85 rfus, respectively. The inclusion of PTX as a control of apoptosis-mediated death showed reduced fluorescence of 225 ± 28 rfus, however, this was not significant.

After 4 h VSMC treatment with free-IOX, empty-NIV and IOX-NIV, a significant increase in toxicity-associated fluorescence of empty- and IOX-NIV treated VSMCs was observed ($p < 0.001$; Figure 4.19). In contrast to the IOX-induced reduction in viable VSMC fluorescence, a comparable increase in toxicity fluorescence was not observed. Empty-NIV treatment of VSMCs at a concentrations of 0.50 and 0.99 mM lead to a toxicity fluorescence of 3828 ± 303 and 3093 ± 137 rfus, respectively. IOX-NIV treatment also significantly increased toxicity fluorescence which was 1950 ± 310 and 2287 ± 260 rfus after treatment with 1.36 and 0.95 mM, respectively. Significantly greater levels of toxicity were observed when comparing NIV-treated VSMCs to the signal obtained from live VSMCs (205 ± 40 rfus) and PTX-treated VSMCs, which were included as a control for apoptosis-mediated cytotoxicity (425 ± 362 rfus). Similar to previous analysis of viability, there was no significant difference between the untreated live control, and the PTX-treated VSMC control.

VSMC caspase-3/ -7 expression, which was measured as an indicator of apoptosis, after treatment with free-IOX, or empty- and IOX-NIV was not found to be significantly increased in comparison to the control of untreated cells ($p = 0.211$; Figure 4.20). Despite an increase in in VSMC luminescence treated with 100 nM PTX - from 262 ± 23 in untreated VSMCs, to 388 ± 349 in PTX-treated, the increase in fluorescence was not found to be significantly different from any other measurement which is likely related to the high SD observed between different measurements of PTX-treated VSMCs.
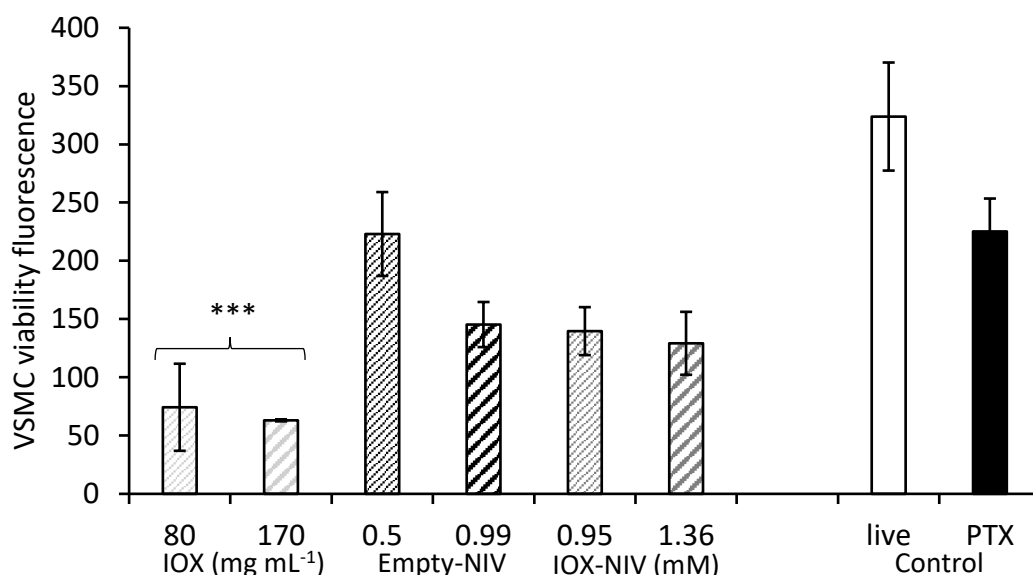
Figure 4.18: Detection of fluorescence representative of VSMC viability during the performance of the ApoTox-Glo™ assay. *VSMCs were exposed to free-IOX, empty- and IOX-NIV for 4 h prior to the addition of substrate for the detection of cell viability using fluorescence wavelengths of 400_{ex} and 505_{em} nm. Treatment with 100 nM paclitaxel (PTX) was used as a control for the induction of apoptosis-mediated cytotoxicity. Equivalent encapsulated IOX concentration range within IOX-NIVs was 0.90 and 1.29 mg mL^{-1}, respectively (*** p < 0.001 in comparison to the live control1; n = 3; ± SD).*
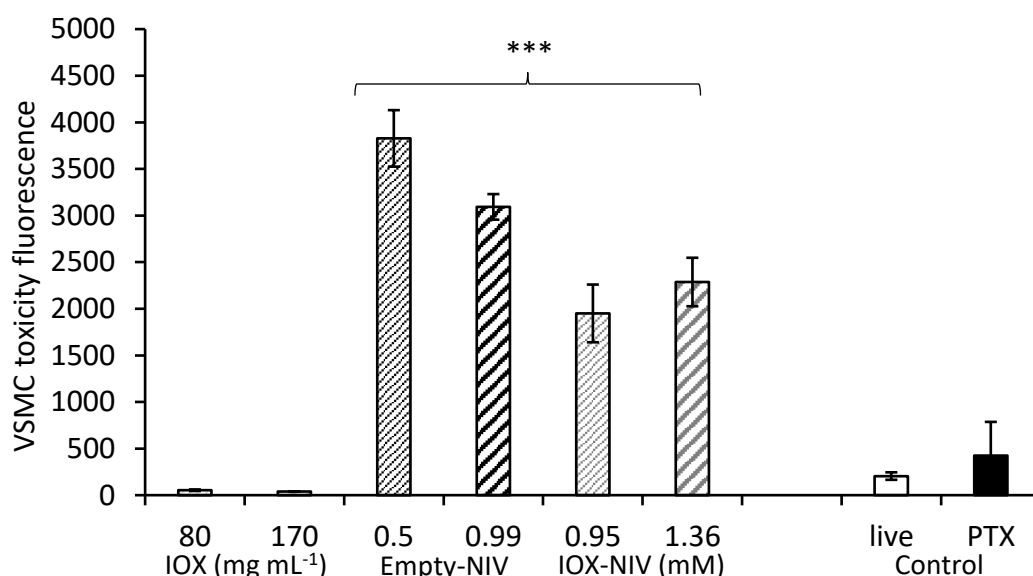
Figure 4.19: Fluorescent detection of VSMC toxicity during the performance of the ApoTox-Glo™ assay. *VSMCs were exposed to free-IOX, empty- and IOX-NIV for 4 h prior to the addition of substrate for the detection of cell death using fluorescence wavelengths of 485_{ex} and 520_{em} nm. Treatment with 100 nM paclitaxel (PTX) was used as a control for the induction of apoptosis-mediated cytotoxicity. Equivalent encapsulated IOX concentration range within IOX-NIVs was 0.90 and 1.29 mg mL^{-1}, respectively (**** p < 0.001 in comparison to live and dead cell controls; n = 3; ± SD).*
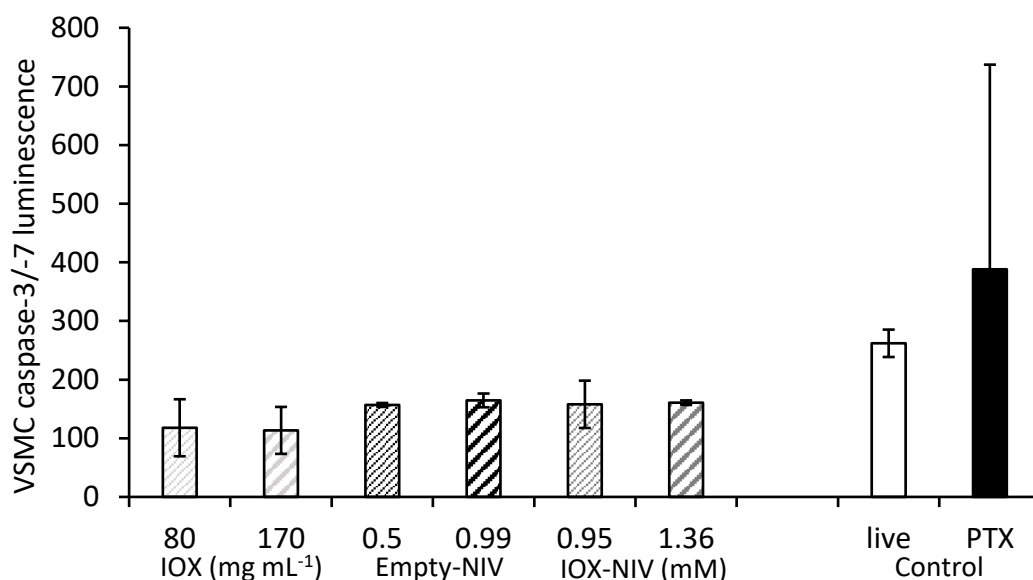
Figure 4.20: Luminescent detection of VSMC apoptotic activity during the performance of the ApoTox-Glo™ assay. *VSMCs were exposed to free-IOX, empty- and IOX-NIV for 4 h prior to the addition of substrate for the detection of caspase-3/ -7 using luminescence. Treatment with 100 nM paclitaxel (PTX) was used as a control for the induction of apoptosis. Equivalent encapsulated IOX concentration range within IOX-NIVs was 0.90 and 1.29 mg mL^{-1}, respectively (p = 0.211; n = 3; ±SD).*

In comparison to VSMC analysis of the effect of IOX, empty-NIV and IOX-NIV, all treatment groups were found to express significantly reduced fluorescence representative of viable HUVECs after 4 h treatment (Figure 4.21). Live cells, which were untreated HUVECs, expressed a fluorescent intensity of 1177 ± 97 rfu, in comparison, the negative control of dead HUVECs, which were treated with 50 % (*v/v*) DMSO, expressed a significantly lower signal of 3 ± 3 rfu ($p < 0.001$). Cell viability was ~50 % lower for most treatment groups which was also significantly different to the positive control ($p < 0.001$). In addition to this, HUVEC exposure to 170 mg mL^{-1} IOX resulted in a further significant reduction in viable cells in comparison to the reduction observed after HUVEC exposure to just 80 mg mL^{-1} IOX whereby HUVECs expressed a fluorescence of 196 ± 59 and 543 ± 32 rfu, respectively ($p < 0.001$).

Measurement of fluorescence indicative of cytotoxicity shows an absence of signal for the positive control dead HUVECs treated with 50 % DMSO. Despite this, the cytotoxicity fluorescence measured from the HUVEC live control (1168 ± 127 rfu) was significantly less than all of the NIV-treated samples (Figure 4.22; $p < 0.001$), a similar effect was observed previously when VSMCs were exposed to NIVs. HUVECs treated with 80 or 170 mg mL^{-1} IOX did not express an increase in cytotoxicity signal but again, similar to the VSMC response, both of these treatment groups expressed a signal lower than the viable cell control. Measured cytotoxicity fluorescence was 473 ± 86 and 102 ± 28 rfus after exposure to 80 and 170 mg mL^{-1}

IOX, respectively (Figure 4.22; p < 0.001). HUVECs treated with empty-NIV at concentrations of 0.31 and 0.46 mM increased the cytotoxicity fluorescence from 1168 ± 127 rfu to 3425 ± 543 and 4447 ± 1349 rfu, respectively. HUVECs treated with IOX-NIV at concentrations of 0.63 and 1.2 mM produced similarly high fluorescent intensities at 3699 ± 329 and 3381 ± 1177 rfu, respectively.

HUVEC apoptotic activity was analysed upon detection of luminescence representative of caspase-3/ -7 after 4 h treatment with either free-IOX, empty-NIV or IOX-NIV. The luminescent signal gained for the dead control was significantly lower than the signal produced from the live HUVEC control. An appropriate positive control for the induction of apoptosis was not included in these set of experiments and only a negative control of dead cells (treated with 50 % (v/v) DMSO) was included for the purpose of the toxicity signal measured previously. The only treatment group which produced a significantly greater apoptotic signal in comparison to live, viable HUVECs was after 4 h treatment with 170 mg mL^{-1} IOX whereby HUVECs expressed a luminescence of 640 ± 64 which was significantly greater than the HUVEC live control group which expressed a luminescence of 467 ± 45 (Figure 4.23; p < 0.001). An additional significant relationship was observed upon analysis of the decrease in caspase-3/ -7 activity when comparing the live control with HUVECs treated with 0.63 mM IOX-NIV which expressed a signal of 314 ± 76, however, this was not indicated due to the fact that the signal level was below that of viable HUVECs.
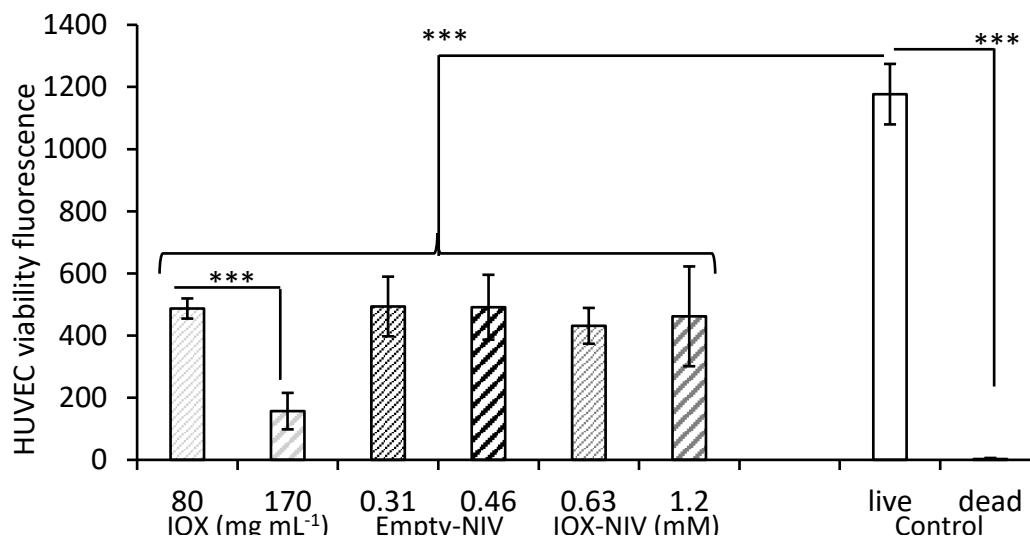
Figure 4.21: Detection of fluorescence representative of HUVEC viability during the performance of the ApoTox-Glo™ assay. *HUVECs were exposed to free-IOX, empty- and IOX-NIV for 4 h prior to the addition of substrate for the detection of cell viability using fluorescence at wavelengths of 400_{ex} and 505_{em} nm. Treatment with 50 % (v/v) DMSO was used as a control for cell death. Equivalent encapsulated IOX concentration range within IOX-NIVs was 0.60 and 1.14 mg mL^{-1}, respectively (*** p < 0.001; n = 3; ± SD).*
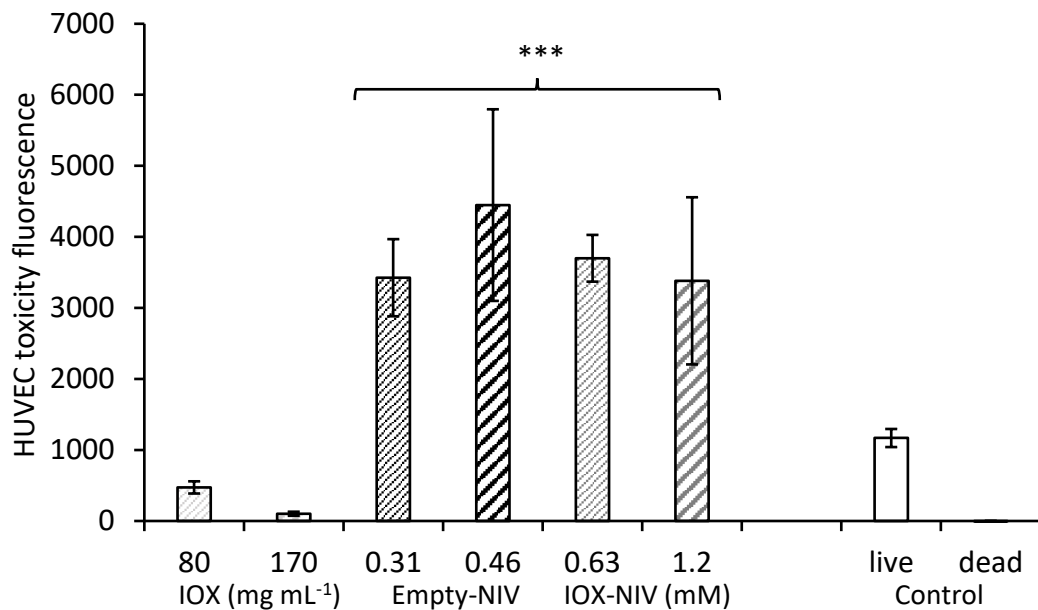
Figure 4.22: Fluorescent detection of HUVEC toxicity during the performance of the ApoTox-Glo™ assay. *HUVECs were exposed to free-IOX, empty- and IOX-NIV for 4 h prior to the addition of substrate for the detection of cell death using fluorescence at wavelengths of 485_{ex} and 520_{em} nm. Treatment with 50 % (v/v) DMSO was used as a control for cell death (*** p < 0.001 in comparison to the live cell control; n = 3; ± SD).*
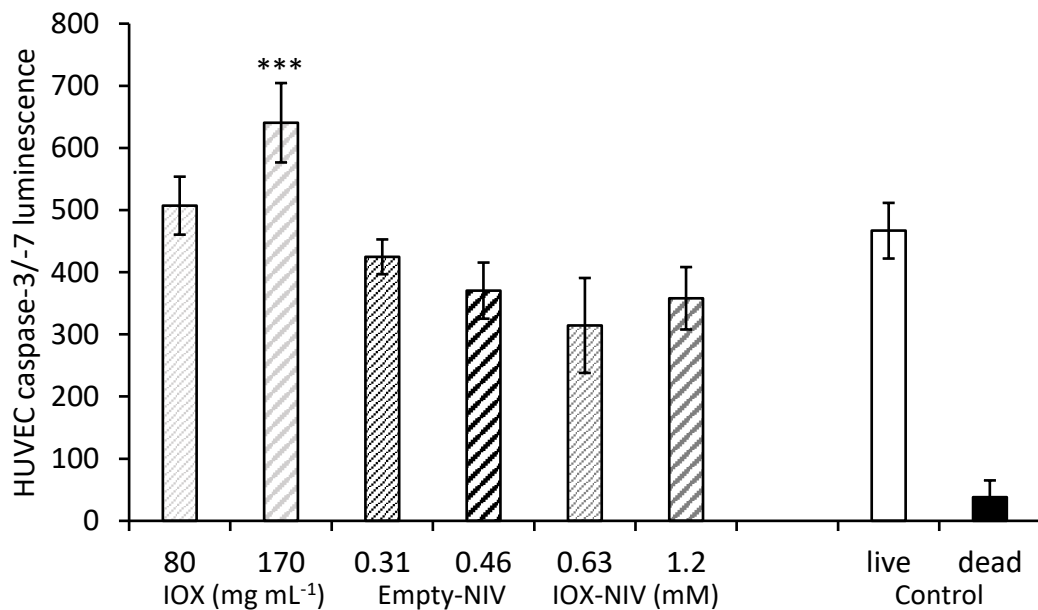
Figure 4.23: Luminescent detection of HUVEC apoptotic activity during the performance of the ApoTox-Glo™ assay. *HUVECs were exposed to free-IOX, empty- and IOX-NIV for 4 h prior to the addition of substrate for the detection of caspase-3/ -7 using luminescence. Treatment with 50 % (v/v) DMSO was used as a control for cell death (*** p < 0.001 in comparison to the live cell control; n = 3; ± SD).*

4.5 Discussion

4.5.1 Role of osmolality on IOX-mediated HEK-293 metabolic activity, proliferation and cytotoxicity

Previously published research is in agreement with the results which demonstrate the ability of low osmolar RCM to exert a time- and concentration-dependent decrease in HEK-293 metabolic activity that is independent of osmolarity (Romano *et al.*, 2008). These conclusions could be made when comparing RCM response to that obtained after exposure to mannitol as an equi-osmolar control. The decision to use mannitol was based on the fact that mannitol is a known osmotic diuretic, similar to IOX, and previous research has indicated a role for mannitol-based hyperosmolarity in HUVEC dissociation and cell death through apoptosis (Malek *et al.*, 1998). The unexpected concentration-dependent increase in HEK-293 metabolism after mannitol exposure may have been related to mannitol-based signal interference, rather than an ability to directly enhance metabolic activity. This is due to the fact that mannitol itself is not actively metabolised and is inert to mammalian cells, instead, it is a common metabolic agent in plants (Patel and Williamson, 2016). Despite this, duplicate background samples, whereby culture media plus mannitol and Resazurin were analysed, did not lead to the generation of a concentration-dependent fluorescent signal in the absence of cells. Further investigation could include analysis of the effects of an alternative hyperosmolar agent, or involve longer exposure times. In comparison to the experimental design shown here, Shen and Kamen (2012) reported a decrease in HEK-293 proliferation and viability after long-term exposure and routine culturing in hyperosmolar NaCl solutions, however, subjection of cells to prolonged exposure times does not reflect the short half-life of RCM *in vivo.*

In addition to previous experiments, the CellTox™ Green assay was performed as a real-time kinetic "no-step" assay to determine the influence of time on IOX toxicity. CellTox™ Green offers a direct method for the detection of toxicity as it utilises a dye that increases in fluorescence when intercalated with DNA released dying cells (Section 4.1.3). Despite the measurement of fluorescence being carried out at a number of different time points as described in the manufacturer's protocol, a significant loss in the positive control signal between 6 and 24 h was observed. This was in opposite to data presented by the manufacturer who reported continual, real-time analysis of toxicity using a number of cytotoxic agents over the course of a total of 72 h (Worzella et al., n.d.). A peak in signal from positive control HEK-293s was observed after 2 h incubation, therefore data was presented from the 2 h time point. At this time point there was no significant increase in CellTox™ fluorescence after HEK-293 exposure to IOX at concentrations up to 324 mg mL^{-1}, suggesting there was no

IOX-induced death, even the live negative control expressed a slightly greater signal in comparison to all IOX-treated samples. In addition, the lysis control provided in the kit produced a significantly greater signal > 5x the negative control. Microscopic visualisation of HEK-293s at the end of the experiment (24 h) detected drastic alterations in morphology, including a concentration-dependent reduction in HEK-293 adherence which was observed after treatment with IOX concentrations between 43 and 96 mg mL^{-1}. The loss in adherence after treatment with 216 mg mL^{-1} IOX was accompanied by a loss in the visualisation of distinct cell membranes between neighbouring cells and the formation of extended appendages between large masses of cells. Previous research has made links between tubular formation in endothelial cells under hyperosmolar conditions induced by both glucose and mannitol (Madonna *et al.*, 2016). Similarities can be observed between morphological changes observed after IOX exposure and those reported to occur during hyperosmotic stress which activates focal adhesion kinases in order to protect against hyperosmotic-induced apoptosis (Lunn and Rozengurt, 2004), as well as in the prevention of hyperosmotic-independent loss-of-adherence or anchorage-induced apoptosis (Frisch *et al.*, 1996). Visualisation of masses of undefined cells with thin, networking, appendages, resembling filopodia (Section 4.4.2), have also been described upon exposure of cells to hyperosmotic stress as a result of actin filament reformation (Lunn and Rozengurt, 2004). After HEK-293 treatment with higher concentrations of IOX (324 mg mL^{-1}) no adherent cells were visualised and there was little resemblance to viable untreated HEK-293s. Instead, few large aggregates were found to be floating in the media which is likely to be indicative of cell death. This treatment group shared a greater resemblance to the lack of cells observed in the lysis buffer control, which in opposite to test samples, expressed a high level of fluorescence indicative of toxicity at time points ≤ 6 h (Section 4.4.2). The vast difference in cellular appearance (24 h post-exposure) and the inability to detect CellTox fluorescence (6 h post-exposure) may have been related to the kinetics of IOX-induced toxicity, as any cell death which occurred after the 6 h time point may not have been detected due to a loss in CellTox signal, as seen upon analysis of the positive control at 24 h (Section 4.4.2). In order to quantify any toxicity linked with the IOX-destruction of HEK-293 morphology, the performance of an end-point assay may have been more appropriate.

Jensen *et al.* (2011) studied the effects of IOX on NRK 52-E renal epithelial cells in a time-dependent manner. The first detectable effects of IOX was a rapid reduction in metabolic activity, as determined through the use of the MTT assay, whereby after 30 min treatment with 324 mg mL^{-1} IOX reduced metabolism to 45 % which decreased further with time, reaching 6 % after 24 h. These results are similar to the effects of IOX on HEK-293 metabolism as

determined using Resazurin whereby 13 % of metabolically active viable cells were measured after 24 h incubation with 324 mg mL^{-1} IOX (Section 4.4.3). Interestingly, Jensen *et al.* (2011) was unable to detect cytotoxicity until 12 and 24 h post-treatment using trypan blue analysis and through scoring cell death in terms of necrotic and apoptotic activity. This study highlights the importance of timing in the detection of IOX-associated toxicity and may explain why the reduction in HEK-293 metabolism could be easily quantified, while alterations in toxicity could not be confirmed using CellTox analysis. In contrast, an absence of toxicity in combination with a reduction in metabolism and proliferation has been reported in a single study by Sawmiller *et al.* (1998) who measured toxicity based on the expression of lactate dehydrogenase.

4.5.2 Toxicity profile and EC50s of IOX on HEK-293, VSMCs and HUVECs based on the measurement of cell metabolism

The Resazurin metabolic indicator assay was also performed in order to characterise the toxic profile of IOX which could be used to obtain EC50 values for HEK-293s, VSMC and HUVECs. Despite potential differences when comparing *in vitro* EC50s with toxicity *in vivo* the characterisation of toxicity profiles is an essential step in the drug development process. HEK-293 experiments involved exposure to IOX for 24 h while vascular cells were exposed to IOX for 2 h, which was previously described as the half-life of IOX (Olsson *et al.*, 1983). The EC50 values for the different cell types was similar, between 124 and 152 mg mL^{-1} (section 4.4.3). This is in agreement with previous research which evaluated the toxicity of IOX after exposure within the spinal column. *In vitro* cytotoxicity of nucleus pulposus cells was similar to the results obtained here, whereby, after 18 h exposure to 175 mg mL^{-1} IOX cell viability was reduced to 40 % (Matheny and Moehlenbruck, 2010). Based on the calculated EC50s, the order of greatest susceptibility to IOX-associated reduction in metabolism was VSMC > HUVEC > HEK-293. HEK-293s were found to have the greatest EC50 value, and hence lowest IOX susceptibility, in comparison to the other cell types. The combination of extended exposure time and the requirement for a high IOX concentration to induce a 50 % reduction in metabolism could suggest that HEK-293 cells are more robust and not as sensitive to the effects of IOX when compared to cells of vascular origin. This result may seem surprising as the majority of preventative measures associated with the avoidance of RCM-associated disease focus on the function of the kidneys, however, if the negative effects of IOX administration could be prevented in the vasculature, downstream events related to the kidneys may be circumvented. The protection of the vasculature from immediate exposure to RCM upon sequestering it within a delivery system may offer another advantage in support of an IOX-NIV delivery system. When comparing the two cellular components of the

vasculature, VMSCs were shown to be the most sensitive to the action of IOX indicated by the lowest EC50 value. Endothelial cells are likely to be the first point of contact after IV administration of RCM and in turn appear to be more resistant to the negative effects of low osmolar non-ionic RCM. SMCs were also reported to be more greatly influenced by the anti-proliferation effect of IOX, in comparison to endothelial cells (Sawmiller *et al.,* 1998). In relation to vascular sensitivity to osmolarity, the opposite results have been reported, whereby endothelial cells are more susceptible to this mechanism of cytotoxicity (Malek *et al.*, 1998).

Regardless of the cell type, visualisation of metabolically reduced cells, as determined using the Resazurin assay, saw them become rounded and detach from their surface. This occurred to a greater extent when IOX concentration increased. Research performed by Malek *et al.*, (1998) to determine the effect of hyperosmolar agents on endothelial and VSMCs detected the induction of apoptosis related to a change in cellular morphology which was described as a cell rounding and 'cell loss phenomenon', similar to the results gained in the experiments described in this thesis. Exposure of monocytes to IOX has been reported to result in the opening of K^+ channels leading to K^+/ Cl^- and H_2O efflux as an attempt to reduce the extracellular/ intracellular osmotic gradient, which in turn leads to cell shrinkage (Bøyum *et al.*, 2002). This would provide a simple explanation to describe the change in cellular morphology to round spherical cells which lose adhesion capabilities, however, these results do not coincide with initial results which did not find a role for osmolality in altered metabolism exerted by IOX. *In vitro* cell shrinkage occurs as the result of a shift in the cytoskeleton and rearrangement of focal adhesion points, the interactions of which have been shown to play a key role in determining cell survival or death through apoptosis – a feature of which is cell shrinkage (Frisch *et al.*, 1996; Lunn and Rozengurt, 2004). RCM-induction of apoptosis on a variety of renal cell lines has been described elsewhere (Rowe *et al.*, 2016; Ko *et al.*, 2016; Gong *et al.*, 2009), however, further analysis is required to determine whether IOX has induced apoptosis within the experiments outlined in this thesis, however, the reduced metabolic activity combined with cell shrinkage, rounding and loss of adhesion upon exposure to IOX could support cell death through apoptosis.

4.5.3 EC50s of NIVs on VSMCs and HUVECs based on the analysis of metabolic activity *in vitro*

As concluded in the earlier physical characterisation of NIVs, the entrapment of IOX within NIVs is likely to alter the typical pharmacokinetic profile of IOX so that it is no longer filtered through the kidneys, instead, it is likely that IOX-NIVs will be delivered to other organs in the body (Chapter 2 – Formulation and Physical Characterisation of IOX-NIV). *In vitro*

experiments involving the analysis of the effects of empty- and IOX-NIVs, therefore, focused on vascular-derived cells rather than kidney-derived cells. The 22 % EE of IOX within NIVs and subsequent purification through ultracentrifugation means that the final concentration of IOX within NIVs that cells may be exposed to cells is much less than that IOX exposure as a free-drug. Assuming a 22 % EE the treatment of cells with IOX-NIVs at final lipid concentrations of 2.5-0.02 mM would be equivalent to IOX concentrations within the range of 2.37-0.02 mg mL^{-1}, which according to earlier IOX cytotoxicity analysis . In order to compare EC50 values with that described in the literature, concentrations used in this thesis were converted from a molar concentration to weight concentrations (Table 4.8). The EC50s obtained after treatment on VSMC and HUVECs ranged from 447-990 µg mL^{-1} for empty-NIV and 1275-1364 µg mL^{-1} for IOX-NIV. Both ranges covered greater concentrations than that described in the literature for empty-NIVs, whereby, Obeid *et al.* (2016) reported the effect of hydration media on *in vitro* toxicity of empty-NIVs, using the same Resazurin metabolic indicator assay. In contrast to the data reported here Obeid *et al.* (2016) described EC50 values between 140 and 410 µg mL^{-1} suggesting that the formulation and method of synthesis described in this thesis reduced toxicity in comparison to alternative methods and formulations.

Table 4.8: Conversion of NIV EC50 values from molar to mass concentration of total lipid for the comparison with data provided in the literature *(n = 3; ± SD).*

Cell type	Treatment	µM	µg mL^{-1}
VSMC	Empty-NIV	990 ± 1.05	419 ± 0.44
	IOX-NIV	1364 ± 286[1]	577 ± 121
HUVEC	Empty-NIV	447 ± 1.04	190 ± 0.44
	IOX-NIV	1275 ± 1.04[2]	540 ± 0.44
Equivalent encapsulated IOX concentrations of [1]1.29 and [2]1.21 mg mL^{-1}			

Regardless of the cell type chosen, empty-NIVs were observed to exert a significant reduction in metabolism *in vitro* when compared to IOX-NIVs, as represented by the lower EC50 values. Surprisingly, despite the level of toxicity exerted by free-IOX, IOX-entrapment within NIVs did not reduce the EC50 lipid concentration in comparison to empty-NIV, but instead offered a protective effect leading to the requirement higher concentrations in order to match the toxic effect of empty-NIVs. Controversially, antioxidant activity of RCM, including IOX, has previously been reported where they have been found to inhibit superoxide and hydroxyl radical production (Berg *et al.*, 2005). This work appears to be in contrast to the fact that IOX-associated reactive oxygen species (ROS) production has been defined as a contributing factor in RCM-AKI, while N-acetylcysteine antioxidant treatment has been shown to offer protection against RCM-associated renal damage (Yang *et al.*, 2014; Gong *et al.*, 2010).

Despite this, it may be speculated that IOX-NIV exposure *in vitro* can prevent cellular production of ROS as a result of its transmembrane delivery into cells, leading to reduced toxicity. The delivery of antioxidants within a liposome formulation has been reported to offer improved efficacy, in comparison to free-antioxidants, due to the ability of the delivery system to promote delivery across the cell membrane and improve the retention of antioxidants within the cell (Suntres, 2011). In terms of cell-type-based sensitivity, empty-NIVs were found to effect HUVECs to a more significant level in comparison to VSMCs. In contrast, there was no significance when comparing the measured EC50 values of IOX-NIV on VSMCs and HUVECs. Previous research comparing the toxicity of a cationic liposome delivery system on both endothelial and SM cells, using a similar metabolic indicator assay, had shown a slight decrease in SM cell viability in comparison to endothelial cells, this highlights the influence of the final physicochemical characteristics of lipid drug delivery systems and their ability to induce toxic effects (Brito *et al.*, 2008).

4.5.4 Further investigation of IOX, empty-NIV and IOX-NIV vascular insult through the use of the ApoTox-Glo™ assay

Previous investigations into the suitability of the Resazurin assay has identified the potential for the alteration of both viability and morphology as a direct result of Resazurin exposure, which was determined upon comparison of ATP-measured viability after increasing Resazurin exposure times (Riss *et al.*, 2013). However, a negative effect on the morphology of control samples as a result of Resazurin exposure was not observed, therefore, it is likely that any Resazurin-mediated effects on cell viability are related to the cell type tested and concentration of Resazurin, in addition to the time cells ae exposed to Resazurin. The performance of initial assay optimisation experiments carried out prior to the analysis of test materials detected the minimum incubation time required to produce an optimal signal reflective of healthy cells. In addition to this, a comparison between control cells and IOX-treated cells would reduce any interference as all test and control sample will have been incubated with the same concentration of Resazurin or CellTox™ Green reagent. RCM have commonly been reported to induce apoptosis after *in vitro* exposure to HEK-293s (Romano *et al.*, 2008), HUVECs (Zhang *et al.*, 2000), VSMCs and cardiocytes previously (Zhang *et al.*, 1999)

Despite a clear reduction in metabolic activity after exposure to IOX and NIVs the level of IOX-related toxicity was questionable after a combination of assays which analyse directly measure toxicity failed to detect an increase in toxic biomarkers (Section 4.4.2). In addition to the range of metabolic, proliferative and toxicity assays performed previously, an additional triplex assay was utilised to look at the effects of IOX, empty-NIV and IOX-NIV around the

concentrations detected to relate to the EC50 values of different cell types. In addition to the measurement of toxicity and viability as determined by the measurement of fluorescence, the ApoTox-Glo™ assay is able to measure apoptotic activity which is a common theme reported in the literature after *in vitro* exposure to RCM and hyperosmolar agents.

An apoptotic positive control was included during the performance of the ApoTox-Glo™ assay on VSMCs where cells were treated with a concentration of 100 nM PTX, which was previously reported to induce apoptosis in cancerous nasopharyngeal cells *in vitro* (Tan *et al.*, 2002), which was anticipated to act as a combined positive control for both the detection of toxicity and apoptosis, as well as acting as a negative control for viability. However, performance of the assay did not lead to a significant decrease in viability signal in comparison to the live VSMC signal. In addition, the toxic PTX-treated control signal was low and not significantly different than live untreated VSMCs. A slight increase in apoptotic signal measured from PTX-VSMCs was observed, however this was not significantly different to the live VSMC control which may have been attributed to the large standard deviation measured. Rather than continuation with PTX as a positive control for HUVEC toxicity and apoptosis a different control was selected for the performance of the ApoTox-Glo™ assay whereby, HUVECs were exposed to 50 % DMSO as a negative control for viability and positive control for toxicity as success had previously been observed using this treatment type during the performance of the Resazurin assay. Little fluorescence was detected upon the measurement of VSMC viability, however, this was also the case upon measurement of toxicity. As expected, a significant increase in caspase-3/ -7 signal was measured upon exposure of HUVECs to 50 % DMSO. Previous research has shown that human-derived cells exposed to DMSO undergo apoptotic cell death as detected by an initial increase in membrane fluidity and influx of Ca^{2+} and upregulation of NOS activity (Trubiani *et al.*, 2003).

VSMCs and HUVECs were exposed to two different concentrations of free-IOX, empty-NIV and IOX-NIV during the performance of the ApoTox-Glo™ assay which were dependant on the results obtained from the Resazurin assay. VSMC EC50s were determined to be 124 ± 15 mg mL^{-1} IOX, 0.99 ± 0.001 mM empty-NIV and 1.36 ± 0.29 mM IOX-NIV while HUVEC EC50s were 114 ± 12 mg mL^{-1} IOX, 0.45 ± 0.001 mM empty-NIV and 1.28 ± 0.001 mM IOX-NIV. VSMCs and HUVECs were treated with IOX concentrations above and below the calculated EC50s at 70 and 180 mg mL^{-1} IOX. One NIV treatment concentration was equivalent to the predetermined Resazurin-based EC50 calculated for each cell type while the second concentration tested was at a final concentration lower than the determined EC50 in

order to determine whether any effects were likely to be concentration-dependent, a feature which was observed during the performance of the Resazurin assay.

Upon measurement of fluorescence representative of VSMC viability, it was noted that across the different treatment groups the signal was relatively low and peaked at the live control at ~330 rfu. In comparison, the viable fluorescent signal from live, untreated HUVECs was much greater at ~1180 rfu. All VSMC treatment groups expressed viability fluorescence less than the live cell control but only IOX-treated VSMCs showed a significant reduction, however, in contradiction to results from the Resazurin assay, a relationship between IOX concentration and signal reduction was not detected. In comparison, the majority of HUVEC treatment groups – free-IOX, empty-NIV and IOX-NIV – were found to express a similarly significant reduction in viability. The exception to this rule was the greater signal reduction measured from HUVECs treated with 170 mg mL^{-1} IOX which was significantly reduced in comparison to HUVECs treated with 80 mg mL^{-1} IOX highlighting the potential for a concentration-dependent effect.

Interestingly, contrasting results were observed upon the measurement of VSMC and HUVEC toxicity across all treatment groups, whereby an increase in fluorescence was not observed after exposure to IOX, instead a signal increase was observed after NIV exposure to VSMCs and HUVECs. The increase in toxicity fluorescence was not necessarily concentration-dependent. Despite the inability to detect IOX toxicity in either VSMC or HUVEC treatment groups, exposure of HUVECs to the higher concentration of 170 mg mL^{-1} IOX did lead to a significant increase in caspase-3/ -7 activity, which was not observed after VSMC treatment. This may be related to the earlier detection of a greater sensitivity of HUVECs to IOX-associated reduction in metabolism, where a lower EC50 value was reported for HUVECs. In comparison, all NIV treatment groups expressed a caspase-3/ -7 signal less than the live control whether VSMCs or HUVECs were tested.

It is important to note, that during the performance of the ApoTox-Glo™ assay, background signals, which may have the potential to interfere with the accuracy of measurements, were recorded from wells containing test samples in the absence of cells which was subtracted from the fluorescence recorded from cells exposed to the same test samples. Therefore the detection of opposing results is unlikely to be related to test sample interference. The timing behind the measurement of viability, toxicity and apoptosis is an important factor which the manufacturer included a note about in the protocol. Differences in the series of biochemical events that cells undergo after exposure to a cytotoxic agent, and the ability to detect them is likely to occur in

a kinetic and cell-dependent manner. If these variables were further investigated by the performance of a time-response assay, as suggested by the kit manufacturers, more relevant data may have been obtained. The earlier detection of changes in VSMC and HUVEC metabolism were based on the effects after 2 h exposure. In the instance of the ApoTox-Glo™ assay, cells were exposed to test reagents for 4 h, the length of which was increased to account for differences in changes in metabolism in addition to the length of time typically taken for the induction of apoptosis. Despite this, the manufacturer's protocol states the potential for the measurement of reduced cell viability, without an inversely proportional increase in toxicity, in instances where a fast-acting toxic compound is being tested which could subsequently result in an underestimation of cytotoxicity.

4.6   Conclusion and experimental limitations

Although the safety of RCM has significantly improved since their initial development, through the reduction of ionic strength and osmolality, RCM-associated side-effects, including potential renal failure, remains to be a key problem in certain 'at-risk' groups of patients. The exact interactions leading to RCM-associated complications has proven to be a challenge to define, highlighted by the range of conflicting data available within the literature. The properties of RCM which have been the main focus of toxicity studies include osmolality, iodine concentration, and other chemistry-related factors. Despite conflicting data describing the role for osmolality on RCM-associated cell death, one major theme is the common association between RCM-exposure and cell death through apoptosis. The aims of this chapter were to define the toxic concentrations of RCM on renal, HEK-293 cells, and those derived from vascular origin, VSMCs and HUVECs. Initial experiments were performed with a focus on the role of osmolality and IOX concentration on HEK-293 metabolism, proliferation and toxicity. Further analysis was carried out to define the toxicity of both empty- and IOX-NIV, which were formulated and characterised in earlier chapters (Chapter 2 and 3), focused on the effects of these materials on vascular-derived cells VSMCs and HUVECs. An alteration in the typical biodistribution and pharmacokinetic profile of IOX was likely to be expected upon IV administration of IOX within a NIV formulation, whereby the literature shows that small lipid nanoparticles are more likely to be delivered to organs such as the liver and spleen. In comparison free-IOX is rapidly filtered through the kidneys and excreted in the urine. This alteration in biodistribution therefore offers the potential for IOX to bypass the kidneys, which is a key organ involved in the development of RCM-associated disease, which is why NIV toxicity was carried out with a focus on cells of vascular origin. Due to various advantages and disadvantages associated with different techniques commonly used during *in vitro* analysis, a multi-faceted approach was taken whereby contrasting and complimentary techniques were utilised with the goal of being able to further the understanding of IOX-associated damage and the safety of a NIV system.

IOX-associated reductions in HEK-293 metabolism, which is commonly reported as cytotoxicity, in comparison to mannitol solution expressing a similar level of osmolality, opposing results were obtained, suggesting that IOX hyperosmolality was not the most predominant factor leading to the loss in metabolism. In addition to the measurement of HEK-293 metabolism after exposure to increasing concentrations of IOX, a commercially available toxicity kit, CellTox™ Green, which is based on the ability of a dye to bind to nucleic acids of dead cells as a result of increased membrane permeability, was utilised to show that, surprisingly no increase in toxicity was observed even at high IOX concentrations. The

performance of a literature search revealed only one publication was observed to be in agreement that RCM reduced the proliferative capacity of cells, which would also lead to a reduction in metabolism, without the detection of any toxicity (Sawmiller *et al.,* 1998), as the majority of other studies typically show cell death and apoptosis after *in vitro* exposure to a range of different RCM. However, other studies have shown that one of the first cellular features influenced by RCM is metabolic activity which has been reported to occur after as little as 30 min exposure, the detection of toxicity on the other hand may require a much greater exposure time ($\geq$ 12 h) before it can be detected (Jensen *et al.*, 2011).

Prior to initiation of *in vitro* experiments with VSMCs, specific immunohistochemistry techniques it was possible to identify a homogeneous population of VSMCs which had been isolated from rat aorta as a primary culture using the explant method. Successful isolation and identification enabled the use of these cells in *in vitro* toxicology studies to promote our understanding of the effects of the non-ionic, low osmolar RCM, IOX, on vascular-derived cells and the safety of an IOX-NIV system which is an essential stage in drug development prior to commencing with more in-depth *ex vivo* experiments (Chapter 5 - Influence of IOX and IOX-NIV pre-treatment on vascular response to pharmacological agents) which will aid the design of future *in vivo* testing. Despite the absence of toxicity observed after analysis of HEK-293s using the CellTox™ Green assay, the significant reduction in metabolic activity exerted on HEK-293s, VSMCs and HUVECs was investigated further and EC50s were determine for each cell line to reveal the order of sensitivity to be VSMC > HUVEC > HEK-293. Despite the fact that IOX-renal interactions can have severe consequences leading to a risk of mortality, *in vitro* it appeared cells of vascular origin are more sensitive to negative effects of IOX. One benefit of administering IOX within a NIV formulation, in addition to the alteration in pharmacokinetic profile, is the presence of a physical barrier which would inhibit the direct interaction of IOX with cells of the vasculature, further reducing the risk to susceptible patients.

A limitation of this experiment, and future blood vessel response experiments, exists in relation to the inability to directly compare any change in toxicity solely based on the IOX concentration. As a result of the toxic concentrations of both free-IOX and IOX-NIV, in addition to the capacity of NIVs to entrap IOX after purification, a direct comparison of free-IOX and IOX-NIV toxicity could not be made. IOX-entrapment upon hydration, in addition to the purification process led to an overall reduction in IOX concentration. Although a calculated EE of 22 % was in line with previous publications on RCM-liposome EE (Chapter 3 - Validation of an HPLC method for IOX quantification and determination of IOX-NIV

encapsulation efficiency and release), the dilution factor obtained upon hydration in a 10x volume of PBS in addition to the 88 % reduction after purification would lead to an equivalent IOX concentration of 14 mg mL^{-1}, which is less than the initial IOX concentration required to reduce both HEK-293 (74 mg mL^{-1}) and HUVEC (20 mg mL^{-1}) metabolism, but was close to the initial concentration observed to reduce VSMC metabolism (10 mg mL^{-1}) (Section 4.4.3). Therefore, a direct comparison between entrapped and unentrapped IOX concentration could not be compared. In addition to this, in order to obtain the maximum IOX concentration, it would involve administering cells and blood vessels with a lipid concentration of 7.5 mM, which was significantly greater than the toxic lipid concentration obtained after the estimation of IOX-NIV EC50s which was 1.36 ± 0.29 mM and 1.28 ± 0.001 mM for VSMC and HUVECs, respectively (Section 4.4.4). Analysis of a sample where purification was not performed would have enabled a direct comparison of any effect of NIV entrapment in comparison to free IOX. In order to do so, experiments may have been performed without a purification step, instead, EC50 values for free-IOX and IOX-NIV were reported without consideration of the final IOX concentration. Although the level of IOX-NIV entrapment after the hydration stage lead to dilution of IOX to the point where the final IOX concentration exposed to cells would be below the toxic range, comparisons between empty-NIVs and IOX-NIVs through the identification of EC50s were still defined. It was surprising to detect a greater reduction in metabolism when comparing empty-NIV with IOX-NIV, particularly as a result of the earlier detection of decreases in cell metabolism after IOX exposure. However, there is evidence to suggest that this IOX-encapsulation may offer a protective effect related to antioxidant activity exerted by RCM, and its enhanced delivery across the cell membrane as a result of NIV encapsulation.

Similar to the analysis of results obtained upon analysis of HEK-293 response through the use of contrasting and complimentary techniques, the ApoTox-Glo™ triplex assay was utilised to measure the effects of IOX, empty-NIV and IOX-NIV on vascular-derived cells *in vivo*. This was of particular interest due to the inability to detect IOX toxicity in earlier experiments, despite a measured concentration-dependent reduction in metabolism and proliferative capacity in HEK-293s. Despite this, clear results relating to the effects of these agents on VSMCs and HUVECs were not obtained due to the fact that measured reductions in viability were not inversely related to increases in toxicity, and often opposite results were detected for different materials. The inability to detect toxicity may be in agreement with the single study mentioned previously, however, it may simply be related to the timing of analysis. In addition, the apoptotic activity of all test samples on VSMCs and HUVECs, as detected through the measurement of caspase-3/ -7, was often detected to be less than the positive control of live,

untreated cells, except in the instance of HUVECs treated with the higher concentration of 170 mg mL^{-1} IOX. This fact may have been coincidental or it may have been associated to the increased sensitivity of HUVECs as determined through the Resazurin metabolic indicator assay. Future *in vitro* experiments should be designed to challenge the relationship between time and the potential detection of IOX or NIV associated toxicity and apoptosis.

The current data from the Resazurin and CellTox Green assays would be in agreement with research that shows only an effect of IOX on proliferation rather than inducing toxicity, however, this is in contrast to a large number of alternative studies, discussed previously, which predominantly support the detection of a decrease in viability and increased apoptotic activity. As a result of these experiments, the precise mechanisms behind changes in HEK-293 metabolism, proliferation and morphology as a result of exposure to IOX remain unclear, although a decrease in metabolism was confirmed. When using mannitol as a comparison, there was no apparent role for osmolality in the reduction of metabolism and potential toxicity. In terms of morphology, some changes were observed which may have been indicative of hyperosmolarity-induced death, however, the CellTox Green assay did not detect cytotoxicity after 2 h exposure to IOX. It could be that treatment of renal and vascular cells with IOX leads to an induction in apoptosis, similar to what is observed when cells are maintained in a hyperosmolar environment, however, no direct measurements of toxicity were confirmed by the experiments outlined in this chapter. This was partly in relation to the failure of, or lack of appropriate positive controls utilised in toxicity kits. In conclusion, an IOX-reduction in cell metabolism was detected quickly after IOX exposure, however, longer incubation times may be more suitable for the detection of cytotoxicity or apoptosis.

4.7   Appendix

4.7.1   Successful isolation and growth of an homologous population of VSMCs using the explant method
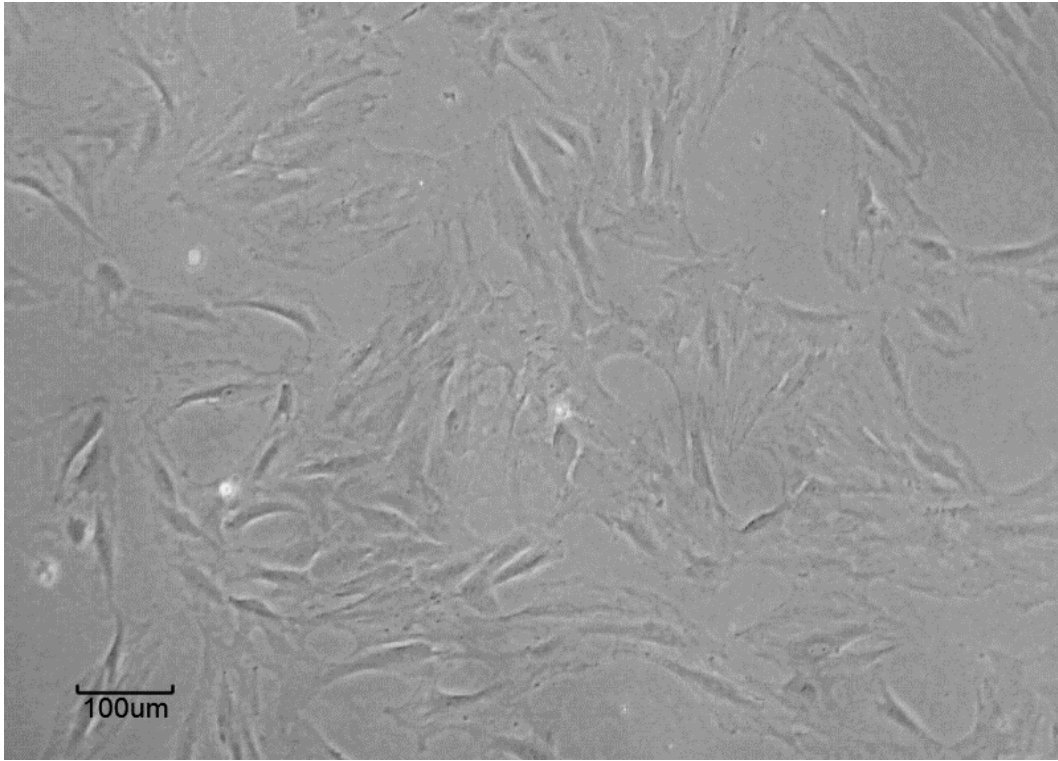
Figure 4.24: Microscopic image of VSMC morphology. *VSMCs were isolated using the explant method and allowed to gain confluency at passage 2 prior to imaging (100x).*
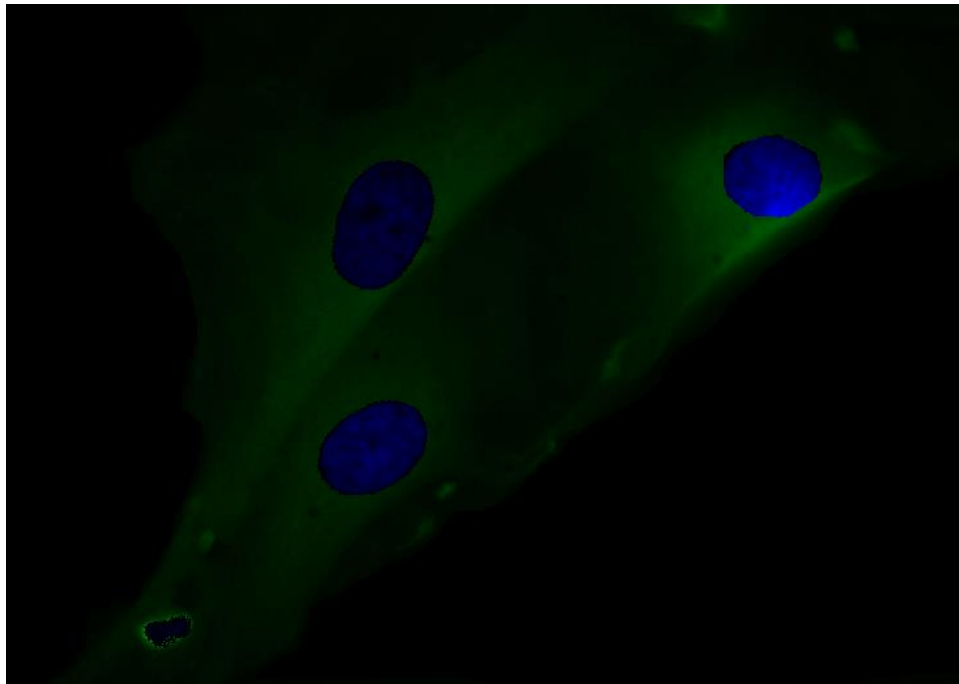
Figure 4.25: Fluorescent imaging of VSMCs stained with VSMC-specific protein MHC. *VSMCs were isolated using the explant method and allowed to proliferate on cover slips after 3 routine passages. Cells were fixed and stained with antibodies against MHC and the nuclear dye Hoechst was used to visualise the nuclei (600x).*
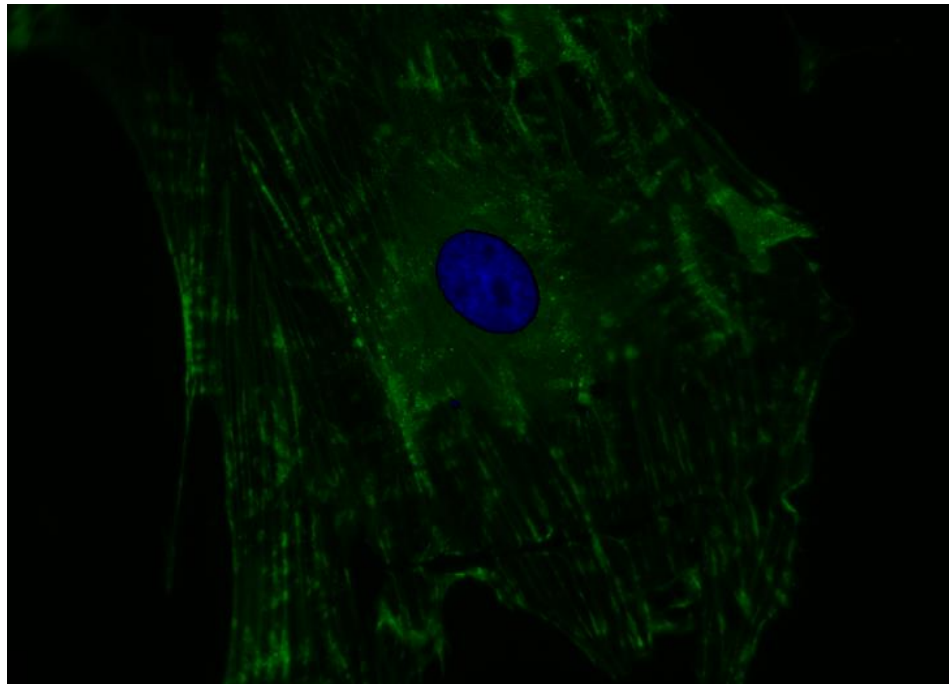
Figure 4.26: Fluorescent imaging of VSMCs stained with antibodies against VSMC-specific α-SM actin. *VSMCs were isolated using the explant method and allowed to proliferate on cover slips after 3 routine passages. Cells were fixed and stained with antibodies against MHC and the nuclear dye Hoechst was used to visualise the nuclei (400x).*

157

4.7.2 Optimisation of parameters for Resazurin
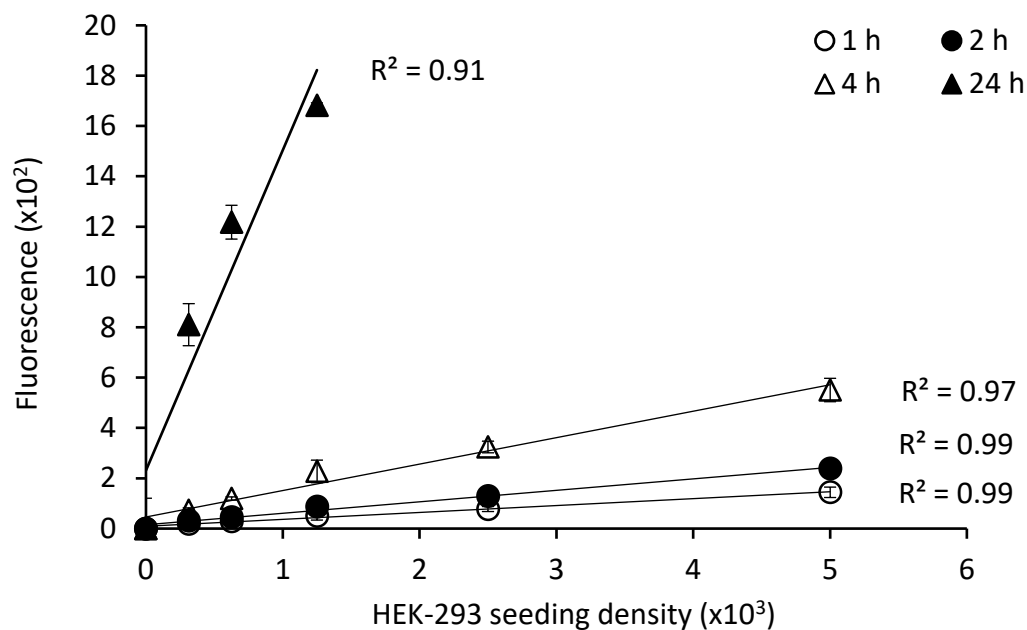
Figure 4.27: Linearity of fluorescent intensity produced by HEK-293s at different seeding densities over increasing incubation times. *(n = 3; ± SD).*
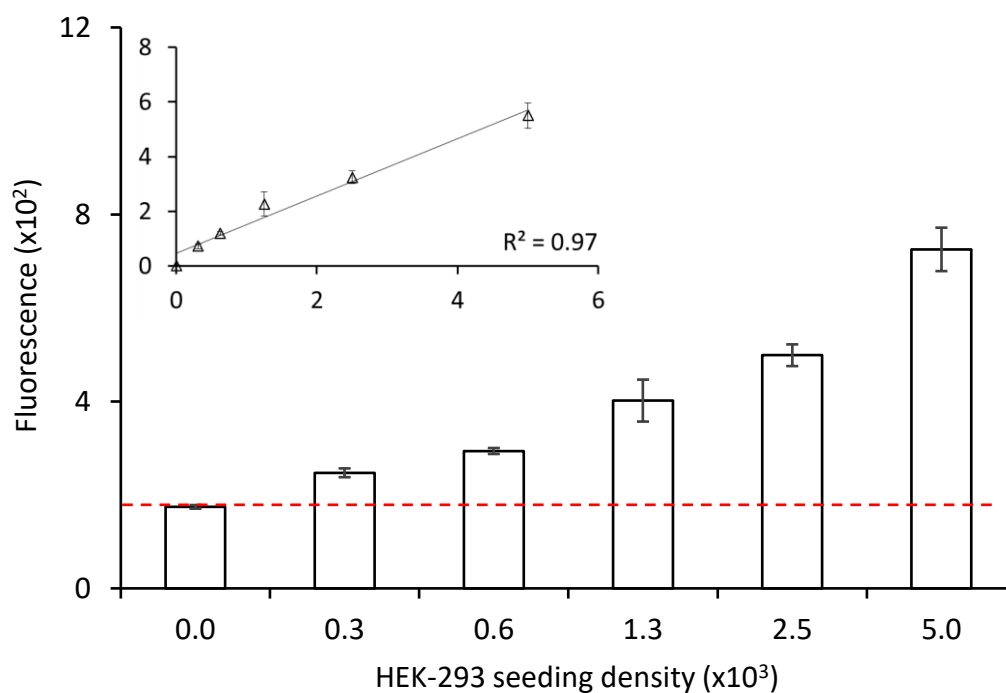
Figure 4.28: Sensitivity of the Resazurin assay for the detection of viable HEK-293s after 4 h incubation. *The dashed line indicates the background fluorescence observed in the absence of cells (n = 3; ± SD).*
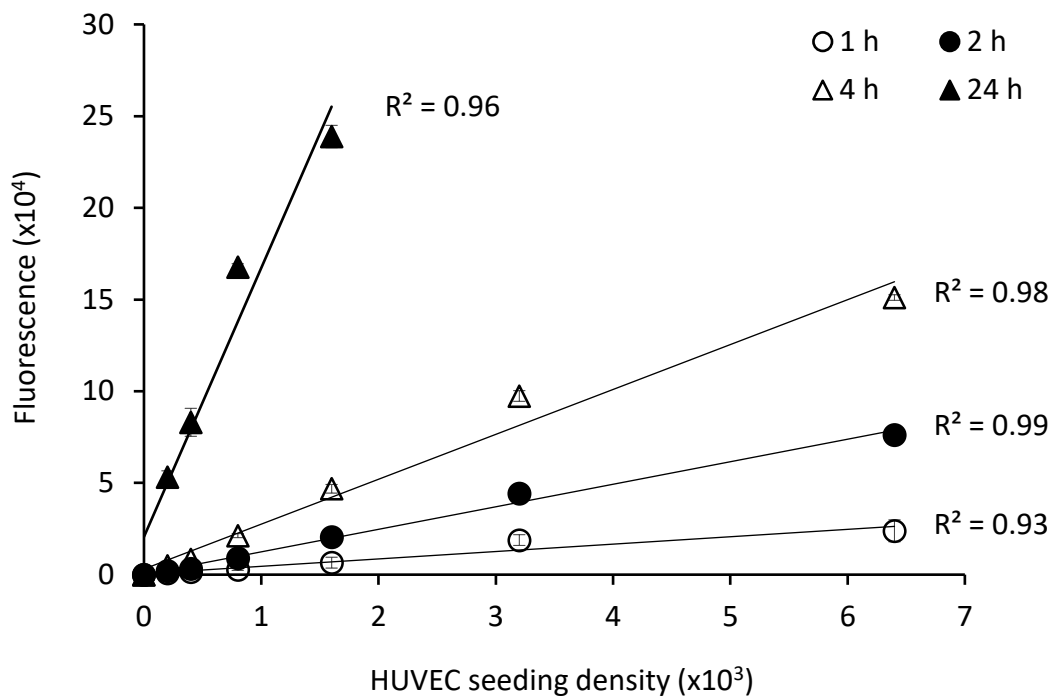
Figure 4.29: Linearity of fluorescent intensity produced by HUVECs at different seeding densities over increasing incubation times. *(n = 3; ±SD).*
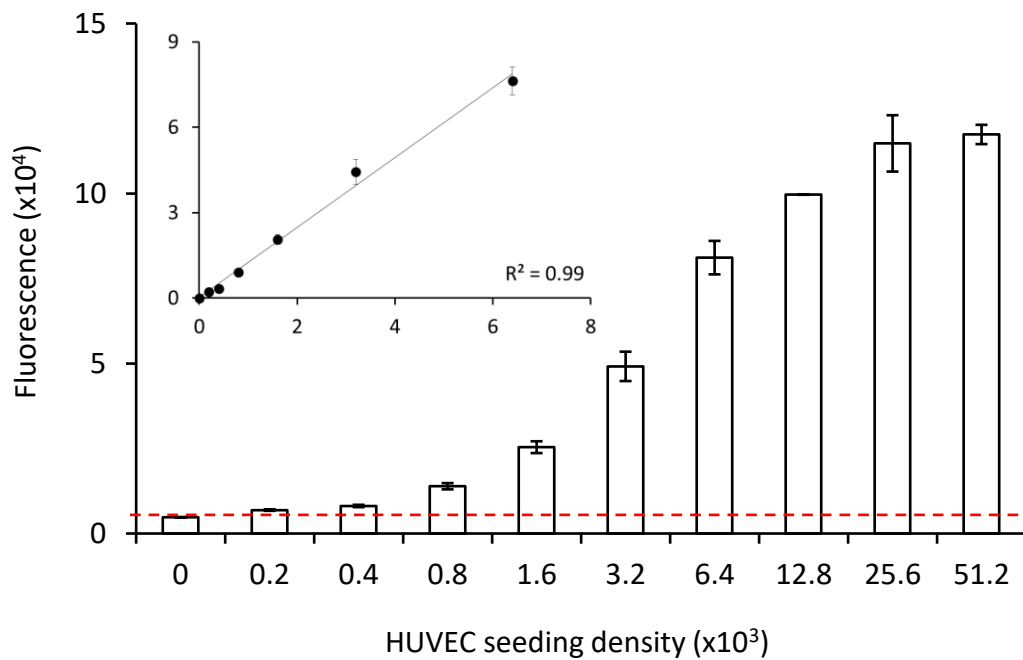
Figure 4.30: Sensitivity of the Resazurin assay for the detection of viable HUVECs after 2 h incubation. *The dashed line indicates the background fluorescence observed in the absence of cells (n = 3; ±SD).*

Chapter 5

Influence of IOX and IOX-NIV
pre-treatment on vascular response
to pharmacological agents

5 Chapter 5 – Influence of IOX and IOX-NIV pre-treatment on vascular response to pharmacological agents

5.1 Introduction

Blood vessels are a key part of the circulatory system - enabling the transport of blood, nutrients and signalling molecules while simultaneously transporting waste products for their removal from the body. Blood vessels are composed of three separate layers (Figure 5.1). The outer adventitia is comprised of connective tissue which offers structural support. The middle layer of the blood vessel is formed of vascular smooth muscle (VSM) which contracts and relaxes - enabling the control of vascular lumen diameter and blood pressure. The effect of vessel tone on blood pressure can be described by multiplying the vascular resistance (R) by the blood flow (Q) which provides the change in pressure (ΔP) (Equation 5.1; Secomb, 2016). Therefore, vasodilation, or reduced VSM tone, exerts the opposite effects on tension and blood pressure. Finally, the inner endothelium consists of a monolayer of endothelial cells (ECs) which have direct contact with nutrients, signalling molecules and pharmacological agents present within the blood. ECs also play a key role in releasing factors which mediate VSM contraction and relaxation.
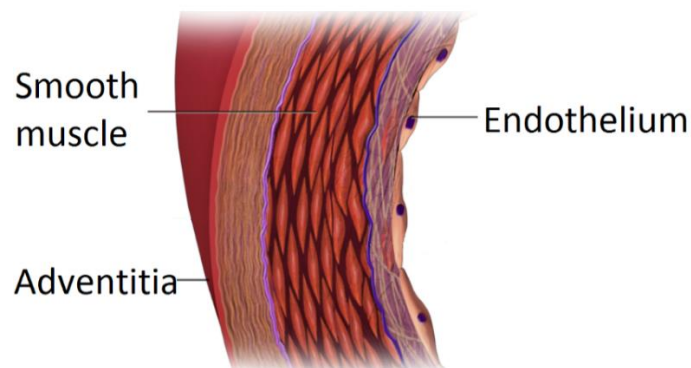
Figure 5.1: Structure of the blood vessel showing 3 distinct layers. *The outer adventitia, the medial smooth muscle layer and the inner endothelial monolayer. Image adapted from: Blausen.com Staff (2014).*

Equation 5.1:

$$\Delta P = Q \times R$$

5.1.1 Typical control of vascular tone

The CNS enables a rapid-response mechanism for ensuring blood pressure homeostasis. A decrease in blood volume, and hence pressure, can be sensed by baroreceptors present in the carotid sinus which results in decreased signalling to the brain. The sympathetic autonomic nervous system responds to the decreased signalling and sends electrical signals to the heart causing stronger cardiac contraction and increased vascular resistance. The parasympathetic nervous system has an opposing effect which leads to a rapid reduction in blood pressure when required (Thomas, 2011). In addition to autonomic control, the renin-angiotensin-aldosterone system (RAAS) regulates systemic blood flow and vascular resistance through neurohormonal control involving a number of organs the kidneys, adrenal cortex, liver and brain which in turn release factors which directly influence vascular tone. The liver plays an important role in its release angiotensinogen which is cleaved by renin releasing it into the bloodstream. Angiotensinogen is cleaved to form angiotensin I which acts upon the endothelium cleaving angiotensin I to angiotensin II using angiotensin converting enzymes. Angiotensin II acts upon a number of different target cell types which exert different functions – 1) VSM cells undergo vasoconstriction which increases vascular resistance (Touyz and Schiffrin, 1997), 2) water retention within the kidneys leads to an increase in blood volume, 3) the brain senses angiotensin II in the blood sending an electrical signal leading to the release of antidiuretic hormone (ADH) from the pituitary gland (Liyanarachchi and Debono, 2017). ADH causes both vasoconstriction within blood vessels and renal water reabsorption across channels within the nephron leading to an increase in blood volume (Bernstein *et al.*, 2014). ADH is also released in response to other factors, primarily, increased blood osmolarity – as detected by osmoreceptors The presence of ADH within the blood vessel acts directly on VSM cells resulting in vasoconstriction and an increase in resistance and pressure.

General VSM health can be tested by monitoring the response in vascular tone to pharmacological agents. KCl is a pharmacological agent which induces VSM constriction through membrane depolarisation and activation of voltage-gated Ca^{2+} channels in a receptor-independent manner (Figure 5.2). This is referred to as a relatively simple, non-specific method which bypasses receptor-mediated vasoconstriction. Contraction of VSM under the control of KCl results in an increase in $[Ca^{2+}]i$, Ca^{2+}-calmodulin-dependent myosin light chain (MLC) kinase phosphorylation and activation (Ratz and Miner, 2009). KCl is a gold standard for inducing VSM contraction during the performance of myograph experiments to enable the investigation of alterations in more complex mechanisms of G-protein-coupled receptor (GPCR) activation (Ratz *et al.*, 2005).
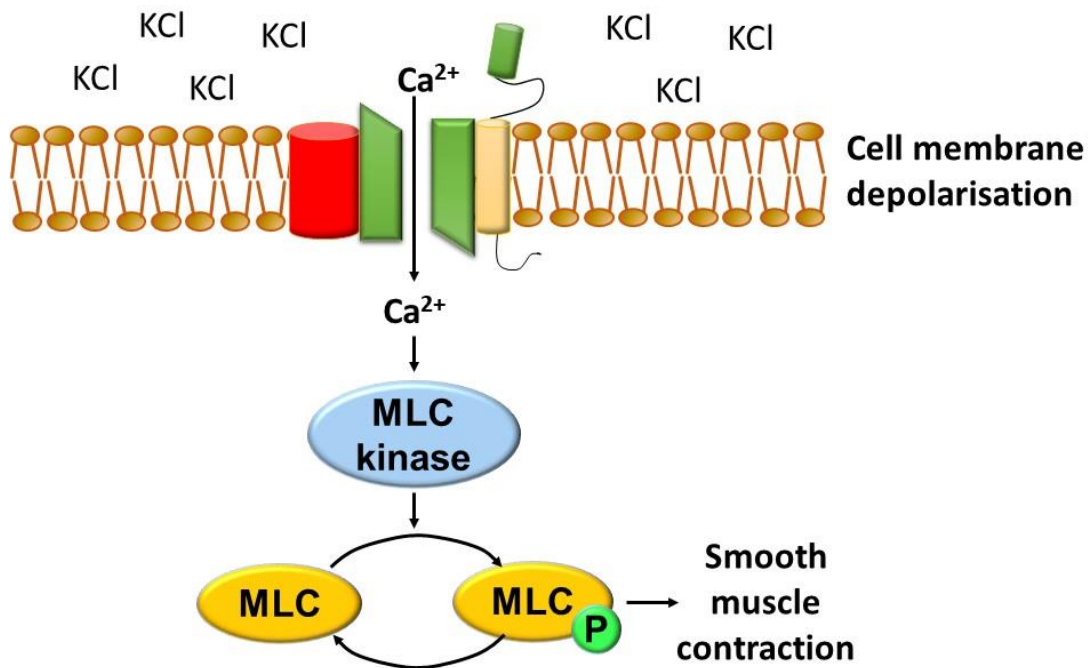
Figure 5.2: KCl-mediated VSM cell contraction. High levels of extracellular KCl leads to VSM membrane depolarisation and activation of voltage-gated Ca²⁺ channels. *The subsequent increase in intracellular Ca^{2+} activates MLC kinase which phosphorylates MLC inducing VSM contraction. MLC – myosin light chain.*

A more specific type of VSM-mediated contraction involves activation of α_1-adrenergic receptors which form a subgroup of the GPCRs. α_1-adrenergic receptors may be activated by a number of different agonists including hormones, neurotransmitters and drugs (Dinh *et al.*, 2009; Grimm *et al.*, 2006). α_1-adrenergic receptors are highly expressed on the surface of VSM cells and play an important role in VSM contraction and sensitivity to Ca^{2+} (Terzic *et al.*, 1992, Reynolds and Dubyak, 1985). Dysfunction of these contractile processes are known to contribute to vascular diseases including asthma and pulmonary hypertension which makes GPCRs a key target for drug development (Wright *et al.*, 2013). Phenylephrine (PE) specifically targets the α_1-adenergic receptor which induces vasoconstriction and an increase in blood pressure through stimulation of phospholipase C. The specificity of PE towards VSM-mediated vasoconstriction has meant that this molecule has become key in understanding vascular dysfunction in *ex vivo* models and it has played an important role in gaining an understanding of the function of α1-adrenergic receptors. (Figure 5.3).
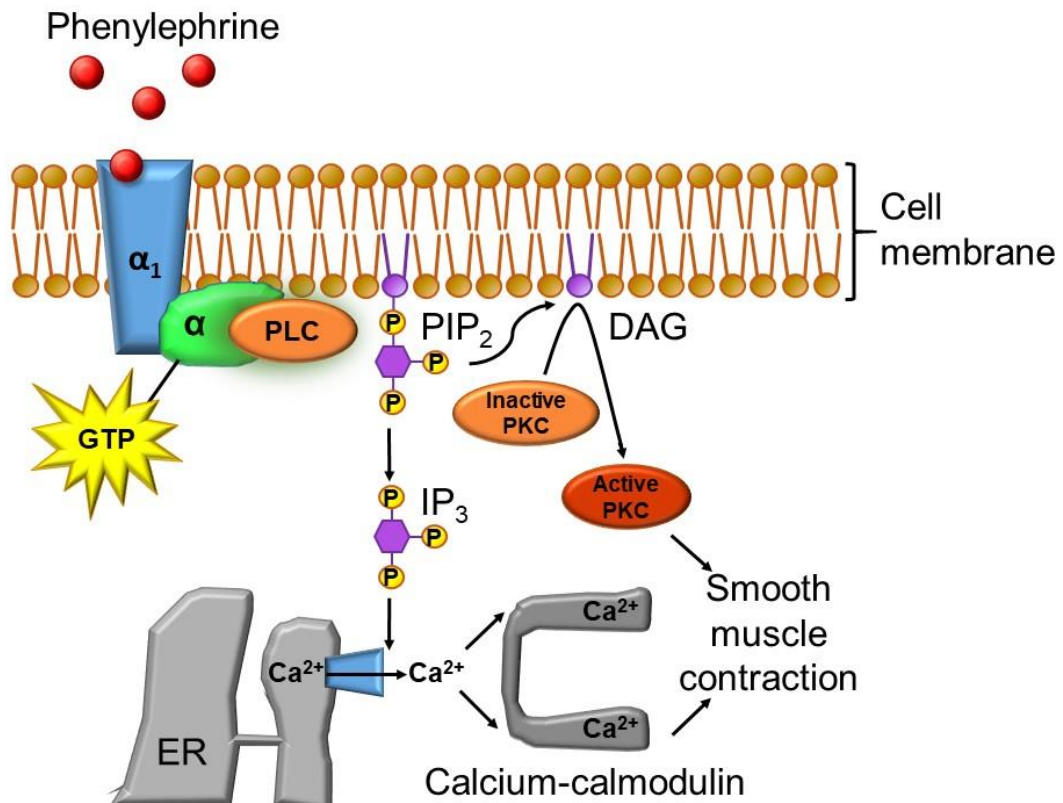
Figure 5.3: VSM-mediated contraction as a result of PE-activation of the α1-adrenergic receptor. *PE specifically interacts with α1-adrenergic receptors which are expressed on VSMCs. Subsequent PLC activation leads to phosphorylation of membrane-bound PIP2 and the release of IP3 into the cytosol, while leaving DAG complexed to the membrane. IP3 increases intracellular Ca2+ upon release from the ER. Ca2+ forms a complex with calmodulin which causes SMC contraction. In addition, membrane-bound activates intracellular PKC which also contributes to VSM contraction. PE – phenylephrine, PLC – phospholipase C, PIP2 - phosphatidylinositol 4,5 – bisphosphate, IP3 - inositol triphosphate, ER – endoplasmic reticulum, PKC – protein kinase C.*

In addition to the complex neurohormonal mechanisms which have systemic control over blood pressure, a number of mechanisms also exist which enable fine tuning of vascular tone within localised areas of the body. Under certain conditions requirements for nutrients at specified organs is of greater demand in comparison to that required in other areas of the body. For example, during exercise skeletal muscles undertaking strenuous activity require more oxygen in comparison to the rest of the body as a result of increased metabolic activity (Hellsten *et al.*, 2012b). In these instances tissues release metabolites, such as and adenosine, which act on nearby blood vessels promoting vasodilation and increased blood flow to the desired site without the requirement of increasing cardiac output (Hellsten *et al.*, 2012). Control of blood vessel vasodilation through endothelial release of -nitric oxide (NO) occurs when inactivated caveolin-bound endothelial nitric oxide synthase (eNOS), expressed on the cell membrane, is released due to increased intracellular calcium ([Ca^{2+}]i) (Bucci *et al.*, 2000).

Endogenous NO agonists (i.e. acetylcholine (ACh) and adenosine) increase $[Ca^{2+}]i$ levels by inducing its release from the endoplasmic reticulum and subsequent uptake of extracellular Ca^{2+} upon activation of Ca^{2+}-activated K^+ channels (Allard *et al.*, 1996). $[Ca^{2+}]i$ binds to calmodulin within the cytoplasm causing a conformational change enabling eNOS binding and conversion of L-arginine to NO (Palmer *et al.*, 1988). NO diffuses across the endothelial membrane and into nearby VSM cells where it binds to the enzyme, soluble guanylyl cyclase (sGC). Activated sGC converts GTP to cGMP, decreasing VSM tension and reducing $[Ca2+]i$, further promoting vasodilation (Arnold *et al.*, 1977; Archer *et al.*, 1994). This endothelial-dependent control of VSM tone can be tested through the use of vascular response experiments in order to determine the effect of drugs on VSM function, in an endothelial-dependent manner.

In comparison to both KCl and PE, ACh exerts an opposing, vasodilatory effect on VSM upon interaction with GPC-muscarinic receptors (MRs) expressed on the endothelial layer, rather than being a direct target of VSM (Furchgott and Zawadzki, 1980). Activation of MRs results in endothelial production of NO which has a relaxing effect on the adjacent VSM (Figure 5.4; Hofmann *et al.*, 1992).
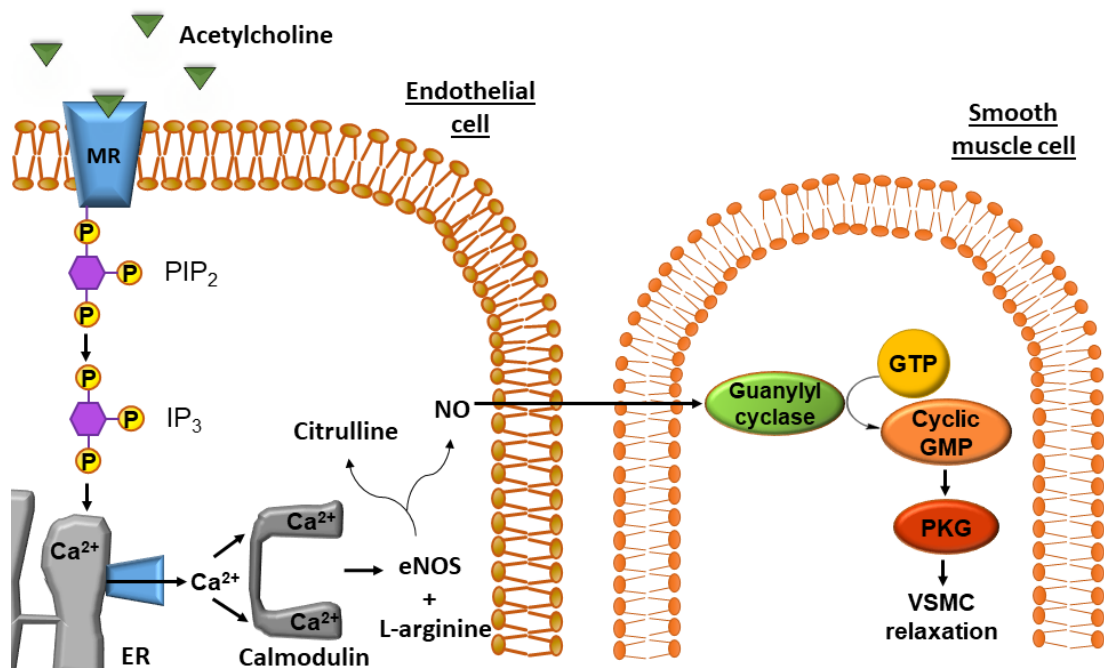
Figure 5.4: ACh activation of GPCR, MR, present on endothelial cells resulting in endothelial-dependent VSM cell relaxation. *MRs expressed on the surface of endothelial cells are activated by ACh. PIP$_2$ phosphorylation leads to the release of IP$_3$ into the cytosol and intracellular Ca^{2+} release from the ER. Ca^{2+} creates a complex with calmodulin leading to the production of eNOS, which when combined with L-arginine leads to the synthesis of citrulline and NO. NO diffuses across the VSM cell membrane and into neighbouring VSM cells leading to activation of guanylyl cyclase, cGMP and protein kinase G resulting in endothelial-dependent VSM relaxation. GPCR – G-protein-coupled receptor, MR – muscarinic receptor, ACh – acetylcholine, PIP$_2$ – phosphatidylinositol 4,5 – bisphosphate, IP$_3$ – inositol triphosphate, ER – endoplasmic reticulum, eNOS – endothelial nitric oxide synthase, NO – nitric oxide, GTP – guanosine triphosphate, GMP – guanosine monophosphate, PKG – protein kinase G.*

Sodium nitroprusside (SNP) is a pharmacological molecule which is utilised for the immediate control of high blood pressure due to its ability to induce generalised relaxation of blood vessels in a manner which is both receptor- and endothelium-independent. The mechanism by which SNP causes vasodilation is related to the fact that this molecule is a NO-donor which directly activates sGC leading to VSM relaxation (Figure 5.5; Moncada and Higgs, 2006). The measurement of vascular response to SNP during myograph experiments reflects the ability of VSM relaxation in a way that is independent of typical endothelial control.
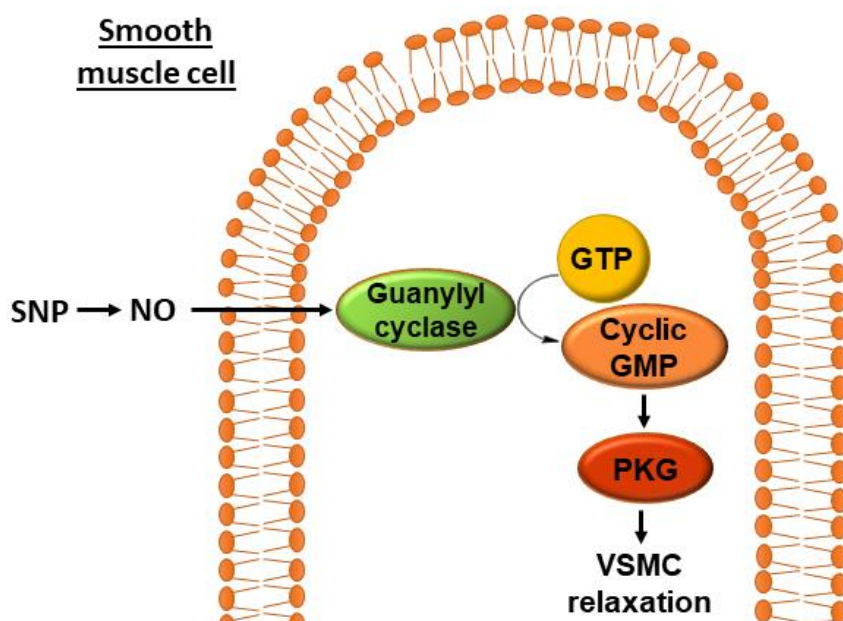
Figure 5.5: The pharmacological action of SNP leading to receptor-independent VSM cell relaxation. *The presence of SNP, as an NO donor, directly releases NO in receptor-independent manner. NO diffuses across the VSM cell membrane activating guanylyl cyclase which uses GTP to produce cyclic GMP which in turn activates PKG inducing VSM cell relaxation. SNP – sodium nitroprusside, NO – nitric oxide, GTP – guanosine-5'-triphosphate, PKG – protein kinase G, VSMC – vascular smooth muscle cell.*

5.1.2 Vascular dysfunction and RCM-AKI and CIN

Maintenance of vascular and endothelial structure and function is of utmost importance as dysfunction of normal physiology is known to contribute to a range of vascular disease states which can have negative consequences on renal function. Conditions including advanced age (Stacul *et al.*, 2011), diabetes (Heyman *et al.*, 2013), and hypertension (Conen *et al.*, 2006) have been associated with RCM-AKI and CIN. Many individuals suffering from these conditions also express a greater susceptibility to cardiovascular and renal disease (Andreucci *et al.*, 2014). The link between an altered vascular and renal state and patient susceptibility to RCM-AKI will be discussed.

VSM cells are known to undergo phenotypic switching which alters cellular morphology and physiology. In young healthy individuals, VSM cells express a differentiated contractile phenotype, however, VSM cells of the aged patient shows conversion to a dedifferentiated proliferative 'synthetic' phenotype (Bochaton-Piallat *et al.*, 1993). Physiological changes in VSM cells are associated with a host of physical changes in the blood vessel such as increased stiffness, risk of sclerotic plaque formation (McCaffery *et al.*, 1988) and calcification (Atkinson, 1985). The vasculature of the elderly patient is more prone to degeneration and

extracellular matrix degradation which negatively impacts the ability to maintain healthy control of blood pressure and flow. This in turn increases susceptibility to cardiovascular and renal disease (Gussenhoven *et al.*, 1991). A combination of these complex risk factors are likely to be associated with an increased susceptibility to RCM-AKI within the elderly patient (Mehran and Nikolsky, 2006).

Two other conditions which have been identified to predispose individuals to RCM-AKI are hypertension and diabetes (Conen *et al.*, 2006; Heyman *et al.*, 2013). In addition hypertension exists as a co-morbidity within the diabetic patient - the American Diabetes Association (2003) estimates that the prevalence of hypertension within the diabetic population is between 20 and 60 %. Similar to the elderly, these individuals are prone to the development of cardiovascular and renal disease, as well as susceptibility to RCM-AKI and CIN. One key feature of these patient groups is endothelial dysfunction. Spontaneously hypertensive rat models suffer from persistent renal vasoconstriction related to compromised release and action of vasodilators such as NO and PGI_2 (Michel *et al.*, 2007). In a spontaneous diabetic rat model the aorta was found to express an attenuated response to endothelium-dependent ACh, but not SNP or PE, which highlights underlying endothelial-dysfunction (Durante *et al.*, 1988). Chemically-induced diabetic rat models have also shown enhanced renal vasoconstriction to adenosine associated with reduced NO production and/ or responsiveness (Pflueger *et al.*, 1999). An understanding of the underlying dysfunction present in these patient groups may provide a link between the role of the vasculature and enhanced susceptibility to RCM-associated damage.

In addition to the link between endothelial dysfunction and the development of AKI-RCM within the diabetic patient, CIN studies have also identified the requirement for decreased renal function as a key contributing factor. Nikolsky *et al.* (2004) investigated the occurrence of RCM-associated CKD after percutaneous coronary intervention to discover renal disease was significantly higher in diabetic patients with CKD undergoing dialysis (27 %) in comparison to diabetic patients with CKD but not receiving dialysis (15 %). This highlights that co-morbidities associated with at-risk patients constitute an important perquisite in their likelihood to develop significant AKI after exposure to RCM.

The prevalence of an aging population with increased vascular and renal co-morbidities, alongside the increased use of RCM-enhanced bio-imaging highlight the importance of taking more significant precautions to avoid RCM-AKI which can be potentially fatal (Royal College of Radiologists, (2015/16); Tonelli and Riella, 2014). Although complete avoidance of RCM administration and CT scanning is usually recommended for patients identified as high risk

(Beckett *et al.*, 2015), the risk to patients with unknown or borderline susceptibility remains high.

Myography offers a way to measure transversal isometric tension exerted by blood vessels in response to pharmacological stimuli independent of normal homeostatic or CNS-mediated control of blood pressure. It is a useful technique for the analysis of vessel function and has commonly been used to enhance understanding of specific vascular disease states, as well as in the development of pharmacological agents for the treatment of disease (Enomoto *et al.*, 2014; Sun *et al.*, 2017). It is possible to determine the origin of alterations in vascular response, such as whether they are VSM- or endothelial-dependent, through vessel exposure to specific vascular mediators (Syyong *et al.*, 2009). Wire myography is a useful tool for measuring vascular function as a result of disease or pharmacological intervention. Comparing IOX-exposed vessel response to the response after IOX-NIV exposure will provide additional information on the suitability of IOX-NIV for the preservation of vascular functional and avoidance of potential downstream damage within the kidneys. Commonly used pharmacologic agents with specific cell- and receptor-mediated targets have been outlined (Table 5.1).

Table 5.1: Commonly used pharmacological agents for the study of vascular function and their respective actions.

Agonist	Action
KCl	Receptor-independent VSM contraction (voltage-gated Ca^{2+} channels)
PE	Receptor-dependent VSM contraction (α_1-adrenergic receptor)
ACh	Endothelium receptor-dependent vasodilation (muscarinic receptor)
SNP	Endothelium-independent vasodilation

5.2 Specific chapter aims and experimental limitations

The aim of this chapter was to build on previous *in vitro* experiments which tested the toxicity profile of both free-IOX and IOX-NIV on ECs and VSMCs *in vitro.* Through the use of a wire myograph the effects of IOX and IOX-NIV exposure on typical vascular response to pharmacological standards were compared. The objectives required to meet this aim are to:

- Successfully isolate rat aorta and confirm vessel health prior to analysis.
- Compare normal vessel response to pharmacological standards after exposure to IOX and IOX-NIV
- Determine sensitivity and dose-response curves to determine the effect of IOX and IOX-NIV pre-treatment on vessel response.

Encapsulation of the RCM, iohexol (IOX), within NIVs may offer the potential to reduce RCM-AKI risk for patients with defined or unknown susceptibilities. Comparing IOX-exposed vessel response to the response after IOX-NIV exposure will provide additional information on the suitability of IOX-NIV for the preservation of vascular functional and avoidance of potential downstream damage within the kidneys. Prior to further explanation of experiments and the data analysis, it is important to highlight potential limitations identified before and after the performance of these studies in order to address potential uncertainties that may arise when reading this chapter. Similar limitations exist in these experiments as those reported at the end of the *in vitro* experiments (Chapter 4 – *In vitro* Toxicity of IOX, IOX-NIV and empty-NIV). Whereby, a direct correlation between IOX toxicity and IOX-NIV toxicity could not be made as a result of the reduced mount of IOX within IOX-NIVs as a result of the encapsulation and purification process. Despite this, EC50 values for both IOX and IOX-NIV were used to inform decisions on the concentrations used for the analysis of the effect of these two drug products on vascular response.

5.3   Materials and methods

5.3.1   Vessel dissection and preparation

Male Sprague Dawley rats (10-12 weeks, 200-350 g) were housed and cared for following standards outlined by the Animals Procedure Act (1986). Rats had *ad lib* access to standard laboratory chow and water prior to being sacrificed through cervical neck dislocation. The outer fur was decontaminated with 70 % (*v/v*) ethanol prior to transfer to a class II biological safety cabinet. Sterile scissors and forceps were used to dissect the aorta which was collected into a volume of ice-cold Krebs' solution (119 mM KCl, 4.5 mM $NaHCO_3$, 1 mM KH_2PO_4, 1 mM $MgSO_47H_2O$, 11 mM glucose and 2.5 mM $CaCl_2$; degassed with 95: 5 % O_2/ CO_2) and immediately stored on ice. Fat and connective tissue were removed from the aorta and it was cleaned with Krebs' to remove blood and debris. Rings were cut into 4 x 4 mm segments with a scalpel, taking care not to damage the endothelium. The segments were loaded on to the wire myograph.

5.3.2   Experimental set-up and equilibration of wire myograph

A 4-chamber wire myograph (Danish Myo Technology; DMT) with adapted poles, which enable the analysis of large vessels, was used to detect changes in vessel tension after exposure to IOX and IOX-NIV. The rings were mounted on two 40 µm steel poles, the lower one connected to a micrometre to enable stretching of the vessel to an appropriate baseline tension, while the top pole was connected to an isometric force transducer (Figure 5.6). Each chamber was filled with 10 mL Krebs' solution, pre-warmed to 37 °C and subjected to continuous gassing with 95: 5 % (*v/ v*) O_2/ CO_2. The wire myograph was calibrated to a basal tension of 9.18 mN using a 2 g balance. Aorta segments were mounted on to the poles of each chamber and the inner tension was gradually increased to ~9.18 mN over a period of ~15 min using the micrometre. Vessels were allowed to equilibrate for 1 h while the tension was monitored and adjusted to ~9.18 mN every 15 min.
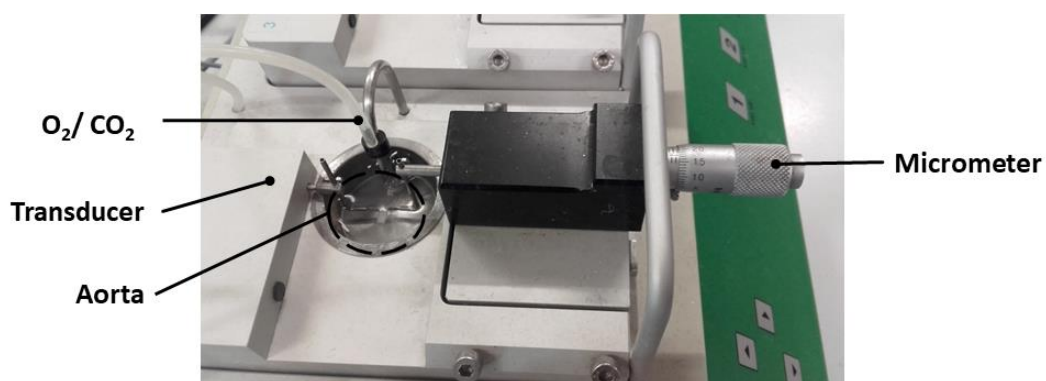
Figure 5.6: DMT myograph chamber with aorta-loaded poles. *The chamber contains 10 mL pre-warmed Krebs' solution which is maintained at 37 °C with gentle O_2/CO_2 (95: 5 % v/v) bubbling. The ~4 mm aorta segment is carefully loaded onto the wire myograph pole arms, one of which is connected to a signal transducer that is sensitive to changes in tension, the other arm is connected to a micrometre which is used to equilibrate aorta tension to a baseline which is similar to that of aorta pressure in vivo.*

5.3.3 Pharmacological agent preparation and aorta tissue activation

All pharmacological agents were obtained from Sigma unless stated otherwise. A stock solution of 1 M KCl was prepared on the day by dissolving 0.746 g KCl in 10 mL Krebs' solution. Stock solutions of PE, ACh and SNP were prepared in Krebs' at a concentration of 1×10^{-1} M and stored at -20 °C. On the day of experiment stock solutions were thawed and 1 in 10 serial dilutions were performed in Krebs' at concentrations ranging from $1 \times 10^{-1} - 10^{-7}$ M.

A normalisation procedure was carried out to ensure optimal vessel response, reproducibility and accuracy of analysis. Equilibrated vessels were exposed to 60 mM KCl (x3), with 3x washing stages and 5 min equilibration in between exposures. On the final exposure to KCl, vessels were also exposed to 1×10^{-6} M PE. The acceptance criteria for vessels was the detection of vessel contraction after exposure to these pharmacological agents. All vessels tested were found to meet this acceptance criteria.

5.3.4 Vessel pre-treatment and analysis of vascular response

After the performance of vessel equilibration and normalisation, vessels were either pre-treated with final concentrations of 142 mg mL^{-1} IOX, 1 mM of purified IOX-NIV (IOX encapsulated equivalent concentration of 0.95 mg mL^{-1}), or PBS as a control, for 1 h at 37 °C. After this, vascular response experiments were carried out by first monitoring the cumulative concentration response to KCl at final concentrations between 5 and 65 mM. Prior to the performance of subsequent response experiments, vessels were washed in Krebs' solution (x3) and allowed to equilibrate until a stable baseline was observed. Following this, vessel response

was monitored upon exposure to cumulative concentrations of PE – between 1×10^{-10} and 10^{-4} M. Again, washing and equilibration stages were performed and vessels were pre-constricted with 1×10^{-6} M PE and the dilatory response to ACh was monitored upon exposure to cumulative concentrations between 1×10^{-10} and 10^{-4} M ACh. Finally, the same process was carried out prior to pre-constriction with PE and the change in tension in the presence of cumulative concentrations of SNP was monitored between the range of 1×10^{-10} and 10^{-4} M.

5.3.5 Data recording and statistical analysis

Data was recorded using MyoDaq software at 1 second intervals and exported using MyoData prior for further analysis using Microsoft Excel, whereby vascular response was analysed first after determining the 10-point moving average in order to minimise variability observed as a result of baseline noise. Contractile response was calculated as a percentage relative to the maximum response of 60mM KCl or 1×10^{-6} M PE. Vessel relaxation to ACh or SNP was measured as a percent reduction relative to the initial pre-constriction induced by 1×10^{-6} M PE. Data was plotted as the mean ± SEM as calculated using Microsoft Excel 2013. Statistical comparisons of sensitivity (EC50; negative log of the concentration of drug required to produce 50 % of the maximum response) and maximum responses between arteries were performed using Student's t-test. EC50 values for ACh and SNP were determined by first plotting a linear line of best fit prior to determining the value 50 % between the maximum and minimum response. Further statistical comparisons of data was performed using ANOVA (Tukey's test) on Minitab v 17.3.1.0. Statistical significance was assumed where $p < 0.05$.

5.4 Results

5.4.1 Effect of IOX and IOX-NIV vessel pre-treatment on vasoconstriction

After vessel pre-exposure to IOX for 1 h, there was a complete loss in voltage-dependent KCl response, as observed after exposure to cumulative concentrations of KCl (Figure 5.7A). Despite a lower average response to cumulative concentrations of KCl in the purified IOX-NIV pre-treated vessels when compared to control vessels, individual sample variation in each treatment group expressed overlapping standard deviation meaning that any differences were non-significant as evident upon performance of ANOVA analysis. Data obtained from control and IOX-NIV response to KCl was also plotted as a % of each vessels maximum response. Due to the absence of response from the IOX pre-treated group this data was not included. Similar KCl-response curves were obtained for both control and IOX-NIV groups, nonetheless, IOX-NIV responses appeared to be shifted to the right (Figure 5.7B). The maximum tension exerted by control vessels was 9.6 ± 3.9 mN while vessels pre-treated with 142 mg mL^{-1} IOX expressed a maximum tension of 0.5 ± 0.5 mN (Table 5.2). Despite the large difference in maximum response when comparing control and IOX-vessels, the results not significant. Similar maximum responses were observed when comparing control and IOX-NIV treated groups, at 9.6 ± 3.9 mN and 7.3 ± 0.9 mN, respectively ($p = 0.3$). In contrast, statistical analysis of the sum of KCl responses for control and IOX pre-treated vessels was significantly different ($p = 0.05$). This was not the case when comparing control and IOX-NIV sum responses ($p = 0.22$; Table 5.2). EC50 values calculated from the % maximum response showed that the control and IOX-NIV pre-treated vessels were not significantly different at 21.9 ± 5.1 mM and 30.6 ± 6.6 mM KCl, respectively (Table 5.2).
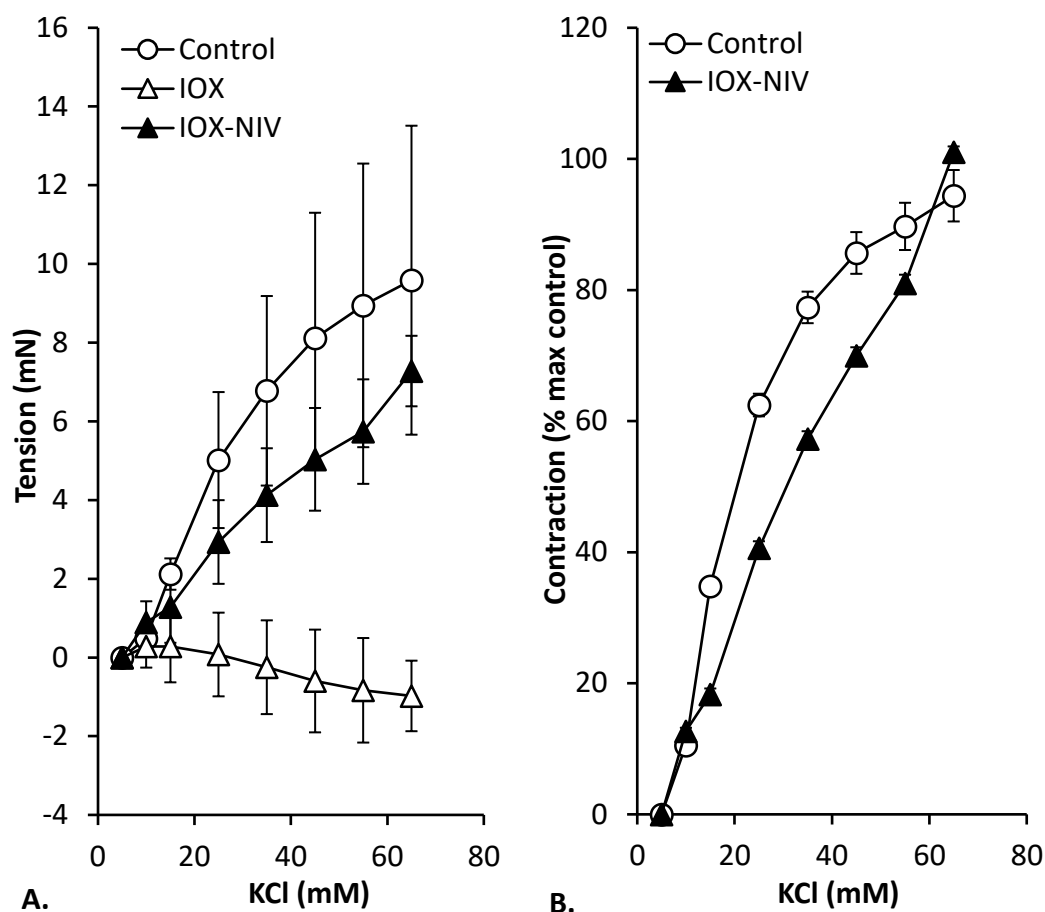
Figure 5.7: KCl cumulative concentration response after 1 h pre-treatment with PBS (control), 142 mg mL^{-1} IOX and 1 mM IOX-NIV. A. *Data was plotted to compare the change in tension, after background subtraction, as a result of increasing KCl concentration* **B.** *Vessel contraction for control vessels and IOX-NIV pre-treated vessels were plotted as a percentage of the vessels maximum response after exposure to a final concentration of 65 mM KCl. 1 mM IOX-NIV encapsulated IOX equivalent after purification = 0.95 mg mL^{-1} (n = 3, ± SEM).*

Table 5.2: Effect of vessel pre-treatment on cumulative response to KCl *(n = 3).*

Treatment	Maximum tension (mN ± SEM)	p-value	Sum of tension (mN ± SEM)	p-value	EC50 (mM ± SEM)	p-value
Control [a]	9.6 ± 3.9	-	41.0 ± 14.9	-	21.9 ± 5.1	-
IOX [b]	0.5 ± 0.5	0.07	-2.0 ± 3.6	0.05*	n/a	-
IOX-NIV [c]	7.3 ± 0.9	0.30	27.3 ± 6.3	0.22	30.6 ± 6.6	0.16

[a]*667 µl PBS;* [b]*142 mg mL^{-1};* [c]*1 mM IOX-NIV; 1 mM IOX-NIV encapsulated IOX equivalent after purification = 0.95 mg mL^{-1}; *p ≤ 0.05 when comparing treated vessels to the control response.*

Overlapping PE dose-response curves were observed upon expression of data as a percentage of maximum vessel response and the EC50 response was estimated to be 10^{-7} M PE regardless of vessel treatment (Figure 5.8). Control vessels exposed to cumulative concentrations of PE exerted a maximum tension of 15.0 ± 2.0 mN, although differences were observed between pre-treatment groups no significant difference was observed – IOX-vessels 12.2 ± 1.4 mN and IOX-NIV-vessels 16.7 ± 2.5 mN (

Table **5.3**). The same was true upon comparison of the sum of PE responses over the course of the experiments which was 49.3 ± 7.6, 42.2 ± 6.9 and 54.5 ± 9.1 mN for control, IOX and IOX-NIV pre-treatment groups, respectively.
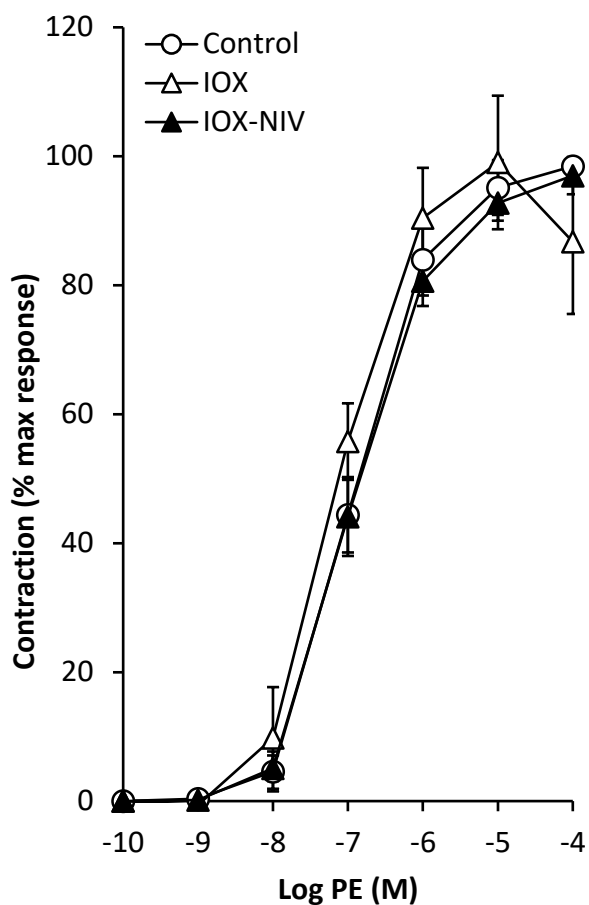
Figure 5.8: PE cumulative concentration response after 1 h vessel pre-treatment with PBS (control), 142 mg mL^{-1} IOX and 1 mM IOX-NIV. *Vessel response was plotted as a percentage increase, in relation to the maximum response obtained at either 10^{-5} or 10^{-4} M PE, as a result of the increase in PE concentration. 1 mM IOX-NIV encapsulated* IOX *equivalent after purification = 0.95 mg mL^{-1} (n = 4, ± SEM).*

Table 5.3: Effect of vessel pre-treatment on cumulative response to PE. *(n =4; ± SEM).*

Treatment	Maximum tension (mN ± SEM)	p-value	Sum of tension (mN ± SEM)	p-value	Log EC50 (M ± SEM)	p-value
Control[a]	15.0 ± 2.0		49.3 ± 7.6	-	-6.9 ± 0.1	-
IOX[b]	12.2 ± 1.4	0.15	42.2 ± 6.9	0.26	-7.2 ± 0.2	0.14
IOX-NIV[c]	16.7 ± 2.5	0.29	54.5 ± 9.1	0.34	-6.9 ± 0.1	0.44

[a]*667 µl PBS;* [b]*142 mg mL^{-1};* [c]*1 mM IOX-NIV; 1 mM IOX-NIV encapsulated* IOX *equivalent after purification = 0.95 mg mL^{-1}.*

5.4.2   Effect of IOX and IOX-NIV vessel pre-treatment on vasodilation

Analysis of vessel responses to ACh as a % of each vessels maximum response would suggest that the control group were the most sensitive as vasodilatory response occurred across the lowest concentration range. In comparison, vasodilatory response was shifted to the right for IOX pre-treated vessels, and further shifted to the right in the IOX-NIV pre-treated group (Figure 5.9).

Further analysis of vessel responses showed no difference in cumulative response across treatment groups during PE pre-constriction, the maximum PE response was much lower in IOX-vessels (6.1 + 2 mN) in comparison to the control group (12.9 + 3 mN), however, this decrease was not found to be significant. Similarly, no significant difference in maximum or cumulative constriction after pre-constriction agent was observed when comparing IOX and IOX-NIV response with the control (Table 5.4). Any differences in average minimum tension after the measurement of vasodilatory response to cumulative concentrations of ACh was non-significant at -2.1 ± 3.5, 0.8 ± 0.5 and 5.6 ± 2.1 mN for the control, IOX or IOX-NIV groups, respectively. However, the cumulative vasodilatory response of both IOX (5.2 ± 1.7 mN) and IOX-NIV (6.3 ± 1.4 mN) was significantly less than the control groups at 14.6 ± 1.5 mN (p = 0.01 and p = 0.005, respectively). Despite this, the average EC50 value calculated from both IOX or IOX-NIV treated vessels were not significantly different from control vessels (Table 5.4).
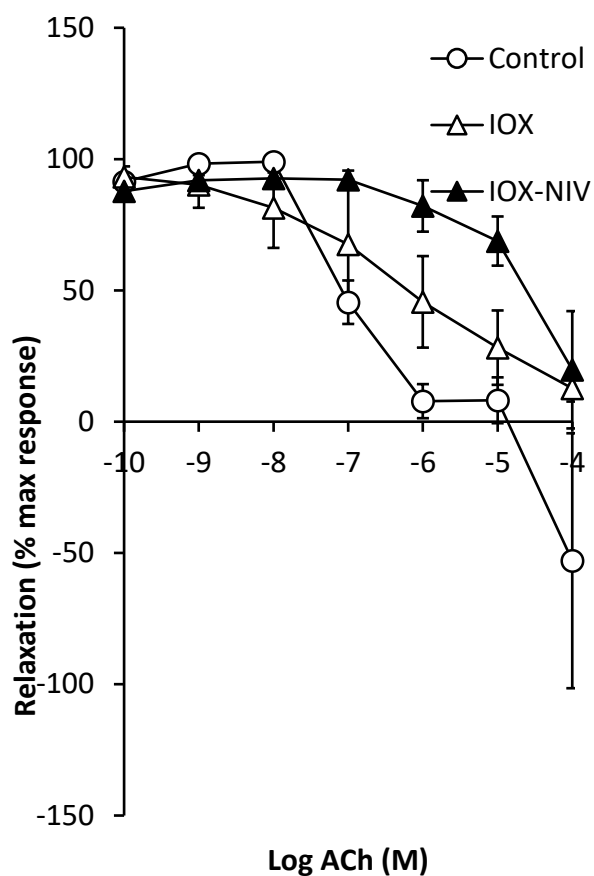
Figure 5.9: ACh cumulative concentration response after 1 h vessel pre-treatment with PBS (control), 142 mg mL^{-1} IOX and 1 mM IOX-NIV (IOX encapsulated equivalent concentration of 0.95 mg mL^{-1}). *Vessel response was plotted as a percentage decrease, in relation to the initial level of contraction induced after exposure to 10^{-5} or 10^{-4} M PE, as a result of the increase in ACh concentration. 1 mM IOX-NIV encapsulated* IOX *equivalent after purification = 0.95 mg mL^{-1} (n = 3, ± SEM).*

Table 5.4: Effect of vessel pre-treatment on PE-contraction and vasodilatory response to ACh. *(n = 3, ± SEM).*

	Pre-constriction response to PE					
Treatment	**Maximum tension (mN ± SEM)**	**p-value**	**Cumulative tension increase (mN ± SEM)**	**p-value**		
Control[a]	12.9 ± 3.0	-	33.7 ± 10.4	-		
IOX[b]	6.1 ± 2.1	0.07	14.0 ± 7.7	0.10		
IOX-NIV[c]	11.9 ± 2.7	0.39	48.2 ± 13.5	0.21		
	Vasodilatory response to ACh					
Treatment	**Minimum tension (mN ± SEM)**	**p-value**	**Cumulative tension decrease (mN ± SEM)**	**p-value**	**Log EC50 (M ± SEM)**	**p-value**
Control[a]	-2.1 ± 3.5	-	14.6 ± 1.5	-	-6.6 ± 0.4	-
IOX[b]	0.8 ± 0.5	0.25	5.2 ± 1.7	0.01*	-6.6 ± 0.8	0.98
IOX-NIV[c]	5.6 ± 2.1	0.07	6.3 ± 1.4	0.005*	-5.7 ± 0.4	0.18

[a]*667 µl PBS*; [b]*142 mg mL^{-1}*; [c]*1 mM IOX-NIV; 1 mM IOX-NIV encapsulated* IOX *equivalent after purification = 0.95 mg mL^{-1}; * p < 0.05, ** p < 0.005 when comparing treated vessels to the control response.*

Vessel responses plotted as a % of each vessels maximum response showed similar to SNP regardless of pre-treatment (Figure 5.10). Similar to the pattern observed when comparing vessel pre-treatment groups and their response to PE as a pre-constricting prior, to the performance of ACh-cumulative concentration response curves, the pre-constriction response was roughly half in the IOX group (5.1 ± 1 mN) in both the control and IOX-NIV groups (~11 ± 3 mN). In this instance the difference in pre-constriction between control and IOX-treated vessels was significantly different (p = 0.04;

Table 5.5). A similar pattern was observed when comparing the cumulative increase in tension after exposure to PE for each treatment group - control group cumulative tension was 16.0 ± 7.3 mN and IOX-pre-treated vessel cumulative response was 5.1 ± 0.9 mN, while IOX-NIV pre-treated vessels expressed a cumulative vasoconstrictive response of 14.6 ± 4.6 mN which was similar to the control group (

Table 5.5). The minimum tension after exposure to cumulative concentrations of SNP produced similar results for each test group – IOX pre-treated vessels expressed a minimum tension of -0.7 ± 0.6 mN and IOX-NIV pre-treated vessels expressed a tension of -2.3 ± 1 mN and differences were non-significant in comparison to the control group at -0.8 ± 0.4 mN. In contrast, the differences in cumulative vasodilatory response to SNP was significantly different when comparing IOX (5.9 ± 1.1 mN) with the control (12.1 ± 2.4 mN) (p = 0.04). The response of IOX-NIV pre-treated vessels was comparable with that of the control at 13.5 ± 3.4 mN. In addition to this, the EC50s for each test group was ~ 10^{-8} M SNP which meant that there were no significant differences when comparing SNP sensitivity of vessels after exposure to free or NIV entrapped IOX.
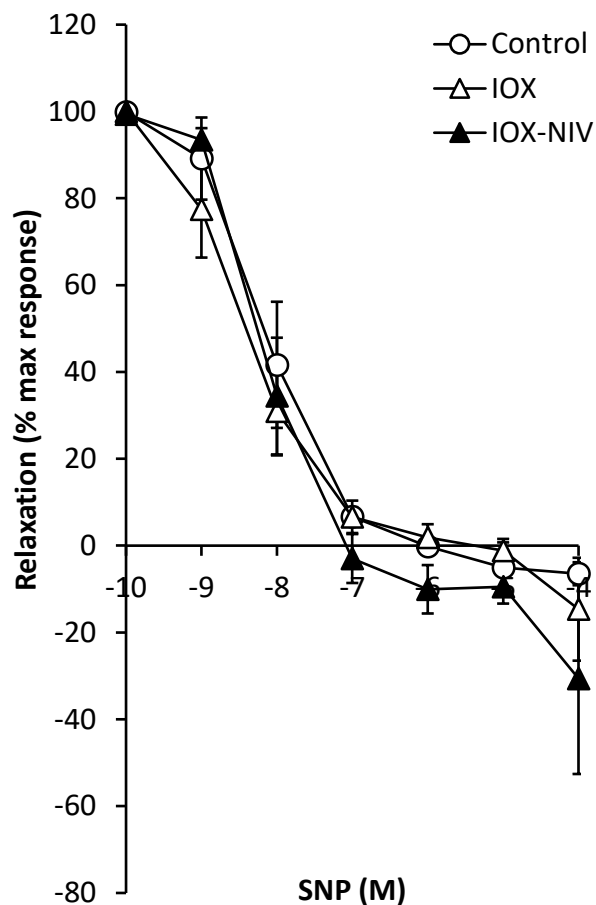
Figure 5.10: SNP cumulative concentration response curve after 1 h vessel pre-treatment with PBS (control), 142 mg mL^{-1} IOX and 1 mM IOX-NIV. *Vessel response was plotted as a percentage decrease, in relation to the initial level of contraction induced after exposure to 10^{-5} or 10^{-4} M PE, as a result of the increase in SNP concentration. 1 mM IOX-NIV encapsulated* IOX *equivalent after purification = 0.95 mg mL^{-1} (n = 4; ± SEM).*

Table 5.5: Effect of vessel pre-treatment on PE-contraction and vasodilatory response to SNP.

Treatment	Maximum tension (mN ± SEM)	p-value	Cumulative tension increase (mN ± SEM)	p-value		
	Pre-constriction response to PE					
Control [a]	11.3 ± 2.6	-	16.0 ± 7.3	-		
IOX [b]	5.1 ± 0.9	0.04*	5.1 ± 0.9	0.12		
IOX-NIV [c]	11.2 ± 3.2	0.50	14.6 ± 4.6	0.44		
Treatment	**Minimum tension (mN ± SEM)**	**p-value**	**Cumulative tension decrease (mN ± SEM)**	**p-value**	**Log EC50 (M ± SEM)**	**p-value**
	Vasodilatory response to SNP					
Control [a]	-0.8 ± 0.4	-	12.1 ± 2.4	-	-7.9 ± 0.3	-
IOX [b]	-0.7 ± 0.6	0.48	5.9 ± 1.1	0.04*	-8.0 ± 0.5	0.9
IOX-NIV [c]	-2.3 ± 1.2	0.11	13.5 ± 3.4	0.36	-7.7 ± 0.3	0.6

[a]*667 µl PBS*; [b]*142 mg mL^{-1}*; [c]*1 mM IOX-NIV; 1 mM IOX-NIV encapsulated IOX equivalent after purification = 0.95 mg mL^{-1}; *p ≤ 0.05 when comparing treated vessels to the control response*

5.5 Discussion

Myograph experiments were utilised to examine the implications of blood vessel exposure to IOX and whether the entrapment of IOX within a NIV delivery system may be used to avoid negative effects. After 1 h exposure to PBS, IOX, or IOX-NIV (37 °C) changes in vessel tension, after exposure to well-characterised vasoconstrictive or vasodilatory pharmacological agents, was recorded to measure VSM- and endothelium-induced constriction and relaxation. These experiments build on previous *in vitro* studies which were used to identify the EC50 values of free-IOX, IOX-NIV and empty- NIVs (Chapter 4 – *In vitro* Toxicity of IOX, IOX-NIV and empty-NIV).

The theory that RCM, including IOX, induce vascular relaxation contradicts theories that the pathology of CIN is related to vasoconstriction and increased blood pressure, particularly in the afferent arteriole of the nephron. Pre-existing high blood pressure and vasoconstriction within the diabetic patient is a characteristic which has been linked to an increase in susceptibility to CIN (Caiazza *et al.*, 2014). However, RCM administration has been linked to the induction of both vasoconstriction and vasodilation whereby the vessel of choice used during the experiment appears to influence the response to pharmacological agents. Rauch *et al.* (1997) isolated a range of different rabbit arteries and observed vasoconstriction in the carotid, aorta, iliac and, most importantly the renal artery, but saw an opposite response when analysing the mesenteric and celiac arteries. The greatest intensity of vasoconstriction was observed in the carotid and aortic vessels. Although the underlying renal disease in susceptible patient appears to be the key contributing factor to RCM-AKI. Overall, the current data suggests that the interaction of RCM within the vasculature is in fact specific to certain arteries. Despite this, the results described in these experiments support the theory that RCM exert a negative effect on the aorta leading to altered vascular contractile and dilatory responses.

5.4.1 Effect of IOX and IOX-NIV exposure to vascular response to vasoconstriction-inducing agents

The most notable change in response observed across all myograph experiments was the absence of vasoconstriction upon exposure to increasing concentrations of the depolarising agent KCl after 1 h vessel incubation with IOX. Despite the lack of KCl-mediated response observed in comparison to control vessels, t-test analysis showed that the differences between control and IOX vessels were non-significant. An increase in the number of experiments performed may have detected significance between the dramatically altered vessel responses. Despite this, a significant reduction in the total increase in contraction throughout the course of the experiment when comparing control and IOX treated vessels was detected. The

reduction in KCl response after vessel exposure to IOX suggests that IOX has a direct physiological effect on VSM and hence an alteration in VSM membrane depolarisation. Previous *in vitro* experiments had shown a 50 % reduction in VSMC metabolic activity after 2 h exposure to 124 mg mL^{-1} IOX, equivalent to a final iodine concentration of 57 mg I mL^{-1} (Chapter 4 – *In vitro* toxicity of IOX, IOX-NIV and empty-NIV). Despite this, similar non-ionic RCM and a high osmolar mannitol solution (iopromide, iotrolan and saturated mannitol solution) were reported to have no effect on VSMC-viability or growth, as determined through trypan blue exclusion, after 60 min exposure at a much greater iodine concentration of 250 mg I mL^{-1} (Wang *et al.*, 1998). Previous organ-bath based experiments which utilised perfused dog ear arteries to test the effect of RCM, including IOX, on the endothelium found that RCM act as vasodilators in a concentration-dependent manner resulting in VSM relaxation (Hutcheson *et al.*, 1999). These results were observed in both the performance of a cascade bioassay as well as during the use of endothelium-intact rings. In general, it was found that RCM have a direct effect on the endothelium resulting in the inhibition of NO production, without having a direct effect on the vascular smooth muscle. However conclusions from Hutcheson *et al.*, (1999) had a primary focus on the performance of relaxation studies using ACh and SNP rather than making a comparison between VSM and endothelial-mediated vessel response.

Karstoft *et al.* (1995) suggested that the vasodilatory effect of IOX could be explained by stating that IOX blocks VSM voltage-operated Ca^{2+} channels. This could explain why aorta response to KCl, but not PE, was inhibited after pre-treatment with IOX. After the removal of the endothelial layer Schneider and Rand (1988) continued to observe IOX induced vasoconstriction, therefore concluded that this was initiated through direct VSM toxicity. The effect of IOX on pre-constricted vessels was not a factor tested within the scope of these experiments, however, earlier *in vitro* tests detected a decrease in VSMC performance after measurement using the Resazurin metabolic indicator assay (Chapter 4), as well as the absence of response to KCl, highlight that there is a degree of direct toxicity of IOX on the VSM layer. A second theory which may describe the lack of vascular response to KCl after treatment with IOX at 37 °C is reduced extracellular Ca^{2+} availability. RCM-Ca^{2+} binding has been previously reported in studies utilising ionic RCM, specifically ioxaglate and diatrizoate, whereby a reduction in ionised Ca^{2+} within the blood was detected in conjunction with alterations in electrical signalling within the heart and vasculature. Although these effects were not similarly observed upon exposure to non-ionic RCM such as IOX (Hayakawa *et al.*, 1994). Regardless of the mechanism behind the lack of vascular response to KCl in IOX pre-treated vessels, no altered effect was observed as a result of vascular incubation with 1 mM IOX-NIV which

highlights the safety of vascular exposure to this concentration of lipid. Initial similar KCl-response after IOX-NIV exposure supports the use of NIVs as a drug delivery system.

If the absence of KCl-mediated response was related to a loss in VSM viability, it may also be assumed that PE vasoconstriction would be similarly decreased after IOX treatment. Instead, PE-dose-response curves were not altered after pre-exposure to IOX or IOX-NIV. The maximum tone generated after exposure to a final concentration of 1×10^{-4} M PE was unaltered when comparing control, IOX and IOX-NIV vessel treatment groups. Despite constituting two different methods of inducing vasoconstriction, KCl and PE-mediated downstream signalling is similar. The absence of any difference in PE-mediated response may suggest that the negative effect of IOX *ex vivo* is not necessarily related to an overall reduction in VSM viability.

PE responses measured in this study are in agreement with previous research which supports the theory that non-ionic RCM, including IOX, do not negatively affect muscarinic receptor-mediated VSM contraction and hence the theory that IOX does not directly influence VSMs (Schneider and Rand, 1988). Upon vascular exposure to IOX-NIV at a final lipid concentration of 1 mN, there was no interference with vasoconstriction, either voltage-dependent or α_1-adrenergic receptor-dependent VSM contraction. *In vitro* experiments had estimated a VSMC EC50 of 1.36 ± 0.29 mM after 2 h exposure to IOX-NIV, while HUVEC EC50 was 1.28 ± 0.001 mM, in comparison, blood vessels in a myograph system appear to be more robust and no alteration in function was observed despite the alteration in voltage-dependent response after free-IOX exposure *ex vivo*. It could have been that after the performance of cumulative concentration responses to KCl immediately after IOX treatment lead to a transient loss in vessel response which was regained during the time period between the performances of KCl- and PE-response experiments. Effects of RCM on vascular activity have been found to be reversible, which may explain the recovery of PE-mediated vasoconstriction after the performance of KCl vasoconstriction (Schneider and Rand, 1988). The average time between these experiments was around 1 h, during this time the vessel was washed 3x in fresh Krebs' solution and allowed to settle until a basal tension was reached providing time for the vessel to regain normal activity.

5.4.2 Effect of vascular exposure to IOX and IOX-NIV on vasodilatory response to pharmacological agents

In comparison to control groups, the cumulative vasodilatory response to ACh was different depending on whether vessels were exposed to IOX or IOX-NIV. IOX pre-treated vessel response was shifted to the right while IOX-NIV vessel response expressed a greater shift

suggesting a reduced capacity of vessel dilatory response via endothelial receptor-dependent mechanisms. The sum of vasodilation after pre-treatment with IOX and IOX-NIV was significantly lower than the sum of vasodilation exerted by the control vessels. Both of these factors could indicate either reduced NO production by endothelial cells or decreased sensitivity to the vasodilatory activity of ACh on the muscarinic receptors of endothelial cells. Hutcheson *et al.* (1999) performed organ bath-based experiments using rabbit aorta to determine whether IOX exposure to 10 % (64.7 mg mL^{-1}) or 30 % (194.1 mg mL^{-1}) IOX influenced ACh (endothelium-dependent) and SNP-induced relaxation (minus endothelium) after initial pre-constriction using PE. A concentration-dependent decrease in vessel sensitivity to ACh was observed in the presence of IOX. In conjunction with data obtained upon examination of vascular response to endothelium-independent-SNP vasodilation, Hutcheson *et al.* (1999) had shown the absence of an effect of IOX exposure on SNP-induced relaxation., but highlighting an overall reduced relaxing capacity of smooth muscle cells as a result of RCM pre-incubation.

Differences between the effect of IOX exposure and ACh response reported here and the work described by Hutcheson may have been related to differences in the experimental set-up. Firstly, Hutcheson performed all relaxation experiments in the continuous presence of RCM rather than performing experiments after a 1 h pre-treatment. The negative effects of IOX *in vitro* are often reported after treatment times as little as 1 to 15 min exposure (Zhang *et al.*, 2000). In addition to this, earlier *in vitro* vascular toxicity experiments had detected an alteration in HEK-293 cell division after as little as 10 mins post-exposure the extent of which was not found to be time-dependent over the course off 30 mins (Chapter 4 - In vitro Toxicity of IOX, IOX-NIV and Empty-NIV), therefore it may have been expected that regardless of differences in exposure, similar responses may have been expected. As discussed previously, the effects of RCM on vascular activity have been found to be reversible which may relate to the absence of notable response to ACh-vasodilation (Schneider and Rand, 1988).

Secondly, Hutcheson compensated for any loss of vascular tone related to the presence of RCM by increasing PE concentration 10-fold to 3 µM, ensuring the same degree of pre-constriction prior to the performance of vasodilatory dose-response curves. Ensuring the same degree of vascular tone prior to relaxation experiments may have been beneficial in eliminating interference. Despite no difference in vasoconstriction of aortic segments to PE, in terms of maximum response, cumulative response, or % constriction based on individual vessel response, further experimentation which involved a degree of pre-constriction prior to the analysis of vasodilatory response saw that IOX vessels exerted half the tone in comparison

to both control and IOX-NIV pre-treated vessels. Similar responses to ACh in the IOX and control groups may therefore be attributed to the lower level of pre-tension exerted by IOX-treated vessels, if an equal level of pre-constriction was achieved for each treatment group, an alteration in the dose-dependent response to ACh may have been observed. Previous studies are also in agreement with the theory that a direct endothelium-independent action on VSM plays an important role in the mediation of IRCM-induced vasorelaxation in rabbit aortic rings (Pugh *et al*., 1995; Pitman *et al*., 1996).

5.4.3 Linkage between drug entrapment and anticipated vascular response

A NIV encapsulation efficiency at 22 ± 3 % IOX, was determined in earlier chemical characterisation experiments (Chapter 3 – Validation of HPLC detection of IOX and quantification of encapsulation efficiency and release), corresponding to a final IOX concentration of 142 mg mL^{-1}. Therefore, at a final lipid concentration of 1 mM, IOX-NIV treated vessels would therefore be treated with NIVs entrapping an equivalent IOX concentration of 9.47 mg mL^{-1} which is much less than the concentrations equivalent to the EC50s mentioned previously. During IOX-NIV vessel exposure the influence of the IOX-NIV release profile needs to be considered. According to IOX release studies, after 1 h incubation at 37 °C between 20 and 30 % of entrapped IOX would have leaked from NIVs (Chapter 3 – Validation of HPLC detection of IOX and quantification of encapsulation efficiency and release). This suggests that vessel exposure to IOX would have been less than the toxic range measured *in vitro,* between 1.89 and 2.84 mg mL^{-1} IOX, but would have also been in combination with the NIV lipid components. Despite the concentration of IOX entrapped within or released from NIVs being below the toxic range observed during *in vitro* exposure to cells of vascular origin, the level of encapsulation within IOX-NIV is likely to be sufficient enough to provide attenuation required for bio-imaging. Previous experiments have shown that liposomes with an iodine entrapment of 34.8 mg I mL^{-1} delivered intravenously to rabbits at 475 mg I kg^{-1} body weight successfully provided contrast enhancement (Kao *et al.*, 2003). The iodine-equivalent concentration of IOX within NIVs prepared in this study was therefore 52 % greater than that reported in previous studies. It may therefore be assumed at this stage, a non-toxic IOX-NIV system could present a safe and effective option for contrast-enhanced bio-imaging. Although further experiments should be performed to determine the attenuation power of this vesicle system.

5.6   Conclusion and future experiments

Exposure to IOX leads to altered vascular function. The most significant change was in response to KCl, a gold-standard for VSM contraction which is exerted through membrane depolarisation and activation of voltage-dependent Ca^{2+} channels. After IOX exposure, vessels were found to lose all response to increasing KCl concentrations. In comparison, IOX-NIV exposed vessels showed similar maximum, cumulative and EC50 responses to that expressed by the control. The lack of vascular response to KCl highlights a direct effect of IOX on VSM contractility due to a loss in normal function. Interestingly, more-specific methods of inducing VSM contraction, through exposure to α_1-adrenergic receptor agonist, PE, was not altered after exposure to IOX or IOX-NIV. This suggests that although there was reduced VSM response to KCl, the VSM was still able to contract through activation of specific receptors. This suggests that the effect of IOX on vascular response may have not simply been related to an overall decrease in VSM viability, however, IOX may decrease extracellular Ca^{2+} availability or block voltage-operated Ca^{2+} channels directly.

Despite no differences being observed after exposure to IOX or IOX-NIV in terms of cumulative, max or EC50 responses to PE, a significant decrease in tone was observed after pre-constriction with 1×10^{-6} M PE prior to the performance of relaxation experiments. The reduced pre-constriction of IOX-exposed vessels may have masked any significant alteration in endothelial-mediated VSM relaxation which may have been observed upon exposure to increasing ACh concentrations in terms of % max response or calculated EC50s. Similarly no significant alteration in SNP, endothelium-independent relaxation of VSM in terms of the estimated EC50 values was apparent regardless of whether vessels were exposed to IOX or IOX-NIV. The significant reduction in IOX pre-treated vessel cumulative vasodilatory response to ACh and SNP is suggestive of an alteration in responsiveness to vasodilatory agents – a feature commonly reported throughout the literature. Endothelial dysfunction is also a common symptom expressed by patients with CIN-predisposing morbidities, the exacerbation of an altered endothelial response upon exposure to RCM may provide evidence to explain the mechanism of susceptibility in certain patient groups.

Differences in the initial vascular tone in experiments involving pre-constriction with PE, such as ACh and SNP-cumulative concentration response curves, may have contributed to the lack of differences in response as a % between different treatment groups. Preferably, each vessel used in each sample group would express the same level of initial pre-constriction when treated with a specific dose of PE, however differences were observed between vessels subjected to different pre-treatments which meant additional dosages of PE were sometimes given. Despite

this, earlier experiments had shown similar degrees of vasoconstriction during PE cumulative concentration response curves. In terms of result interpretation, the initiation of different baselines pre-constrictions, which was significantly lower in the IOX pre-treatment group, meant that the amount of pre-existing tension which could have been relaxed was greatly reduced, and therefore it may be assumed that the concentration of relaxing agent required to reduced similar levels of vasodilation will also be reduced within these treatment groups. Future work should focus on exerting the same degrees of vascular tone during pre-constriction of different treatment groups.

More clinically relevant data may have been obtained if experiments compared the performance of blood vessels derived from susceptible patient groups, or from animal model equivalents. This is due to the fact that AKI as a result of IOX exposure is not common within healthy patients, instead, a link between vascular and renal dysfunction and patient susceptibility to RCM-AKI is key. Isolation of vessels from an aged or diabetic or hypertensive hosts may have provided more clinically-relevant results. Experiments which compare the results obtained here, using healthy animal vessels, could be compared to vessels from hosts with physiologically abnormal vessels, such as aorta obtained from diabetic or aged rat models could improve our understanding of disease and whether NIVs could be used to prevent complications in at-risk patient groups. In addition, the rat aorta is a common vessel of choice in studies looking as the effects of RCM on the vasculature, the large size of the vessel offers an advantage relating to and ease of use when performing contractile experiments. Although RCM is commonly used for imaging of the vasculature around the heart, the renal artery may provide more clinically relevant data as it is the kidney which suffers the most damage after RCM administration.

Similar to *in vitro* study improvement, it may have been advantageous to perform experiments where the IOX concentration was normalised between IOX and IOX-NIV groups. Rather than removing unentrapped IOX from the external NIV media, the analysis of IOX-NIVs with both entrapped and unentrapped IOX would have enabled the opportunity for a direct comparison based on IOX concentration which would enabled conclusions to be made as to whether the entrapment of IOX offered a level of protection against alterations in vascular response to key pharmacological agents. It may have also been beneficial to further investigate NIV toxicity by pre-exposing vessels to equal concentrations of empty-NIV in addition to IOX-NIV. Despite this, no significant effect of IOX-NIV on vascular response to the various pharmacological agents was observed in comparison to the untreated control group. Earlier *in vitro* experiments tested the effect of IOX, empty-NIV and IOX-NIV on cells from both

endothelial and vascular cell origin (Chapter 4 – *In vitro* Toxicity of IOX, IOX-NIV and empty-NIV). Here a similar toxicity profile was observed regardless of IOX-entrapment therefore it may also be assumed that there would be no difference in *ex vivo* results, particularly in a system completely absent of IOX.

Further experiments are required to confirm the efficacy of IOX-NIV *in vivo* while the incorporation of diabetic, aged, or hypertensive rats may provide a more relevant assessment of the risk of dysfunction in RCM-AKI key risk groups.

Chapter 6

General conclusions

6.   Chapter 6 - General conclusion and future work

The overall aim of this thesis was to formulate an established NIV formulation as a novel delivery system for IOX, with an end goal of achieving a reliable and effective preventative measure against the development of potentially fatal RCM-CIN or AKI. The current absence of preventative and treatment mechanisms acts as a burden to the healthcare system, in addition to patients and their families. The development of such a preventative option would be of financial interest as well as reducing hospital-associated morbidity and mortality. The theory that NIVs may be a viable option to prevent undesirable or toxic IOX interactions, within the vasculature or renal system, stems from the success observed from using NIVs, and alternative lipid-based delivery systems, to reduce systemic toxicity associated with chemotherapeutics and antibiotics, for example. Therefore, it was proposed that a novel application for NIVs would be their use in the prevention of RCM-associated damage. Throughout each stage of development, parameters important to ensure the ease of transfer of a lipid delivery system from research and development, to the clinical setting were considered.

Initial synthesis of IOX-NIVs led to the observation of an unexpected phenomenon, whereby vesicles were not observed to form until after further dilution of hydrated molten lipids. This affect was also not reported in any of the liposome preparations which have been described in the literature(Burke *et al.*, 2007; Karathanasis *et al.*, 2009b; Samei *et al*., 2009; Zheng *et al*., 2006), nor through the use of this formulation or method of NIV preparation (Alsaadi, 2011; Mulle*n et al.*, 2000). In comparison to empty-NIVs, whereby the lipids were hydrated in PBS, IOX-NIVs appeared to be in a pro-vesicle form, likely to be the result of CPP – essentially, a balance between lipid and drug concentration. Hydration of the lipid-drug mix using an aqueous phase resulted in the self-assembly of IOX-NIVs which was visualised through a change in colour, from clear to opaque. Size characterisation of the pro-IOX-NIV form did not generate results indicative of the presence of particles whether this was based on particle size analysis using DLS, or through microscopic analysis using AFM. Characterisation of fully formed IOX-NIVs identified the presence of a narrow size distribution and average particle diameter which is compatible with the requirement to administration RCM intravenously. A desired size between 100 and 200 nm was achieved, therefore, it can be expected that IOX-NIV will express a different pharmacokinetic biodistribution in comparison to free-IOX which is rapidly filtered through the kidneys. Instead, due to their size, IOX-NIVs would be more likely to be recognised by the MPS and distributed within the liver and spleen.

The homologous size and negative surface charge of IOX-NIVs supported the electrochemical stability of the system, meaning that, when stored at temperatures of 4 and 25 °C, IOX-NIVs

retained both their initial physical, chemical and IOX-entrapment properties throughout the course of the entire stability experiment. In contrast, an increase in IOX-NIV size, PDI, loss in electronegativity and IOX-entrapment was observed after long-term storage at extreme temperatures of 50 °C. The detection of an alteration in IOX-NIV physical properties occurred to a lesser extent after storage at 37 °C, however, the gradual decline in EE remained almost identical to IOX-NIV stored at 50 °C. IOX-NIV expressed physical and chemical stability for the whole 37 weeks when stored at 4 and 25 °C, a reduced shelf-life of 21 weeks could be recommended upon storage at a temperature ≤ 37 °C, or up to 8 weeks at temperatures ≤ 50 °C. The performance of long-term analysis of empty-NIVs and IOX alone, using the same conditions as described for IOX-NIVs, would assist in uncovering whether the change in colour after long-term IOX-NIV incubation (> 1 month) at increased temperatures was in fact related to alterations in IOX chemistry or the degradation of lipid components, either through oxidation or some other chemical process. Regardless of the cause of the change in IOX-NIV appearance, this alteration subsequently lead to IOX-NIV physical and chemical decline. The generation of results relating to lipid quantification through the use of an ELSD-HPLC method may have been able to conclude whether the temperature- and time-dependent decrease in IOX-NIV stability was related to a specific lipid component. An ELSD-HPLC method for the quantification of NIV components has been described elsewhere (Alsaadi *et al.*, 2013), however, unexpected interferences meant that the results were invalid and unfortunately could not be reanalysed. Additional experiments whereby the long-term stability of hydrated IOX-NIV is monitored would make a useful comparison to stability of the formulation in its pro-form. These results would be able to address the theory formulation storage as a pro-IOX-NIV offers enhanced stability. If pro-IOX-NIVs were found to retain their stability better than IOX-NIVs the requirement for the use of lyophilisation as a preservation technique may not be necessary.

IOX EE within NIVs was quantified using a robust and accurate HPLC method, validated using FDA analytical method guidelines. The percentage of IOX entrapment was at the typical level expected for the incorporation of a hydrophilic drug within the core of a lipid delivery system. Previous research which developed RCM-liposomes had expressed EEs of the same value, ~20 %, therefore in terms of EE there was no specific advantage over the use of NIVs rather than liposomes. IOXs release from NIVs under physiological conditions which mimic conditions of the body had shown a typical hydrophilic drug release profile characterised by a 'burst' release, whereby, the majority of IOX leaked from NIVs within the initial 24 h after the initiation of dialysis. These experiments could have been improved by creating more

physiologically relevant conditions, the incorporation of FCS within the saline release media would better mimic the properties of blood.

The *in vitro* work carried out in this thesis is in support of the evidence reported in the literature in terms of anticipated IOX toxicity as determined through the Resazurin-metabolic indicator assay, but the data is also in line with NIV cytotoxic ranges currently reported. Additional benefits may have been achieved upon testing *in vitro* toxicity using un-purified IOX-NIV as this would have enabled a direct comparison between free-IOX and IOX-NIV toxicity profiles using normalised IOX concentrations. Instead, current data makes it difficult to determine whether there is a true reduction in toxicity through the encapsulation of IOX within NIVs.

After the isolation of rat aorta, the different endothelial and vascular components of the vasculature were observed to have reasonable viability and responsiveness which highlights the quality of the method used. IOX caused a significant reduction in receptor-independent vasoconstriction in the presence of K^+ ions. Although results could not be directly compared based on IOX concentration, exposure to IOX-NIV had no effect on vessel response. Similar to the experimental design of the *in vitro* work, benefits may be gained from the performance of further vascular performance experiments which incorporates the analysis of toxicity of IOX-NIV without purification. This would allow for normalisation of IOX concentration enabling a direct comparison of free- and IOX-NIV toxicity, and whether entrapment offers any advantage in this instance. IOX did not impair vessel response to other pharmacological constricting or relaxing agents.

Performance of myographic experiments on vessels obtained from animals suffering from currently identified RCM-associated AKI and CIN would provide useful data in comparison to that gained from healthy animals as described in this thesis. Due to the fact that the development of RCM-AKI or CIN has been linked to the presence of underlying renal and vascular disease states, the analysis of response from vessels obtained from a pre-disposing disease state such as the diabetic, aged or hypertensive model may provide more relevant information. Performance of this experiment could add to our current understanding of RCM-associated disease and whether IOX-NIVs can infer a level of protection.

Guidelines produced by the FDA for preferred liposomal characterisation at the research and development stage outlined a number of other properties that were not outlined within the scope of the work carried out in this thesis. This included the definition of NIV lamellarity for which a commonly used technique for the determination of lamellar number is FFEM. As mentioned as a way to improve analysis of IOX-NIV behaviour in conditions which mimic

the environment after administration, the FDA guidelines also recommend testing the interaction of a lipid delivery system with proteins which are strongly concentrated within serum. The importance of this relates to the fact that protein interactions interferes with biodistribution, half-life, drug-leakage and stability. This highlights the importance of effective design of experiments. Other parameters which the FDA recommend reporting on include viscosity, phase transition behaviours, the influence of salt exposure and characterisation of structure.

Beyond physical, chemical and *in vitro* characterisation of IOX-NIVs, the next logical stage in development would be the use of *in vivo* models for the determination of safety and potential dosage analysis. Additional chemical analysis to clearly characterise the lipid components both post-synthesis and throughout storage conditions is necessary to identify the presence of contaminants and potential methods of IOX-NIV degradation. Promising results are presented throughout the literature in terms of RCM-liposomes, the efficacy of IOX-NIVs as a contrast enhancing agent still remains to be tested.

7. Bibliography

Abdelkader, H., Alani, A. W. G., & Alany, R. G. (2014). Recent advances in non-ionic surfactant vesicles (niosomes): Self-assembly, fabrication, characterization, drug delivery applications and limitations. *Drug Delivery*, *21*(2), 87–100.

Abe, S., Fukuda, H., Tobe, K., & Ibukuro, K. (2016). Protective effect against repeat adverse reactions to iodinated contrast medium: Premedication vs. changing the contrast medium. *Eur Radiol*, *26*, 2148–2154.

Adler-Moore, J. P., & Proffitt, R. T. (2008). Amphotericin B lipid preparations: what are the differences? *Clinical Microbiology and Infection*, *14*, 25–36.

Ahmed, S., Gogal, R. J., & Walsh, J. (1994). A new rapid and simple non-radioactive assay to monitor and determine the proliferation of lymphocytes: an alternative to [3H]thymidine incorporation assay. *J Immunol Methods*, *170*, 211–224.

Akbarzadeh, A., Rezaei-Sadabady, R., Davaran, S., Joo, S. W., Zarghami, N., Hanifehpour, Y., Samiei, M., Kouhi, M., & Nejati-Koshki, K. (2013). Liposome: classification, preparation, and applications. *Nanoscale Research Letters*, *8*(1), 102.

Akiyama, M., Nakada, T., Sueki, H., Fujisawa, R., & Iijima, M. (1998). Drug eruption caused by nonionic iodinated X-ray contrast media. *Acad Radiol*, *5*, S159-161.

Al-sulti, Z. S. (2017). Mitochondrial regulation of vascular smooth muscle cell proliferation and migration in atherogenesis and restenosis. *[Thesis] The University of Strathclyde*.

Alberts, D. S., Liu, P. Y., Wilczynski, S. P., Clouser, M. C., Lopez, A. M., Michelin, D. P., Lanzotti, V. J., Markman, M., & Southwest Oncology Group. (2008). Randomized trial of pegylated liposomal doxorubicin (PLD) plus carboplatin versus carboplatin in platinum-sensitive (PS) patients with recurrent epithelial ovarian or peritoneal carcinoma after failure of initial platinum-based chemotherapy (Southwest Onc. *Gynecol Oncol*, *108*, 90–94.

Ali, M. H., Kirby, D. J., Mohammed, A. R., & Perrie, Y. (2010). Solubilisation of drugs within liposomal bilayers: Alternatives to cholesterol as a membrane stabilising agent. *Journal of Pharmacy and Pharmacology*, *62*, 1646–1655.

Allard, B., Bernengo, J. C., Rougier, O., & Jacquemond, V. (1996). Intracellular Ca2+ changes and Ca2+-activated K+ channel activation induced by acetylcholine at the endplate of mouse skeletal muscle fibres. *J Physiol*, *15*, 337–349.

Almén, T. (1969). Contrast Agent Design: Some Aspects on the Synthesis of Water Soluble

Contrast Agents of Low Osmolality. *J Theor Biol*, *24*, 216–226.

Almén, T. (1995). Visipaque - As step forward, a historical review. *Acta Radiologica*, *399*, 2–18.

Almén, T., Aspelin, P., & Nilsson, P. (1980). Aortic and pulmonary arterial pressure after injection of contrast media into the right atrium of the rabbit. Comparison between metrizoate, ioxaglate and iohexol. *Acta Radiol Suppl.*, *362*(37–41).

Almgren, M., Edwards, K., & Karlsson, G. (2000). Cryo transmission electron microscopy of liposomes and related structures. *Colloids and Surfaces A: Physicochemical and Engineering Aspects*, *174*(1–2), 3–21.

Alsaadi, M. (2011). Non-Ionic Surfactant Vesicles as a Delivery System for Cisplatin. *Thesis [PhD] University of Strathclyde*, (October).

Alsaadi, M., Italia, J. L., Mullen, A. B., Ravi Kumar, M. N. V., Candlish, A. A., Williams, R. A. M., … Carter, K. C. (2015). The efficacy of aerosol treatment with non- ionic surfactant vesicles containing amphotericin B in rodent models of leishmaniasis and pulmonary aspergillosis infection. *Journal of Controlled Release*, *160*(3), 685–691.

Alsaadi, M. M., Christine Carter, K., & Mullen, A. B. (2013). High performance liquid chromatography with evaporative light scattering detection for the characterisation of a vesicular delivery system during stability studies. *Journal of Chromatography A*, *1320*, 80–85.

Andreucci, M., Faga, T., Pisani, A., & Sabbatini, M. (2014). Acute kidney injury by radiographic contrast media: Pathogenesis and prevention. *BioMed Res Int*, *Epub*, doi: 10.1155/2014/362725.

Andreucci, M., Faga, T., Serra, R., De Sarro, G., & Michael, A. (2017). Update on the renal toxicity of iodinated contrast drugs used in clinical medicine. *Drug Healthc Patient Saf*, *22*, 25–37.

Ansari, L., Shiehzadeh, F., Taherzadeh, Z., Nikoofal-Sahlabadi, S., Momtazi-borojeni, A. A., Sahebkar, A., & Eslami, S. (2017). The most prevalent side effects of pegylated liposomal doxorubicin monotherapy in women with metastatic breast cancer: a systematic review of clinical trials. *Cancer Gene Therapy*, *24*, 189–193.

Archer, S., Huang, J., Hampl, V., Nelson, D., Shultz, P., & Weir, E. (1994). Nitric oxide and cGMP cause vasorelaxation by activation of a charybdotoxin-sensitive K channel by cGMP-dependent protein kinase. *Proc Natl Acad Sci U S A*, *91*, 7583–7587.

Arnold, W., Mittal, C., Katsuki, S., & Murad, F. (1977). Nitric oxide activates guanylate cyclase and increases guanosine 3':5'-cyclic monophosphate levels in various tissue preparations. *Proc Natl Acad Sci U S A*, *74*, 3203–3207.

Association, A. D. (2003). Treatment of Hypertension in Adults With Diabetes. *Diabetes Care*, *26*(Suppl 2), s80–s82.

Ates, B., Abraham, L., & Ercal, N. (2008). Antioxidant and free radical scavenging properties of N-acetylcysteine amide (NACA) and comparison with N-acetylcysteine (NAC). *Free Radic Res*, *42*, 372–377.

Atkinson, J. (1985). Age-related medial elastocalcinosis in arteries: mechanisms, animal models, and physiological consequences. *J Appl Physiol*, *105*, 1643–1651.

Avgoustakis, K., Beletsi, A., Panagi, Z., Klepetsanis, P., Karydas, A., & Ithakissios, D. (2002). PLGA-mPEG nanoparticles of cisplatin: in vitro nanoparticle degradation, in vitro drug release and in vivo drug residence in blood properties. *J Control Release*, *79*, 123–135.

Awasthi, V. D., Garcia, D., Goins, B. a., & Phillips, W. T. (2003). Circulation and biodistribution profiles of long-circulating PEG-liposomes of various sizes in rabbits. *International Journal of Pharmaceutics*, *253*(1–2), 121–132.

Azmins, M. N., Florence, A. T., Handjani-Vila, R. M., Stuart, J. F. B., Vanlerberghe, G., & Whittake, J. S. (1985). The effect of non-ionic surfactant vesicle (niosome) entrapment on the absorption and distribution of methotrexate in mice. *J Pharm Pharmacol*, *37*, 237–242.

Baig, M., Farag, A., Sajid, J., Potluri, R., Irwin, R. B., & Khalid, H. M. I. (2014). Shellfish allergy and relation to iodinated contrast media: United Kingdom survey. *World J Cardiol*, *6*, 107–111.

Baillie, a J., Florence, a T., Hume, L. R., Muirhead, G. T., & Rogerson, a. (1985). The preparation and properties of niosomes--non-ionic surfactant vesicles. *The Journal of Pharmacy and Pharmacology*, *37*(12), 863–868.

Baillie, A. J., Coombs, G. H., Dolan, T. F., & Laurie, J. (1986). Non-ionic surfactant vesicles, niosomes, as a delivery system for the anti-leishmanial drug, sodium stibogluconate. *Journal of Pharmacy and Pharmacology*, *38*(7), 502–505.

Baker, D. H. (2004). Iodine toxicity and its amelioration. *Exp Biol Med (Maywood)*, *229*, 473–478.

Bangham, A. D., & Horne, R. W. (1964). Negative staining of phospholipids and their structural modification by surface-active agents as observed in the electron microscope.

Journal of Molecular Biology, *8*, 660–668.

Barrett, B., Parfrey, P., Vavasour, H., O'Dea, F., Kent, G., & Stone, E. (1992). A comparison of nonionic, low-osmolality radiocontrast agents with ionic, high-osmolality agents during cardiac catheterization. *N Engl J Med*, *326*, 431–436.

Beckett, K., Moriarity, A., & Langer, J. (2015). Safe Use of Contrast Media: What the Radiologist Needs to Know. *RadioGraphics*, *35*, 1738–1750.

Berg, K., Skarra, S., Bruvold, M., Brurok, H., Karlsson, J. O. G., & Jynge, P. (2005). Iodinated radiographic contrast media possess antioxidant properties in vitro. *Acta Radiologica*, *46*(8), 815–822.

Bernstein, K., Giani, J., Shen, X., & Gonzalez-Villalobos, R. (2014). Renal angiotensin-converting enzyme and blood pressure control. *Curr Opin Nephrol Hypertens*, *23*, 106–112.

Billström, A., Hietala, S. O., & Wirell, S. (1987). Effects of metrizoate and iohexol on the liver at visceral angiography. *Acta Radiol*, *28*, 707–710.

Blausen.com Staff. (2014). Medical gallery of Blausen Medical 2014. *WikiJournal of Medicine*, *1*(Accessed: 17 September 2018), DOI:10.15347/wjm/2014.010.

Bochaton-Piallat, M., Gabbiani, F., Ropraz, P., & Gabbiani, G. (1993). Age influences the replicative activity and the differentiation features of cultured rat aortic smooth muscle cell populations and clones. *Arterioscler Thromb Vasc Biol*, *13*, 1449–1455.

Bodin, A., Linnerborg, M., Nilsson, J. L. G., & Karlberg, A.-T. (2003). Structure Elucidation, Synthesis, and Contact Allergenic Activity of a Major Hydroperoxide Formed at Autoxidation of the Ethoxylated Surfactant C12E5. *Chem. Res. Toxicol.*, *16*, 575–582.

Bolstad, B., Borch, K. W., Grynne, B. H., Lundby, B., Nossen, J. O., Kloster, Y. F., Kristoffersen, D. T., & Andrew, E. (1991). Safety and Tolerability of Iodixanol. A Dimeric, Nonionic Contrast Medium: An Emphasis on European and Clinical Phases I and II. *Invest Radiol*, *26*, S201-204.

Bøyum, A., Fjerdingstad, H., Martinsen, I., Lea, T., & Løvhaug, D. (2002). Separation of human lymphocytes from citrated blood by density gradient (NycoPrep) centrifugation: Monocyte depletion depending upon activation of membrane potassium channels. *Scandinavian J Immunol*, *56*, 76–84.

Bozzuto, G., & Molinari, A. (2015). Liposomes as nanomedical devices. *International Journal of Nanomedicine*, *10*, 975–999.

Brar, S., Aharonian, V., Mansukhani, P., Moore, N., Shen, A., Jorgensen, M., Dua, A., Short, L., & Kane, K. (2014). Haemodynamic-guided fluid administration for the prevention of contrast-induced acute kidney injury: the POSEIDON randomised controlled trial. *Lancet*, *383*, 1814–1823.

Brewer, J. M., & Alexander, J. (1992). The adjuvant activity of non-ionic surfactant vesicles (niosomes) the BALB / c humoral response to bovine serum albumin. *Immunol*, *75*, 570–575.

Briguori, C., Manganelli, F., Scarpato, P., Elia, P., Golia, B., Riviezzo, G., Lepore, S., Librera, M., Villari, B., Colombo, A., & Ricciardelli, B. (2002). Acetylcysteine and contrast agent-associated nephrotoxicity. *J Am Coll Cardiol*, *40*, 298–303.

Brito, L., Little, S., Langer, R., & Amiji, M. (2008). Poly(beta-amino ester) and cationic phospholipid-based lipopolyplexes for gene delivery and transfection in human aortic endothelial and smooth muscle cells. *Biomacromolecules*, *9*, 1179–1187.

Bucci, M., Gratton, J., Rudic, R., Acevedo, L., Roviezzo, F., Cirino, G., & Sessa, W. (2000). In vivo delivery of the caveolin-1 scaffolding domain inhibits nitric oxide synthesis and reduces inflammation. *Nat Med.*, *6*, 1362–1367.

Bumbăcea, R., Petruţescu, B., Bumbăcea, D., & Strâmbu, I. (2013). Immediate and delayed hypersensitivity reactions to intravascular iodine based radiocontrast media -- an update. *Pneumologia*, *62*, 47–51.

Burke, S.J., Annapragada, A., Hoffman, E.A., Chen, E., Ghaghada, K.B., Sieren, J., van Beek, E. J. (2007). Imaging of Pulmonary Embolism and t-PA Therapy effects using MDCT and Liposomal Iohexol Blood Pool Agent - Preliminary Results in a Rabbit Model. *Acad Radiol*, *14*(3), 355–362.

Caiazza, A., Russo, L., Sabbatini, M., & Russo, D. (2014). Hemodynamic and tubular changes induced by contrast media. *Biomed Res Int*, doi: 10.1155/2014/578974.

Candeias, L. P., MacFarlane, D. P. S., McWhinnie, S. L. W., Maidwell, M. L., Roeschlaub, C. A., Sammes, P. G., & Whittlesey, R. (1998). The catalysed NADH reduction of resazurin to resorufin. *J. Chem. Soc., Perkin Trans. 2*, *0*, 2333–2334.

Carrion, F. J., De la Maza, A., & Parra, J. L. (1994). The influence of ionic strength and lipid bilayer charge on the stability of liposomes. *Journal of Colloid and Interface Science*, *164*, 78–87.

Carter, K. C., Baillie, a J., & Mullen, a B. (1999). The cured immune phenotype achieved by treatment of visceral leishmaniasis in the BALB/c mouse with a nonionic surfactant vesicular formulation of sodium stibogluconate does not protect against reinfection. *Clinical and Diagnostic Laboratory Immunology*, *6*(1), 61–65.

Carter, K., Sundar, S., Spickett, C., Pereira, O., & Mullen, A. (2003). The in vivo susceptibility of Leishmania donovani to sodium stibogluconate is drug specific and can be reversed by inhibiting glutathione biosynthesis. *Antimicrob Agents Chemother*, *47*, 1529–1535.

Carugo, D., Bottaro, E., Owen, J., Stride, E., & Nastruzzi, C. (2016). Liposome production by microfluidics: potential and limiting factors. *Scientific Reports*, *6*, 25876.

Cavalier, E., Rozet, E., Dubois, N., Charlier, C., Hubert, P., Chapelle, J.-P., Krzesinski, J.-M., & Delanaye, P. (2008). Performance of iohexol determination in serum and urine by HPLC: validation, risk and uncertainty assessment. *Clinica Chimica Acta; International Journal of Clinical Chemistry*, *396*(1–2), 80–85.

Cevc, G., & Richardsen, H. (1999). Lipid vesicles and membrane fusion. *Adv. Drug. Deliv.*, *38*, 207–232.

Chaloemsuwiwattanakan, T., Sangcakul, A., Kitiyakara, C., Nacapricha, D., Wilairat, P., & Chaisuwan, P. (2016). Simple and fast analysis of iohexol in human serums using micro-hydrophilic interaction liquid chromatography with monolithic column. *J Sep Sci*, *39*, 3521–3527.

Chamley-Campbell, J., Campbell, G. R., & Ross, R. (1979). The smooth muscle cell in culture. *Physiol Rev*, *1*, 1–39.

Chase, E. N., & Kricheff, I. I. (1965). The Comparison of the Complication Rates of Meflumine Iothalamate and Sodium Diatrizoate in Cerebral Angiography. *Am J Roentgenol*, *95*, 852–856.

Chen, L. (1978). Microcirculation of the spleen: and open or closed circulation? *Science*, *201*, 157–159.

Choi, H. S., Liu, W., Misra, P., Tanaka, E., Zimmer, J. P., Itty Ipe, B., Bawendi, M. G., & Frangioni, J. V. (2007). Renal clearance of quantum dots. *Nature Biotechnology*, *25*(10), 1165–1170.

Chou, S. Y., Porush, J. G., & Faubert, P. F. (1990). Renal medullary circulation: hormonal control. *Kidney Int*, *37*, 1–13.

Christiansen, C. (2005). X-ray contrast media—an overview. *Toxicol*, *209*, 185–187.

Conacher, M., Alexander, J., & Brewer, J. M. (2001). Oral immunisation with peptide and protein antigens by formulation in lipid vesicles incorporating bile salts (bilosomes). *Vaccine*, *19*(20–22), 2965–2974.

Conen, D., Buerkle, G., Perruchoud, A., Buettner, H., & Mueller, C. (2006). Hypertension is an independent risk factor for contrast nephropathy after percutaneous coronary intervention. *Int J Cardiol*, *110*, 237–241.

Cormack, A. M. (1979). Nobel Lecture: Early two-dimensional reconstruction and recent topics stemming from it. *Med Phys*, *209*(4464), 1482–1486.

Danila, D., Partha, R., Elrod, D. B., Lackey, M., Casscells, S. W., & Conyers, J. L. (2009). Antibody-Labeled Liposomes for CT Imaging of Atherosclerotic Plaques. *Tex Heart Inst J*, *36*(5), 393–403.

Davidson, E. M., Barenholz, Y., Cohen, R., Haroutiunian, S., Kagan, L., & Ginosar, Y. (2010). High-dose bupivacaine remotely loaded into multivesicular liposomes demonstrates slow drug release without systemic toxic plasma concentrations after subcutaneous administration in humans. *Anesth Analg*, *110*, 1018–1023.

Dawson, P. (1991). Factors dictating iodinated contrast agent toxicity. *In: Katayama, M, Brasch R C Eds. New Dimensions in Contrast Media*, *Amsterdam:*, 66–71.

Dawson, P., & Clauss, W. (Eds). (1998). Advances in X-ray contrast: collected papers. In *Kluwer Academic Publishers*.

De Baere, S., Smets, P., Finch, N., Heiene, R., De Backer, P., Daminet, S., & Croubels, S. (2012). Quantitative determination of exo- and endo-iohexol in canine and feline samples using high performance liquid chromatography with ultraviolet detection. *J Pharm Biomed Anal*, *61*, 50–56.

Derjaguin, B., & Landau, L. (1993). Theory of the stability of strongly charged lyophobic sols and of the adhesion of strongly charged particles in solutions of electrolytes. *Prog Surf Sci*, *43*, 30–59.

Dimov, K., Kastner, E., Hussain, M., Perrie, Y., & Szita, N. (2017). Formation and purification of tailored liposomes for drug delivery using a module-based micro continuous-flow system. *Sci Rep*, *7*, 12045.

Ding, Y., Zhang, X., Xu, Y., Cheng, T., Ou, H., Li, Z., An, Y., Shen, W., Liu, Y., & Shi, L. (2018). Polymerization-induced self-assembly of large-scale iohexol nanoparticles as contrast agents for X-ray computed tomography imaging. *Polymer Chemistry*, *9*(21), 2926–2935.

Duarte, M., Giordani, R. B., De Carli, G. A., Zuanazzi, J. A., Macedo, A. J., & Tasca, T. (2009). A quantitative resazurin assay to determinate the viability of Trichomonas vaginalis and the cytotoxicity of organic solvents and surfactant agents. *Exp Parasitol*, *123*, 195–198.

Ducker, G. S., Chen, L., Morscher, R. J., Ghergurovich, J. M., Esposito, M., Teng, X., Kang, Y., & Rabinowitz, J. D. (2016). Reversal of Cytosolic One-Carbon Flux Compensates for Loss of the Mitochondrial Folate Pathway. *Cell Metabolism*, *24*(4), 640–641.

Dulińska, I., Targosz, M., Strojny, W., Lekka, M., Czuba, P., Balwierz, W., & Szymoński, M. (2006). Stiffness of normal and pathological erythrocytes studied by means of atomic force microscopy. *Journal of Biochemical and Biophysical Methods*, *66*(1–3), 1–11.

Durante, W., Sen, A., & Sunahara, F. (1988). Impairment of endothelium-dependent relaxation in aortae from spontaneously diabetic rats. *Br. J. Pharmacol*, *94*, 463–468.

EMEA. (2006). ICH Topic Q2 (R1) Validation of analytical procedures: Text and methodology. *ICH Harmonised Tripartite Guideline*, 1–15.

Enomoto, M., Pan, J., Shifrin, Y., & Belik, J. (2014). Age dependency of vasopressin pulmonary vasodilatory effect in rats. *Pediatr Res*, *75*, 315–321.

Erdogan, S., Ozer, A. Y., & Ektzoglu, M. (2006). Gamma irradiation of liposomal phospholipids. *FABAD J Pharm Sci*, *31*, 182–190.

Farthing, D., Sica, D. A., Fakhry, I., Larus, T., Ghosh, S., Farthing, C., Vranian, M., & Gehr, T. (2005). Simple HPLC-UV method for determination of iohexol, iothalamate, p-aminohippuric acid and n-acetyl-p-aminohippuric acid in human plasma and urine with ERPF, GFR and ERPF/GFR ratio determination using colorimetric analysis. *Journal of Chromatography B: Analytical Technologies in the Biomedical and Life Sciences*, *826*(1–2), 267–272.

FDA. (2015). Analytical Procedures and Methods Validation for Drugs and Biologics. *Guidance for Industry*, 1–15.

Felgner, P. L., Gadek, T. R., Holm, M., Roman, R., Chan, H. W., Wenz, M., Northrop, J. P., Ringold, G. M., & Danielsen, M. (1987). Lipofection: a highly efficient, lipid-mediated DNA-transfection procedure. *Proc Natl Acad Sci USA*, *84*, 7413–7417.

Firkins, J. L., & Eastridge, M. L. (1994). Assessment of the effects of iodine value on fatty acid digestibility, feed intake, and milk production. *J Dairy Sci.*, *77*, 2357–2366.

Food and Drug Administration. (2015). LLiposome Drug Products Chemistry, Manufacturing, and Controls; Human Pharmacokinetics and Bioavailability; and Labeling Documentation Guidance for Industry. *Pharmaceutical Quality*, *Revision 1*(October), 1–13.

Food and Drug Administration. (2018). Liposome Drug Products Chemistry, Manufacturing, and Controls; Human Pharmacokinetics and Bioavailability; and Labeling Documentation

Guidance for Industry. *Pharmaceutical Quality*, (April), 1–15.

Forssen, E. A., & Ross, M. E. (1994). DaunoXome® Treatment of Solid Tumours: Preclinical and Clinical Investigations. *J Liposome Res*, *4*, 481–512.

Foster, S. J., & Sovak, M. (1988). Isomerism in Iohexol and Ioxilan. *Invest Radiol*, *Suppl 1*, S106–S109.

Franzé, S., Selmin, F., Samaritani, E., Minghetti, P., & Cilurzo, F. (2018). Lyophilization of Liposomal Formulations: Still Necessary, Still Challenging. *Pharmaceutics*, *10*, pii: E139. doi: 10.3390/pharmaceutics10030139.

Frisch, S., Vuori, K., Ruoslahti, E., & Chan-Hui, P. (1996). Control of adhesion-dependent cell survival by focal adhesion kinase. *J Cell Biol*, *134*, 793–799.

Furchgott, R., & Zawadzki, J. (1980). The obligatory role of endothelial cells in the relaxation of arterial smooth muscle by acetylcholine. *Nature*, *288*, 373–376.

Gabizon, A., Catane, R., Uziely, B., Kaufman, B., Safra, T., Cohen, R., Martin, F., Huang, A., & Barenholz, Y. (1994). Prolonged circulation time and enhanced accumulation in malignant exudates of doxorubicin encapsulated in polyethylene-glycol coated liposomes. *Cancer Res1*, *54*, 987–992.

Gabizon, A., & Martin, F. (1997). Polyethylene glycol-coated (pegylated) liposomal doxorubicin. Rationale for use in solid tumours. *Drugs*, *54*, 15–21.

Gawrys, O., Polkowska, M., Roszkowska-Chojecka, M., Gawarecka, K., Chojnacki, T., Swiezewska, E., Masnyk, M., Chmielewski, M., Rafa Owska, J., & Kompanowska-Jezierska, E. B. (2014). Effects of liposomes with polyisoprenoids, potential drug carriers, on the cardiovascular and excretory system in rats. *Pharmacological Reports : PR*, *66*(2), 273–278.

Geenen, R. W. F., Kingma, H. J., & van der Molen, A. J. (2013). Contrast-induced nephropathy: pharmacology, pathophysiology and prevention. *Insights into Imaging*.

Geraghty, R., Capes-Davis, A., Davis, J., Downward, J., Freshney, R., Knezevic, I., Lovell-Badge, R., Masters, J., Meredith, J., Stacey, G., Thraves, P., Vias, M., & UK, C. R. (2014). Guidelines for the use of cell lines in biomedical research. *Br J Cancer*, *111*, 1021–1046.

Giannakis, S., Jovic, M., Gasilova, N., Pastor Gelabert, M., Schindelholz, S., Furbringer, J. M., Girault, H., & Pulgarin, C. (2017). Iohexol degradation in wastewater and urine by UV-based Advanced Oxidation Processes (AOPs): Process modeling and by-products identification. *J Environ Manage*, *195*, 174–185.

205

Glück, R., Mischler, R., Finkel, B., Que, J. U., Scarpa, B., & Cryz, S. J. J. (1994). Immunogenicity of new virosome influenza vaccine in elderly people. *Lancet.*, *16*, 160–163.

Goldbach, P., Brochart, H., Wehrlé, P., & Stamm, A. (1995). Sterile filtration of liposomes: Retention of encapsulated carboxyfluorescein. *International Journal of Pharmaceutics*, *117*, 225–230.

Gong, X., Celsi, G., Carlsson, K., Norgen, S., & Chen, M. (2010). N-acetylcysteine amide protects renal proximal tubular epithelial cells against iohexol-induced apoptosis by blocking p38 MAPK and iNOS signaling. *Am J Nephrol*, *31*, 178–188.

Gong, X., Celsi, G., Carlsson, K., Norgren, S., & Chen, M. (2009). N-acetylcysteine amide protects renal proximal tubular epithelial cells against iohexol-induced apoptosis by blocking p38 MAPK and iNOS signaling. *Am J Nephrol*, *31*, 178–788.

Gonzalez, R. J., & Tarloff, J. B. (2001). Evaluation of hepatic subcellular fractions for Alamar blue and MTT reductase activity. *Toxicology in Vitro*, *15*(3), 257–259.

Grainger, R. G. (1980). Osmolality of intravascular radiological contrast media. *Br J Radiol.*, *53*, 739–746.

Gregoriadis, G. (1973). Drug entrapment in liposomes. *FEBS Letters*, *36*(3), 292–296.

Gregoriadis, G., & Perrie, Y. (2010). Liposomes. *In: Encyclopedia of Life Sciences. John Wiley & Sons, Ltd*, 1–8.

Gregoriadis, G., & Ryman, B. E. (1971). Liposomes as carriers of enzymes or drugs: a new approach to the treatment of storage diseases. *Biochem J.*, *124*(5), 58P.

Grimm, M., Mahnecke, N., Soja, F., El-Armouche, A., Haas, P., Treede, H., Reichenspurner, H., & Eschenhagen, T. (2006). The MLCK-mediated α1-adrenergic inotropic effect in atrial myocardium is negatively modulated by PKCε signaling. *Br J Pharmacol*, *148*, 991–1000.

Grit, M., Underberg, W., & Crommelin, D. (1993). Hydrolysis of saturated soybean phosphatidylcholine in aqueous liposome dispersions. *J Pharm Sci*, *82*, 362–366.

Grit, M., Zuidam, N. J., Underberg, W. J. M., & Crommelin, D. J. A. (1993). Hydrolysis of Partially Saturated Egg Phosphatidylcholine in Aqueous Liposome Dispersions and the Effect of Cholesterol Incorporation on Hydrolysis Kinetics. *Journal of Pharmacy and Pharmacology*, *45*(6), 490–495.

Gryparis, E. C., Mattheolabakis, G., Bikiaris, D., & Avgoustakis, K. (2007). Effect of

Conditions of Preparation on the Size and Encapsulation Properties of PLGA-mPEG Nanoparticles of Cisplatin. *Drug Deliv.*, *14*, 371–380.

Gussenhoven, M., Ravensbergen, J., van Bockel, J., Feuth, J., & Aarts, J. (1991). Renal dysfunction after angiography; a risk factor analysis in patients with peripheral vascular disease. *J Cardiovasc Surg*, *32*, 81–86.

Gutierro, I., Hernández, R. M., Igartua, M., Gascón, a. R., & Pedraz, J. L. (2002). Size dependent immune response after subcutaneous, oral and intranasal administration of BSA loaded nanospheres. *Vaccine*, *21*(1–2), 67–77.

Hamid, R., Rotshteyn, Y., Rabadi, L., Parikh, R., & Bullock, P. (2004). Comparison of alamar blue and MTT assays for high through-put screening. *Toxicology in Vitro*, *18*(5), 703–710.

Han, W., Zhu, D., Wu, L., Chen, Q., Guo, S., & Gao, P. (2009). N-acetylcysteine-induced vasodilation involves voltage-gated potassium channels in rat aorta. *Life Sci*, *84*, 732–737.

Handjani-Vila, R., Ribier, A., Rondot, B., & Vanlerberghie, G. (1979). Dispersions of lamellar phases of non-ionic lipids in cosmetic products. *Int J Cosmet Sci*, *1*, 303–314.

Harashima, H., Sakata, K., Funato, K., & Kiwada, H. (1994). Enhanced hepatic uptake of liposomes through complement activation depending on the size of liposomes. *Pharm Res*, *11*, 402–406.

Haschek, E., & Lindenthal, O. T. (1896). A contribution to the practical use of the photography according to Röntgen. *Wien Klin Wochenschr*, *9*, 63.

Hayakawa, K., Okuno, Y., Fujiwara, K., & Shimizu, Y. (1994). Effect of iodinated contrast media on ionic calcium. *Acta Radiol*, *35*, 83–87.

Heeremans, J., Gerritsen, H., Meusen, S., Mijnheer, F., Gangaram Panday, R., Prevost, R., Kluft, C., & Crommelin, D. (1995). The Preparation of Tissue-Type Plasminogen Activator (t-PA) Containing Liposomes: Entrapment Efficiency and Ultracentrifugation Damage. *J Drug Target*, *3*, 301–310.

Hellsten, Y., Nyberg, M., Jensen, L. G., & Mortensen, S. P. (2012a). Vasodilator interactions in skeletal muscle blood flow regulation. *The Journal of Physiology*, *590*(24), 6297–6305.

Hellsten, Y., Nyberg, M., Jensen, L., & Mortensen, S. (2012b). Vasodilator interactions in skeletal muscle blood flow regulation. *J Physiol*, *590*, 6297–6305.

Heyman, S. N., Rosenberger, C., Rosen, S., & Khamaisi, M. (2013). Why is diabetes mellitus

a risk factor for contrast-induced nephropathy? *BioMed Research International*, *2013*.

Hidalgo, J. F., & Zamora, R. (2005). Interplay between the maillard reaction and lipid peroxidation in biochemical systems. *Ann N Y Acad Sci*, *1043*, 319–326.

Hofmann, F., Dostmann, W., Keilbach, A., Landgraf, W., & Ruth, P. (1992). Structure and physiological role of cGMP-dependent protein kinase. *Biochim Biophys Acta*, *30*, 51–60.

Hong, K., Drummond, D. C., & Kirpotin, D. (2016). *Liposomes Useful for Drug Delivery. U.S. Patent No. US20160030341 A1*.

Hou, S., Bushinsky, D., Wish, J., Cohen, J., & Harrington, J. (1983). Hospital-acquired renal insufficiency: A prospective study. *Am J Med*, *74*, 243–248.

Hounsfield, G. N. (1973). *Computerized Tansverse Axial Scanning (Tomography): Part I. Description of System* (pp. 1016–1022). pp. 1016–1022.

Hu, C., & Rhodes, D. (1999). Proniosomes: a novel drug carrier preparation. *Int J Pharm*, *185*, 23–35.

Huang, H., Dunne, M., Lo, J., Jaffray, D. A., & Allen, C. (2012). Comparison of Computed Tomography – and Optical Image – Based Assessment of Liposome Distribution. *Mol Imaging*, *0*(0), 1–13.

Huang, X., Caddell, R., Yu, B., Xu, S., Theobald, B., Lee, L. J., & Lee, R. J. (2010). Ultrasound-enhanced Microfluidic Synthesis of Liposomes. *Anticancer Res.*, *30*, 463–466.

Hutcheson, I. R., Griffith, T. M., Pitman, M. R., Towart, R., Gregersen, M., Refsum, H., & Karlsson, J. O. (1999). Iodinated radiographic contrast media inhibit shear stress- and agonist-evoked release of NO by the endothelium. *British Journal of Pharmacology*, *128*(2), 451–457.

ICH Harmonised Tripartite Guideline. (2005). Validation of Analytical Procedures: Text and Methodology Q2 (R1). *International Conference on Harmonization*, 1–13.

Ingle, J. J., & Crouch, S. (1988). Spectrochemical Analysis. *New Jersey (Prentice Hall)*.

Israelachvili, J. (2011). Intermolecular & surface forces 3rd edition. *Academic Press, Elsevier*.

Jacobi, U., Waibler, E., Schulze, P., Sehouli, J., Oskay-Özcelik, G., Schmook, T., Sterry, W., & Lademann, J. (2005). Release of doxorubicin in sweat: first step to induce the palmar-plantar erythrodysesthesia syndrome? *Annals of Oncol*, *16*, 1210–1211.

Jemnitz, K., Veres, Z., Monostory, K., Kóbori, L., & Vereczkey, L. (2008). Interspecies differences in acetaminophen sensitivity of human, rat, and mouse primary hepatocytes. *Toxicology in Vitro*, *22*(4), 961–967.

Jensen, H., Doughty, R. W., Grant, D., & Myhre, O. (2011). The effects of the iodinated X-ray contrast media iodixanol, iohexol, iopromide, and ioversol on the rat kidney epithelial cell line NRK 52-E. *Renal Failure*, *33*(4), 426–433.

Jost, G., Pietsch, H., Lengsfeld, P., Hütter, J., & Sieber, M. A. (2010). The impact of the viscosity and osmolality of iodine contrast agents on renal elimination. *Invest Radiol*, *45*, 255–261.

Jousma, H., Talsma, H., Spies, F., Joosten, J., Junginger, H., & Crommelin, D. (1987). Characterization of liposomes. The influence of extrusion of multilamellar vesicles through polycarbonate membranes on particle size, particle size distribution and number of bilayers. *Int J Pharm*, *35*, 263–274.

Júnior, A. D., Mota, L. G., Nunan, E. A., Wainstein, A. J., Wainstein, A. P., Leal, A. S., Cardoso, V. N., & De Oliveira, M. C. (2007). Tissue distribution evaluation of stealth pH-sensitive liposomal cisplatin versus free cisplatin in Ehrlich tumor-bearing mice. *Life Sci.*, *80*, 659–664.

Junyaprasert, V. B., Teeranachaideekul, V., & Supaperm, T. (2008). Effect of Charged and Non-ionic Membrane Additives on Physicochemical Properties and Stability of Niosomes. *AAPS PharmSciTech*, *9*(3), 851–859.

Kalra, M. K., Maher, M. M., D'Souza, R., & Saini, S. (2004). Multidetector Computed Tomography Technology. Current Status and Emerging Developments. *J Comput Assist Tomogr*, *28*, S2-6.

Kanny, G., Pichler, W., Morisset, M., Franck, P., Marie, B., Kohler, C., Renaudin, J. M., Beaudouin, E., Laudy, J. S., & Moneret-Vautrin, D. A. (2005). T cell-mediated reactions to iodinated contrast media: evaluation by skin and lymphocyte activation tests. *J Allergy Clin Immunol*, *115*, 179–185.

Kanter, P. M., Bullard, G. A., Pilkiewicz, F. G., Mayer, L. D., Cullis, P. R., & Pavelic, Z. P. (1993). Preclinical toxicology study of liposome encapsulated doxorubicin (TLC D-99): comparison with doxorubicin and empty liposomes in mice and dogs. *In Vivo.*, *7*, 85–95.

Kanzaki, T., & Sakagami, H. (1991). Late Phase Allergic Reaction to a CT Contrast Medium (Iotrolan). *J Dermatol*, *18*, 528–531.

Kao, C., Hoffman, E., Beck, K., & Bellamkonda, RV Annapragada, A. (2003). Long-residence-time nano-scale liposomal iohexol for X-ray-based blood pool imaging. *Acad*

Radiol, *10*, 475–483.

Karathanasis, E., Chan, L., Balusu, S. R., D'Orsi, C. J., Annapragada, A. V, Sechopoulos, I., & Bellamkonda, R. V. (2008). Multifunctional nanocarriers for mammographic quantification of tumor dosing and prognosis of breast cancer therapy. *Biomaterials*, *29*(36), 4815–4822.

Karathanasis, E., Chan, L., Karumbaiah, L., McNeeley, K., D'Orsi, C. J., Annapragada, A. V, Sechopoulos, I., & Bellamkonda, R. V. (2009). Tumor vascular permeability to a nanoprobe correlates to tumor-specific expression levels of angiogenic markers. *PloS One*, *4*(6), e5843.

Karathanasis, E., Suryanarayanan, S., Balusu, Sri, R., McNeeley, K., Sechopoulos, I., Karellas, A., Annapragada, A. V., & Bellamkonda, R. V. (2009). Imaging Nanoprobe for Prediction of Outcome of Nanoparticle Chemotherapy using Mammography. *Radiology*, *250*(2), 398–406.

Karstoft, J., Bååth, L., Jansen, I., & Edvinsson, L. (1995). Vasoconstriction of isolated arteries induced by angiographic contrast media. A comparison of ionic and non-ionic contrast media iso-osmolar with plasma. *Acta Radiol*, *36*, 312–316.

Katayama, H., Yamaguchi, K., Kozuka, T., Takashima, T., Seez, P., & Matsuura, K. (1990). Adverse reactions to ionic and nonionic contrast media. A report from the Japanese Committee on the Safety of Contrast Media. *Radiol*, *175*, 621–628.

Katzberg, R. (1997). Urography into the 21st century: new contrast media, renal handling, imaging characteristics, and nephrotoxicity. *Radiol*, *204*, 297–312.

Katzberg, R. W., & Haller, C. (2006). Contrast-induced nephrotoxicity: Clinical landscape. *Kidney Int*, *69*, S3-7.

Kaur, G., & Dufour, J. M. (2012). Cell lines: Valuable tools or useless artifacts. *Spermatogenesis*, *2*(1), 1–5.

Killen, D. a, Foster, J. H., & Scott, H. W. (1962). Toxic reactions incident to urokon aortography as related to the volume of contrast medium injected. *Annals of Surgery*, *155*, 472–476.

Kim, I. Y., Lee, S. B., Lee, D. W., Song, S. H., Seong, E. Y., & Kwak, I. S. (2012). Long-term effect of radiocontrast-enhanced computed tomography on the renal function of chronic kidney disease patients. *Clinical and Experimental Nephrology*, *16*(5), 755–759.

Kim, S., Chatelut, E., Kim, J. C., Howell, S. B., Cates, C., Kormanik, P. A., & Chamberlain, M. C. (1993). Extended CSF cytarabine exposure following intrathecal administration of DTC 101. *J Clin Oncol.*, *11*, 2186–2193.

Kirby, C., Clarke, J., & Gregoriadis, G. (1980). Effect of the cholesterol content of small unilamellar liposomes on their stability in vivo and in vitro. *The Biochemical Journal*, *186*(2), 591–598.

Klonoff, D. C. (2009). The increasing incidence of diabetes in the 21st century. *J Diabetes Sci Technol.*, *3*, 1–2.

Ko, G., Bae, S., Hong, Y., Pyo, H., & Kwon, Y. (2016). Radiocontrast-induced nephropathy is attenuated by autophagy through regulation of apoptosis and inflammation. *Hum Exp Toxicol*, *35*, 724–736.

Kolbe, A. B., Hartman, R. P., Hoskin, T. L., Carter, R. E., Maddox, D. E., Hunt, C. H., & Hesley, G. K. (2014). Premedication of patients for prior urticarial reaction to iodinated contrast medium. *Abdom Imaging*, *39*, 432–437.

Konings, A. W. T. (1984). Lipid peroxidation in liposomes. *In: Gregoriadis, G. (Ed.) Liposome Technology*, *1*(Boca Raton, CRC Press Inc), 139–161.

Koppele, J. . Te, & Thurman, R. . (1990). Phagocytosis of Kupffer cells predominates in pericentral regions of the liver lobule. *Am J Physiol*, *22*, G814–G821.

Krause, M. R., & Regen, S. L. (2014). The Structural Role of Cholesterol in Cell Membranes: From Condensed Bilayers to Lipid Rafts. *Acc. Chem. Res.*, *47*, 3512–3521.

Kshirsagar, A., Poole, C., Mottl, A., Shoham, D., Franceschini, N., Tudor, G., Agrawal, M., Denu-Ciocca, C., Magnus Ohman, E., & Finn, W. (2004). N-acetylcysteine for the prevention of radiocontrast induced nephropathy: a meta-analysis of prospective controlled trials. *J Am Soc Nephrol*, *15*, 761–769.

Kwok, C. S., Pang, C. L., Yeong, J. K., & Loke, Y. K. (2013). Measures used to treat contrast-induced nephropathy: Overview of reviews. *Brit J Radiol*, *86*(1021).

Ladbrooke, B. D., Williams, R. M., & Chapman, D. (1968). Studies on lecithin-cholesterol-water interactions by differential scanning calorimetry and X-ray diffraction. *Biochim Biophys Acta.*, *150*, 333–340.

Lai, D. Y. (2015). Approach to using mechanism-based structure activity relationship (SAR) analysis to assess human health hazard potential of nanomaterials. *Food and Chemical Toxicology*, 1–7.

Lancelot, E., Idée, J. M., Laclédère, C., Santus, R., & Corot, C. (2002). Effects of two dimeric iodinated contrast media on renal medullary blood perfusion and oxygenation in dogs. *Invest Radiol*, *37*, 368–375.

Lenhard, D. C., Pietsch, H., Sieber, M. A., Ernst, R., Lengsfeld, P., Ellinghaus, P., & Jost, G. (2012). The osmolality of nonionic, iodinated contrast agents as an important factor for renal safety. *Invest Radiol*, *47*, 503–510.

Lewington, A., MacTier, R., Sutton, A., Smith, D., & Downes, M. (2013). Prevention of Contrast Induced Acute Kidney Injury (CI-AKI) in adult patients on behalf of The Renal Association, British Cardiovascular Intervention Society and Royal College of Radiologists. *[Last Accessed 2019 May 06]*, http://www.renal.org/ docs/default-source/guidelin.

Liu, D., Liu, F., & Song, Y. (1995). Recognition and clearance of liposomes containing phosphatidylserine are mediated by serum opsonin. *Biochim Biophys Acta*, *1235*, 140–146.

Liu, F., & Liu, D. (1996). Serum independent liposome uptake by mouse liver. *Biochim Biophys Acta - Biomembranes*, *1278*, 5–11.

Liyanarachchi, K., & Debono, M. (2017). Physiology of the pituitary, thyroid, parathyroid and adrenal glands. *Surgery*, *35*, 542–555.

Loftsson, T. (2014). Degradation Pathways. *Drug Stability for Pharmaceutical Scientists*, 63–104.

Lunn, J. A., & Rozengurt, E. (2004). Hyperosmotic stress induces rapid focal adhesion kinase phosphorylation at tyrosines 397 and 577: Role of Src family kinases and Rho family GTPases. *J Biol Chem*, *279*(43), 45266–45278.

MacAskill, M. G. (2014). Inflammatory and proliferative characteristics of late arteriovenous fistula stenosis: therapeutic potential of diclofenac. *[Thesis] The University of Strathclyde*.

Madonna, R., Giovannelli, G., Confalone, P., Renna, F., Geng, Y.-J., & De Caterina, R. (2016). High glucose-induced hyperosmolarity contributes to COX-2 expression and angiogenesis: implications for diabetic retinopathy. *Cardiovasc Diabetol*, *15*, DOI 10.1186/s12933-016-0342-4.

Maede, H. (2012). Vascular permeability in cancer and infection as related to macromolecular drug delivery, with emphasis on the EPR effect for tumor-selective drug targeting. *Proc Jpn Acad Ser B Phys Biol Sci*, *88*, 53–71.

Maherani, B., Arab-tehrany, E., Kheirolomoom, A., Reshetov, V., Jose Stebe, M., & Linder, M. (2012). Optimization and characterization of liposome formulation by mixture design. *Analyst*, *137*, 773–786.

Malek, A., Goss, G., Jiang, L., Izumo, S., & Alper, S. (1998). Mannitol at Clinical Concentrations Activates Multiple Signaling Pathways and Induces Apoptosis in Endothelial

Cells Editorial Comment. *Stroke*, *29*, 2631–2640.

Malvern. (n.d.). Nano Series Training Manual. *Chapter 1: Zeta Potential Theory*, 1–20.

Mandal, T. K., & Chatterjee, S. (1980). Ultraviolet- and Sunlight-induced Lipid Peroxidation in Liposomal Membrane. *Radiat Res*, *83*, 290–302.

Marasca, E., Greetham, D., Herring, S. D., & Fisk, I. D. (2016). Impact of nitrogen flushing and oil choice on the progression of lipid oxidation in unwashed fried sliced potato crisps. *Food Chem*, *199*, 81–86.

Mastouri, R., Sawada, S. G., & Mahenthiran, J. (2010). Current noninvasive imaging techniques for detection of coronary artery disease. *Expert Rev Cardiovasc Ther*, *8*, 77–91.

Matheny, S. A., & Moehlenbruck, J. (2010). Iohexol, an iodinated radiopaque contrast agent, demonstrates toxicity to rabbit and sheep nucleus pulposus (NP) cells in vitro. *Spine*, *21*, 2338–2345.

Matsumura, Y., & Maeda, H. (1986). A new concept for macromolecular therapeutics in cancer chemotherapy: mechanism of tumoritropic accumulation of proteins and the antitumor agent smancs. *Cancer Res*, *46*, 6387–6392.

Matumoto-Pintro, P., Murakami, A., Vital, A., Croge, C., da Silva, D., Ospina-RojaAna, I., & Guerra, A. (2017). Effects of storage time and temperature on lipid oxidation of egg powders enriched with natural antioxidants. *Food Chem*, *228*, 463–468.

McCaffery, T., Nicholson, A., Szabo, P., Weksler, M., & Weksler, B. (1988). AGING AND ARTERIOSCLEROSIS The increased proliferation of arterial smooth muscle cells isolated from old rats is associated with increased platelet-derived growth factor-like activity. *J Exp Med*, *167*, 163–174.

Mcdonald, R. J., Mcdonald, J. S., Bida, J. P., Carter, R. E., Fleming, C. J., Williamson, E. E., & Kallmes, D. F. (2013). Intravenous Contrast Material – induced Nephropathy: Causal or Coincident Phenomenon? *Radiol*, *267*(1), 106–118.

Mehran, R., & Nikolsky, E. (2006). Contrast-induced nephropathy: definition, epidemiology, and patients at risk. *Kidney International. Supplement*, (100), S11–S15.

Meth, M. J., & Maibach, H. I. (2006). Current Understanding of Contrast Media Reactions and Implications for Clinical Management. *Drug Saf*, *29*, 133–141.

Michel, F., Man, R., & Vanhoutte, P. (2007). Increased spontaneous tone in renal arteries of

spontaneously hypertensive rats. *Am J Physiol Heart Circ Physiol*, (293), H1673-1681.

Miller, C. R., Bondurant, B., McLean, S. D., McGovern, K. A., & O'Brien, D. F. (1998). Liposome−Cell Interactions in Vitro: Effect of Liposome Surface Charge on the Binding and Endocytosis of Conventional and Sterically Stabilized Liposomes. *Biochemistry*, *37*, 12875–12883.

Moncada, S., & Higgs, E. A. (2006). The discovery of nitric oxide and its role in vascular biology. *Br J.Pharmacol.*, *147 Suppl*(0007–1188 (Print) LA–eng PT–Journal Article SB–IM), S193–S201.

Monnard, P.-A., Oberholzer, T., & Luisi, P. L. (1997). Entrapment of nucleic acids in liposomes. *Biochimica et Biophysica Acta (BBA) - Biomembranes*, *1329*, 39–50.

Morcos, S., Thomsen, H., & Webb, J. (1999). Contrast-media-induced nephrotoxicity: a consensus report. Contrast Media Safety Committee, European Society of Urogenital Radiology (ESUR). *Eur Radiol*, *9*, 1602–1613.

Mrowietz, C., Franke, R. P., & Jung, F. (2012). Influence of different radiographic contrast media on the echinocyte formation of human erythrocytes. *Clin Hemorheol Microcirc*, *50*, 35–47.

Mukundan, S., Ghaghada, K. B., Badea, C. T., Kao, C.-Y., Hedlund, L. W., Provenzale, J. M., Johnson, G. A., Chen, E., Bellamkonda, R. V., & Annapragada, A. (2006). A liposomal nanoscale contrast agent for preclinical CT in mice. *AJR. American Journal of Roentgenology*, *186*(2), 300–307.

Mullen, A. B., Baillie, A. J., Carter, K. C., & Uchegbu (Ed.), I. F. (2000). Synthetic Surfactant Vesicles: Niosomes and Other Non-phospholipid Vesicular Systems. *Overseas Publishers Association*, 96–113.

Mullen, A. B., & Carter, K. C. (1997). Comparison of the efficacies of various formulations of amphotericin B against murine visceral leishmaniasis. *Antimicrob. Agents Chemother.*, *41*, 2089–2092.

Nash, K., Hafeez, A., & Hou, S. (2002). Hospital-acquired renal insufficiency. *Am J Kidney Dis*, *39*, 930–936.

Nasseri, B. (2005). Effect of cholesterol and temperature on the elastic properties of niosomal membranes. *Int J Pharm*, *26*, 95–101.

NICE. (2013). Acute kidney injury: Prevention, detection and management. *Clinical Guideline CG169*, https://www.nice.org.uk/guidance/cg169/.

NICE. (2014). Chronic kidney disease in adults: assessment and management. *Clinical Guideline CG182*, https://www.nice.org.uk/guidance/cg182.

Nikolsky, E., Mehran, R., Turcot, D., Aymong, E., Mintz, G., Lasic, Z., Lansky, A., Tsounias, E., Moses, J., Stone, G., Leon, M., & Dangas, G. (2004). Impact of chronic kidney disease on prognosis of patients with diabetes mellitus treated with percutaneous coronary intervention. *Am J Cardiol*, *94*, 300–305.

Nobelprize.org. (n.d.). The Nobel Prize in Physiology or Medicine 1979. *Nobel Prize Media AB 2014*, http://www.nobelprize.org/nobel_prizes/medicine/la.

Novelline, R. (1997). Squire's Fundamentals of Radiology. *Harvard University Press*, *5th editio*, 1.

Nyman, U., & Almén, T. (1980). Effects of contrast media on aortic endothelium. Experiments in the rat with non-ionic monomeric and monoacidic dimeric contrast media. *Acta Radiol Suppl.*, *362*, 65–71.

Nyman, U., Ekberg, O., & Aspelin, P. (2016). Torsten Almén (1931–2016): the father of non-ionic iodine contrast media. *Acta Radiol*, *57*, 1072–1078.

O'Brien, M. E., Wigler, N., Inbar, M., Rosso, R., Grischke, E., Santoro, A., … CAELYX Breast Cancer Study Group. (2004). Reduced cardiotoxicity and comparable efficacy in a phase III trial of pegylated liposomal doxorubicin HCl (CAELYX/Doxil) versus conventional doxorubicin for first-line treatment of metastatic breast cancer. *Ann Oncol*, *15*, 440–449.

O'Sullivan, B., Al-Bahrani, H., Lawrence, J., Campos, M., Cázares, A., Baganz, F., Wohlgemuth, R., Hailes, H., & Szita, N. (2012). Modular microfluidic reactor and inline filtration system for the biocatalytic synthesis of chiral metabolites. *J Mol Catal B: Enzym*, *77*, 1–8.

Obeid, M. A., Khadra, I., Mullen, A. B., Tate, R. J., & Ferro, V. A. (2016). The effects of hydration media on the characteristics of non-ionic surfactant vesicles (NISV) prepared by microfluidics. *International Journal of Pharmaceutics*.

Olsson, B., Aulie, A., Sveen, K., & Andrew, E. (1983). Human pharmacokinetics of iohexol. A new nonionic contrast medium. *Invest Radiol*, *18*, 177–182.

Oussoren, C., Zuidema, J., Crommelin, D. J. a, & Storm, G. (1997). Lymphatic uptake and biodistribution of liposomes after subcutaneous injection. II. Influence of liposomal size, lipid composition and lipid dose. *Biochimica et Biophysica Acta - Biomembranes*, *1328*(2), 261–272.

Palmer, R., Ashton, D., & Moncada, S. (1988). Vascular endothelial cells synthesize nitric oxide from L-arginine. *Nature*, *333*, 664–666.

Park, S., Cha, J., Nam, J., Kim, M., Park, S., Park, E., Lee, H., & Kim, H. (2014). Formulation optimization and in vivo proof-of-concept study of thermosensitive liposomes balanced by phospholipid, elastin-like polypeptide, and cholesterol. *PLoS ONE*, *9*, e103116.

Pasternaka, J., & Williamson, E. (2012). Clinical pharmacology, uses, and adverse reactions of iodinated contrast agents: A primer for the non-radiologist. *Mayo Clin Proc*, *87*, 390–402.

Patel, T. K., & Williamson, J. D. (2016). Mannitol in Plants, Fungi, and Plant-Fungal Interactions. *Trends Plant Sci*, *21*, 486–497.

Patil, Y. P., & Jadhav, S. (Eds). (2015). Preparation of liposomes for drug delivery applications by extrusion of giant unilamellar vesicles. *Nanoscale and Microscale Phenomena: Fundamentals and Applications*, 17–29.

Payne, N., Browning, I., & Hynes, C. (1986). Characterization of proliposomes. *J Pharm Sci*, *75*, 330–333.

Payne, N., Timmins, P., Ambrose, C., Ward, M., & Ridgway, F. (1986). Proliposomes: A Novel Solution to an Old Problem. *J Pharm Sci*, *185*, 23–35.

Peer, D., Karp, J., Hong, S., Farokhzad, O., Margalit, R., & Langer, R. (2007). Nanocarriers as an emerging platform for cancer therapy. *Nat Nanotechnol*, *2*, 751–760.

Pereira-lachataignerais, J., Pons, R., Panizza, P., & Courbin, L. (2006). *Study and formation of vesicle systems with low polydispersity index by ultrasound method*. *140*, 88–97.

Perrin, C., Vu, V., Matthijs, N., Maftouh, M., Massart, D., & Vander Heyden, Y. (2002). Screening approach for chiral separation of pharmaceuticals Part I. Normal-phase liquid chromatography. *J Chromatogr A*, *947*, 69–83.

Persson, P. B. (2005). Editorial: contrast medium-induced nephropathy. *Nephrol Dial Transplant*, *20 Suppl 1*, i1.

Petros, R. a, & DeSimone, J. M. (2010). Strategies in the design of nanoparticles for therapeutic applications. *Nature Reviews. Drug Discovery*, *9*(8), 615–627.

Pflueger, A., Osswald, H., & Knox, F. (1999). Adenosine-induced renal vasoconstriction in diabetes mellitus rats: role of nitric oxide. *Am J Physiol*, *276*, F340-346.

Prado, E. L., & Dewey, K. G. (2014). Nutrition and brain development in early life. *Nutr Rev*, *72*, 267–284.

Quintavalle, C., Brenca, M., De Micco, F., Fiore, D., Romano, S., Romano, M. F., Apone, F., Bianco, a, Zabatta, M. a, Troncone, G., Briguori, C., & Condorelli, G. (2011). In vivo and in vitro assessment of pathways involved in contrast media-induced renal cells apoptosis. *Cell Death & Disease*, *2*(5), e155.

Radiologists, R. C. of. (n.d.). Information submitted to Health Education workforce planning and education commissioning round - 2015/16. *Clin Radiol*, https://www.rcr.ac.uk/sites/default/files/document.

Rampersad, S. N. (2012). Multiple applications of alamar blue as an indicator of metabolic function and cellular health in cell viability bioassays. *Sensors*, *12*(9), 12347–12360.

Ratz, P. H., Berg, K. M., Urban, N. H., Miner, A. S., Paul, H., Berg, K. M., Urban, N. H., & Miner, A. S. (2005). Regulation of smooth muscle calcium sensitivity: KCl as a calcium-sensitizing stimulus. *Am J Physiol Cell Physiol*, (288), C769-783.

Ratz, P., & Miner, A. (2009). Role of protein kinase Cζ and calcium entry in KCl-induced vascular smooth muscle calcium sensitization and feedback control of cellular calcium levels. *J. Pharmacol. Exp. Ther*, *328*, 399–408.

Rauch, D., Dresche, P., Knes, J. M., & Madsen, P. O. (1997). Variable effects of iodinated contrast media on different rabbit arteries in vitro. *Urol Res*, *25*, S21-23.

Reynolds, E., & Dubyak, G. (1985). Activation of calcium mobilization and calcium influx by alpha 1-adrenergic receptors in a smooth muscle cell line. *Biochem Biophys Res Commun*, *130*, 627–632.

Riss, T. L., Moravec, R. A., Niles, A. L., & Minor, L. (2013). Cell Viability Assays. *Assay Guidance Manual [Internet]. Bethesda (MD): Eli Lilly & Company and the National Center for Advancing Translational Sciences*, Available from: http://www.ncbi.nlm.nih.gov/books/.

Romano, G., Briguori, C., Quintavalle, C., Zanca, C., Rivera, N. V, Colombo, A., & Condorelli, G. (2008). Contrast agents and renal cell apoptosis. *European Heart Journal*, *29*(20), 2569–2576.

Romberg, B., Oussoren, C., Snel, C. J., Hennink, W. E., & Storm, G. (2007). Effect of liposome characteristics and dose on the pharmacokinetics of liposomes coated with poly(amino acid)s. *Pharmaceutical Research*, *24*(12), 2394–2401.

Röntgen, W. (1895). Ueber eine neue Art von Strahlen. Vorläufige Mitteilung. *Aus Den*

Sitzungsberichten Der Würzburger Physik.-Medic. Gesellschaft Würzburg, 137–147.

Rowe, E., Rowe, V., Biswas, S., Mosher, G., Insisienmay, L., Ozias, S., Gralinski, M., Hunter, J., & Barnett, J. (2016). Preclinical studies of a kidney safe iodinated contrast agent. *J Neuroimaging*, *26*, 511–518.

Rudnick, M. R., Goldfarb, S., Wexler, L., Ludbrook, P. A., Murphy, M. J., Halpern, E. F., Hill, J. A., Winniford, M., Cohen, M. B., & VanFossen, D. B. (1995). Nephrotoxicity of ionic and nonionic contrast media in 1196 patients: A randomized trial. *Kidney Int*, *47*, 254–261.

Ruggiero, A., Villa, C., Bander, E., Rey, D., Bergkvist, M., Batt, C., Manova-Todorova, K., Deen, W., Scheinberg, D., & McDevitt, M. (2010). Paradoxical glomerular filtration of carbon nanotubes. *Proc Natl Acad Sci USA*, *107*, 12369–12374.

Ruysschaert, T., Marque, A., Duteyrat, J.-L., Lesieur, S., Winterhalter, M., & Fournier, D. (2005). Liposome retention in size exclusion chromatography. *BMC Biotechnol*, *5*, 11.

Saarinen-Savolainen, P., Jarvinen, T., Taipale, H., & Urtti, A. (1997). Method for evaluating drug release from liposomes in sink conditions. *Int J Pharm*, *159*, 27–33.

Sadat, U., Usman, A., Boyle, J., Hayes, P., & Solomonc, R. (2015). Contrast Medium-Induced Acute Kidney Injury. *Cardiorenal Med*, *5*, 219–228.

Safirstein, R., Andrade, L., & Vieira, J. (2000). Acetylcysteine and nephrotoxic effects of radiographic contrast agents--a new use for an old drug. *N Engl J Med*, *343*, 210–212.

Sakai, H., Tomiyama, K., Sou, K., Takeoka, S., & Tsuchida, E. (2000). Poly(ethylene glycol)-Conjugation and Deoxygenation Enable Long-Term Preservation of Hemoglobin-Vesicles as Oxygen Carriers in a Liquid State. *Bioconjugate Chem.*, *11*, 425–432.

Samei, E., Saunders, R. S., Badea, C. T., Ghaghada, K. B., Hedlund, L. W., Qi, Y., Yuan, H., Bentley, C. R., & Mukundan, S. (2009). Micro-CT imaging of breast tumors in rodents using a liposomal, nanoparticle contrast agent. *International Journal of Nanomedicine*, *4*, 277–282.

Sarin, H. (2010). Physiologic upper limits of pore size of different blood capillary types and another perspective on the dual pore theory of microvascular permeability. *J Angiogenes Res*, *2*, 14.

Sarker, S. D., Nahar, L., & Kumarasamy, Y. (2007). Microtitre plate-based antibacterial assay incorporating resazurin as an indicator of cell growth, and its application in the in vitro antibacterial screening of phytochemicals. *Methods*, *42*, 321–324.

Sawmiller, C. J., Powell, R. J., Quader, M., Dudrick, S. J., Sumpio, B. E., & Cronenwett, J. (1998). The differential effect of contrast agents on endothelial cell and smooth muscle cell growth in vitro. *Journal of Vascular Surgery*, *27*(6), 1128–1140.

Schneider, K. M., & Rand, M. J. (1988). Vasodilatation and vasoconstriction in the rabbit isolated aorta. Effects of ioxilan, iohexol, and diatrizoate. *Invest Radiol.*, *23*(S150-152).

Schwertner, H. A., & Weld, K. J. (2015). High-performance liquid-chromatographic analysis of plasma iohexol concentrations. *J Chromatogr Sci*, *53*, 1475–1480.

Secomb, T. W. (2016). Hemodynamics. *Compr Physiol*, *6*, 975–1003.

Seeliger, E., Flemming, B., Wronski, T., Ladwig, M., Arakelyan, K., Godes, M., Möckel, M., & Persson, P. B. (2007). Viscosity of contrast media perturbs renal hemodynamics. *J Am Soc Nephrol*, *18*, 2912–2920.

Sendeski, M., Patzak, A., & Persson, P. B. (2010). Constriction of the vasa recta, the vessels supplying the area at risk for acute kidney injury, by four different iodinated contrast media, evaluating ionic, nonionic, monomeric and dimeric agents. *Invest Radiol*, *45*, 453–457.

Senior, J. H. (1987). Fate and behavior of liposomes in vivo: a review of controlling factors. *Crit Rev Ther Drug Carrier Syst*, *3*, 123–193.

Sessa, G., & Weissmann, G. (1968). Phospholipid spherules (liposomes) as a model for biological membranes. *Journal of Lipid Research*, *9*(3), 310–318.

Shabir, G. (2004). A practical approach to validation of HPLC methods under current good manufacturing practices. *Journal of Validation Technology*, *10*, 210–218.

Shehata, T., Kimura, T., Higaki, K., & Ogawara, K. (2016). In-vivo disposition characteristics of PEG niosome and its interaction with serum proteins. *Int J Pharm*, *512*, 322–328.

Shen, C. F., & Kamen, A. (2012). Hyperosmotic pressure on HEK 293 cells during the growth phase , but not the production phase , improves adenovirus production. *J Biotech*, *157*(1), 228–236.

Siddik, Z. H., Jones, M., Boxall, F. E., & Harrap, K. R. (1988). Comparative distribution and excretion of carboplatin and cisplatin in mice. *Cancer Chemother Pharmacol*, *21*, 19–24.

Siddiqui, M., AlOthman, Z., & Rahman, N. (2017). Analytical techniques in pharmaceutical analysis: A review. *Arab J Chem*, *10*, S1 409-421.

Sobral, N. C., Soto, M. A., & Carmona-ribeiro, A. M. (2008). *Characterization of DODAB / DPPC vesicles*. *152*, 38–45.

Soenen, S., Brisson, A., & De Cuyper, M. (2009). Addressing the problem of cationic lipid-mediated toxicity: the magnetoliposome model. *Biomaterials*, *30*, 3691–3701.

Solanki, Himanshu K. Pawar, D. D., Shah, D. A., Prajapati, V. D., Jani, G. K., Mulla, A. M., & Thakar, P. M. (2013). Development of Microencapsulation Delivery System for Long-Term Preservation of Probiotics as Biotherapeutics Agent. *Biomed Res Int.*, *620719*.

Sosale, N., Spinler, K., Alvey, C., & Discher, D. (2015). Macrophage engulfment of a cell or nanoparticle is regulated by unavoidable opsonization, a species-specific "Marker of Self" CD47, and target physical properties. *Curr Opin Immunol*, *35*, 107–112.

Sovak, M., Ranganathan, R., & Speck, U. (1982). Nonionic Dimer: Development and Initial Testing of an Intrathecal Contrast Agent. *Radiology1*, *142*, 115–118.

Speck, U., Bohle, F., Krause, W., Martin, J. L., Miklautz, H., & Schuhmann-Giampieri, G. (1998). Delayed Hypersensitivity to X-Ray CM: Possible Mechanisms and Models. *Acad Radiol*, *5*, S162-165.

Stacul, F., van der Molen, A. J., Reimer, P., Webb, J. a W., Thomsen, H. S., Morcos, S. K., Almén, T., Aspelin, P., Bellin, M.-F., Clement, O., & Heinz-Peer, G. (2011). Contrast induced nephropathy: updated ESUR Contrast Media Safety Committee guidelines. *European Radiology*, *21*(12), 2527–2541.

Stjerndahl, M., & Holmberg, K. (2003). Synthesis and chemical hydrolysis of surface-active esters. *J Surfactants Detergs*, *6*, 311–318.

Stott, B., Vu, M., McLemore, C., Lund, M., Gibbons, E., Brueseke, T., Wilson-Ashworth, H., & Bell, J. (2008). Use of fluorescence to determine the effects of cholesterol on lipid behavior in sphingomyelin liposomes and erythrocyte membranes. *J Lipid Res*, *49*, 1202–1215.

Stride, E., & Saffari, N. (2003). Microbubble ultrasound contrast agents: a review. *Proceedings of the Institution of Mechanical Engineers. Part H, Journal of Engineering in Medicine*, *217*(6), 429–447.

Subramanian, S., Tumlin, J., Bapat, B., Zyczynski, T. (2007). Economic Burden of Contrast-Induced Nephropathy: Implications for Prevention Strategies. *J Med Econ*, *10*(2), 119–134.

Sułkowskia, W., Pentaka, D., Nowaka, K., & Sułkowskab, A. (2005). The influence of temperature, cholesterol content and pH on liposome stability. *J Mol Struct*, 737–747.

Sun, S., Tong, W., Guo, Z., Tuo, Q., Lei, X., Zhang, C., Liao, D., & Chen, J. (2017). Curcumin enhances vascular contractility via induction of myocardin in mouse smooth muscle cells. *Acta Pharmacol Sin*, *38*, 1329–1339.

Suntres, Z. (2011). Liposomal antioxidants for protection against oxidant-induced damage. *J Toxicol*, *Epub*, doi: 10.1155/2011/152474.

Svetina, S., & Zeks, B. (2002). Shape behavior of lipid vesicles as the basis of some cellular processes. *Anat Rec*, *268*, 215–225.

Swaminathan, V., Mythreye, K., O'Brien, E. T., Berchuck, A., Blobe, G. C., & Superfine, R. (2011). Mechanical Stiffness Grades Metastatic Potential in Patient Tumor Cells and in Cancer Cell Lines. *Cancer Res*, *71*(15), 5075–5080.

Syyong, H., Chung, A., Yang, H., & van Breemen, C. (2009). Dysfunction of endothelial and smooth muscle cells in small arteries of a mouse model of Marfan syndrome. *Br J Pharmacol*, *158*, 1597–1608.

Takatsuki, H., Furukawa, T., Liu, Y., Hirano, K., Yoshikoshi, A., & Sakanishi, A. (2004). Effect of contrast media on vascular smooth muscle cells. *Acta Radiologica (Stockholm, Sweden : 1987)*, *45*(6), 635–640.

Tan, G., Heqing, L., Jiangbo, C., Ming, J., Yanhong, M., Xianghe, L., Hong, S., & Li, G. (2002). Apoptosis induced by low-dose paclitaxel is associated with p53 upregulation in nasopharyngeal carcinoma cells. *Int J Cancer*, *97*, 168–172.

Taylor, K. M. G., & Elhissi, A. M. A. (2016). Preparation of Liposomes for Pulmonary Delivery using Medical Nebulizers. *Liposome Technology: Liposome Preparation and Related Tecniques Ed. G. Gregoriadis*, *CRC Press*, 67–83.

Taymouri, S., & Varshosaz, J. (2016). Effect of different types of surfactants on the physical properties and stability of carvedilol nano-niosomes. *Adv Biomed Res*, *5*, 48.

Tepel, M., van der Giet, M., Schwarzfeld, C., Laufer, U., Liermann, D., & Zidek, W. (2000). Prevention of radiographic-contrast-agent-induced reductions in renal function by acetylcysteine. *N Engl J Med*, *20*, 180–184.

Terzic, A., Pucéat, M., Clément, O., Scamps, F., & Vassort, G. (1992). Alpha 1-adrenergic effects on intracellular pH and calcium and on myofilaments in single rat cardiac cells. *J Physiol*, *447*, 275–292.

Thomas, G. (2011). Neural control of the circulation. *Adv Physiol Educ*, *35*, 28–32.

Thomsen, H. S., & Morcos, S. K. (2000). Radiographic contrast media. *BJU Int*, *86 Suppl 1*, 1–10.

Tiderius, C. J., Olsson, L. E., Leander, P., Ekberg, O., & Dahlberg, L. (2003). Delayed gadolinium-enhanced MRI of cartilage (dGEMRIC) in early knee osteoarthritis. *Magnetic Resonance in Medicine : Official Journal of the Society of Magnetic Resonance in Medicine / Society of Magnetic Resonance in Medicine*, *49*(3), 488–492.

Toh, R.-M., & Chiu, G. N. C. (2013). Liposomes as sterile preparations and limitations of sterilisation techniques in liposomal manufacturing. *Asian J Pharm Sci*, *8*, 88–95.

Tolentino, L. F., Tsaia, S. F., Witt, M. D., & French, S. W. (2004). Fatal fat embolism following amphotericin B lipid complex injection. *Experimental and Molecular Pathology*, *77*, 246–248.

Tonelli, M., & Riella, M. (2014). Chronic kidney disease and the aging population. *Indian J Nephrol*, *24*, 71–74.

Torchilin, V. P., & Weissig, V. (1990). Liposomes: A Practical Approach. *Ed. R.R.C. New; Oxford University Press; Oxford,*.

Törnqvist, E., Annas, A., Granath, B., Jalkesten, E., Cotgreave, I., & Öberg, M. (2014). Strategic focus on 3R principles reveals major reductions in the use of animals in pharmaceutical toxicity testing. *PLoS ONE*, *9*(7), 1–11.

Touyz, R., & Schiffrin, E. (1997). Angiotensin II regulates vascular smooth muscle cell pH, contraction, and growth via tyrosine kinase-dependent signaling pathways. *Hypertension*, *30*, 222–229.

Trcka, J., Schmidt, C., Seitz, C. S., Bröcker, E. B., Gross, G. E., & Trautmann, A. (2008). Anaphylaxis to iodinated contrast material: nonallergic hypersensitivity or IgE-mediated allergy? *Am J Roentgenol*, *190*, 666–670.

Trubiani, O., Salvolini, E., Staffolani, R., Di Primio, R., & Mazzanti, L. (2003). DMSO modifies structural and functional properties of RPMI-8402 cells by promoting programmed cell death. *Int J Immunopathol Pharmacol*, *16*, 253–259.

Uchegbu, I. (1998). The biodistribution of novel 200-nm palmitoyl muramic acid vesicles. *Int J Pharm*, *162*, 19–27.

Uchegbu, I. F., Double, J. A., Turton, J. A., & Florence, A. T. (1995). Distribution, metabolism and tumoricidal activity of doxorubicin administered in sorbitan monostearate (Span 60) niosomes in the mouse. *Pharm Res*, *12*, 1019–1024.

Uchegbu, I. F., & Vyas, S. P. (1998). Non-ionic surfactant based vesicles (niosomes) in drug delivery. *Int J Pharm*, *172*, 33–70.

USP. (n.d.). <1225> Validation of Compendial Procedures. *General Information*, 1–5.

Vaisman, B., Shikanov, A., & Domb, A. (2005). Normal phase high performance liquid chromatography for determination of paclitaxel incorporated in a lipophilic polymer matrix. *J Chromatogr A*, *1064*, 85–95.

Valenzuela, A., Sanhueza, J., & Nieto, S. (2003). No TitleCholesterol oxidation: health hazard and the role of antioxidants in prevention. *Biol Res.*, *36*, 291–302.

van Meer, G. (1989). Lipid traffic in animal cells. *Annu Rev Cell Biol*, *5*, 247–275.

Van Norman, G. A. (2016). Drugs, Devices, and the FDA: Part 1: An Overview of Approval Processes for Drugs. *JACC: Basic to Translational Science*, *1*(3), 170–179.

van Swaay, D., & deMello, A. (2013). Microfluidic methods for forming liposomes. *Lab on a Chip*, *13*(5), 752–767.

Vitor, M. T., Bergami-Sanots, P. C., Barbuto, A. M., & de la Torre, L. G. (2013). Cationic Liposomes as Non-Viral Vector for RNA Delivery in Cancer Immunotherapy. *Recent Pat Drug Deliv Formul*, *7*, 99–110.

Vladisavljević, G., Khalid, N., Neves, M., Kuroiwa, T., Nakajima, M., Uemura, K., Ichikawa, S., & Kobayashi, I. (2013). Industrial lab-on-a-chip: Design, applications and scale-up for drug discovery and delivery. *Adv Drug Deliv Rev*, *65*, 1626–16263.

Von Hoff, D. D., Layard, M. W., Basa, P., Davis, H. L. J., Von Hoff, A. L., Rozencweig, M., & Muggia, F. M. (1979). Risk factors for doxorubicin-induced congestive heart failure. *Ann Intern Med*, *91*, 710–717.

Vora, B., Khopade, A. J., & Jain, N. K. (1998). Proniosome based transdermal delivery of levonorgestrel for effective contraception. *J Controlled Release*, *54*, 14–165.

Wallace, S. J., Li, J., Nation, R. L., & Boyd, B. J. (2013). Drug release from nanomedicines: Selection of appropriate encapsulation and release methodology. *Drug Deliv Transl Res*, *2*, 284–292.

Wallingford, V. H. (1953). The Development of Organic Iodine Compounds as X-Ray Contrast Media. *Journal of the American Pharmaceutical Association*, *42*, 721–728.

Walsh, C., Ou, K., Belliveau, M, N., Leaver, J, T., Wild, W. A., Huft, J., Lin, P. J., Chen, S., Leung, A. K., Lee, J. B., Hansen, C. L., Taylor, R. J., Ramsay, E. C., & Cullis, P. . (2004). Microfluidic-based manufacture of siRNA-lipid NPs for therapeutic applications. *Methods Mol Biol*, *1141*, 109–120.

Wang, Y., Chan, P., & Morcos, S. (1998). The effect of radiographic contrast media on human vascular smooth muscle cells. *Br J Radiol*, *71*, 376–380.

Wartiovaara, J., Ofverstedt, L., Khoshnoodi, J., Zhang, J., Mäkelä, E., Sandin, S., Ruotsalainen, V., Cheng, R., Jalanko, H., Skoglund, U., & Tryggvason, K. (2004). Nephrin strands contribute to a porous slit diaphragm scaffold as revealed by electron tomography. *J Clin Invest*, *114*, 1475–1483.

Wei, X., Geng, F., He, D., Qiu, J., & Xu, Y. (2005). Liposomal Contrast Agent for CT Imaging of the Liver. *Conf Proc IEEE Eng Med Biol Soc*, *6*, 5702–5705.

Weisbord, S. D., & Palevsky, P. M. (2008). Prevention of contrast-induced nephropathy with volume expansion. *Clin J Am Soc Nephrol*, *3*, 273–280.

Whillier, S., Raftos, J., Chapman, B., & Kuchel, P. (2009). Role of N-acetylcysteine and cystine in glutathione synthesis in human erythrocytes. *Redox Rep*, *14*, 115–124.

Widmark, J. M. (2007). Imaging-related medications: a class overview. *Proceedings (Baylor University. Medical Center)*, *20*(4), 408–417.

Witten, D. M., Hirsch, F. D., & Hartman, G. (1973). Acute reactions to urographic contrast medium: incidence, clinical characteristics and relationship to history of hypersensitivity states. *Am J Roentgenol Radium Ther Nucl Med*, *119*, 832–840.

Worzella, T., Niles, A., Hengstl, T., Fejtl, M., Oberdanner, C., & Merlino, J. (n.d.). Real-time cytotoxicity analysis using CellTox™ green cytotoxicity assay and the Tecan Infinite® 200 PRO with gas control module. *(Last Accessed 26 July 2018)*, https://www.promega.co.uk/resources/pubhub/real-ti.

Wright, D. B., Tripathi, S., Sikarwar, A., Santosh, K. T., Perez-Zoghbi, J., Ojo, O. O., Irechukwu, N., Ward, J. P. T., & Schaafsma, D. (2013). *Regulation of GPCR-mediated SMC contraction - implications for asthma and pulmonary hypertension* (pp. 121–131). pp. 121–131.

Xu, S., Fu, J., Chen, J., Xiao, P., Lan, T., Le, K., Cheng, F., He, L., Shen, X., Huang, H., & Liu, P. (2009). Development of an optimized protocol for primary culture of smooth muscle cells from rat thoracic aortas. *Cytotechnology*, *61*(1–2), 65–72.

Xu, X., Khan, M. a., & Burgess, D. J. (2012). Predicting hydrophilic drug encapsulation inside unilamellar liposomes. *International Journal of Pharmaceutics*, *423*(2), 410–418.

Xu, X., Khan, M., & Burgess, D. (2012). A quality by design (QbD) case study on liposomes containing hydrophilic API: II. Screening of critical variables, and establishment of design space at laboratory scale. *Int J Pharm*, *423*, 543–553.

Yang, Y., Yang, D., Yang, D., Jia, R., & Ding, G. (2014). Role of reactive oxygen species-mediated endoplasmic reticulum stress in contrast-induced renal tubular cell apoptosis. *Nephron Exp Nephrol*, *128*, 30–36.

Yoshioka, T., Sternberg, B., & Florence, A. T. (1994). Preparation and properties of vesicles (niosomes) of sorbitan monoesters (Span 20,40,60 and 80) and a sorbitan triester (Span 85). *Int J Pharm*, *105*, 1–6.

Zhang, H., Holt, C., Malik, N., Shepherd, L., & Morcos, S. (2000). Effects of radiographic contrast media on proliferation and apoptosis of human vascular endothelial cells. *Br J Radiol*, *73*, 1034–1041.

Zhang, J., Duarte, C., & Ellis, S. (1999). Contrast medium- and mannitol-induced apoptosis in heart and kidney of SHR rats. *Toxicol Pathol*, *27*, 427–435.

Zheng, J., Liu, J., Dunne, M., Jaffray, D. a, & Allen, C. (2007). In vivo performance of a liposomal vascular contrast agent for CT and MR-based image guidance applications. *Pharmaceutical Research*, *24*(6), 1193–1201.

Zheng, J., Muhanna, N., De Souza, R., Wada, H., Chan, H., Akens, M. K., Anayama, T., Yasufuku, K., Serra, S., Irish, J., Allen, C., & Jaffray, D. (2015). A multimodal nano agent for image-guided cancer surgery. *Biomaterials*, *67*, 160–168.

Zheng, J., Perkins, G., & Kirilova, A. (2006). Multimodal Contrast Agent for Combined Computed Tomography and Magnetic Resonance. *Invest Radiol*, *41*(3), 339–348.